TILTS, GLOBAL TECTONICS

AND EARTHQUAKE PREDICTION

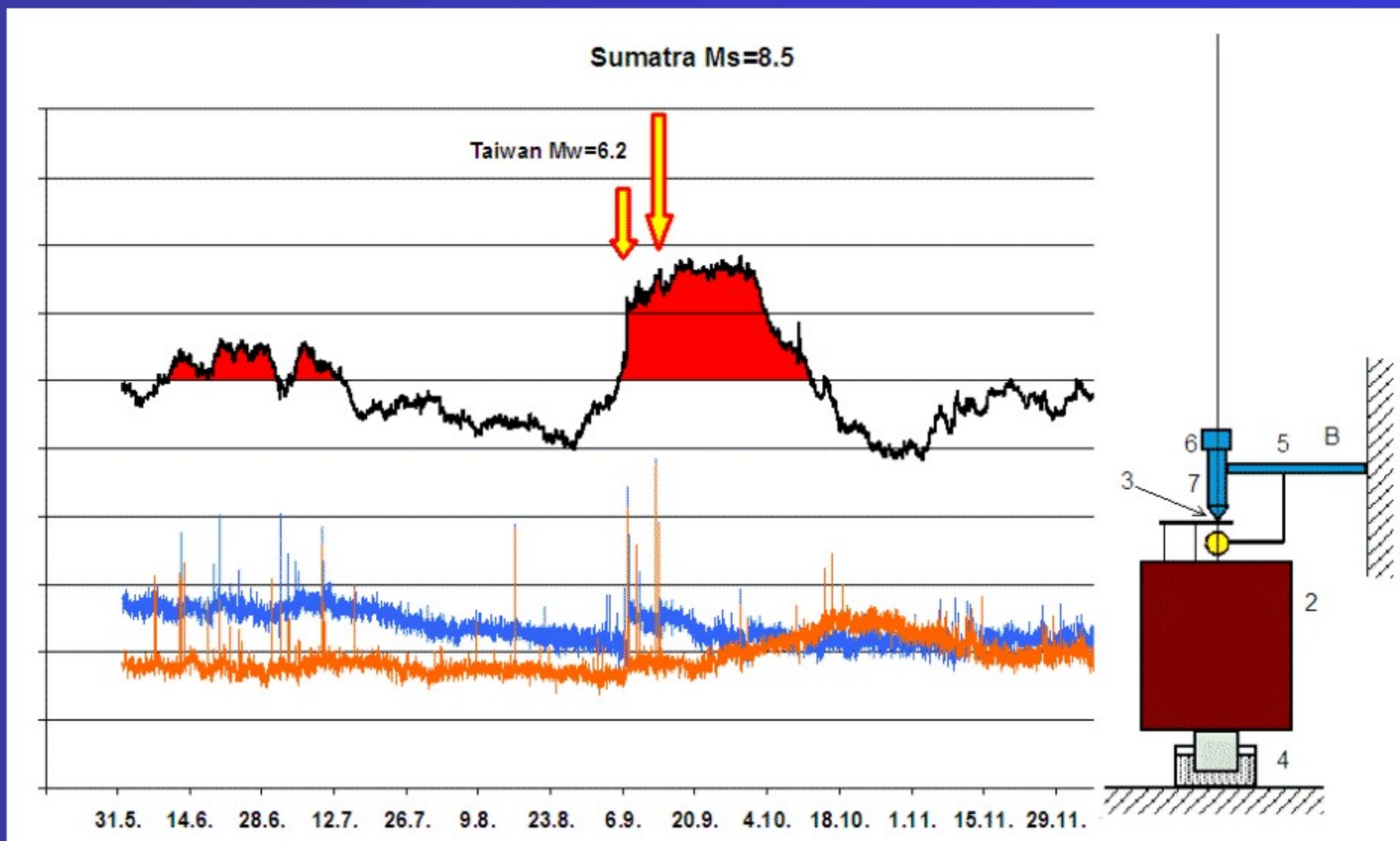

Pavel Kalenda
Libor Neumann
et al.

World Organization for Scientific Cooperation

Pavel Kalenda, Libor Neumann et al.

TILTS, GLOBAL TECTONICS AND EARTHQUAKE PREDICTION

SWB

London, 2012

TILTS, GLOBAL TECTONICS AND EARTHQUAKE PREDICTION

Pavel Kalenda[1], Libor Neumann[2] et al.

[1] IRSM CAS CZ, V Holešovičkách 41, Praha 8, Czech Republic, pkalenda@irsm.cas.cz
[2] Anect a.s., A.Staška 79, Praha 4, Czech Republic

Authors (bold) and co-authors of chapters:
Jiří Málek (chap. 4.1, 4.4, 4.6, 4.7)
IRSM CAS CZ, V Holešovičkách 41, Praha 8, Czech Republic.
Lumír Skalský (chap. **3.1**, 4.2., 4.3., 4.4., 4.6)
IG CAS CZ, Příbram, Czech Republic.
Václav Procházka (chap. 9.2, 9.5)
Ústav skla a keramiky, VŠCHT Praha, Technická 5, Czech Republic.
Lubor Ostřihanský (chap. **4.5**, **9.1**, 9.3)
Nad Palatou 7, 150 00 Praha 5, Czech Republic.
Tomáš Kopf (chap. **3.5**)
Mathematical Institute of the Silesian University at Opava,
Na Rybníčku 1, 746 01 Opava, Czech Republic.
Ivo Wandrol (chap. 3.6)
Mathematical Institute of the Silesian University at Opava,
Na Rybníčku 1, 746 01 Opava, Czech Republic.

Pavel Kalenda, Libor Neumann et al. TILTS, GLOBAL TECTONICS AND EARTHQUAKE PREDICTION. SWB, London, 247 p.

ISBN 978-9952-451-18-4

SWB
London, 2012

Kalenda, P., Neumann, L., et al. Tilts, Global Tectonics And Earthquake Prediction, SWB 2010, London.

Contents

"Bah, no one but fools and charlatans
try to predict earthquakes!"
Charles E. Richter

1. INTRODUCTION

Prediction of earthquakes – the Holy Grail of seismology and its most important aim – seems to have been an unattainable goal for generations of seismologists. Going back as far as the 6th century (Varahamihira 505 – 587), there are records of anomalous phenomena observed prior to some earthquakes, such as animal behaviour or unusual clouds in the sky (Times of India 2001). The first professional station, focusing on the animal behaviour prior to earthquakes, was constructed in 1968 in Hsingtai, China, after the city was hit by the M=6.8 earthquake (Munidasa 2009).

1.1. Development of Earthquake Prediction Science Based on Measurements

According to Scholz (1997), **the 1970s** were a productive period; in 1973, he and his colleagues Lynn Sykes and Yash Aggarwal put forward the dilatancy-diffusion theory in an attempt to explain a great variety of phenomena that had been observed to shortly precede earthquakes. That period culminated with a successful prediction. The "Geomagnetic Storm Double Time Method" developed by Tiezheng Zhang during 1968-1969 is the first successful earthquake prediction method based on geomagnetic measurements (Zhang, 2002) (Note 1). The initial success accomplished by Zhang significantly encouraged Chinese researchers to develop a series of other earthquake prediction techniques based on various types of geophysical measurements during the 1970s, which unfortunately, are not well documented by papers in English, thus are not well known by researchers in other countries.

Raising the level of interest even higher, the Chinese government announced in 1975 that it had successfully predicted a magnitude 7.5 earthquake and that the city of Haicheng had been evacuated in advance,

saving thousands of lives. The prediction was made on the basis of anomalous water levels in wells, anomalous behaviour of animals and, in the last period prior to the mainshock, of the anomalous increase of seismic activity. (Note 1)

That period of euphoria was quickly replaced by one of disenchantment after Tangshan was hit by a strong M=7.6 earthquake on July 28, 1976, claiming between 240,000 and 650,000 lives. Paradoxically, after the earthquake, clear precursors were found, in animal behaviour (Munidasa 2009) in the amount of the hutch water pumped from the nearby mine (Fujita 1997), in water table level changes in boreholes, and in ground resistivity (Chu et al.1996). A great number many more types of precursors were well documented in papers and books after the Tangshan earthquake, but not in English.

However, during the devastating Tangshan earthquake, a situation similar to the 1975 Haicheng earthquake developed in the Qinglong County nearby Tangshan. The Qinglong County government paid full attention to a prediction based on „The analysis of scientific data acquired by seven major techniques, including crustal stress and electrical measurements, indicated that there was a good possibility that this region would be struck by a significant earthquake between July 22 and August 5, 1976", and adopted a series of earthquake prevention measures resulting in no casualties in the Qinglong county during the Tangshan earthquake. This was documented in detail and described by a UN report in 1996 as the „Qinglong County

Note 1

Predicting the 1975 Haicheng Earthquake (Wang, 2006), a joint paper by Canadian and Chinese seismologists, reported that the Haicheng Earthquake Observatory, based on telluric current observations, at noontime on Feb., 4, 1975, the day of occurrence, concluded that an earthquake "greater than *M* 4–5" might occur "within three hours". They immediately reported their prediction by phone to the Haicheng County's Earthquake Office, and hand delivered their writtern prediction by bicycle to the same office. However, this prediction was disregarded by the paper as „The merit of the massive amateur involvement in microscopic precursory monitoring before the Haicheng earthquake is in its educational effects, as discussed in the Basis for Evacuation Decisions section, not in its scientific contribution."

Miracles“. (Note 2)

The 1980s and 1990s were characterised by the development of new prediction techniques, e.g. VAN method (Varotsos & Alexopoulous 1984a, 1984b, GRL 1996), based on the measurement of electro-magnetic waves or based on statistical nuances of seismicity (algorithms "M8", "CN", "SSE", "RTP") (Keilis-Borok & Kossobokov 1990, Keilis-Borok & Rotwain 1990, Keilis-Borok et al. 2002, Levshina & Vorobieva, 1992).

Note 2

The detailed report “Integration of Public Administration and Earthquake Science: The Best Practice Case of Qinglong County“ conducted by the UN Global Programme during 1995 – 1996 which confirmed:

“On the evening of July 16, 1976, scientist Chengmin Wang of the SSB's Analysis and Prediction Department, speaking to a session of 60 attendees, explained that professional earthquake monitoring groups and lay detection centers had reported abnormal signals for the Beijing-Tianjin-Tangshan-Bohai-Zhangjiakou region relating to a possible earthquake. The analysis of scientific data acquired by seven major techniques, including crustal stress and electrical measurements, indicated that there was a good possibility that this region would be struck by a significant earthquake between July 22 and August 5, 1976.”

Paying full attention to the warnings by the above prediction, “By July 26th, temporary earthquake tents were set up. Led by County Secretary Ran Guangqi, who moved into an earthquake tent himself, over 60% of Qinglong County's more than 470,000 residents moved out of their homes. Those who did not move were instructed to keep their doors and windows open at all times to avoid being trapped in case of an earthquake.“

In Qinglong County (115 km from Tangshan), more than 180,000 buildings were destroyed by the GTE; over 7,000 of these totally collapsed. However, only one person died, and he died of a heart attack. Meanwhile, in the city of Tangshan and in all its other surrounding counties, more than 240,000 people were crushed to death and 600,000 were seriously injured. Five hours after the earthquake, Qinglong County dispatched the first medical team to the disaster zone, and within a very short time, sent relief teams to Tangshan to help with rescue work and transport of the wounded.

Source: Integration of Public Administration and Earthquake Science: The Best Practice Case of Qinglong County, documented by UN:
http://www.globalwatch.org/ungp/qinglong.htm
http://unpan1.un.org/intradoc/groups/public/documents/undp/unpan032134.pdf
http://unpan1.un.org/intradoc/groups/public/documents/undp/unpan032135.pdf
http://unpan1.un.org/intradoc/groups/public/documents/undp/unpan032136.pdf

Many prediction techniques were examined during an experiment in Parkfield, California, USA area where a so-called "characteristic" earthquake with M≈6 magnitude within a period of 22 years (Bakun & Lindh 1985) was expected. The National Earthquake Prediction Evaluation Council Program (NEPEC) (Bakun et al., 1987) was created to add instruments as considered necessary to measure physical properties prior to, during, and after the anticipated earthquake (USGS 1994). The following values were measured: Creep: At present, there are 12 creepmeters in operation. Two Colour Electronic Distance Meter (EDM): This network has been in operation since 1985 giving a complete record of strain accumulation and slip on the ridge of the San Andreas Fault, 5 to 15 km southeast of the nucleation zone of the 1966 earthquake. GPS: There are now about a dozen continuous GPS sites operating in the Parkfield region. Dilatational Stress: Eight borehole dilatometers installed in the mid to late 1980s. Strain Tensor: Of the three three-component strainmeters installed in late 1980s, all are working. Water Wells: Changes in levels of several water wells in the Parkfield area have been recorded since the mid 1980s. Northern California Seismic Network (NCSN or Calnet). High Resolution Seismic Array: In the mid 1980s, ten seismometers were installed in the boreholes to improve the level of detection of micro-earthquakes. California Strong Motion Instrumentation Program (CSMIP). Electromagnetic networks: Changes in the magnetic field, resistivity, and electric field, have been recorded at several sites since the late 1980s.

The Parkfield experiment failed for the most part. And it was not until the 28th of September 2004, 11 years after the forecast time window had ended, that the predicted seismic event with a M=6 magnitude was observed in the Parkfield area (USGS 2009). After the assessment of all the methods deployed in Parkfield, geophysicists reported that even in 2004, their data had not identified any reliable precursors (Harris & Arrowsmith 2006).

The situation was even more problematic for forecasting efforts in Japan. While the US earthquake program focused mainly on mitigation, the Japanese program became entirely a prediction program. By 1978 it was no longer called a research program and became committed to predicting a magnitude 8 earthquake in a highly populated and developed part of the country - the Tokai district on the Suruga Bay, west of Tokyo. But, on

January 17 1995, a powerful earthquake with a magnitude of 7.3 hit Kobe, Japan. Nearly 4600 people were killed and more than 200,000 were made homeless (Kinki 2002). The 1995 Kobe earthquake pointed to a lack of balance in the Japanese program. But, similar to the earthquake in Tangshan, the Kobe earthquake showed retrospectively that the mainshock had been preceded by a host of precursors as pointed out by Paul Silver and Hiroshi Wakita (1996).

The failure of those forecasting programs resulted in criticism of the prediction process itself (Geller et al. 1997, Main et al. 1999). Geophysicists pointed to the chaos theory and credited the randomness of earthquake to the critical state dominating over most of areas on the Earth (Bak & Tang 1989, Sornette & Sornette 1989). The result of theoretical analyses of seismicity from the deterministic chaos point of view was that it is not possible to predict particular earthquakes, i.e. to establish where, when and what magnitude they will be. In the critical state of the environment any event may occur in a given time. The observed quakes can be small as well as big, only their probability will be governed by the G-R distribution law (Gutenberg & Richter 1954). General scepticism dominating after the unsuccessful predictions of earthquakes in the USA and Japan and theoretical analysis of their predictability led to a sharp reduction of grants into that research field. As R. Geller wrote (1997a): "The cumulative effect of these and other specious claims (predictions), extensively reported by the media, has been to give ordinary citizens and government officials the incorrect impression that earthquakes can be predicted. This not only leads to wasting funds on pointless prediction research, it also leads to neglect of practical precautions that could save lives and reduce property damage when a quake comes."

In the following years, not only grants into the research of possible predictions of earthquakes were reduced but also the results in this field were not published in scientific papers. For instance, amateur seismologist J. Berkland, who verified the relation between the earthquakes and tides, and even professional seismologists (Zschau, Varostos, Keilis-Borok) were criticised (Masood 1995, VAN 1996) and even ridiculed, see the header epigraph (Geller 1997a, 1997b). With various excuses, many had not been

allowed to publish in prestigious journals and then they were blamed for not publishing in the impacted periodicals, as shown e.g. by Geller (1997b).

The situation in China was slightly different. Although mainstream seismologists hesitated and were cautious about stating full support to "earthquakes can not be predicted", and instead stated that "**Studies in EQ prediction require long term science accumulation and require persistent exploration by one generation following another**", which in fact meant that earthquake prediction is impossible by the present generation (Zhang et al. 2001). A number of researchers practicing earthquake prediction in China (without any support from the government) continued their efforts in research based on measurements and analysis of various geophysical parameters. They reported their results in papers published by various journals in Chinese.

1.2. Methods Used for the Prediction of Earthquakes

In spite of that lack of support, many researchers continued developing forecasting methods in 1980s and 1990s both on a private and professional or on a semi-professional bases. **The electro-magnetic methods** stemming from the VAN methods (Thanassoulas 1991, Thanassoulas & Tselentis 1993, Thanassoulas & Tsatsaragos 2000, Biagi et al. 2001, 2004) could be considered promising earthquake forecasting methods. Freund's work (F. Freund 2002, Bleier & Freund 2005, Freund et al. 2006) explaining how some phenomena are occurring in magmatic rocks at the time of stress change and at the beginning of their rupture have been supportive of electro-magnetic methods. Since the electro-magnetic field and ions expand into the surrounding environment, it is possible to observe such effects both between the lithosphere and the atmosphere (Shalimov 1992, Pulinets 1998, Molchanov 2004) and in the atmosphere itself (Masayasu & Yabashi 1994, Eftaxias, et al. 2003, Molchanov 2003), in the ionosphere (Hayakawa & Sato 1994, Calais et al. 1995, Borisov et al. 2001, Naaman et al. 2001, Silina 2001, Calais et al. 2003, Ducic 2003, Plotkin 2003, Popov 2003, Heki 2004, Liu et al. 2004, Pulinets & Boyarchuk 2004) and even in outer space (Calais et al. 1998, Němec et al. 2005, Němec et al. 2009). A prediction method based on the observation of "earthquake clouds" in the high atmosphere that sometimes appear above the areas of future earthquakes

(Gorny et al. 1988, Times of India 2001, Shou 1999, 2004, Uda & Maeda 2006), Guo & Wang 2008) is likely to be based on the same physical principle. The electromagnetic MDCB method used in China is analogical to the VAN method, but the sensors do not measure electromagnetic waves. They measure the electric current between two electrodes (capacitors) (Wang et al. 2002).

A method based on a possible earthquake triggering by **tides** (Tamrazyan 1967, Shlien 1972, Kartvelishvili 1988) is another widely developing way of prediction. They found correlation between tides and earthquakes and in some cases electromagnetic energy field pulses (e.g. geologist Jim Berkland and analytical chemist E.D. Glass (1996, 1999, 2004)). It is possible to calculate tides quite easily anywhere on the Earth since the position of two main objects to induce the tides, Moon and Sun (Melchior 1983, Tamura 1987), is known. As early as more than 100 years ago the seismologists considered the possibility of earthquake triggering by tides (Schuster 1897). Most analyses, however, have shown a very low correlation between the earthquakes and earth tides (Knopoff 1964, Heaton 1982). A more conclusive correlation has been observed between the ocean tides and volcano activity in the coastal areas or on the ocean ridges (Mauk & Johnston 1973, McNutt & Beavan1981, Rydelek et al. 1988, Shirley 1988, Rydelek et al. 1992, Emter 1997, Wilcock 2001, Tolstoy et al. 2002, Cochran et al. 2004 Stroup et al. 2007) or earth tides and seismic swarms (Klein 1976, Fischer et al. 2006). In their experiments with rock specimens, Lockner & Beeler (1999) and Beeler & Lockner (2003) have shown why the link between the earth tides and earthquakes is relatively weak. Earth tides induce stress on the faults in order of kPa (Melchior 1983), which is one order less than natural stress fluctuations in rocks. However, the latest works show that if the analysis includes the seismic events of one type only, then the triggering by tides is non-accidental and significant. It is possible to determine both location and occurrence times for major earthquakes (Tanaka et al. 2002a, Tanaka et al. 2006a, Tanaka 2006b, Sue 2009). For example, C. Thanassoulas uses such effect to improve the estimate of the earthquake occurrence time in areas determined by means of the VAN method (Thanassoulas et al. 2001). Hyakawa et al. (2009), too, have found a similar relation between the tides and electro-magnetic fields. As well, the

Load-Unload Response Ratio (LURR) method (Yin et al. 1995, Yin et al. 2000) using the non-linearity of the seismicity response to the tides (Kagan 1994, Keilis-Borok & Soloviev 2003) is based on the possible triggering of earthquakes by tides.

Unfortunately, a general mistrust of the earthquake prediction based on the tidal triggering (Vidale et al. 1998, Cochran & Vidale 2006) led to the situation when this method was not used for prediction of one of the most powerful recent earthquakes in Sumatra (M=9.3). It hit Sumatra on Boxing Day, 2006 at 00:58:53, exactly 1 day and 1 hour prior to the maximum tide potential, the largest in the last 18.6 years. Only ex-post, a number of works have shown that the earthquake and its aftershocks had been triggered by tides (Crockett et al. 2006) and were predictable (Tanaka 2006b, 2010). This earthquake was predicted for example by N. Venkatanathan .[(Note 3)]

Other methods of the earthquake prediction such as the **ground water table** measurement (Wakita 1975, Wakita 1996, Yamaguchi 1980, Wang 1984, Wang et al. 1984, Roeloffs 1988, Chu et al.1996, Roeloffs & Quilty 1997, King et al. 1999, Contadakis & Asteriadis 2001, Yaltirak et al. 2005) or measurement of ground water chemical changes (Keramova 2003, Keramova 2005, Inan et al. 2008) are mostly used in China and Japan. In China, fluids are now measured at 294 stations, almost the same number of stations as those measuring deformation (358) and half the number measuring the geo-electro-magnetic field (Shi et al. 2009). As shown by Matsumoto et al. (2007), both methods of fluid measurement reflect the changes of stress in collectors and on deep faults.

Note 3

Venkatanathan predicted that the main event would occur on 26 December 2004 at 00:30 (GMT) with probable epicentre at 3.54 N latitude and 97.17E longitude, which is located near the coast of Banyak Island, Sumatra, Indonesia with magnitude around 5.0 to 7.0 (report of University of Madras 2004). The actual event occurred on the same day at 00:58 (GMT), with the actual epicentre at 3.3 N latitude and 95.8 E longitude. The difference in distance between the predicted and the actual epicentre was just 157 km and with a time difference of only 28 minutes.

The measurement of **radon gas** in water has been widely used since the earthquake in Tashkent in 1966, when the radon anomalies were conclusively observed (Ulomov & Mavashev 1971, Asada 1982). Interest in radon as an earthquake signal peaked in the 1970s in California (Hough 2009). The radon anomalies are put in connection with movements on faults prior to earthquakes point to stress variations in rocks, which release radon gas, a product of radioactive uranium decay (Virk & Singh 1994, Wakita 1996). Chyi et al. (2002) and Richon et al. (2003).

The earthquake prediction in Aquila (Italy) (April 5, 2009, M=6.3) by G. Giuliani (Dorigo 2009) proved to be a classic example of the present day mainstream science mistrust of the possibilities of imminent earthquake prediction. G. Giuliani, an expert in radioactivity measurement, had constructed a new instrument for radon gas detection (Giuliani 2004). Using that instrument he had been performing measurements of radon gas concentrations in the Aquila area for more than 10 years. He was criticized by geophysicists and government officials, when he published the earthquake prediction (Dorigo 2009). He had fought a huge internal fight. The probability of a correct prediction with parameters $M \geq 5$, T=14 days and R=200 km was mere 2%, but it proved to be correct. Prior to that, G. Giuliani himself predicted a far bigger event in a smaller time and size window, thus furthering his scientific reputation.

Thermal anomalies (Qiang et al. 1990, Xu et al. 1991, Liperovsky et al. 2005, Freund et al. 2006) might be observed at the same time as radon gas and aerosol or ion emanation. Such anomalies were first measured in boreholes together with other parameters of fluids (Asteriadis & Livieratos 1989). And with the development of space programs and techniques for remotely surveying the Earth, thermal methods have become more important with respect to the possibilities of monitoring large areas of the Earth's surface with anomalous temperatures in real time (Tronin 1996, Tronin et al. 2002, Ouzounov & Freund 2004, Saraf & Choudhury 2004, Saraf & Choudhury 2005, Choudhury et al. 2006).

Most seismologists prefer to forecast earthquakes using the analysis of **seismicity** itself. Apart from the above mentioned statistical analyses of seismicity using the M8 algorithms (Keilis-Borok & Kossobokov 1990) or

CN algorithms (Keilis-Borok & Rotwain 1990) where mainly gaps (Wyss & Haberman 1988, Scholz 1988) preceding the mainshock or clustering of events both in time and space are searched for (Keilis-Borok & Kossobokov 1990, Di Luccio et al.1997, Di Giovambattista & Tyupkin 2001, Di Giovambattista & Tyupkin 2004), the most frequently used method is monitoring of the foreshock activity (Papazachos 1975, Dodge & Beroza 1995, Jones & Molnar 1979, Jones et al. 1982, Molchan & Dmitrieva 1990, Ogata et al. 1995, Rastogi & Mandal 1999). The foreshock activity analysis has shown that prior to the earthquake series, a so-called "nucleation stage" may be observed when the earthquake is inevitable. And it can occur spontaneously even if the stress on the fault is reduced (Ohnaka 1992). Recognition of this nucleation stage would lead to an immediate prediction of the mainshock.

The principal problem of the imminent prediction based on seismicity seems to be the fact that depending on the homogeneity/heterogeneity of rocks and friction on faults, foreshock activity might or might not precede the mainshock (Sobolev & Ponomarev 1996).

The previously discussed methods attempt to identify precursors that appear in the last stage prior to the earthquake and distinguish them from normal processes that appear in the time periods between the major events. The trouble is that all precursors appearing prior to the mainshock appear between major events as well. Only their intensities vary as well as the magnitudes of the observed earthquakes. At any moment the stress tensor in the rocks changes resulting in deformations inducing both the seismic events and their precursors (Reid 1911). In order to be able to distinguish a precursor of a small event from a precursor of a main shock, it is necessary to somehow measure the absolute value of stress in the rocks, both continuously and in a vast areas (Yaolin Shi et al. 2009) and thus estimate the amount of the accumulated energy that may be released during the earthquake.

Since we are not able to directly measure **stress in the rocks** in seismogenic depths under the surface, i.e. unlike in the areas near the Earth surface, such as mines or boreholes (Staš et al. 2005), we have to use indirect methods to measure at least some components of the stress tensor.

By means of measuring the water table in boreholes it is possible to measure the relative value of omni-directional stress in the collector (Wakita 1975). However, it is very difficult to establish the direction of the principal component of stress tensor. Additionally, the reaction of the water table level to stress is strongly anisotropic (Zhang et al. 2008). The situation is similar when measuring radon gas (Matsumoto et al. 2007). Therefore, methods have been introduced, based on the measurement of rock deformation that are intended to show how the value and direction of stress inducing deformations is changing. From the instrumentation point of view, tilt-measuring methods started to be used first (Melchior 1983, Braitenberg et al. 2006). However, they were not used to predict earthquakes. They registered only occasionally anomalous tilt not related to tides (Skalský 1963, Skalský & Pícha 1965) or preceding earthquakes (Biagi et al. 1976, Braitenberg 1999). Later on, strain measurement accompanied the tilt meters (Brimich 2006) and again, in a few cases, only the changes have been observed prior to the earthquakes (Kaczorowski 2007). Both methods were deployed in Parkfield as well. But prior to the 2004 earthquake they did not identify anything helpful (Johnston et al. 2004, Harris & Arrowsmith 2006). Strain measurement is broadly used in China (Li et al. 2003) and the measurements were performed there in 358 areas in 2009 (Shi et al. 2009).

In connection space program developments, predominantly horizontal deformations started to be measured using GPS (Bo et al. 2007, Tada 2008) as well as vertical deformations using InSAR (Feigl et al. 1995, Wright et al. 1999). Despite the fact that volcano eruptions have been predicted using both techniques (Abidin et al. 2006, Janssen 2007), when deformations reached tens of centimetres, in isolated cases only, the micro-anomalies (micro-deformations) have been measured preceding the biggest seismic events (Lundgren 2002, Caporali et al. 2005, Borghi et al. 2009). Liu and Shao (1999) have explained the characteristics of crust movement on the Fujian coast, which may be related to the Taiwan 7.8 earthquake of December 21, 1999.

One of the least developed methods able to indirectly measure the omni-directional pressure in rocks is **gravimetry (**Hayes et al. 2006). In 2009, the

Atropatena network of stations was put into operation on the Euro-Asian lithospheric plate able to detect the tectonic (stress) waves generated in the centre of future earthquakes (Khalilov 2009).

One of the most important conclusions of the ISESEP 09 International Conference On Earthquake Prediction in Beijing says that for imminent prediction it is necessary to measure stress in rocks continuously, using direct or indirect methods so that we are able to measure the absolute value of stress and its variations in time (Crampin & Gao 2009, Shi et al. 2009). Since we have analysed possible earthquake predictions based on seismicity for many years, we drew the conclusion that this is not the most appropriate method due to the fact that all seismic events originate at the end of the process of rock rupturing. It is not possible to monitor seismicity deep under the Earth's surface with sufficient accuracy to be able to continuously report on the rupture process.

Dear reader, this book is not aimed at describing and evaluating **all** of the forecasting methods that might be used to predict earthquakes. In that respect, we refer to more comprehensive works, namely by T. Rikitake (1976, 1982), K. Mogi (1985), Ma Zongjin et al. (1990), C. Lomnitz (1994) or S. Mukherjee (2006). We would simply like to show in this book that it is actually possible to predict earthquakes. We are going to present our own results of measurements of micro-deformations of massif using vertical static pendulums. Based on that, we will show how it would be possible to predict the place and time and magnitude of future earthquakes. Since different chapters of this book address different subjects it is possible to skip over some of them. If you would like to learn about our measurements we recommend going directly to Chapter 5. If you would like to read about the model of movement of lithospheric plates and/or with prediction of earthquakes only, please proceed directly to Chapters 9 and 10.

In Chapter 2, we are going to show why the earthquakes are predictable.

In Chapter 3, we are going to theoretically evaluate exogenous effects that might be the triggering mechanisms for earthquakes including tides (Skalský, Kalenda), change in the Earth rotation speed (LOD) (Ostřihanský), gravitational non-tidal forces (Neumann), and thermo-elastic

waves, and we will discuss how stress and deformation penetrate from the surface areas to deeper locations in the crust and to surrounding areas (Kopf, Wandrol).

In Chapter 4, we are going to show which triggering mechanisms have been discovered with regard to world seismicity, in coal mines, and in seismicity in California and in Italy. And we will try to determine their influence on the triggering of a number of major earthquakes (Kalenda, Málek, Skalský, Ostřihanský).

In Chapter 5, we are going to describe the equipment for measuring the micro-deformation of rocks that we use for measuring tilts (Neumann).

In Chapter 6, we are going to present and analyse the results of the micro-tilt measurement of massif both on the surface and underground since 2007 (Neumann, Kalenda).

In Chapter 7, we are going to show how it is possible to interpret the measured tilt data (Kalenda, Neumann).

In Chapter 8, we are going to compare our results of deformation measurements with other deformation measurement methods and methods of indirect stress measurement.

In Chapter 9, we will sketch out a working model of the lithosphere plate movement resulting from the deformation measurements. That model will form a basis for the interpretation of the observed deformation measurement anomalies for forecasting earthquakes (Kalenda, Neumann, Procházka, Ostřihanský).

In Chapter 10, we will propose how it is possible to predict earthquakes based on indirect stress measurements using vertical static pendulums. Using examples from the years 2007 to 2010, we will show which seismic events could have been predicted and which ones were actually predicted (Kalenda, Neumann).

2. EARTHQUAKE PREDICTABILITY / ACCIDENTALITY

2.1. System and Earthquake Predictability

Before we start looking for earthquake precursors, fault zone energy accumulation mechanisms, fault zone energy sources, and triggering mechanisms for major earthquakes, we need to ask a more basic question: Can earthquakes be predicted?

Earthquakes result from processes that start with the accumulation of energy in a fault zone. It is stored as deformation energy (strain energy) in the rock layers and is released by long-period events (creep, slow slip events – SSE, tremors) or short-period events (micro-earthquakes, earthquakes). Are there any physical, chemical, geological, geographical or any other events or combinations of events that can be objectively identified and measured? Or, can we describe the system where the energy is accumulated, and where at the end there might be major earthquake? Is it possible to determine an approximate amount of accumulated energy and the distance between the system and the strength limit? If the answer is "yes" then it should be possible to predict at least some earthquakes.

The claim that there is a 100% certainty that such objectively determinable precursors or their combinations can never be observed before major earthquakes is foolish at best. Nevertheless, this is what R.Geller (1997b), A. Sornette & D. Sornette (1989), K. Ito & M. Matsuzaki (1990), or I. Main (1994, 1995, 1999) said on the basis of the theoretical analysis of seismicity and its description by means of Gutenberg-Richter law (1954) and systems in critical state (Bak & Tang 1989, Bak 1996). According to what they say, it would not be possible to predict deterministically individual earthquakes, i.e. determine within defined magnitude range and a defined area and time window. Thus, only when seismic risk can be predicted (Kanamori et al. 1997) can construction standards be improved to withstand the predicted velocity of movements and the acceleration at the given places calculated on the basis of the seismic response (Moczo et al. 1987, Galis et al. 2008).

Only in those cases, where there is at least one phenomenon or at least one combination showing the current state of the system, can the answer to the question about the predictability of earthquakes be "yes".

The aim of earthquake prediction is to correctly determine the inner state of the rockmass in the particular area and determine if the precursors of the earthquake point only to a small earthquake or to an earthquake large enough to bring the system to its critical state, where the probability of a major earthquake occurring increases substantially, or we can be certain about a future earthquake at a predictable time.

The inner state of the system 'rockmass-stress-deformation' can be observed by means of its response to the outside stimuli (external forces). In a number of experiments we have analysed this response. In chapter 4.1 we analysed if all the events responded to outside stimuli (external forces) or if they appeared accidentally. In agreement with the results of Per Bak et al. (2002) we will show that all the seismic events can be divided into two categories – events that depend on each other, and independent, random events. The group of dependent events shows a strong non-random dependence on the external forces (tides, diurnal non-tidal period). On the contrary it is probable that independent events do not depend on the outside stimuli (external forces). This means that their character is stochastic, exactly the same as B. Geller (1997b) or I. Main (1994) theoretically predicted. The fact that the group of stochastic events exists and creates only a part of all seismic events tell us:

1) The system 'rockmass-stress-deformation' is predictable and it is possible to measure its response to the external forces and so assess the state of the system.

2) Only a certain percentage of major earthquakes will be predictable because the stochastic events are unpredictable. That, however, does not exclude the predictability of the system by other than seismic precursors. However, natural science repeatedly teaches us, all seen to be „stochastic events" sooner or later turn into „non-stochastic events" as soon a some smart or lucky researcher discovers some unknown reasons behind such „stochastic events".

2.2. Nucleation period – time to mainshock

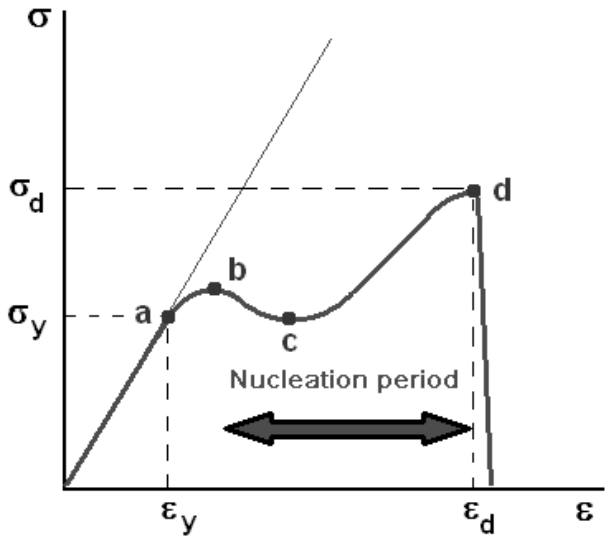

Fig. 2.1: Definition of nucleation period:
a – proportional limit, b – upper yield limit, c – lower yield limit, d – failure limit, (σ_y, ε_y) – deformation on the proportional limit, σ_d – tensile strength, ε_d – sensibility.

Now we know that the system 'rockmass-stress-deformation' is predictable. However, we are not sure that we will be able to predict individual earthquakes in real time. The predictability depends on how quickly the system responds to the increase of the stress (or the change of its orientation), for how long it is near the critical point, and how long the so called '**nucleation period' is** between exceeding the critical point and the main deformation (Li 1987, Dieterich 1987, 1994, Ohnaka 1992, Roy & Marone 1996). The nucleation period *sensu lato* is the period in which the growth of the main deformation is detectable. It is different from the nucleation phase *sensu stricto* proposed by Beroza & Ellsworth (1996) during which the growth of the crack or deformation becomes unstoppable. This nucleation period *sensu stricto* can be defined as the period during which the deformation exceeds the strength limit (point **d** on the stress-strain diagram, see Fig. 2.1)

Nucleation period *sensu lato* in the broad sense can be defined as the period before the main event, when the linear response of the rockmass changes into non-linear and Hook's law is no longer valid, and when the first irreversible deformations in the substantial mass of the material

appears. This period follows the moment when the deformation exceeds the upper yield limit (point **b** on the stress-strain diagram).

According to Beeler & Lockner's (2003) rock sample testing, the nucleation period should depend on the speed of the stress accumulation approximately, according to the relationship

$$\log T\,[\text{years}] = 2\pi^* 0.8 / \tau \quad , \qquad (2.1)$$

where τ is stress increase during one year period for specified magnitude and area. Beeler a Lockner estimated the value $\tau = 0.33 – 0.0667$ MPa/year for San Andreas area. Dieterich (1994) described a more conservative relationship

$$\log T\,[\text{years}] = 0.8 / \tau \quad . \qquad (2.2)$$

For selected forshocks Rikitake (1976) discovered a similar relationship

$$\log T\,[\text{days}] = 0.76\,M - 1.83 \quad . \qquad (2.3)$$

The real detectable nucleation period will be smaller because we are not able to detect the smallest variations in precursors and also because the real rockmass will be different from the ideal one, or the friction will exceed the average value. However, Sobolev & Ponomarev (1996) showed, in the case of bigger external cyclic forces the same rockmass under the same stress circumstances will have a longer nucleation period since the friction on the fault will decrease. Lockner & Beeler (1999) a Beeler & Lockner (2003) came to the same conclusions.

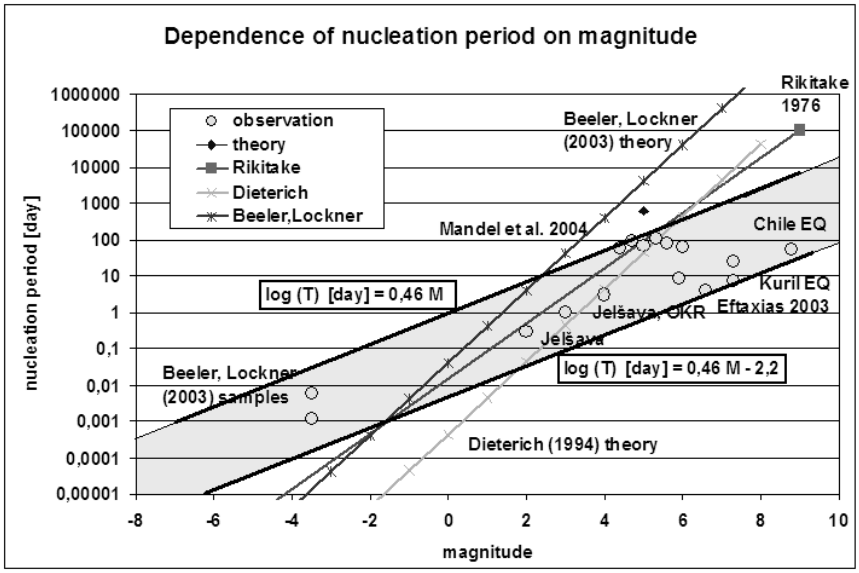

Fig. 2.2: The dependence of nucleation period on magnitude.

We analysed the observed nucleation periods in rock samples (Beeler & Lockner 2003), in samples of sandstones with various grain size matrix (Janas – pers. comm.), in rock bursts at Ostrava-Karviná Coal Basin (OKD) (coal + sandstone), in rock bursts at Jelšava (pottasium) (Kalenda & Pompura 1997), and in observed earthquakes (Mandal et al. 2004, Eftaxias et al. 2003, Kalenda et al. 2009). The results show that the detectable nucleation period is much shorter and can be approximately described by the relationship (see Fig. 2.2)

$$\log T\,[\text{day}] = 0.46\,M - 2.2 \qquad (2.4)$$

It is obvious that the nucleation period does not have a strict lower threshold, so it is not possible to propose that all major (M>6), and all catastrophic earthquakes (M>8) cant be predicted under all circumstances existing on the Earth. However, it is possible to predict at least those events with M>6 whose nucleation periods are longer than 1 day.

3. THEORY OF EXTERNAL FORCES

Many external forces and outside stimuli influence can act on the Earth at the same time, leading to its deformation. Some of the external forces only trigger earthquakes. Others can trigger them and at the same time they can be the sources of accumulated earthquake energy (see Chapter 9). In this Chapter, the most important exogenous forces will be discussed, largely from the point of view of earthquake triggering.

The tidal influence of the Moon and the Sun on the solid Earth, oceans, and atmosphere has been well described from the historical point of view. The second triggering mechanism for earthquakes can be associated with variations in the rotation of the Earth – Length Of the Day (LOD), which is partly connected with tides and tidal friction, and partly with nutation of the Earth and with climate changes. The third, up-to date unpublished triggering mechanism of earthquakes, can be associated with gravity field variations on the spinning sphere (Earth surface). The fourth triggering mechanism can be connected with the disproportion between the barycentre of the Solar system and actual position of the Sun. The fifth, and most dominant triggering mechanism, can be connected with solar irradiance of the Earth's surface and with climate changes that can lead to generation of thermoelastic waves (Hvožďara et al. 1988).

3.1. Tides

The result of mutual gravitational influence of space bodies is called by attribute 'tidal'. The simplest model for understanding of this term is the rigid Earth model (see Fig. 3.1). Its basic parameter is tidal potential. The other parameters like tidal force and its components or static ocean tides as well as additional parameters for real elastic Earth models as tidal tilts, lineal, areal, volume and shear tidal strains (relative tidal

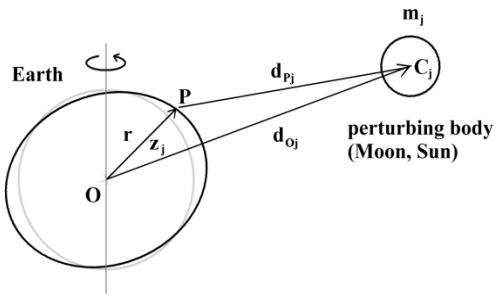

Fig. 3.1: Definition of parameters of perturbing body.

deformations) or horizontal and vertical tidal displacements can be derived from this basic tidal potential.

The gravitational force $\mathbf{F_{O,j}}$ of the perturbing body B_j with the mass $\mathbf{m_j}$ acting in the centre O of the rigid Earth at the distance $\mathbf{d_{O,j}}$ from the centre C_j of the perturbing body B_j is given by the well-known relation

$\mathbf{F_{O,j}} = \mathbf{G m_j} / (\mathbf{d_{O,j}})^2$, where **G** is the gravitational constant, so that its potential $\mathbf{W_{O,j}} = \mathbf{G m_j} / \mathbf{d_{O,j}}$.

Similarly hold for arbitrary point P on the Earth's surface at the distance $\mathbf{d_{P,j}}$ from the centre C_j of the perturbing body Bj relations

$$\mathbf{F_{P,j}} = \mathbf{G m_j} / (\mathbf{d_{P,j}})^2 , \quad \mathbf{W_{P,j}} = \mathbf{G m_j} / \mathbf{d_{P,j}} . \qquad (3.1)$$

Table 1 Parameters of Earth – Moon system

Earth	Moon
mass $M = 5.9734\ 10^{24}$ kg	$m = M/81.33$
radius $r = 6.37103\ 10^6$ m	$R = 1.7379\ 10^6$ m
angular rotation	
velocity $\Omega = 2\pi/(86164.1\ )$s	$\omega_m = \omega$
momentum radius $r_e = \sqrt{0.331}$	$r_m = \sqrt{0.394}$
	current orbital parameters
	semi-major axis dp = $3.8440\ 10^8$ m
	derivative a = 3.82 cm/yr by laser lunar ranging
	angular velocity $\omega = 2\pi/(27.32166$ d)
	eccentricity e = 0.05490

If only the gravitational force of perturbing body B_j exists then their potential on the Earth's surface in the point P with respect to the Earth's centre will be

$$\mathbf{W_{P,O,j}} = \mathbf{G m_j} / \mathbf{d_{O,j}} + [\mathbf{G m_j} / (\mathbf{d_{O,j}})^2] \,.\, \mathbf{r} \,.\, \cos(\mathbf{z_j}) , \qquad (3.2)$$

where $\mathbf{z_j}$ is zenith distance of the perturbing body B_j in the point P.

As the direct gravitation force of perturbing body $\mathbf{F_{P,j}}$ (with its potential $\mathbf{W_{P,j}}$ (3.1)) is in action in the point P at the same time as the force $\mathbf{F_{P,O,j}}$ (with its potential $\mathbf{W_{P,O,j}}$ (3.2)) , the tidal force with its tidal potential $\mathbf{V_{P,j,R}}$ would be (3.1)-(3.2) (index R denotes the rigid Earth)

$$\mathbf{V_{P,j,R}} = \mathbf{W_{P,j}} - \mathbf{W_{P,O,j}} = \mathbf{G m_j}/\mathbf{d_{P,j}} - \mathbf{G m_j}/\mathbf{d_{O,j}} .[1+(\mathbf{r}/\mathbf{d_{O,j}}).\cos(\mathbf{z_j})]. \qquad (3.3)$$

Because from the triangle POC_j (see Fig. 3.1) is evident

$(\mathbf{d_{P,j}})^2 = (\mathbf{d_{O,j}})^2 + \mathbf{r}^2 - 2\mathbf{r} \,.\, \mathbf{d_{O,j}} \,.\, \cos(\mathbf{z_j})$, (3.4)

we can expand (3.3) into the polynom

$$V_{P,j,R} = (Gm_j / d_{O,j}) \sum_{l=2}^{\infty} [(r / d_{O,j})^l . P_l(\cos(z_j)] \,, \quad (3.5)$$

where $\mathbf{P_l}(\cos \mathbf{z_j})$ are Legendre's polynoms.

If we use the average distances $\mathbf{c_{O,j}}$ instead of the true distance to the perturbing body

$\mathbf{d_{O,j}} = \mathbf{c_{O,j}} \,.\, (\mathbf{d_{O,j}} / \mathbf{c_{O,j}})$, (3.6)

then the tidal potential in the point P on the rigid Earth for all perturbing bodies of mass $\mathbf{m_j}$, j = 1,..,N will obtain the form

$$V_{P,R} = \sum_{j=1}^{N} \{ Gm_j \sum_{l=2}^{\infty} [(r^l / {c_{O,j}}^{l+1}) \,.(c_{O,j} / d_{O,j})^{l+1} . P_l(\cos(z_j)]\} \,. \quad (3.7)$$

The function $\cos(\mathbf{z_j})$ can be expressed using geocentrical latitude ψ of the point P and declination δ_j and hour angle $\mathbf{t_j}$ of the perturbing body B_j by

$\cos(\mathbf{z_j}) = \sin\psi \,.\, \sin\delta_j + \cos\psi \,.\, \cos\delta_j \,.\, \cos \mathbf{t_j}$. (3.8)

The hour angle $\mathbf{t_j}$ can be expressed by Greenwich time $\mathbf{H_G}$, geographical longitude λ of the point P and right ascension α_j of the perturbing body B_j

$\mathbf{t_j} = \mathbf{H_G} + \lambda - \alpha_j$. (3.9)

The geocentrical latitude ψ of point P and its distance $\mathbf{r}$ from the Earth's centre $\mathbf{O}$ could be than written as

$\psi = \text{arc tg}(\mathbf{r_b} / \mathbf{r_a})$, $\mathbf{r} = \mathbf{a_0} \,.\, (\mathbf{r_a}^2 + \mathbf{r_b}^2)^{½}$, (3.10)

where

$\mathbf{r_a} \equiv (\mathbf{r} \,.\, \cos\psi) / \mathbf{a_0} = [(1 - \mathbf{e_0}^2 \,.\, \sin^2\varphi)^{-½} + \mathbf{h} / \mathbf{a_0}] \,.\, \cos\varphi$,

$\mathbf{r_b} \equiv (\mathbf{r} \,.\, \sin\psi) / \mathbf{a_0} = [(1 - \mathbf{e_0}^2) \,.\, (1 - \mathbf{e_0}^2 \,.\, \sin^2\varphi)^{-½} + \mathbf{h} / \mathbf{a_0}] \,.\, \sin\varphi$,

$\mathbf{a_0}$, resp. $\mathbf{e_0}$ are main semi-axis and excentricity of reference ellipsoid,

φ , resp. $\mathbf{h}$ are geographical latitude and altitude of the point $\mathbf{P}$.

If we denote

$$P_l(z_j) = \sum_{m=0}^{l} P_l^m(90° - \psi) . P_l^m(90° - \delta_j) . \cos(mt_j) \quad (3.11)$$

where

$\mathbf{P_l^m}(\mathbf{x}) = \{[2(\mathbf{l}-\mathbf{m})!]/(\mathbf{l}+\mathbf{m})!\}^{½} . \sin^{\mathbf{m}}\mathbf{x} . d^{\mathbf{m}} \mathbf{P_l}(\mathbf{x}) / d(\cos \mathbf{x})^{\mathbf{m}}]$ for $\mathbf{m} = 1, 2, ..., \mathbf{l}$,

$\mathbf{P_l^0}(\mathbf{x}) = \mathbf{P_l}(\mathbf{x}) = [1/(2\mathbf{l} . \mathbf{l}!)] . [d^{\mathbf{l}} / d\,\mathbf{x}^{\mathbf{l}}] (\mathbf{x}^2 - 1)^{\mathbf{l}}$,

then we can express the tidal potential of all perturbing bodies on the rigid Earth as

$$V_{P,R} = \sum_{j=1}^{N} \{Gm_j \sum_{l=2}^{\infty} [(r^l / c_{O,j}{}^{l+1}) .(c_{O,j} / d_{O,j})^{l+1} . P_l(z_j)]\} . \qquad (3.12)$$

It is evident from (3.9), (3.11) and (3.12) that parameter **m** describes the frequency characteristics of tidal spectrum: m=0 long-period part, m=1 diurnal part, m=2 semidiurnal part, m=3 third part of the day and m=4 quarter part of the day. Parameter m>4 (and then I>4) are not used now.

Already G.H.Darwin (1883) found that it is not operative to use the ephemeredes of all perturbing bodies in all time steps of tidal potential evaluation. He replaced the equatorial coordinates by ecliptically and he published the first harmonious development of tidal potential in 1883, using the best quality formulas of mean longitudes of Moon and Sun. Such principle is using till this time, because of its advantageous for the evaluation of tidal potential of semi-elastic model of the Earth.

So far, many harmonious developments of tidal potential were used (Doodson, 1921, Cartwright & Tayler 1971, Cartwright & Edden 1973, Büllesfeld 1985, Roosbeek 1996), which contained 378 up to 12,935 tidal waves.

We used as a comparable basis for global seismicity the tidal potential that was calculated with help of our programs (Skalský 1991) using Tamura's development of tidal potential into 1200 tidal waves (Tamura 1987) and mostly used Wahr-Dehant-Zschau tidal model of the Earth (Wahr 1981, Dehant 1987, Zschau and Wang 1987).

The tidal potential $\mathbf{X_{P,t}}$ at point P on the Earth in the time **t** after reference time **T,** when all characteristics of i-th tidal wave were evaluated, was expressed first by Darwin (1883) as the sum of 'tidal members', today called 'tidal waves'. This tidal potential is now expressed for all of models of the Earth (rigid, semi-elastic, elastic global or elastic local) in the form of sum of finite numbers of 'tidal waves'

$$X_{P,t} = \sum_{i=1}^{n} \{F_i.G_i.K_{i,T}.\cos(\Phi_{i,T} + \omega_{i,T}.t + \kappa_i + u_i.90°)\}, \qquad (3.13)$$

where

$\mathbf{G_i}$ is geodetic coefficient of the **i**-th tidal wave, which is quite complicated function of the basic astronomic constants of perturbing body $\mathbf{B_j}$, of referential ellipsoid and of the characteristics of the point P and parameters **l** and **m**, which was used by derivation of the **i**-th tidal wave,

$\mathbf{K_{i,T}}$, $\mathbf{\Phi_{i,\,T}}$ and $\boldsymbol{\omega_{i,T}}$ are amplitude coefficient, phase and angular frequency of the **i**-th tidal wave for the reference time **T**, which were determined using harmonic development of the relationship (3.12),

$\boldsymbol{\kappa_i}$ denotes the phase shift according to the global model values. For the rigid Earth model $F_i = 1$ a $\kappa_i = 0$,

$\mathbf{u_i}$ is integer multiplier of angle 90°, which allows to use only positive values in (3.13) and so to use only function 'cosinus' ($u_i = 0, -1, +1$ or $+2$).

85 most significant tidal waves were denoted by their historical Darwin's alphanumeric names (2 - 4 characters) - e.g. K_1, O_1, M_2, S_2, N_2, etc.

Doodson (1921) introduced special 6-digit number (called Doodson's argument number) for all tidal waves according to their increasing frequency. He used the fact, that the phase and the frequency of each tidal wave can be expressed as integer combination of 6 basic astronomic parameters:

$\boldsymbol{\tau}$ = mean lunar time (counted from the lower transit of the Moon),
s = mean tropic longitude of the Moon,
h = mean tropic longitude of the Sun,
p = mean tropic longitude of the lunar perigee,
N' = **-N**, where **N** is mean tropic longitude of the ascending lunar node,
$\mathbf{p_S}$ = mean tropic longitude of the perihelion.

If we express this combination as $\mathbf{C} = a \,.\, \boldsymbol{\tau} + b \,.\, \mathbf{s} + c \,.\, \mathbf{h} + d \,.\, \mathbf{p} + e \,.\, \mathbf{N'} + f \,.\, \mathbf{p_S}$,

where $0 \le a \le 4$ and the other integer b, c, d, e, f are in the range from -5 to +5, then such tidal wave will have argument number $a\,(b + 5)\,(c + 5)\,.\,(d + 5)\,(e + 5)\,(f + 5)$,

so that e.g. the greatest diurnal tidal wave **K_1** has Doodson's argument number 165.555 .

In 1987 Tamura extended 6 parameters of 2 more parameters, which express the perturbations of Jupiter and Venus

f_7 = argument of Jupiter's opposition,
f_8 = argument of Venus's conjunction.

Tides show all of basic and half periods of perturbing bodies, i.e. Moon and Sun and the periods of spinning Earth. The dominant tidal periods are mainly semi-diurnal periods (12.000 h for S_2, 12.421 h for M_2 and 12.658 h for N_2), diurnal periods (23.934 h for most important wave K_1, 24.066 h for P_1 and 25.819 for O_1), interference fortnightly periods (high tides), interference semi-annual and annual periods, 4.425-years long period of variation of moon perigee and 18.6-years lunar nodal period.

The tidal influence concerns all of the volume of the Earth, although its amplitude decreases towards the centre of the Earth and toward the poles.

3.2. LOD

The rotation of the Earth can be measured by the inverted parameter – Length Of the Day (LOD). According the theory, the LOD increases and rotation of the Earth Ω is getting smaller (Verbunk 2002).

$$J = \frac{Mm}{M+m} R_p^2 \omega + r_e^{\,2} M r^2 \Omega + r_m^2 m R^2 \omega_m , \qquad (3.14)$$

where parameters of the Earth and Moon are in Table 1

Since the Moon has much smaller mass and radius than the Earth, we ignore its angular momentum in what follows. In our assumption of no external perturbers, J is a constant and its value is found by entering the values listed in Table 1 in eq. 3.14.

In eq. 3.14 R_p, Ω and ω are functions of time. We define

$$I = r_e^{\,2} M r^2 \qquad (3.15)$$

and eliminate ω from eq. 3.14 using Kepler's law

$$\omega^2 = \frac{G(M+m)}{R_p^{\ 3}} \tag{3.16}$$

to find

$$J = Mm\sqrt{\frac{GR_p}{M+m}} + I\Omega \tag{3.17}$$

The tidal forces of the Moon slow down the rotation of the Earth, i.e. Ω is getting smaller. Eq. 3.17 shows that the angular momentum thus lost by the Earth is added to the angular momentum of the lunar orbit, which implies that the distance Rp between the Earth, and the Moon increases.

The development of LOD during past 2450 M.y. (since Proterozoic) shows shorter days and months in the past time (Williams 2000). Paleotidal and paleorotational values provided by late Neoproterozoic (~620 M.y.) tidal rhythmites in South Australia are validated by these tests and indicate 13.1+/-0.1 synodic (lunar) months/yr, 400+/-7 solar days/yr, a length of day of 21.9+/-0.4h and a relative Earth-Moon distance a/a_0 of 0.965+/-0.005. The mean rate of lunar recession since that time is 2.17+/-0.31cm/yr, which is little more than half the present rate of lunar recession of 3.82+/-0.07cm/yr obtained by lunar laser ranging.

The secular deceleration of the Earth rotation has a long-time influence on the mutual movements between separated layers (layering), mostly between the mantle and the crust, and between the core and the mantle. With respect to the lower layers, because the upper layers have a greater moment of inertia *I*, the upper layers will drift to the west during the deceleration of the Earth (Ostřihanský 1997). So, the secular deceleration of the Earth by tidal friction can support the westward drift of lithosphere plates (see Chapter 9.1).

The deformation of the Earth, as a product of tidal influence, is a reason for changes of its moment of inertia *I*. The changes of moment of inertia *I* lead to variations in the spin of the Earth, i.e. variations of LOD according to relation 3.17, because the angular momentum of the system *J* must remain constant. The LOD variations were confirmed by direct measurement of LOD (Aoki et al. 1982) (see Fig. 3.2).

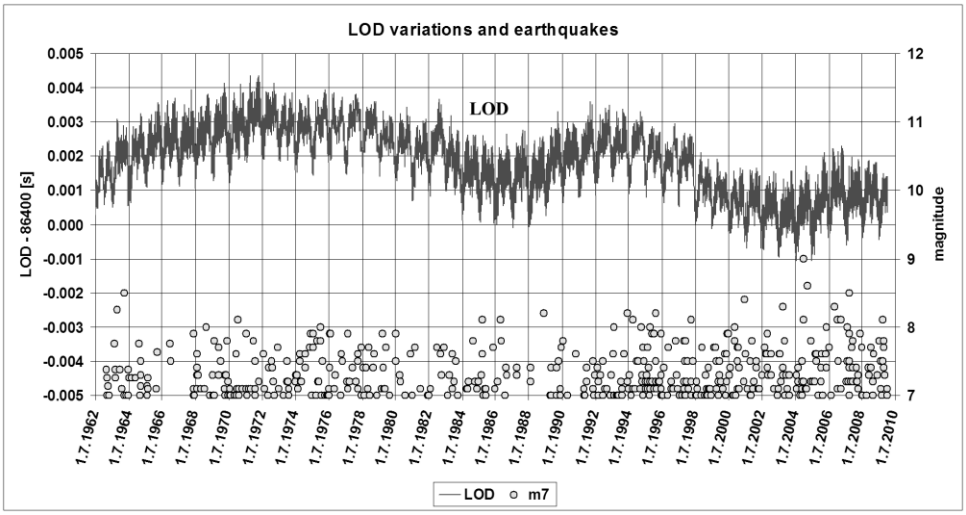

Fig. 3.2: LOD variations (according to IERS 2010) and world seismicity (ANSS 2010).

The most important periods of LOD are fortnightly and semi-annual tidal periods (with minimum LOD around July 21), annual periods, and the lunar nodal period (18.6 years). If we remove the tidal member of LOD from LOD variations, the remaining variations are mainly associated with Chandler's wobble (period ca. 14 months) and the approximately 30-years long interference period between crust and mantle. According to Bobova et al. (1993) – "There is statistical relationship between variations in Chandler oscillations amplitude and nontidal changes of LOD with r=0.98".

Due to tidal friction, some rotational energy causes the heating of the rock mass. If we use the value of derivative *a* measured by lunar ranging, we derive a required current energy dissipation of about 3.5 terrawatt (i.e. $3.5\ 10^{12}$Watt $\approx 1.1\ 10^{20}$ J/y).

The energy, which is connected with changes of spin rotational energy, is much higher (Varga et al. 2005). It depends on the rotation period as

$$\Delta E_{rot} = \frac{1}{2} C\Omega^2 \Delta\Omega = C\Omega^2 \frac{\Delta LOD}{LOD} \tag{3.18}$$

For the most important tidal periods the dissipations of energy according to (3.18) can be: For T=18.6 years – 3.1 10^{20} J, S_{sa} (semi-annual) – 3.4 10^{20} J, M_m (monthly) – 3.9 10^{20} J, M_f (fortnightly) – 7.4 10^{20} J, M_{tm} – 1.4 10^{20} J (Varga et al. 2005). All of them are comparable with the energy of an earthquake with M=9 according to the old empirical relationship (Lomnitz 1994)

$$\log E[J] = 4.4 + 1.5M \,. \tag{3.19}$$

If we suppose that only a small part of the accumulated elastic energy is radiated by seismic energy from the focus (according to our measurements in mines it is only 0.1-1% of entire accumulated energy), then we can write that tides and changes of Earth rotation (LOD) could not be the main mechanisms of energy accumulation. The tides and/or LOD can only work to trigger earthquakes.

3.3. Gravity – spinning sphere in homogenous gravity field

Gravity can produce, besides tides and their "by-product" (changes of LOD), other effects, which have never been proposed as earthquake triggering mechanisms. With the following discussion we will analyse the influence of gravity on the dipole, which can be, for example, the rock mass on both sides of the fault and which is placed on the spinning sphere (Earth's surface). Other effects can be observed if this dipole is going to be in non-homogenous gravity field (e.g. the central gravity field).

Assume that we have a sphere with radius ***R***. A mass dipole is on the sphere surface. The dipole consists from two mass points A and B having the same mass ***m*** and placed relatively close to one another.

The sphere is placed in an external homogenous static gravity field of magnitude ***e***. The field consists of two orthogonal components. The component $\boldsymbol{e_1}$ having the direction of the spinning axes of the sphere, and the orthogonal component $\boldsymbol{e_2}$ that is perpendicular to the spinning axes i.e. the component parallel to the equator plane of the sphere.

The sphere revolves with constant angular speed $\boldsymbol{\omega}$. The angle $\boldsymbol{\varphi}$ is angle between the sphere coordinate system origin and direction of external gravity field component $\boldsymbol{e_2}$ in time $\boldsymbol{t_0}$.

Let us analyse the force interaction of the gravity field with mass dipole in the general position on the sphere surface (see Fig 3.3).

The coordinate system is fixed to the sphere. The dipole position is given by $\boldsymbol{\eta}$ and $\boldsymbol{\xi}$ coordinates of the dipole centre of mass i.e. coordinates of the centre of where $\boldsymbol{A}$ and $\boldsymbol{B}$ points join.

The dipole is described by relative $\boldsymbol{\Delta\eta}$ and $\boldsymbol{\Delta\xi}$ coordinates.

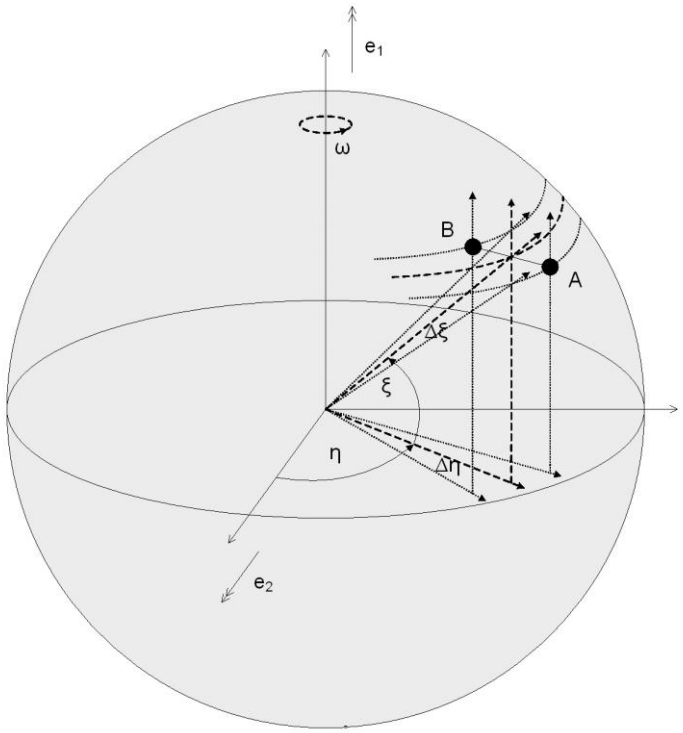

Fig. 3.3: The mass dipole in the coordinate system.

Let us calculate the force mass point interaction components caused by the external gravity field. We will work with the unit force i.e. with the

force interacting with the mass unit. The force caused by spinning axis field component $\boldsymbol{e_1}$ we will mark by index ***1***. The force caused by equator field component $\boldsymbol{e_2}$ we will mark by index ***2***.

The force component in the direction of the centre of the sphere will be marked by index ***r.*** The component in the meridian direction will be marked by index ***m.*** And the component in the direction parallel to the equator will be marked by index ***p***.

$$\begin{aligned} f_{r1} &= e_1 \sin\xi \\ f_{m1} &= e_1 \cos\xi \\ f_{p1} &= 0 \end{aligned} \qquad (3.20) \qquad \begin{aligned} f_{r2} &= e_2 \cos\xi \ \cos\eta \\ f_{m2} &= e_2 \sin\xi \cos\eta \\ f_{p2} &= e_2 \sin\eta \end{aligned} \qquad (3.21)$$

The dipole force interaction will be calculated as the force difference in A and B points $\left(\vec{f}_A - \vec{f}_B\right)$. The spinning sphere is described by the equation $\eta = \omega t + \varphi$.

$$\begin{aligned} \Delta f_{r1} &= 2e_1 \cos\xi \sin\Delta\xi \\ \Delta f_{m1} &= -2e_1 \sin\xi \sin\Delta\xi \\ \Delta f_{p1} &= 0 \end{aligned} \qquad (3.22)$$

$$\begin{aligned} \Delta f_{r2} &= -2e_2\left(\cos\Delta\xi \cos\xi \sin(\omega t+\varphi)\sin\Delta\eta + \cos\Delta\eta \sin\xi \cos(\omega t+\varphi)\sin\Delta\xi\right) \\ \Delta f_{m2} &= -2e_2\left(\cos\Delta\eta \sin\xi \sin(\omega t+\varphi)\sin\Delta\eta - \cos\Delta\xi \cos\xi \cos(\omega t+\varphi)\sin\Delta\xi\right) \\ \Delta f_{p2} &= 2e_2 \cos(\omega t+\varphi)\sin\Delta\eta \end{aligned} \qquad (3.23)$$

We can slightly simplify the equations for small angles $\boldsymbol{\Delta\eta}$ and $\boldsymbol{\Delta\xi}$.

$$\begin{aligned} \Delta f_{r2} &\approx -2e_2\left(\cos\xi \sin(\omega t+\varphi)\sin\Delta\eta + \sin\xi \cos(\omega t+\varphi)\sin\Delta\xi\right) \\ \Delta f_{m2} &\approx -2e_2\left(\sin\xi \sin(\omega t+\varphi)\sin\Delta\eta - \cos\xi \cos(\omega t+\varphi)\sin\Delta\xi\right) \\ \Delta f_{p2} &= 2e_2 \cos(\omega t+\varphi)\sin\Delta\eta \end{aligned} \qquad (3.24)$$

We can see that the interaction of the spinning axes component of the external gravity field is time independent if the field is constant. The interaction can be time dependent only in cases where the external field is changing in time.

The force interaction of the equator component of the external gravity field is time dependent, periodical with the period equal with the spinning period of the sphere. This is true even in the case when the external field is constant in time.

Let us analyse the force interaction of the dipole in more detail. We have plain ***P*** perpendicular to the sphere surface placed in the centre of where the ***A*** and ***B*** points join. The plain is placed that way to be perpendicular to where the ***A*** and ***B*** points join (see Fig 3.4).

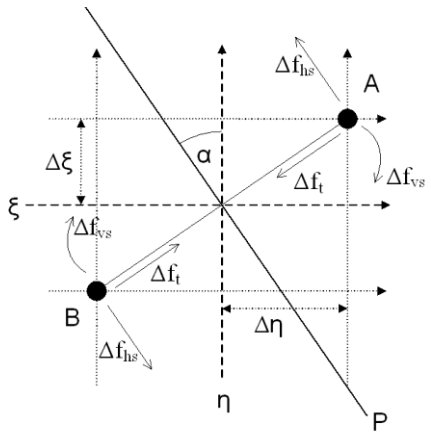

Fig. 3.4: Coordinates and forces related to the mass dipole.

The plain ***P*** is simple model of a fault.

Let us analyse the forces causing a shear stress in the fault model. We will analyse the shear stress in the horizontal and vertical directions (***Δf_hs*** and ***Δf_vs***) and shear force ***Δf_t***. We will focus only on the components caused by the equator component $\boldsymbol{e_2}$ (periodical components) of the external gravity field.

By decomposition of the previously calculated forces we found:

$$\Delta f_{vs} = -e_2\left(\cos\Delta\xi\,\cos\xi\,\sin(\omega t+\varphi)\sin\Delta\eta + \cos\Delta\eta\,\sin\xi\,\cos(\omega t+\varphi)\sin\Delta\xi\right)$$

$$\Delta f_{hs} = e_2\left(\begin{array}{l}\left(\cos\Delta\eta\,\cos\xi\,\sin\Delta\xi\sqrt{\frac{\Delta\eta^2}{\Delta\eta^2+\Delta\xi^2}} - \sin\Delta\eta\sqrt{\frac{\Delta\xi^2}{\Delta\eta^2+\Delta\xi^2}}\right)\cos(\omega t+\varphi)\\ -\left(\cos\Delta\xi\,\sin\xi\,\sin\Delta\eta\sqrt{\frac{\Delta\eta^2}{\Delta\eta^2+\Delta\xi^2}}\right)\sin(\omega t+\varphi)\end{array}\right)$$

$$\Delta f_{t} = -e_2\left(\begin{array}{l}\left(\cos\Delta\eta\,\cos\xi\,\sin\Delta\xi\sqrt{\frac{\Delta\xi^2}{\Delta\eta^2+\Delta\xi^2}} + \sin\Delta\eta\sqrt{\frac{\Delta\eta^2}{\Delta\eta^2+\Delta\xi^2}}\right)\cos(\omega t+\varphi)\\ -\left(\cos\Delta\xi\,\sin\xi\,\sin\Delta\eta\sqrt{\frac{\Delta\xi^2}{\Delta\eta^2+\Delta\xi^2}}\right)\sin(\omega t+\varphi)\end{array}\right)$$

(3.25)

We can see the existence of periodical forces with a frequency given by the sphere spinning caused by an external constant gravity field that can cause fault shear in a horizontal as well as in a vertical direction. Simultaneously the external gravity field leads to existence of periodical change of shear force perpendicular to the fault plain.

The forces are directly proportional to the equator component magnitude e_2 of the external gravity field and approximately directly proportional to the $\Delta\eta$ and $\Delta\xi$ i.e. to the distance between points ***A*** and ***B***. And they are dependent on the ratio of $\Delta\eta$ and $\Delta\xi$ i.e. angle α.

The forces act on the whole sphere surface. And they can cause periodical stress of the material on the whole sphere surface.

The magnitude of the forces is not dependent on the distance of the ***A*** and ***B*** points from the centre of the sphere. If the external gravity field gets through the sphere mass, it will produce the same forces inside the sphere. Let us note that the forces are related to the unit mass of points ***A*** and ***B***.

The triggering mechanism described above will show the diurnal period, because it is controlled by the mutual positions of the Sun and the Earth. And its influence will be maximal near the Earth's equator.

3.4. Gravity – Sun and Barycentre Position Asymmetry Influence (SIM)

Chapter 3.3 concludes that the external homogenous gravity field causes periodical force moments at the surface of the spinning sphere. The force period is equal to the spinning velocity of the sphere relative to the external gravity field.

The goal of this chapter is to analyse the external gravity field with respect to the Earth's trajectory in the space. The present chapter should answer questions regarding whether or not a gravity field can cause significant periodical force interactions on the Earth's surface or below the surface.

We will focus our analysis only on significant gravity fields, and exclude all fields with demonstrably negligible value. We will use static Newton's gravity model (Newton's law of universal gravitation) in the first part of analysis.

$$\hat{F}_{12} = -G\frac{m_1 m_2}{\left|r_{12}\right|^2}\hat{r}_{12} \tag{3.26}$$

The model does not include any physical effects related to velocity, does not include gravity field propagation velocity (i.e. the propagation velocity is unlimited), and does not include any physical effects related with speed of mass.

The basic physical abstraction regarding the movement of the Earth (together with the Sun and the Moon) is based on the use of Newton's force model. The commonly used abstraction expects equivalence between Earth inertial mass and Earth gravity mass. The abstraction uses the existence of balance between gravity acceleration of the Earth-Sun system with the Earth inertial acceleration. Due to the mass ratio of the Earth and the Sun the movement of the Sun is neglected.

The zero value and time independent gravity field exists in the centre of gravity of the Earth as the result of the abstraction.

We can take into account the actual size of the Earth and the respective gravity field of the Moon. We get the classical static tide force generation model with M_2 (12.42h), S_2 (12.00h), K_1 (23.93h) and O_1 (25.82h) dominant modes. Maximal values of tidal accelerations are $1.1\ 10^{-7}$g for the Moon tidal acceleration and $0.52\ 10^{-7}$g for the Sun tidal acceleration (**g** is standard gravity acceleration on the Earth surface). We will use the values as the reference value for the significant evaluation of analysed gravity fields.

The reason why this value is used as the limit of significance is that only fields greater or comparable with the tide related fields can have triggering effects on significant numbers of earthquakes. Smaller fields triggering effect should be negligible compared to the tide field effect.

The first analysis deals with other Solar system planets. We analyse the gravity field in place on the Earth's trajectory. The following table shows maximal value of the gravity field relative to the gravity acceleration on the Earth's surface (Ax/g), to the maximal values of tidal acceleration of the Moon (Ax/TM) and the Sun (Ax/TS) on the Earth's surface.

We can see from calculated values that the gravity fields of Jupiter and Venus are comparable with the tidal field on the Earth's surface. Jupiter's gravity field can have a value equal to about 60% of maximal tidal acceleration of the Sun.

The direct gravity fields of the planets are not the only possible source of external gravity on the Earth's surface. We will analyse the gravity interaction of the Earth with the Sun in more detail. We will analyse the possible 'variation' of the Sun's gravity field, the possible difference from the equilibrium of the Sun's gravity field, and the Earth inertial acceleration.

The absolute size of the Sun's gravity field on the Earth's surface is about $6.1\ 10^{-4}$ g, i.e. about 5 200 times greater than the maximal tidal acceleration of the Moon. This means that a relatively small variation of the Sun gravity field could have greater effect on the Earth's surface than the tidal effects.

Table 2 Relative gravity fields of Solar system planets. Ax – observed body, g – normal gravity on the Earth's surface, TM – tidal acceleration of Moon, TS – tidal acceleration of Sun

	Ax/g	Ax/TM	Ax/TS
Mercury	2.70E-10	0.0023	0.0052
Venus	1.89E-08	0.1629	0.3661
Mars	7.22E-10	0.0062	0.0140
Jupiter	3.28E-08	0.2823	0.6347
Saturn	2.40E-09	0.0207	0.0465
Uranus	7.99E-11	0.0007	0.0015
Neptune	3.73E-11	0.0003	0.0007
Pluto	2.79E-15	0.0000	0.0000

Let us analyse the influence of the Sun's motion relative to the Solar system's centre of gravity. This attempt is the same as the analysis of Solar Internal Motion (SIM) made by Charvátová (1988, 1997). It is the first approximation of the motion of the Sun in an inertial coordinate system.

The Earth is visualised as a mass point $\boldsymbol{m_1}$ and the Sun as a mass point $\boldsymbol{m_2}$ in the following figure.

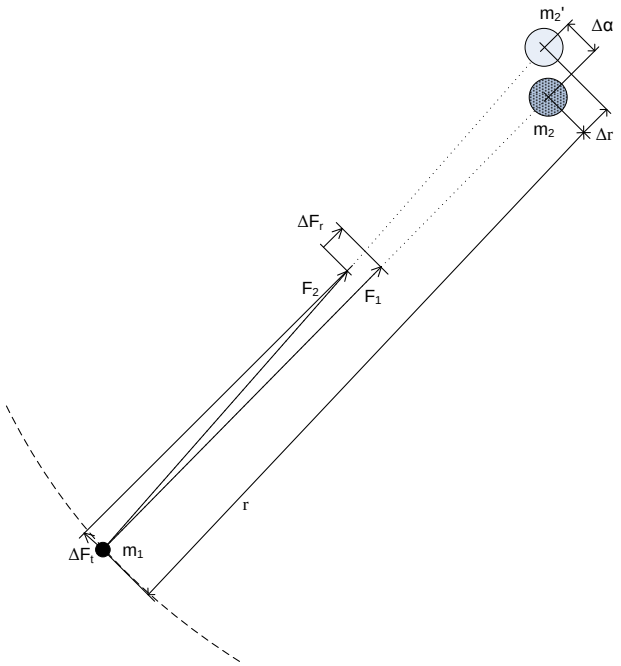

Fig. 3.5: Differential gravity field diagram.

We suppose that m_2 point has many times greater mass than m_1, the system is in dynamic balance with respect of Newton's law and the m_1 trajectory is close to the circle with the centre close to point m_2.

We analyse gravity field variation ΔF_r and ΔF_t in point m_1 if the mass point m_2 is moved to point m_2' i.e. the position of mass point m_2 was changed at $\Delta\alpha$ and Δr. This means that the gravity force was changed from F_1 to F_2. We take into account only a very small change. The dynamic effects are not included. The result is:

$$\begin{aligned} \Delta F_r &\cong -2F\frac{\Delta r}{r} \\ \Delta F_t &\cong F\Delta\alpha \end{aligned} \tag{3.27}$$

We can see that for small differences in position of the mass point m_2 the difference of the gravity field in the place m_1 is approximately directly proportional to the difference of mass point position m_2. The difference cannot be balanced by the inertial acceleration of mass point m_1 (it is not dependent on the new position of mass point m_2). The difference has the same influence to the mass point m_1 as the additional external gravity field. We can name the additional gravity field as 'differential'.

Now we will analyse the possible cause of the position change of the Sun in the inertial coordinate system. We work with Newton's law. In this case the Sun moves around the Solar system centre of gravity to enable the Solar system centre of gravity to be at rest.

We can calculate moments of every planet in the Solar system and find the sum total. We get maximal possible difference of the Sun's position relative to the Solar system's centre of mass. It is about 0.01 AU (Astronomical unit). We found that only the contributions of Jupiter, Saturn, Neptune and Uranus are significant.

We can compare the relative maximal "differential" field value component $\Delta F_r/F$ caused by the Sun's move from the Solar system centre of gravity to the maximum distance calculated as the sum of all planet

momentums with the maximum Moon tide acceleration. We observed that the maximum 'differential' gravity field could be about 200 times greater than the Moon tide field. This means that if the Sun moves only 1% of the maximal distance it creates an external gravity field greater than the maximal sum of Moon and Sun tidal fields.

The orientation of 'differential' gravity field can be of any direction in the ecliptic plane.

If we want to analyse the influence of the 'differential' gravity field on the Earth's surface, we should know the Earth's trajectory curvature (it is related with the Earth inertial acceleration) and the position of the Sun relative to the Solar systems centre of gravity (it is related with the Earth gravitational acceleration) both with a precision greater than 0.1%. That precision is comparable with about 15% of maximal tidal forces on the Earth's surface.

All attempts to do the analysis of the relationship with the needed precision failed.

The use of the simplest physical model based on a static gravity model i.e. a model based on Newton's law and mass point abstraction creates great issue with calculating the relationship between the time variation of trajectories of the Earth and the Sun. The model cannot be solved analytically. The only way to do this is with a numerical solution.

Numerical integration needs initial conditions. We don't know position and speed of the Sun relatively to the Solar systems centre of gravity. We can only use speculations or hypothesis.

We can use hypothesis claiming that the position and speed of all planets in the Solar system are known and an astronomical approximation of planet positions gives the right positions and velocities of the planets. We use the idea that the position and velocity of the Sun can be calculated as a negative position and the velocity of the sum of planets momentums divided by the Sun's mass.

We can numerically integrate the set of differential equation with the initial conditions and use Newton's law of universal gravitation (equation 3.26) as a gravity field model.

It is possible to observe from that numeric model, that the Earth approximately follows the Sun on the track of the Sun around the Solar system's centre of gravity. The Sun's trajectory is very complex. The distance between the Sun and the Earth is time dependent and it is slightly different from the theoretical ellipse.

This means that the time dependent 'differential' gravity field should exist on the Earth. But the precision quantitative estimation or prediction of the time dependence of the 'differential' field could be only speculative. The physical credibility of the calculations is limited for the following reasons:

- The Sun's diameter is described as 1 390 000 km i.e. 0.01AU. It is comparable with the maximum distance of the Sun from the Solar system's centre of gravity, and the huge amount of the Sun's mass is in more distant locations from the Solar system's centre.
- The movement of the Sun is assumed to be caused by more than the effects of the movement of the Sun around the Solar system's centre of gravity e.g. by the jet propulsion effect of the Sun's eruption.
- Newton's law does not include any dynamic gravity interaction, and does not consider gravity field components dependent on the mass velocity.
- We do not know the gravity field propagation velocity and any of the effects related with limited propagation velocity. This does not mean that the effect does not exist or that it has no significant effect in the Solar system.
- Time dependency of the 'differential' field is unknown.

The general physical analysis conclusions of chapters 3.3 and 3.4 are:

- It was analytically confirmed that the external homogenous and time constant gravity field causes periodical force stress on the Earth's

surface. The stress has a periodical character, which can cause or increase the probability of an earthquake occurring.

- It was analytically confirmed, that at least two different types of external gravity fields can be comparable with the maximal tidal fields caused by the Sun and Moon on the Earth's surface (without giving consideration to the above mentioned 'differential' field):
    - Newton's gravity field of Jupiter and Venus
    - 'Differential' gravity field of the Sun
- The maximum magnitude of the 'differential' gravity field of the Sun could be about 200 times greater than maximum tidal field on the Earth's surface.
- All of such 'perturbations' of the gravity field will have diurnal (circadian) and much longer periods on the Earth's surface.
- It was found that the current level of knowledge of theoretical physics is not sufficient for reasonably precise prediction of the size and time dependency of the 'differential' gravity field of the Sun on the Earth's surface. The time dependency of its magnitude is currently unpredictable. It could be similar to pseudorandom time dependence with very significant influence of Jupiter and Saturn (due to theirs dominant influence to the Solar system's centre of gravity).

Those conclusions create the conditions for the decision to try to do measurements of real long-term dependency of the gravity field on the Earth's surface (see Chapter 5).

3.5. Thermoelastic strain

It has been observed for quite a long time that variations in the surface temperature of the Earth produce thermoelastic effects in the rock beneath (Berger 1975). While a part of the effect is relevant to the surface only (Harrison & Herbst 1977), another part penetrates deeper into the rock. As models show, this happens even if the rock is covered by a layer of loose material (Ben-Zion & Leary 1986) and the results are supported by measurements in the field (Berger & Wyatt 1973, Ben-Zion & Leary 1986, Hvoždara & Brimich 1988, Prawirodirdjo et al. 2006, Kalenda 2010). While mostly viewed as a source of unwanted noise in the measurement of

thermoelastic strain and tilt measurements, to be subtracted in the analysis of other effects, the role of these thermoelastic effects remains still to be fully appreciated as a source and a trigger factor to large scale events, in particular earthquakes. The involved sources may seem small at first but their consistent consequences accumulated over time and their ability to send a system already close to the breaking point over the edge may easily be underestimated (see Chapter 9).

In this section we will collect the essential facts of thermoelasticity in the relevant, linear regime to fix the notation, then, as a first step of a model building effort, we will review and discuss the model of J. Berger (Berger 1975) refined in (Ben-Zion & Leary 1986), and in the last section, the alternative approach of M. Hvoždara and L. Brimich (Hvoždara & Brimich 1988). The results are summarized in the conclusion.

3.5.1. Thermoelasticity

The basic notions of elasticity theory are the description of stress in a solid through the stress tensor and the deformation of the solid through the strain tensor (further details concerning this section may be found, e.g., in (Landau & Lifschitz 1983)). The stress tensor σ_{ij} is a symmetric tensor describing the force per area $\sigma_{ij}n_i$ in a plane with unit normal vector n_i (Einstein summation is assumed for repeated indices). The strain tensor u_{ij} is the leading term in the expansion of distance change between points of the solid due to deformations. If $u_i(x)$ is the displacement vector in point x of the initial position of a point in the solid, then the strain tensor is given as

$$u_{ij} = \frac{1}{2}\left(\frac{\partial u_i}{\partial x_j} + \frac{\partial u_j}{\partial x_i} + \frac{\partial u_k}{\partial x_i}\frac{\partial u_k}{\partial x_j} \right) \quad , \qquad (3.28)$$

where the last term may be ignored due to small relative deformations involved in the situations considered. As an aside, it may be noted that in this approximation, it is possible to decompose uniquely any relative displacement $\frac{\partial u_i}{\partial x_j}$ into strain u_{ij} and a local infinitesimal rotation ω_{ij}:

$$\frac{\partial u_i}{\partial x_j} = u_{ij} + \omega_{ij}\,, \tag{3.29}$$

where

$$\omega_{ij} = \frac{1}{2}\left(\frac{\partial u_i}{\partial x_j} - \frac{\partial u_j}{\partial x_i}\right). \tag{3.30}$$

In the absence of other than contact forces, the total volume force density can be given through the stress tensor as $\frac{\partial \sigma_{ij}}{\partial x_j}$ which leads to the equilibrium condition

$$\frac{\partial \sigma_{ij}}{\partial x_j} = 0\ . \tag{3.31}$$

As all our considerations will be restricted to the linear approximation, this equation will be sufficient as other constant forces, in particular gravity, can be understood as being cancelled out by some base level stress, while σ_{ij} denotes the departure from this base level stress.

The relationship between strain and stress can be obtained in line with general thermodynamic principles from the free energy *F*:

$$\sigma_{ij} = \frac{\partial F}{\partial u_{ij}} \tag{3.32}$$

Under the assumption of the isotropy of the material, the expansion of *F* up to second order in terms of the first order variables of strain u_{ij} and temperature fluctuation $T\text{-}T_0$ can be easily obtained through general symmetry arguments:

$$F = F_0 - K\alpha(T - T_0)u_{ii} + \frac{\lambda}{2}(u_{ii})^2 + \mu u_{ij}u_{ij} + \text{higher order terms} \tag{3.33}$$

The absence of first order terms is enforced by the assumption of equilibrium at vanishing first order variables of the expansion. The second order terms are the only ones that can be formed without violating isotropy (symmetry under rotations). The constants λ, μ of the solid material are known as Lame coefficients. The split of the constant of the first term into the product of constants K, α is a physically motivated convention.

Restricting to the second order in the expansion of *F*, we obtain from (3.32) Hook's law:

$$\sigma_{ij} = -K\alpha(T - T_0)\delta_{ij} + \lambda u_{kk}\delta_{ij} + 2\mu u_{ij} \tag{3.34}$$

In these considered cases, increases in temperature resulting from mechanical work are negligible (see Landau & Lifschitz 1983 for a detailed discussion) and therefore the temperature field *T* can be considered as being a parameter and solved independently from the heat equation:

$$\frac{\partial T}{\partial t} = \kappa \nabla^2 T \tag{3.35}$$

The heat equation (3.35), Hook's law (3.34) and the equilibrium condition (3.31) together with the definition of the strain tensor (3.28) give, together with the appropriate boundary conditions, a complete description of thermoelasticity and allow us to, at least in principle, find a solution for the displacement vector field u_i. They form the general framework of the models discussed below.

These basic equations, can however, manifest themselves in different forms due to a number of common reparametrizations of the constants and due to algebraic rearrangements. In order to make it easier to compare different sources, we round off the general discussion with a collection of often-encountered definitions and relationships.

The compression module *K*, already encountered in (3.33), is given by

$$K = \lambda + \frac{2}{3}\mu \tag{3.36}$$

The Young module *E* and the Poisson number σ are given by the compression module *K* and the torsion module μ as

$$E = \frac{9K\mu}{3K + \mu} \qquad \sigma = \frac{1}{2}\frac{3K - 2\mu}{3K + 2\mu} \tag{3.37}$$

with the inverse relationships

$$\mu = \frac{E}{2(1+\sigma)} \qquad K = \frac{E}{3(1-2\sigma)} \tag{3.38}$$

Hook's law (3.34) becomes then

$$\sigma_{ij} = -K\alpha(T - T_0)\delta_{ij} + \frac{E}{1+\sigma}\left(u_{ij} + \frac{\sigma}{1-2\sigma}u_{kk}\delta_{ij}\right) \tag{3.39}$$

or, after an algebraic rearrangement,

$$u_{ij} = -\beta(T - T_0)\delta_{ij} + \frac{1}{E}\left[(1+\sigma)\sigma_{ij} - \sigma\sigma_{kk}\delta_{ij}\right] \tag{3.40}$$

with

$$\beta = \frac{\alpha}{3}\frac{1+\sigma}{1-2\sigma} \quad . \tag{3.41}$$

3.5.2. Berger's model

Berger's model considers a half-space of elastic material with horizontal coordinates *x,z* vertical coordinate (depth) *y* and with a surface temperature given by a harmonic wave with amplitude τ_0, angular frequency ω and wave number *k*:

$$T = \tau_0 e^{i(\omega t + kx)} \tag{3.42}$$

It is further assumed that only plane strain exists, i.e., any quantity is symmetric with respect to translation and reflection of the horizontal *z*-axis. In particular, $u_z = 0$ and

$$u_{zz} = 0 \tag{3.43}$$

Note also, that (3.42) respects this symmetry. From (3.43) we have

$$\sigma_{zz} = \sigma(\sigma_{xx} + \sigma_{yy}) - E\beta T \quad , \tag{3.44}$$

which cannot be zero. So, while there is no dependence of any variable on *z* and only differential equations in spatial coordinates *(x,y)* and time *t* need to be solved, the presence of the third spatial dimension has consequences for the solutions.

The first step is to solve the heat equation (3.35) with boundary condition (3.42). This gives

$$T = \tau_0 e^{-\gamma y} e^{i(\omega t + kx)}, \quad \gamma = k\sqrt{1 + \frac{i\omega}{\kappa k^2}} \quad , \quad \text{with } \mathrm{Re}\,\gamma > 0\,. \tag{3.43}$$

The second step is to solve the equilibrium condition (3.31). That becomes in our case of plane strain:

$$\frac{\partial \sigma_{xx}}{\partial x} + \frac{\partial \sigma_{xy}}{\partial y} = 0 \tag{3.44}$$

$$\frac{\partial \sigma_{yx}}{\partial x} + \frac{\partial \sigma_{yy}}{\partial y} = 0 \tag{3.45}$$

These can be understood as integrability conditions for vectors σ_{xi} and σ_{yi} giving as their general solutions potentials *P,Q* such that:

$$\sigma_{xx} = \frac{\partial P}{\partial x} \quad , \qquad \sigma_{xy} = \frac{\partial P}{\partial y} \quad , \tag{3.46}$$

$$\sigma_{yx} = \frac{\partial Q}{\partial x} \quad , \qquad \sigma_{yy} = \frac{\partial Q}{\partial y} \quad , \tag{3.47}$$

but since in addition $\sigma_{xy} = \sigma_{yx}$, we have additionaly

$$\frac{\partial P}{\partial y} + \frac{\partial Q}{\partial x} = 0 \qquad\qquad , \tag{3.48}$$

which can be, in turn, understood as an integrability condition for the vector *(P,Q)* with potential ψ as the general solution

$$P = \frac{\partial \psi}{\partial x} \quad , \qquad Q = -\frac{\partial \psi}{\partial y} \quad , \tag{3.49}$$

Thus we have

$$\sigma_{xx} = \frac{\partial^2 \psi}{\partial y^2} \qquad \sigma_{yy} = \frac{\partial^2 \psi}{\partial x^2} \qquad \sigma_{xy} = \frac{\partial^2 \psi}{\partial y \partial x} \tag{3.50}$$

Hook's law permits us to calculate strains u_{xx}, u_{xy} and u_{yy} from the obtained stress tensor. But they are also subject to an integrability condition following from their definition through the two components of displacement according to (3.28). This gives a further condition on ψ :

$$\nabla^4 \psi + \frac{E\beta}{1-\sigma} \nabla^2 T = 0 \tag{3.51}$$

The boundary conditions required in (Berger 1975) are

$\sigma_{yy} = \sigma_{xy} = 0$ for $y = 0$, i.e., at the surface, (3.52)

$\sigma_{ii} = 0$ for $y \longrightarrow \infty$ (3.53)

and the resulting expressions for strain are found in (Berger 1975) to be

$$u_{xx} = \left(\frac{1+\sigma}{1-\sigma}\right)\left(\frac{k}{\gamma+k}\right)\beta\tau_0 e^{i(\omega t+kx)}\left\{\left[2(1-\sigma)+\frac{k}{\gamma-k}-ky\right]e^{-ky}-\frac{k}{\gamma-k}e^{-\gamma y}\right\} \tag{3.54}$$

$$u_{yy} = \left(\frac{1+\sigma}{1-\sigma}\right)\left(\frac{k}{\gamma+k}\right)\beta\tau_0 e^{i(\omega t+kx)}\left\{\left[-2\sigma-\frac{k}{\gamma-k}+ky\right]e^{-ky}-\frac{\gamma^2}{k(\gamma-k)}e^{-\gamma y}\right\} \tag{3.55}$$

$$u_{xy} = \left(\frac{1+\sigma}{1-\sigma}\right)\left(\frac{k}{\gamma+k}\right)\beta\tau_0 e^{i(\omega t+kx)}\left\{\left[\frac{\gamma}{\gamma-k}-ky\right]e^{-ky}-\frac{\gamma}{\gamma-k}e^{-\gamma y}\right\} \tag{3.56}$$

For realistic values, the real part of γ^2 can be ignored and γ approximated by

$$\gamma \approx (1+i)\sqrt{\frac{\omega}{2\kappa}} \tag{3.57}$$

and moreover

$$\frac{k}{\gamma} << 1 \tag{3.58}$$

The latter makes terms containing $e^{-\gamma y}$ negligible compared to terms containing e^{-ky} for greater depths *y* and we can approximate then:

$$u_{xx} = \left(\frac{1+\sigma}{1-\sigma}\right)\frac{k}{\gamma}\beta\tau_0 e^{i(\omega t+kx)}e^{-ky}\left[2(1-\sigma)-ky\right] \tag{3.59}$$

$$u_{yy} = \left(\frac{1+\sigma}{1-\sigma}\right)\frac{k}{\gamma}\beta\tau_0 e^{i(\omega t+kx)}e^{-ky}\left[-2\sigma+ky\right] \tag{3.60}$$

$$u_{xy} = \left(\frac{1+\sigma}{1-\sigma}\right)\frac{k}{\gamma}\beta\tau_0 e^{i(\omega t+kx)}e^{-ky}\left[1-ky\right] \tag{3.61}$$

Since the key factor in these expressions governing the penetration depths of the considered effects is e^{-ky}, we may conclude that the effects of surface temperature variations are comparable with the wavelength of variations on the surface.

3.5.3. The model of Hvoždara and Brimich

While J.Berger simplified the full 3-dimensional model by imposing plane strain, the model of M. Hvoždara and L. Brimich makes the more radical assumption of line strain and independence on horizontal directions.

Denoting again the vertical coordinate in half-space measuring depth by *y*, the conditions may be expressed as

$$u_x = u_z = 0, \qquad u_y = u_y(y,t), \qquad T = T(y,t) \tag{3.62}$$

The only non-zero component of the strain tensor is the u_{yy}. The model of Berger can be further simplified by the additional requirements of Hvoždara and Brimich. While this model is an interesting modification, the calculations in (Hvoždara & Brimich 1988) are not entirely correct. On page 130 of their work, they use the constant in the determination of integration from the free boundary conditions on the surface. Hook's law (3.34) without the term corrected for temperature variations is valid in elasticity but not in thermoelasticity. The consequence is a non-vanishing of stress at infinity and other spurious effects contradicting Berger's results and physical intuition (like infinite displacement at infinity).

3.5.4. Conclusion

Berger's model and the discussions and refinements following it show that while diurnal and annual temperature variations on the Earth's surface penetrate to a depth, at most several meters, forces associated with those surface layer thermal variations have an impact on stress and strain at considerable depths. And they could, therefore, be important to earthquake triggering processes (see Chapter 9). The influence of these processes is moderated, but not removed by the presence of a layer of loose material on top of the rock forming the bulk of the Earth's crust, as discussed in (Ben-Zion & Leary 1986). More detailed future models are needed to assess the full consequences of surface temperature induced thermoelasticity.

3.6. Numerical model of thermoelastic strain

As a first step, the numerical model of thermoelastic strain was evaluated. We used the measured curves of temperature development in

various latitudes with steps of 10 degrees during the whole year. As an example the temperature development in Helsinki in January and July is on the Fig. 3.6 a,b.

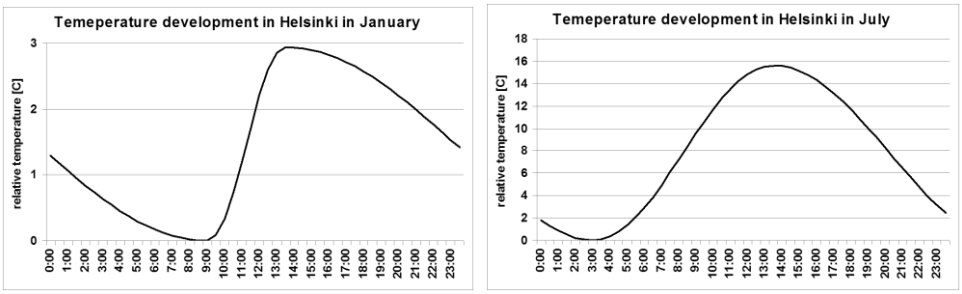

Fig. 3.6: Relative temperature development in Helsinki in January and in July.

The temperature profile in continental rocks according to the relationship (3.43) was calculated in one-day steps in a one-year cycle for each latitude. The same temperature profile was calculated in 30-minute steps in any one-day cycle. Both cycles were superpimposed and the relative temperature development was calculated in 30-minute steps during one year. Then the relative strains ε_{xx}, ε_{yy} and ε_{zz} (3.44) in the far field can be evaluated as integral to temperature profile multiplied by linear thermal expansion coefficient α (3.34). Because the attenuation of thermal wave with the depth is high, the far field should be in the order of one kilometer outside the expanded block. So we are able to evaluate the relative strains of each block and to evaluate the principal component of stress tensor. This depends mainly on the geometry and geographical position of continents.

The maximum and minimum strain in diurnal period was evaluated and the annual strain development was calculated for the points on the border of continents. Japan (140.625E, 50N) and Italy (16.47E, 40N) were chosen as examples (see Fig. 3.7a, b). The principal component of relative strain changes its direction in time in both cases. At the end of March the direction is towards the continent. It is the result of the contraction of the Eurasian lithosphere plate after winter. In the case of Italy, it is in the direction of NE and, in the case of Japan, it is in the direction of NW. The opposite direction can be seen in September. This is the result of the expansion of the Eurasian lithosphere plate after summer.

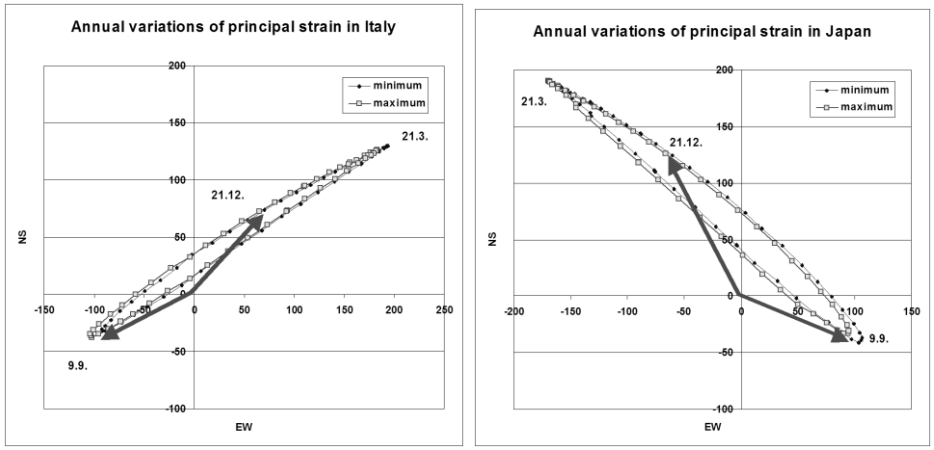

Fig. 3.7: Annual variations of principal strain in Italy and Japan.

The result of annual variation of strain is in accordance with measurements of tilt in Grotta Gigante (Braitenberg et al. 2006), which show the turning points in March (NE) and November (SW) and with the relative motion of Italy in NNR-NUVEL-1 model, measured by the GPS stations (DeMets et al. 1990, Braitenberg et al. 2001). The direction of principal strain component in Japan is in accordance with slip direction of the Phillipine or the Pacific plates against the Japanese arc (Hirose & Obara 2005).

This very important conclusion was arrived at by the evaluation of direction and relative amplitude of diurnal variations of strain between minimal and maximal strains, i.e. during the first part of the day when the Sun is rising (see Fig. 3.8a, b).

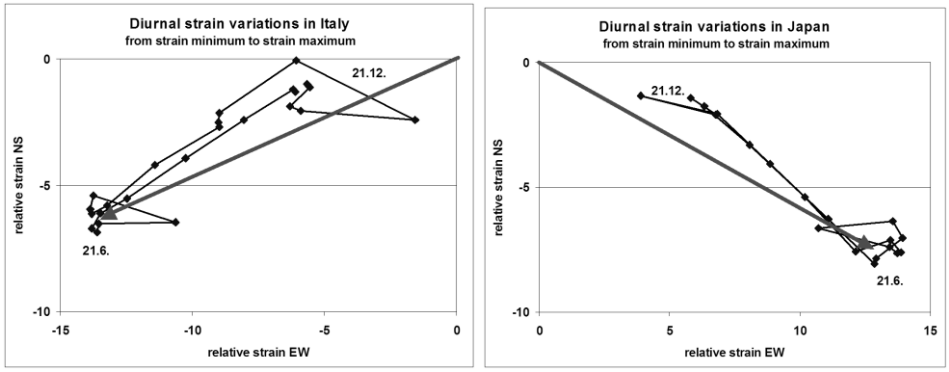

Fig. 3.8: Diurnal relative strain variations in Italy and Japan.

Both curves of diurnal strain variations show their minimum of their lengths in winter and maximum in summer, but both show southern orientation (SE for Italy, SW for Japan), which is directly opposite to the relative motion in NNR-NUVEL-1 model (DeMets et al. 1990).

The result is that the annual variations of strain due to thermal expansion and annual thermoelastic wave transfer manage the direction of the principal stress component. On the other hand, the diurnal variations of strain manage the movement of lithosphere plates.

4. EXPERIMENTS WITH SEISMICITY AND TESTS OF EFFECTS

The aim of this chapter is to analyse what important roles exogenous forces can play as triggers of earthquakes and to test their influence. In the first experiment (chapter 4.1) we will analyse the seismic response to the external stimuli on two groups of seismic events – dependent and independent (or non-random and random), which were divided by methodology of Per Bak et al. (2002). In subsequent chapters we will discuss the seismic events triggered by tides around the world (Chapter 4.2) as well as in the scale of area of mining (Chapter 4.3). The discovery of splitting of tidal periods (Chapter 4.4) led us to finding another triggering mechanism, generated by tides – variations of rotation of the Earth, i.e. changes of the Length Of the Day (LOD) parameter (Chapter 4.5). The non-linearity of seismic response on the tides will be discussed in the next Chapter 4.6. This non-linearity becomes the basis of one of prediction method of earthquakes – Load Unload Response Ratio (LURR) (Yin et al. 2002, Zhang et al. 2004).

We will find in the Chapter 4.7 that in addition to the tidal triggering mechanism there are other mechanisms, mostly with diurnal periods, that can trigger earthquakes even more strongly than tides. The long-time climate cycles correlate well with global seismicity (Chapter 4.8). Other less important exogenous stimuli can trigger earthquakes. They would include atmosphere pressure variations, precipitations, snow cover and floods (Chapter 4.9).

4.1. Random and non-random seismic events and their response to the external forces in the Palm Spring area

Per Bak et al. (2002) showed that both members of a pair of seismic events could be described by three parameters – the magnitude of the smaller of the two, and their distance in space and time. When they discovered this, they showed that simple scaling law could describe all of the pairs of seismic events, which are slightly different for independent seismic events to the ones that are dependent on one another. This fact can be used for simple separation of both groups of seismic events. We tested

the seismic response of both groups on external triggering mechanisms and so we analysed the response of the whole system 'rock-mass – stress – earthquake' to external forces and its predictability.

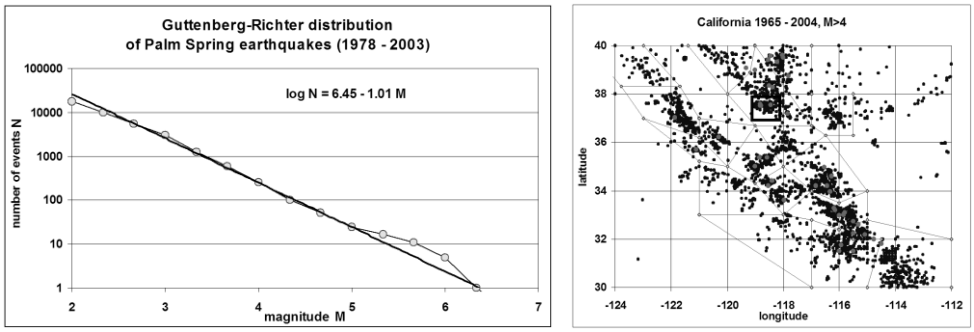

Fig. 4.1a,b: G-R distribution of Palm Springs area earthquakes 1978 – 2003 (ANCC 2005).

For a predictability test we used the data from ANSS Composite Catalogue (ANCC 2004) for the period 1980 – 2004 and a sub-catalogue from the Palm Springs area (37.2-37.9N;-118.2-119.2E) because the whole area is covered by a dense network of seismometers, which makes it possible to register and to localise all of seismic events with M≥2 (see Fig.4.1a). The area is separated from the other seismically active areas in the locality. The mechanisms of all seismic events could be similar and less dependent or more independent to other seismic events in the surrounding area. The events with m≥2 were used for the detailed analyses. This sub-catalogue contains 18228 seismic events (see Fig. 4.1a and 4.1b).

We implemented the methodology of Per Bak et al. (2002) on all subsequent pairs of seismic events by the inter-event time and the magnitude of the smaller of them. We did not use the third parameter – distance between events because the whole area under study is relatively small. Then we evaluated the frequency – inter-event time distributions for groups of seismic events within a magnitude range. The step of the magnitude range was 0.2 for magnitude between M=2 and M≥4 (see Fig. 4.2). All of distributions show that the nearly linear character from the side of smaller inter-event time is present and only the distributions of groups of bigger magnitudes are less smooth, because they include a smaller number of seismic events. All of distributions show the truncated character from the side of bigger inter-event time. They show their upper limit. The most

important is the fact that the inter-event time of transition point between linear and truncated part of all distributions of all magnitude range are nearly the same. This transition point, according to Per Bak et al., is the border between dependent (non-random) and independent (random) seismic events. These transition points are very visible if all of distributions are recalculated with respect to their linear part of distribution (see Fig. 4.3).

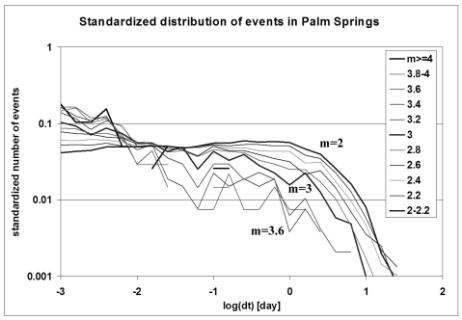

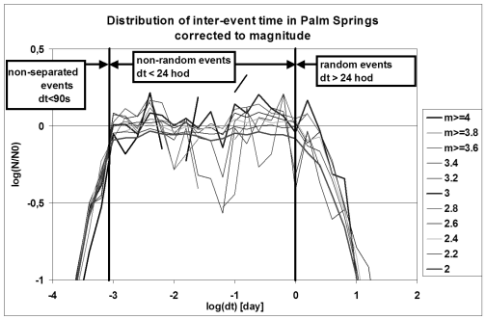

Fig. 4.2 and 4.3: Distribution of inter-event time depending on magnitude of smaller event

It can be stated that the distribution of inter-event time has three parts. In the first part there are the pairs of seismic events, which are inseparable, due to their small inter-event time less than 90 s (see Fig. 4.3). We suppose that if we could separate both events, the distribution would continue linearly to the smallest inter-event time up to infinity. In the second – linear part of distributions – there are present mainly non-random (dependent) seismic events. The number of random and non-random seismic events in the transition point between linear part and truncated part of the distribution is the same. In the truncated part of distribution there are present mainly random (independent) seismic events. We determined the transition point, i.e. its inter-event time, on the basis of deviation of distribution from linear part of more than 3σ. Surprisingly, the transition points of all distributions had nearly the same inter-event time, approximately of 24 hours. It can be stated than the events in Palm Spring area, which are separated by more than one day are mostly independent and *vice versa*. This does not mean that both groups contain only random on non-random events, but the minority is low. By this simple methodology we could separate all of the seismic events into groups of random and non-random events (see Fig. 4.4).

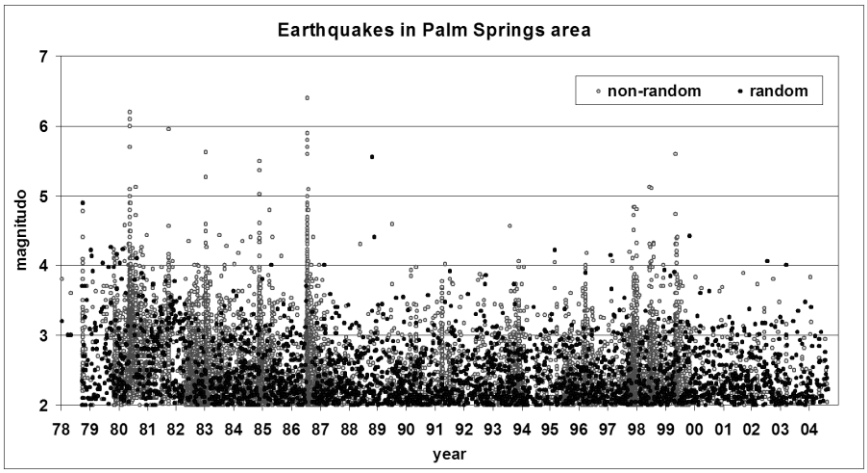

Fig. 4.4: Distribution of random and non-random earthquakes in time.

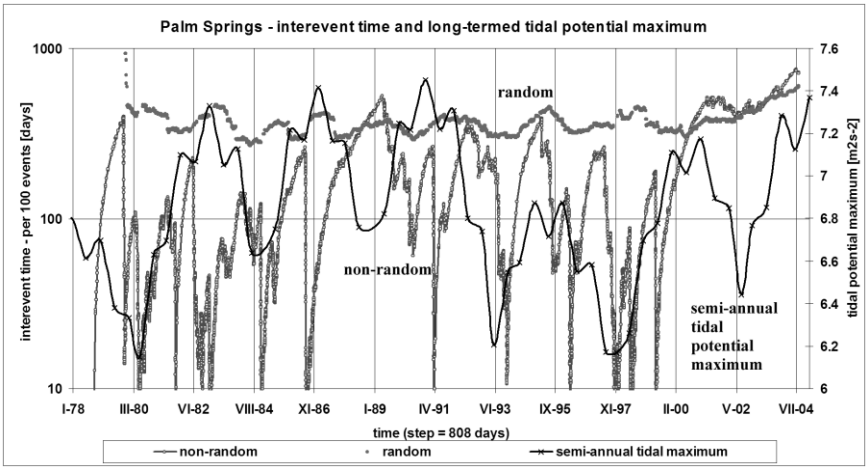

Fig. 4.5: Development of inter-event time in Palm Spring area in time.

The features of both groups of events are very interesting. The non-random events are mostly in the aftershock sequences of big earthquakes (see Fig.4.4). That was expected. On the other hand, the random seismic events are in aftershock sequences as well, for no apparent reason. The distribution of random seismic events in time is nearly constant (see Fig. 4.5), but it is evident that the number of random seismic events is less in the period of beginning of aftershock sequences. This can be the consequence of imperfect separation of both groups in time of anomalous high seismic activity. But the ratio between inter-event time during aftershock sequence

and before it is only 1.5 for random events and for non-random events is greater than 100. It is interesting that the period of approximately 808 days (4.425/2 years) dominates in the non-random activity (see Fig.4.5).

The number of dependent events, which is greater than the number of random events, even in the foreshock period, shows that the continual measurement of the state of the system is possible in the time before the mainshock. It was not surprising to us that some of the mainshocks were independent (random) earthquakes that were not preceded by foreshocks and also not followed by aftershocks (for example the event on October 19, 1988). Such events fulfilled the theoretical supposition about chaotic behaviour of seismicity (Turcotte 1992). It is the reason why not all of seismic events can be predicted.

We statistically tested the correlation between various tidal periods and seismicity using the Schuster's test (Tsuruoka et al., 1995; Tanaka et al., 2002a and 2002b). We started our analysis by moon perigee period (4.425 years). In the Schuster's test, each earthquake is represented by a unit length vector in the direction φ_i. Because the tidal stress period does not always equal 4.425-years, we transformed the time shifts to the phase angles φ_i by setting 0° to the maximum and 360° to the next maximum of 4.425-year tidal potential.

The vector sum D over N earthquakes

$$D^2 = \left(\sum_{i=1}^{N} \cos \varphi_i \right)^2 + \left(\sum_{i=1}^{N} \sin \varphi_i \right)^2 \qquad (4.1)$$

is then evaluated, which equals zero if φ_i angles are distributed randomly. The significance of level p to reject the null hypothesis that the earthquakes occur randomly regardless of the phase angle is given as

$$p = \exp(-D^2/N), \qquad (4.2)$$

which ranges between 0 and 1. The smaller probability p is, the higher is the confidence that the distribution of phase angles is not random.

Histograms of the number of earthquakes in the moon perigee period of both groups of random and non-random events can be seen on Figure 4.6 and 4.7 respectively. Non-random events show the high level of their dependence on this tidal cycle, but the period is divided into two sub-

periods with the length of cca 808 days=4.425/2 years. Both maxims are around the minimum and the maximum of tidal potential. So, the Schuster's test of the whole period is not suitable for such analysis. If we use the Schuster's test for only half-period (by doubling of frequency and than doubling of phase of each event) we obtain the result of conclusive dependence of seismicity on this tidal period on a much higher level than is necessary for confirming it on the statistically significant level 99.9%.

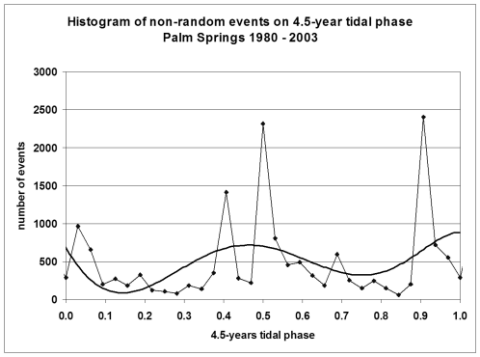

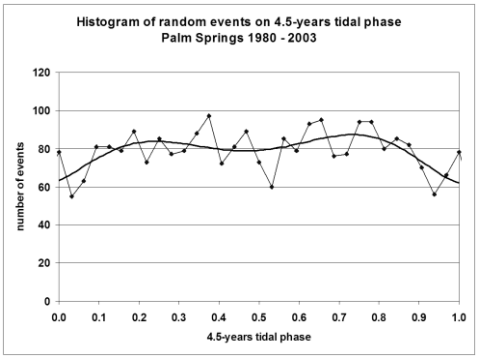

Fig. 4.6 and 4.7: Histogram of dependence of earthquakes on 4.425-years tidal phase.

Histogram of the number of random earthquakes shows that the ratio between extremes of numbers of events is only 3:2 and the minima of number of events corresponds with maxims of non-random events. There is the suspicion that a part of random events was included into the group of non-random events during the aftershock sequences. We can assess their number on the level of 2-3% of non-random events. Then, the histogram of random events during moon perigee period would be flat without significant dependence between seismicity and tidal potential.

The longer tidal period than 4.425 years up to 18.6 years, which is the lunar nodal period, was not tested on the data from Palm Springs area, although this period is visible (see Fig.4.5). We used the global data for such a test (see the next Chapter). Both long tidal period 4.425 and 18.6 years were found in data of North Atlantic Oscillations (NAO) (Berger 2008), so the triggering mechanism of earthquakes cannot be made by direct tidal influence, but indirectly by air pressure variations.

Semi-annual tidal period is dominant too and seismicity shows two maxims during its period (see Fig. 4.8). Unlike the period of 4.425 years, the first maximum of seismicity before tidal potential maximum and the second maximum are shifted of around $\pi/2$, i.e. in the time when the tidal potential influence is at its minimum. The ratio between extremes of number of events is 7:1 and the Schuster's test of non-random events for periods of a quarter of a year or semi-annual periods is far from the statistically significant limit 99.9%. Random events do not show statistically significant dependence on semi-annual tides, because Schuster's test coefficient is p=0.37, which is greater than limit value 0.05 for the limit of the level of 95%. The minima of number of random events show the same phase as maxims of non-random events, which is similar to the situation as in the previous case. The splitting of tidal periods will be analysed in the Chapter 4.4.

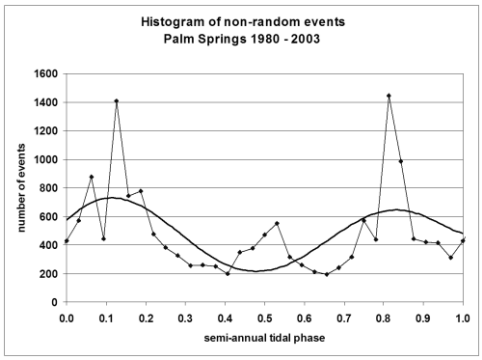

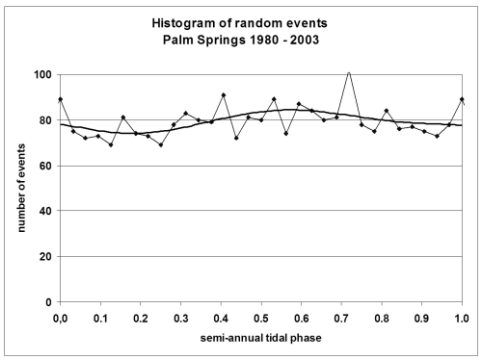

Fig. 4.8 and 4.9: Histogram of dependence of earthquakes on semi-annual tidal phase.

In addition to the diurnal tidal periods, we tested the dependence of seismicity on the non-tidal diurnal period (24:00). This period is present among tidal periods too, but its amplitude is very low in comparison with tidal wave P1 (24:07) (Melchior 1983, Tamura 1987). The histogram of non-random events has two maxims (see Fig.4.10). The first maximum is about 20:00 UT, which is around noon local time (LT). The subsequent maximum is around midnight of LT. The analyse shows that the main maximum is present in all of the groups of seismic events in all of magnitude ranges. The secondary maximum at midnight is present only in the groups of small seismic events. Then we explain the secondary

maximum by better observation conditions during night, when smaller events are registered, unlike during the day when antropogenous noise is higher. If we evaluate the Schuster's test of non-random seismic events for semidiurnal period, the *p* value is far from the statistically significant limit on the level 99.9% ($p<10^{-7}$). The random events do not show any dependence on the semidiurnal cycle (p=0.47) (see Fig. 4.11). More about the analysis of seismicity and its dependence on tidal cycles is described in Kalenda et al. (2006).

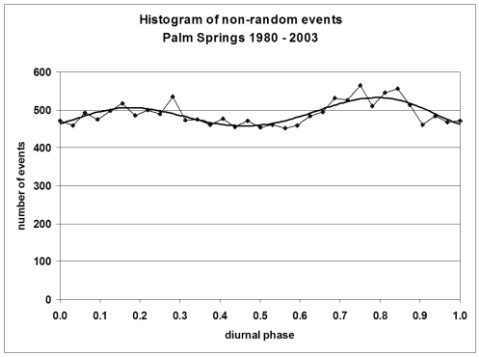

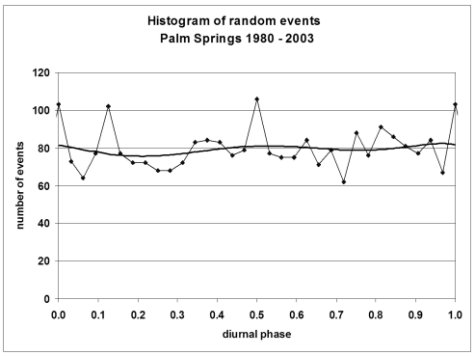

Fig. 4.10 and 4.11: Histogram of dependence of earthquakes on phase of the day (UTC).

All of the seismic events can be divided into two groups – dependent (non-random) and independent (random) events on the basis on their magnitude-space-time distance according to methodology by Per Bak et al. (2002). The group of non-random events shows the statistically significant dependence on external forces like long-period tides and non-tidal diurnal period. It is wrong to assume that all of seismic events are random in time and space and the system 'rock mass – stress – earthquake' is a chaotic system. The opposite is true. We found that the main part of seismic events in Palm Spring area was created by non-random seismic events and such events tell us about the state of the whole system by its response to external forces. The earthquakes are predictable because we are able to measure the response of the system to the external forces and we are able to find the period when the system is approaching a critical state. On the other hand, because the group of random seismic events exists, we will never be able to predict all earthquakes.

4.2. Tidal global experiment

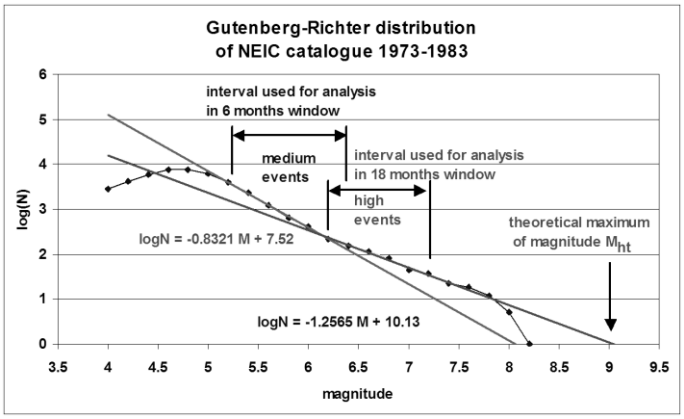

Fig. 4.12: Gutenberg-Richter distribution of all events in NEIC catalogue 1973-1983.

This experiment pertains to the longest tidal periods. Its goal is to determine what influence small amplitude variations of the tidal periods during 18.6-years (moon nodal period) and 4.425-years long (moon perigee period) periods have on global seismicity.

We used, as a comparable basis for global seismicity, the tidal potential that was calculated for Parkfield (USA) for typical foci depths (φ = 36.0° N, λ = 120.5° W, depth = 8 km) with the help of our programs (Skalský 1991) using Tamura's development of tidal potential into 1200 tidal waves (Tamura 1987) and mostly used the Wahr-Dehant-Zschau tidal model of the Earth (Wahr 1981, Dehant 1987, Zschau & Wang 1987). The long-term course of semi-annual maximums of tidal potential for other locations around the world has nearly the same phase (excepting poles) and only different magnitudes.

We determined diurnal maximums of tidal potential and further semi-annual maximums, which represent the whole semi-annual tidal cycle from April 1 to September 30 and from October 1 to March 31. These maximal values (envelopes of maximums) have their quasi-periodical character with medium periodicity about 4.425 years and long periodicity of about 18.6 years (see Fig. 4.13).

Because we don't want to analyse the tidal cycles shorter than half-year, we can say that this envelope of semi-annual maximums of tidal potential,

calculated for one specific place (Parkfield), is a representative of all tidal maximums envelopes at all points on the Earth including the poles.

We used the global data from NEIC catalogue (NEIC 2004) for the years 1973 – 2004 and we analysed medium and high (strong) earthquakes separately, because their Gutenberg-Richter (G-R) distribution according to the relationship

$$\log N = \mathbf{a} - \mathbf{b}\, M \qquad (4.3)$$

were different (see Fig. 4.12). We analysed **a** and **b** parameters of G-R distribution in 6-month time windows for medium events ($\mathbf{a_m}$; $\mathbf{b_m}$) and in 18-month time windows for strong events ($\mathbf{a_h}$; $\mathbf{b_h}$). We calculated theoretical magnitude maximums ($\mathbf{M_{mt}}$; $\mathbf{M_{ht}}$) (see Fig. 4.12) as a crossing point of G-R distribution on the level of 1 event according to formula

$$\mathbf{M_{ht}} = \mathbf{a_h} / - \mathbf{b_h} \qquad (4.4)$$

First of all we analysed the dependence of the number of seismic events in semi-annual windows (see Fig. 4.13). The number of medium events $\mathbf{N_m}$ correlates positively with 18.6-year tides. But, the correlation is not statistically significant (r=0.2). Their correlation with 4.425-year tidal period is not significant at all. On the other hand, the numbers of high events show weak negative correlation with the 4.425-years tidal period. The result is that the tides decrease the friction on the faults from static friction during low tides to quasidynamic during high tides. This is in accordance with tests on rock samples (Sobolev & Ponomarev 1996, Lockner & Beeler 1999).

When we look on the development of coefficients of G-R distribution in time, it can be stated that both coefficients **a** and **b** weakly correlate with tides. The correlation of seismicity is better in the 18.6-year long period than in the 4.425-year long period (see Figs. 4.14 and 4.15). The correlation coefficient r=0.38 is for high events and parameter **a** and r=0.4 is for parameter **b**. For medium events the correlation

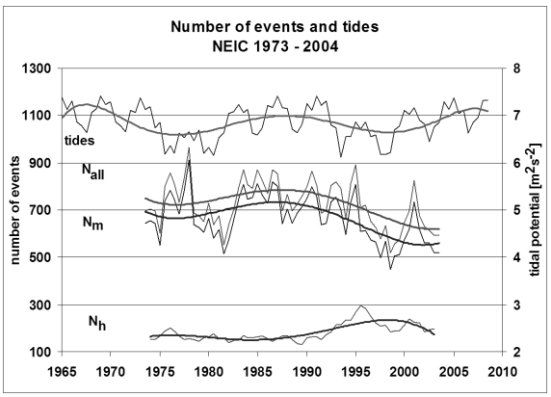

Fig. 4.13: Variation of number of EQs in 6-months time window and tidal amplitude.

coefficient r is around 0.2 for both G-R coefficients. The high value of coefficient **a** during the period of high tides shows the higher risk during this period because the seismic energy release is higher than during the period of low tides. On the other hand, the average energy of one seismic event is less than average. The low values of coefficient **b** during the low tides period (around 0.8) shows that the seismic risk is higher during this period, because the rock mass becomes stronger and the friction on the faults becomes higher. This fact is well documented on the development of theoretical maximum of magnitude, especially for high events ($\mathbf{M_h}$), which is on its maximum during this period of 18.6-year cycle (see Fig. 4.16). The shorter tidal cycle with the period of 4.425-years is also visible on the development of theoretical maximum magnitude $\mathbf{M_h}$ and its correlation coefficient r= -0.46. These results are similar to the results of Kilston & Knopoff (1983), who analysed the seismicity of California between the latitudes of 33 degrees and 36 degrees north and showed that the seismicity correlates significantly with semidiurnal, lunar fortnightly and 18.6-yr periods.

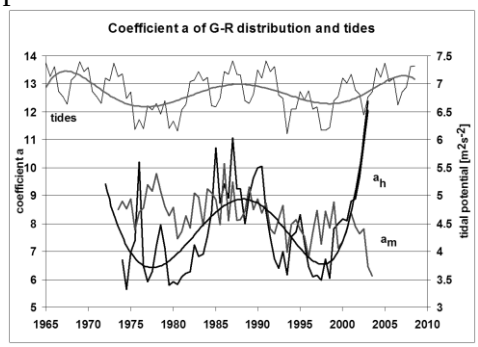

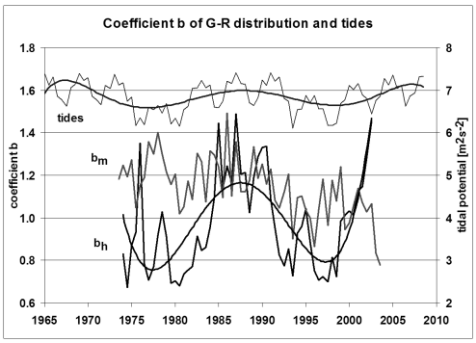

Fig. 4.14 and 4.15: Coefficients **a** and **b** of G-R distribution in time and development of tidal potential.

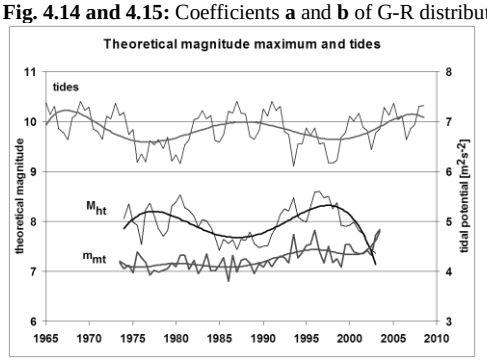

Fig. 4.16: Development of theoretical magnitude maximum and tidal potential.

Small coefficients of correlation of global seismicity and tidal potential showed that the tides are not the only triggering mechanism. Tides and other mechanisms make the conditions for energy accumulation and release.

4.3. Tidal experiment in coal mines

The mining operations were conducted in the most rockburst prone areas of coalfaces No.14736 and 14732 in the collieries in Ostrava-Karviná mine District (OKD) during the years 1995-2001. Because most of seismic events and rockbusts are released by mining operations, it does not make any sense to look for the dependence of numbers of seismic events or energy on tides. However tides can also trigger seismic events as can be deduced from examining Figs. 4.17 and 4.18. Most of the strongest seismic events, which were localised into the roofs of mining coalfaces, were observed during the rising part of semi-annual tidal cycle, however it could be connected with the organisation of mining operations, with small coal production during summer holidays and at the beginning of the year.

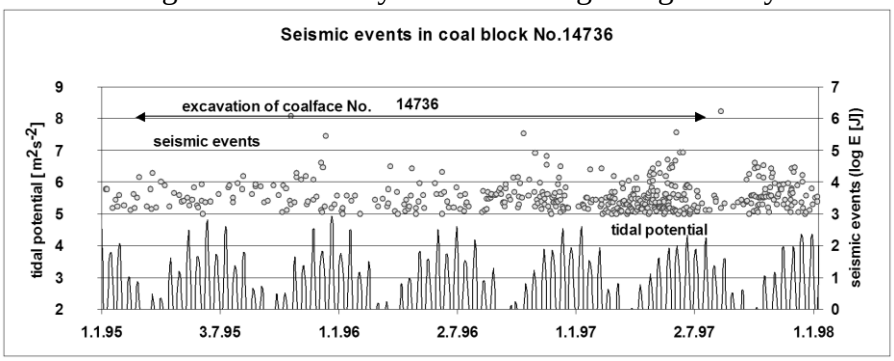

Fig. 4.17: Seismic events in coal block No. 14736 and maximum amplitude of tidal potential.

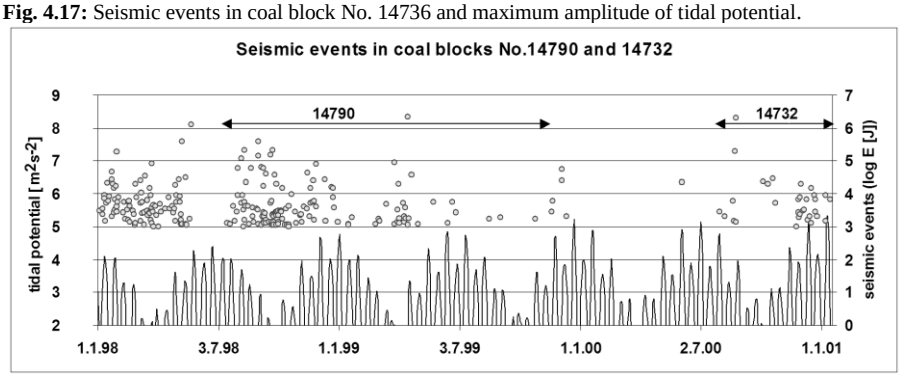

Fig. 4.18: Seismic events in coal block No 14736 and maximum amplitude of tidal potential.

That is why we used the coefficient **b** of G-R distribution (relation 4.3) for the analysis of possible tidal influence on seismicity in coalfaces. This coefficient should depend on the stress state of the massif surrounding the coalface and not on the volume of mined-out coal. We evaluated the coefficient **b** of G-R distribution on the basis of seismological data of seismic events registered in the working area. We used the seismic events in energy classes of 0.3 orders in the range between 30J and 680J. We evaluated the coefficient **b** according to method by Aki-Utsu (Aki 1965, Utsu 1965) in 7-day windows.

The development of coefficient **b** in time (see Fig. 4.19) shows that the coefficient **b** was low and almost independent from tides in the period from November 28 to December 26, 2000, when the major seismic events were observed at the coalface. At that time, intensive mining was dominated in the stress state of the coalface. On the other hand, the coefficient **b** was negative correlation with tides in the period from February 1 to April 1, 2001, when the mining was not so intensive and stronger seismic events with energy greater than 10^4 J were not observed, except blasting. More analysis is in the paper Kalenda & Skalský (2002).

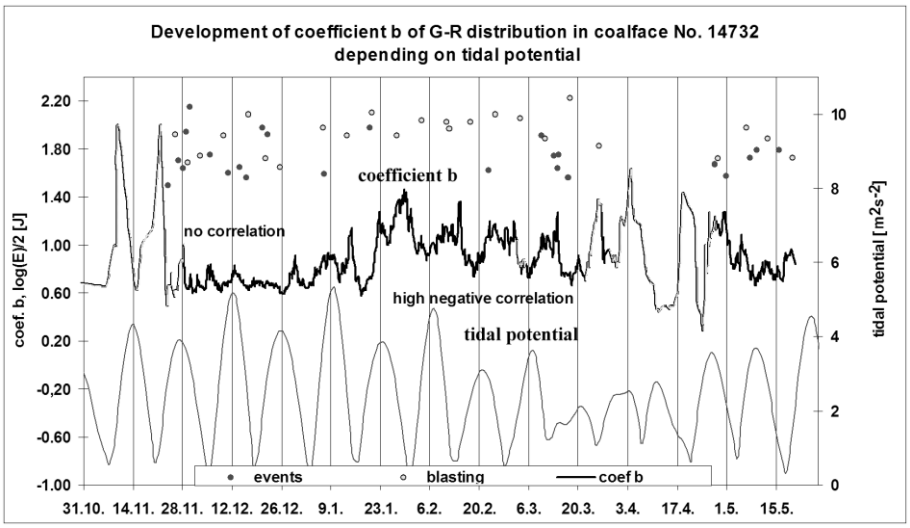

Fig. 4.19: Development of coefficient **b** of G-R distribution in coalface No. 14732.

The analysis of induced seismicity in OKD showed that even in mining conditions, when the seismicity is mostly depending on mining operations, it is possible to monitor the stress state of the rock mass. The tidal influence is, however, subsidiary. And during intensive mining operations it is negligible.

4.4. Splitting of tidal periods

This experiment concerns the doubling (splitting) of the tidal periods, which was discovered in all of the California data and also the data from Palm Springs area (see Chapter 4.1). The reason for that behaviour will be discussed.

We used the same Composite Catalogue of California (ANCC 2004) as in Chapter 4.1 for this analysis in the period from 1/1/1980 to 9/4/2004. This catalogue contains more than 300,000 events and contains all seismic events M≥2 (see Fig.4.20). For consequent analysis and verification of results from a complete catalogue we used the Palm Springs area sub-catalogue (37.2-37.9N;-118.2-119.2E) and events with M≥2 were used for the detailed analyses. The sub-catalogue contains 18,228 seismic events (see Fig. 4.20b).

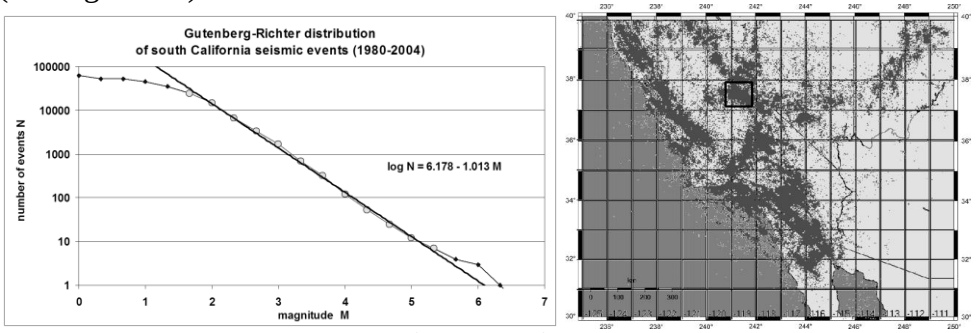

Fig. 4.20a - G-R distribution and **b**- map of southern California earthquakes 1980 – 2004 (ANCC 2005) with Palm Springs area (box).

We defined the tidal phase in the same manner as Tanaka (2002) or Cochran et al. (2004) (see chapter 4.1.). The tidal cycles began at the time of computed Earth tidal potential maximum in the centre of the analysed area. We computed Earth tidal potential for Parkfield (Skalský 1991). The zero phase of annual cycle began around the New Year and this cycle lasted approx. one year and its end was in the time of the next maximum of tidal

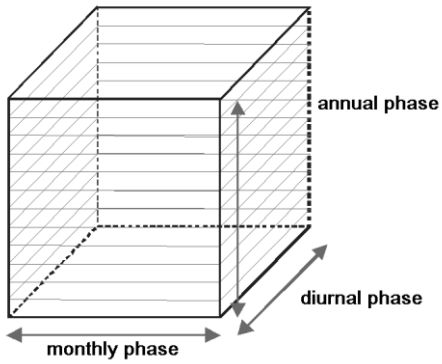

Fig. 4.21: Definition of the 3-D tidal phase space.

potential. The zero phase of semi-annual cycle began around New Year and in June-July. The fortnightly tidal cycle began in the same manner as semi-annual cycle in one of two maxims in the month and ends in the next maxim. Next, we defined the 3-D phase space (see Fig. 4.21).

Now, we are able to compare all of the phases of all tidal cycles in one chart (see Fig. 4.22 in the colour pages in Chapter 9).

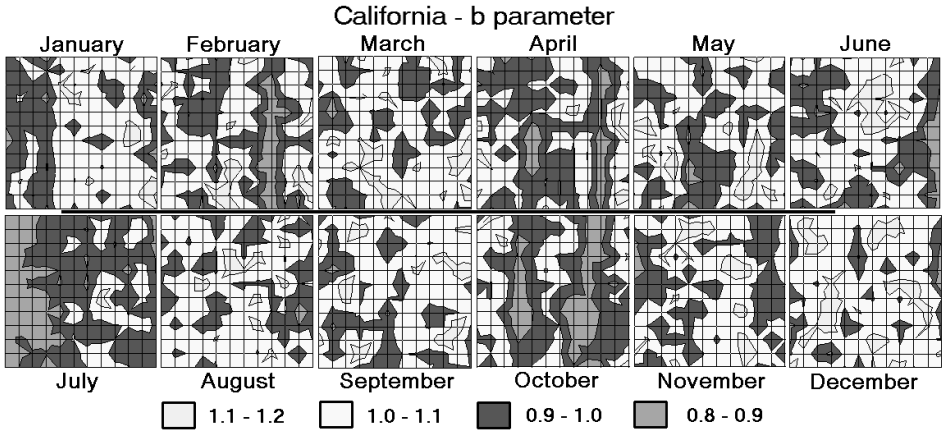

Fig. 4.22: Parameter **b** of G-R distribution of California earthquakes in 3-D phase space (see colour pages too).

The results show, in agreement with the theory, two maxims of seismic events and contemporary two minims of coefficient **b** of G-R distribution at the beginning of the year (December – January) and in the middle of the year (June – July), i.e. in the periods of high tides, when the tidal variations reach their maximum and when Coulomb criterion (CFS) according to relationship (4.5) is the highest. The values of CFS is about 10^4 Pa (Hartzell & Heaton 1989).

$$CFS = \tau_{slip} + f\,\sigma_n \quad , \qquad (4.5)$$

where the shear stress τ_{slip} is evaluated in the slip direction and σ_n is the normal stress in extension and f is the friction coefficient.

Contrary to theoretical suppositions, two minimums of coefficient **b** were observed in April and October (partly in February), i.e. in the period of low tides. The same result was observed from a point of view of monthly periods. One dominant minimum of coefficient **b** and one subsidiary minimum could be found in almost every month. The dominant minimum of coefficient **b** coincided at the beginning of the year with tidal potential maximum. However, in the first and third quarters of the year, the minimum of coefficient **b** coincided with the tidal potential minimum. Such high seismic activity and high seismic risk could not be triggered by tides fulfilling the Coulomb criterion (4.5), but rather by another triggering mechanism, which could be tied with tides. Consequently, some triggering mechanism other than tides must exist.

If we look at the picture 4.24, we will find that the minimums of the Length Of the Day (LOD) parameter (i.e. maximum of rotation of the Earth) is around the low tide periods. That is why the maximum of seismic risk is in April and October and in the low-tide periods, when the Earth rotation is at its maximum. The layers of the Earth are shear strained and layering occurs because the upper layers have greater momentum of inertia. They want to stay on their previous velocity and relatively they want to move to the west with respect to lower layers, which want to rotate rapidly to the east. In other words, the changes of Earth rotation, which are consequence of deformation of the Earth due to tides (see Chapter 3.2), is the second triggering mechanism of earthquakes. Because LOD mechanism is complementary with tides and its maximum of influence is in period of the minimum of the influence of tides, all of statistical tests, like Schuster's tests, for annual or diurnal periods can fail. Both mechanisms can be studied separately in the periods of low and high tides for various focal mechanisms of earthquakes.

Similar situations as the annual or monthly point of view are from the diurnal point of view. Such situations are shown, as best, as possible on the data in December, when four minimums and four maximums can be easily seen in the month-day phase space (see Fig. 4.22 in the colour pages in

Chapter 9). The interesting thing is the rule, which says: "If the minimums of coefficient **b** are in the month of tidal potential maximum (December, January, June, July) then the minimums of coefficient **b** are in the time of fortnightly tidal potential maximum". "If the minimums of coefficient **b** are in the month under study in the time of tidal potential minimum (March, April, September, October), the minimums of coefficient **b** are in the time of fortnightly tidal potential minimum and in the diurnal tidal potential minimum". All of tidal influences are joined by the same rule.

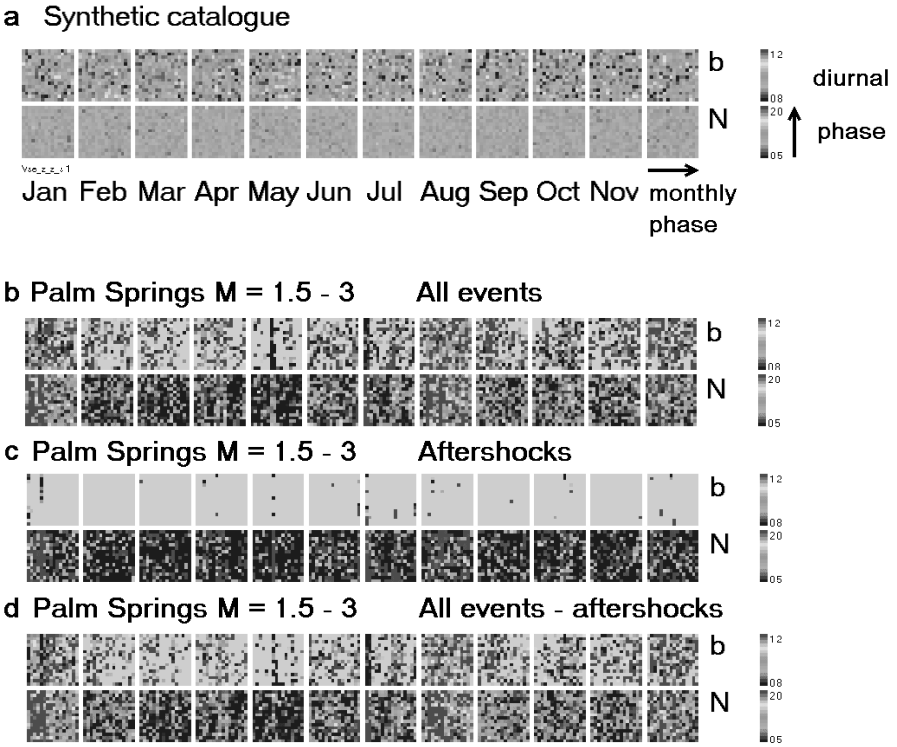

Fig. 4.23: Parameter b of G-R distribution of Palm Springs earthquakes in 3-D phase space. **a)** Synthetic catalogue, **b)** Palm Springs catalogue m = 1 – 3, in period 1980 – 2004 - all events, **c)** aftershocks, **d)** mainshocks. (see colour pages too).

The result, which was made on the whole catalogue from California, was verified on the sub-catalogue from Palm Springs area, which is separated from surrounding areas (see Chapter 4.1). The test of verification was made on the synthetic catalogue, where no dependence of seismicity on

annual, monthly and diurnal tides was observed in 3-D phase space (see Fig.4.23a in the colour pages in Chapter 9). On the other hand, the real catalogue shows the same features as the complete California catalogue. The maximum of number of events occur both in the high- and low-tide periods in all three-space coordinates. The correlation between the whole catalogue (see Fig. 4.23b in the colour pages in Chapter 9) or catalogue of mainshocks (see Fig. 4.23d in the colour pages in Chapter 9) on the tides is higher than the correlation between aftershocks and tides (see Fig. 4.23c in the colour pages in Chapter 9).

4.5. Length of the day (LOD)

The previous experiment showed that the tidal periods are split with one group of earthquakes being triggered during the maximum of Coulomb criterion (4.5) in accordance with the theoretical analysis of movement of the faults, and the second group triggered in the period of low tides, when Coulomb forces are at a minimum and cannot trigger the movements on the fault plane. There must be another triggering mechanism, which is shifted by about $\pi/2$ with the respect to the Coulomb criterion. Such a mechanism can be the rotation of the Earth, i.e. changes of LOD. The approximate relationship between tidal potential and LOD is visible on the Fig. 4.24.

We ran an experiment in the Central Italy, where a high number of normal faults and thrust occurs. The aim was to verify the influence of LOD on the seismicity. We used the earthquake data from the USGS Catalogue (USGS 2010) for the Central Apennines covering the area of coordinates 42°- 43°N and 12.7°- 13.5°E during the period 1974 – 2009. In addition to the 6th April 2009 (M = 6.3) earthquake, this area covers the earthquake Norcia 19th September 1979 (M = 5.9) and Colfiorito 26th September 1997 (M = 4.4) and 12th October 1997 (M = 5.3) covering the chosen rectangle. The most powerful earthquakes in 1979 (Norcia), 1997 (Colfiorito) and 2009 (L'Aquila) occurred in the descending part of the LOD graph, which corresponds to the Earth's rotation velocity increment (see Fig. 4.25). However, from the semi-annual or fortnightly period point of view, all of those events occurred on the ascending slope of the LOD graph (see in detail on Fig.4.26).

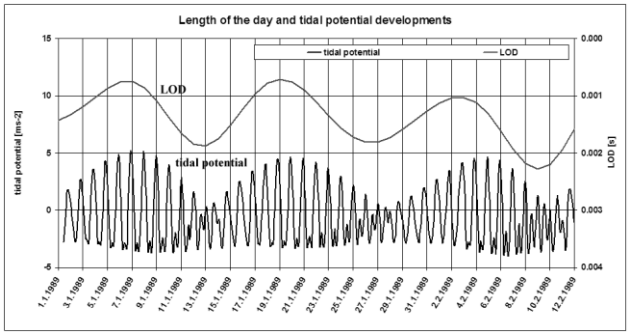

Fig. 4.24: Length of the day and tidal potential.

With the exception of the Norcia earthquake September 19, 1979 and the Colfiorito earthquake on September 26 with its maximum in October 12, 1997, there is a wide and almost continuous earthquake series from 2002 to 2005. This earthquake series (mostly of M<4) corresponds to the speediest Earth rotation that had been recorded during the last 50 years of IERS monitoring. These earthquakes occurred at a time of increased velocity of the Earth's rotation.

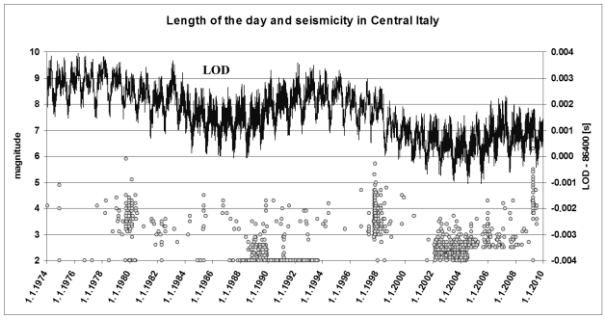

Fig. 4.25: Length of the day and seismicity in Central Italy.

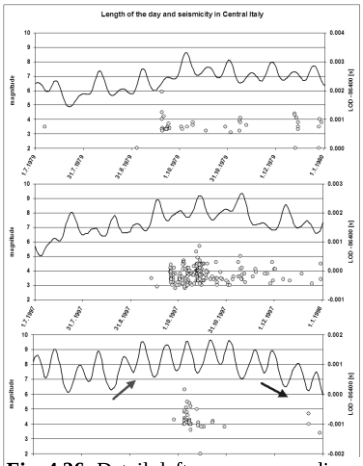

Fig. 4.26: Detail: left arrow – ascending part LOD.

We divided all of seismic events into two groups according to their occurrence time. If they occurred during the fortnightly period, which had longer LOD periods than the previous fortnightly period (red arrow on the Fig. 4.26c), they were signed as 'decelerated' events.

Events that occurred during the descending part of the LOD graph were signed as 'accelerated' events (blue arrow on the Fig. 4.26c). We made two maps of all seismic events from 1974 to 2009 – accelerated and decelerated (see Fig. 4.27).

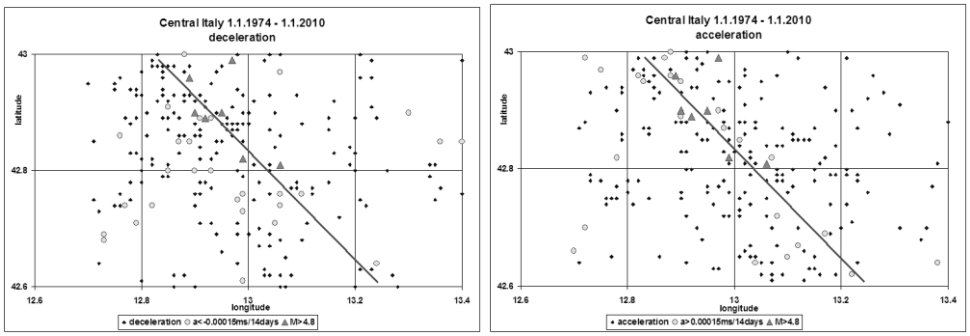

Fig. 4.27: Map of seismic events during **a)** – deceleration, **b)** – acceleration period. Circles – maximums of acceleration/deceleration, red triangles – main shocks.

4.5.1. Geological interpretation

The L'Aquila earthquake occurred in Umbria-Marche-Abruzzi Apennines (Central Italy), which is an area of intensive Plio-Quaternary extensional deformations (Boncio & Lavecchia 2000). The extensional strain field is evident at the surface by NW-SE oriented west dipping normal faults that merge with a high angle and by the low angle NW-SE oriented east dipping normal faults. There are also low angle west dipping thrust faults that have been reactivated in the present-day stress field (Ghisetti & Vezzani 2002). The permanent activity of the extensional system is evidenced by normal faults (master faults, synthetic and antithetic faults) and by regional geomorphology. The carbonate ridges (horsts) form the rigid substrata overlain by Quaternary deposits that fill depressions (grabens). Larger movements of eastern edges of basins also evidence the activity of tectonic structures. The double-acting movement manifests itself as sub horizontal ENE-directed compression and WSW-directed sub vertical subsidence extension (Gasparini et al. 1985) and crustal thinning (Cello et al. 1997). The movement alternating east to west direction represents a tectonic problem that is not easy to resolve. Doglioni 1990 and 1991 has proposed the following solution: "The thrust belt-foredeep-foreland system's progressive migration towards the Adriatic flank would have occurred in response to a mechanism of sinking with the flexural retreat of the Apulian foreland plate. The flexural retreat could be attributed to the existence of movement in the upper mantle that has a direction opposed to that of the subduction of the Apulian plate towards the Tyrrhenian flank".

The problem of such a solution follows from the hypothetic existence of upper mantle movements. Let us concentrate on phenomena evident on the Earth's surface. In the region of L'Aquila the thrust faults and normal faults are almost in a N-S direction. West-dipping Adriatic plate subduction is highly problematic regardless of the non-existence of sea-floor spreading in the Adriatic Sea. A residual Jonian oceanic slab is still occurring in the Calabrian arc (Selvaggi & Chiarabba 1995) as the only evidenced subduction zone in this area manifesting the northward movement of the African plate. The Tyrrhenian Sea is a remnant of a very old oceanic lithosphere, which has remained between Africa-Eurasia after their collision. Such an old oceanic lithosphere (over 180 M.y.) sinks because of gravity related processes and in that manner makes available the space for the plate movements (Ostřihanský 1997; 2004). Subsidence of the Tyrrhenian oceanic plate releases the space for the Central and Southern Apennines movement alternating east and west.

The answer to the question of which forces are behind such alternating movements is easy. It is the Earth's rotation. Forces accelerating the Earth eastward move hanging wall blocks in the direction of the Adriatic Sea rejuvenating sub horizontal Late Miocene-Early Pliocene compressional thrust faults or more recent the normal faults dipping gently eastward (Altotiberina Fault). On the other hand, the westward movement of hanging wall blocks facilitated by the dropping down of the Tyrrhenian oceanic basin is evident by the sub vertical normal faults dipping steeply westward causing subsidence of formed Quaternary basins and manifestation of extensional tectonics characteristic for this region of Apennines. Subsidence and movements along the westward dipping normal faults cause the strongest earthquakes. Earthquakes formed along the eastward thrusting blocks are not strong < 4 M.

The Tyrrhenian Sea is a composed back-arc basin. Therefore no Adriatic slab exists. The Tyrrhenian basin drops down by gravity and the continental lithosphere, with the Apulian foreland plate behind, overrides it. Consequently, the gravitational sinking also of continental lithosphere releases the Apenninian peninsula predisposed to react on the Earth's rotation variations.

The most important finding of this paper is that the earthquakes, which occurred during the Earth's accelerations and decelerations, are situated on the different sides of the Central Apennines. The normal fault (dipping westward) earthquakes are triggered during the Earth's deceleration. The thrust fault earthquakes are triggered during the Earth's acceleration. Therefore the Earth's acceleration engages eastward-directed compression stresses pushing the continental lithosphere of Central Italy to the Adriatic Sea. The tensional stresses, supported by gravitational sinking during the Earth's deceleration, pushes the hanging wall of continental blocks towards the west to the space released by the dropping down of the old Tyrrhenian Sea oceanic lithosphere. This presents a logical explanation of postcollisional extensional collapse of the Apenninic thrust belt. These phenomena confirm the author's opinion (Ostřihanský 1997; 2004) about the sinking of the oceanic lithosphere and the action of external forces influencing the Earth's rotation as being dominant for earthquake triggering and possibly plate movement.

The parameter LOD has, except for the fortnightly and semi-annual components, a longer component as well. The period of approximately 14 months (Chandler period) is typical for polar wobble (Munk & MacDonald 1960). R.S.Gross (2000) from the Jet Propulsion Laboratory has stated that "The principal cause of the Chandler wobble is fluctuating pressure on the bottom of the ocean, caused by temperature and salinity changes and wind-driven changes in the circulation of the oceans".

The length of this long period is the same as the lunar nodal period, i.e. 18.6 years (see Fig. 4.25), which depends on the declination of the Moon with respect to the Earth's equator. This period was recognised on the deformations of the faults and tilt in southern China (Wang et al. 2000).

The question remains, how can small variations of LOD and the changes of stress in the order of 10^{-1} Pa as follows from Wahr (1985) and Gibson & Ma (1998) explain the observed stress change in order of $10^4 – 10^5$ Pa? Authors (Wang et al. 2000) attributed the LOD-correlated decade changes in crustal deformations and stress to the core-mantle coupling mechanism.

4.6. Non-Linear Response – Load-Unload-Response-Ratio (LURR)

One of most important features of the rock mass is its non-linear response to external forces. Earthquakes are a product of this non-linear process. If the stress does not reach the strength limit or the shear stress is not greater than the friction on the fault, the response will be only within the limit of Hook's law. Above these limits earthquakes occur and their numbers and energy will increase (Jaumé & Sykes 1999, Bowman et al. 1998, Sammis et al. 2004). The size of the final addition of external forces that the unstoppable process, leading to the catastrophic earthquake, should be infinitely small. Yin et al. (1995, 2000) used such non-linear behaviour of the process to formulate the LURR hypotheses. They proposed that the measure of the non-linearity is a measure of the non-stability of the process, and its approaching to the critical state close to the strength limit of the rock mass. Although the test of the LURR method showed its prediction power (Yin et al. 2002 Zhang et al. 2004) and the results are in accordance with the theory and modelling experiments (Mora & Place 2002), the results of evaluating the database of California events showed the weak points of the method (Smith & Sammis 2004).

When we analyzed the data from Palm Springs area (see Chapter 4.3), we found that there were two groups of seismic events – one triggered during high tides, and the second triggered during low tides (see Chapter 4.4). That is why we defined two LURR coefficients k_1 and k_2. The first coefficient k_1 is defined in the same way as it was defined by authors of LURR theory (Yin et al. 1995)

$$k_{1,2} = \left(\sum_{i=1}^{N+} m_i \right) / \left(\sum_{i=1}^{N-} m_j \right) \tag{4.6}$$

where $\mathbf{m_i}$ is the magnitude of earthquakes, which occur in the load phase of tidal cycle. This load phase can be defined for LURR coefficient $\mathbf{k_1}$ in the $\pm\pi/2$ surrounding the maximum of CFS criterion in the tidal period. In the case of LURR coefficient $\mathbf{k_2}$ this load phase can be defined in the $\pm\pi/4$ surrounding the average CFS value.

We evaluated the foreshock periods of the most powerful earthquakes in California with M≥5.9 and the results were similar to the analysis of the most powerful earthquakes from Palm Springs, as will be shown in detail.

The first example of the earthquake on September 30, 1981 (M=5.95) shows that both LURR coefficients $\mathbf{k_1}$ and $\mathbf{k_2}$ reached their maximal values (k_1=2.72 resp. k_2=2.95) 3 months before the mainshock (see Fig. 4.28). Coefficient **b** of G-R distribution decreased up to a value of less than 0.6. After the main shock the coefficient $\mathbf{k_1}$ rose and coefficient $\mathbf{k_2}$ remained nearly constant, which was a sign of tidal triggering of the mainshock by process supposed by Yin et al. (1995).

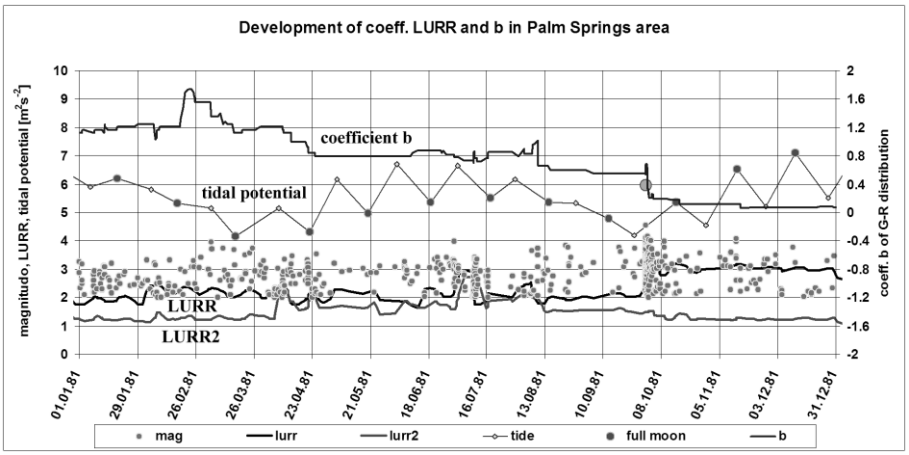

Fig. 4.28: Development of LURR coefficient and coef. b of G-R distribution in 1981.

The second case (on 20.6.1986) shows no significant increasing of both LURR coefficients 6 months before the mainshock (M=5.9) (see Fig. 4.29). On the other hand, the **b** coefficient of G-R distribution was very low (0.4 – 0.6) for a long period before the mainshock. The increasing of both coefficients LURR $\mathbf{k_1}$ and $\mathbf{k_2}$ after the mainshock shows that the time of the mainshock was not random. Instead, it depended on tides as predicted by the theory. Such a mainshock should be predicted only on the basis of **b** coefficient and not on the basis of LURR coefficients. A small increasing of seismic activity is seen before the mainshock.

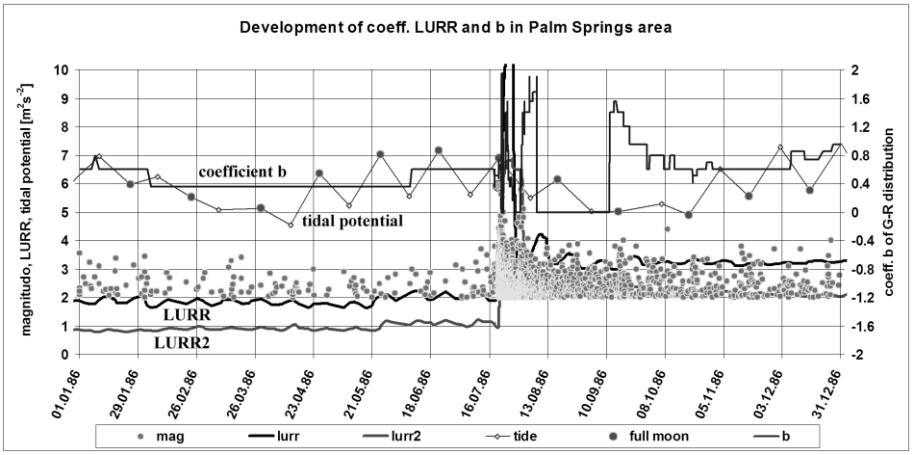

Fig. 4.29: Development of LURR coefficient and coef. b of G-R distribution in 1986.

The third case is very similar to the second one, except for **b,** the coefficient of G-R distribution, which was high for at least 4 months before the mainshock. In this case, the aftershock sequence shows the non-random distribution in time and both LURR coefficients $\mathbf{k_1}$ and $\mathbf{k_2}$ are greater than 7 and 3 respectively. Such a mainshock was unpredictable either on the basis of all LURR coefficients, **b** parameter or by foreshock activity.

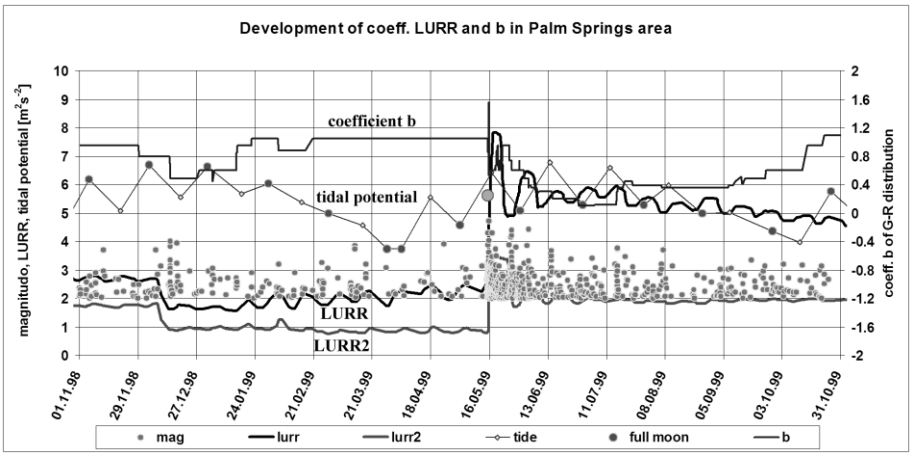

Fig. 4.30: Development of LURR coefficient and coef. b of G-R distribution in 1999.

The analysis of LURR coefficients showed that in cases when tides are the main triggering mechanisms in the area, and during the observed period, the dependence of seismicity on the tides increases before the mainshock. E.Cochran et al. (2004), S. Tanaka (2006a, 2006b) and Y. Sue (2009) showed the same results in the case of specified seismic events according to their focal mechanisms. However, tides could not be the triggering mechanism at all and in that case the foreshock did not show any dependence on tides. The LURR analysis showed that in most cases the tides are not the dominant triggering mechanism in California or, especially, in Palm Springs.

4.7. Test of Non-Tidal Periods in California Seismicity

After the test for tidal periods in seismicity, we tried to test the same Composite catalogue of California earthquakes (ANCC 2004) for non-tidal periods. In this case, the analysis must be made in such a way as to preclude the contamination of analysed periods by tidal periods. So, the easy way was to analyse the seismicity in the window of such length, which was the common multiple of both analysed periods of tides. In the case of the analysis of the diurnal period (24:00) we used the 28-day long time window with an integer number of tidal and non-tidal diurnal periods. In this way, the tidal influence will divide into all of the phases of the non-tidal period as noise. The other way is to use a very long catalogue, in which the tidal influence will divide randomly to all phases of the analysed period.

We used the same tidal periods catalogue (see Chapter 4.4) for the period from January 1, 1970 to April 9, 2004. It contains more than 300,000 events with $m \geq 2$. This catalogue is complete from $m=2$.

We scanned the entire catalogue with constant periods from 0.4 days up to 160 days with the step dt=0.0002 T, where T is the scanning period and dt is the step to next period to be scanned. We assigned a phase φ_i of each earthquake (the phase 0° was defined on 1/1/1900 00:00) and we made a histogram of the phases of all events. Then we evaluated the Schuster's test for each scanned period according (4.1) and (4.2) (see Fig. 4.31).

It did not surprise us to see that the dominant period was the diurnal period 24:00, which has the Schuster's coefficient less than 10^{-70}, which

means absolute certainty. The semidiurnal periods are well established (see in more detail on Fig. 4.32). What was surprising, was the absence of tidal periods of 28 days. It could be the result of non-stability of such periods of time because they are made by the superposition of many tidal periods (components) (Tamura 1987) and the period of 28 days has only an interference character. This leads to the changes in its length and phase (see in detail Kalenda & Skalský 2002). That is why the interference tidal period and its response in seismicity becomes smooth.

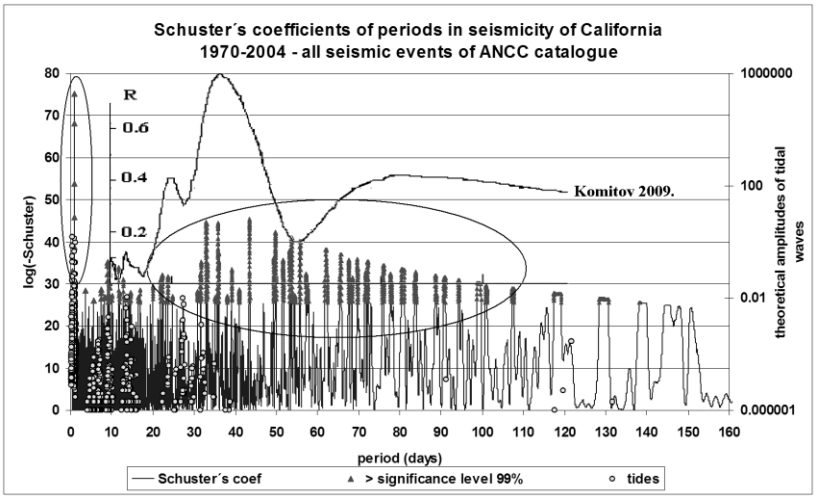

Fig. 4.31: Schuster's coefficients of periods in seismicity of California, tidal periods and Martian's ice cap periods (Komitov 2009).

The second surprise for us was finding dominant periods with their lengths between 30 and 80 days, with the maximum around 33-43 days, which do not correspond with any of the tidal periods. As the similar periods were found by Komitov (2009) in the variations of Martian caps during periods of 'great oppositions' in 1924 and they were well documented in the spectrum of radio emissions from the Sun (Kane et al. 2004), we suppose that such periods (and seismicity) depend on solar activity.

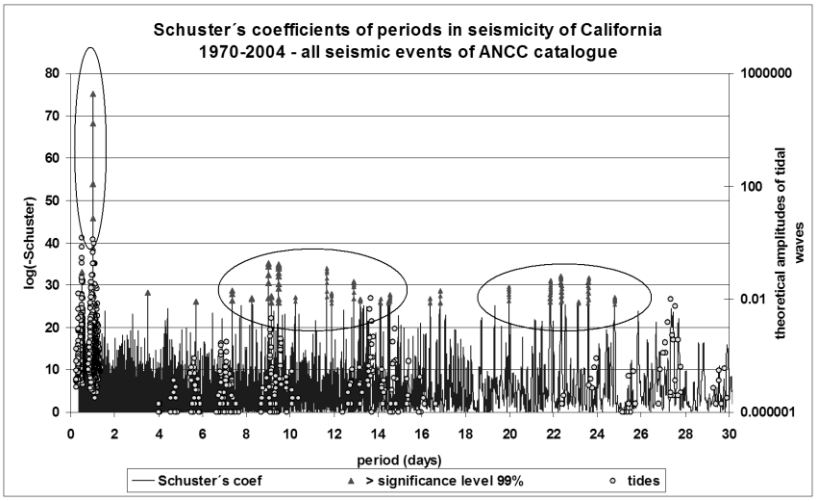

Fig. 4.32: Schuster's coefficients of periods in seismicity of California, tidal periods.

Detailed analyses of non-tidal periods show some groups of stable short periods between 7.3 and 13 days and 20 and 25 days (see Fig. 4.32). Such periods could correspond with periods of solar activity, atmospheric pressure variations or 9-day long tidal variations.

The most dominant period – 24:00 hours – is most probably generated by solar irradiance (see Chapters 3.5 and 9.3) but it can also be generated by direct gravity influence (see Chapters 3.3 and 3.4). Such a diurnal period was observed on tiltmetres underground in Příbram, 1300 m below the surface, where their amplitude was 3 – 10 times greater than the theoretical amplitude of tidal wave P1 (Melchior & Skalský 1969). As we showed previously in Chapter 4.1, most of the observed earthquakes in Palm Spring area were in the afternoon (see Fig. 4.10). But the maximum number of the smallest events of all California was around midnight, when there are the best observation conditions (see Fig. 4.33).

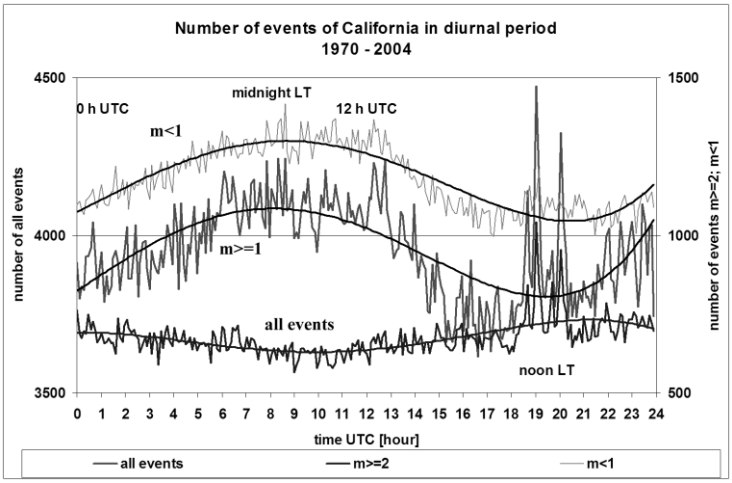

Fig. 4.33: Distribution of events of California 1970 – 2004 in diurnal period.

Another interesting thing was the observation of a stable tidal wave K1 with period T=0.997267 days, i.e. with the length of one sidereal day. Its 'Schuster's coefficient' was $10^{-25.7}$, so it was reliable below the statistical significant limit of 99.9%. It proves the direct gravity influence of our Galaxy on the seismicity of California. Such influence is insignificant, because only small seismic events with magnitude below 1 are triggered (see Fig. 4.34). No influence was observed for seismic events with magnitude greater than 2.

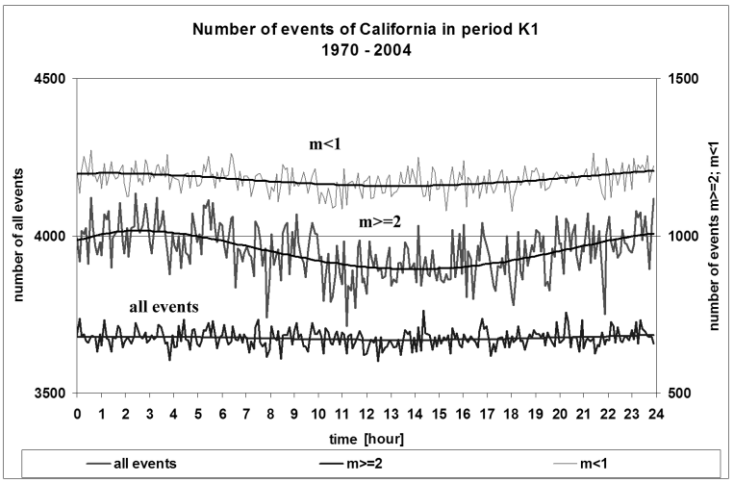

Fig. 4.34: Distribution of events of California 1970 – 2004 in period K1.

The distribution of seismicity in the period of 14 days shows the probably antropogenous influence, i.e. working activity during the week long cycle (see Fig. 4.35). It is evident the minimum number of events on Sunday and the maximum number of events on Wednesday are in the middle of the working week. It should be probably made by contamination of the catalogue by natural seismic events caused by blasting or induced seismic events. The 7-days period is easily observable with the sub catalogue of events with a magnitude of m>2. The diurnal period is easily visible and the variation of number of events is higher during working days than during the weekend.

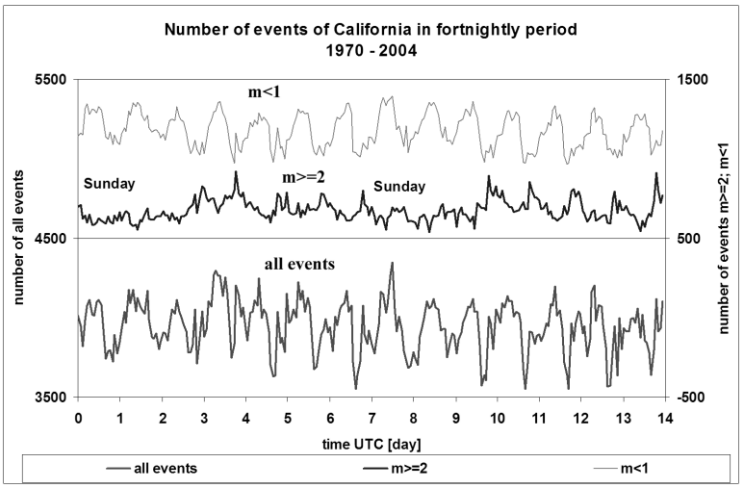

Fig. 4.35: Distribution of events of California 1970 – 2004 in fortnightly period.

Because the annual period contains not only the tidal period (including LOD) but has a thermal component as well, we analysed the reaction of seismicity on all of the triggering processes. It showed that the annual cycle contains two doubled cycles (see Fig. 4.36). Both of the quarter year periods are easily visible only on the sub catalogue of stronger events with m>2. In contrast, the sub catalogue of the smallest events with m<1 shows only semi-annual periods with the maximum number of seismic events in March and September.

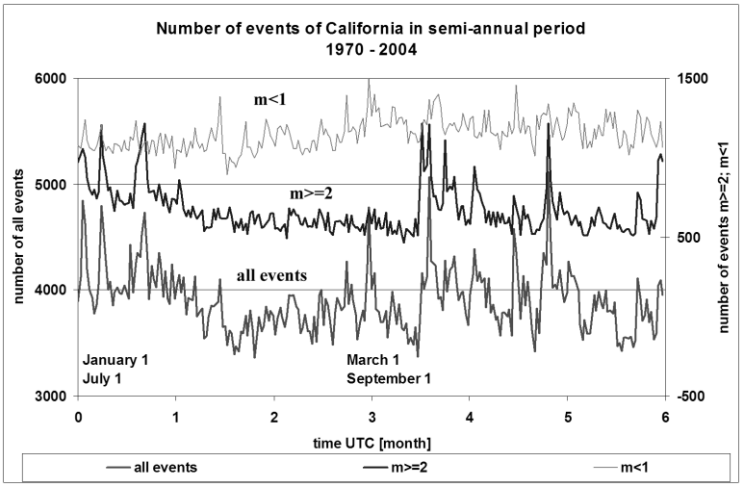

Fig. 4.36: Distribution of events of California 1970 – 2004 in semi-annual period.

4.8. Periods of Halle and Wolf Cycle and Global Climatic Cycles

External forces with a period of exactly 24:00 hours, as it was shown in the previous chapter, can trigger earthquakes. This period is tied with the rotation of the Earth with respect to the Sun, so that the most natural explanation of triggering of earthquakes is due to thermal expansion of rocks, induced by irradiation of the Earth surface. If this is true, then we should observe the long-term variations of seismicity caused by variations of energy flow from the Sun. One of such periods could be a 36-day long period of solar activity variations (see Chapter 4.7). Even longer periods should be observed, connected with 11 or 22 year long cycles (Wolf and Hale cycles).

Are such periods of 11 or 22 years detectable inside seismicity? Wu S. (2005) showed that the large earthquakes occurred during periods of low solar activity. Wej Su & Li (2007) showed that the seismicity correlates positively with periods of reduced solar activity, which associates with rain and floods in valleys. On the other hand Han et al. (2004) showed, that the occurrence dates of most of the big earthquakes in and near faults with west-east strike are close to the maximum years of sunspot numbers,

whereas dates of some big earthquakes, which are not in such faults, are not close to the years of maximum sunspot numbers.

The 11 year long period is, without any doubt, very visible on the activity of mud volcanoes (Gadjiyev et al. 1985, Khain & Khalilov 2008, 2009). It could be caused by small depth of the 'volcanic hearth' in the shallow depths below the surface and could be affected by temperature changes on the surface.

If the Wolff's cycle is detectable on the mud volcanoes, it could be detectable on the shallow seismic activity too, because the foci of seismic events in California are in depths between 6 and 33 km. We chose the ANCC Composite catalogue (ANCC 2010) for this analysis. The catalogue is complete for the period 1900 – 1965 for earthquakes with M>7.5, for the period 1965 – 1978 for earthquakes with M>5 and for the period 1978 – 2010 for earthquakes from M=2 (see Chapter 4.1).

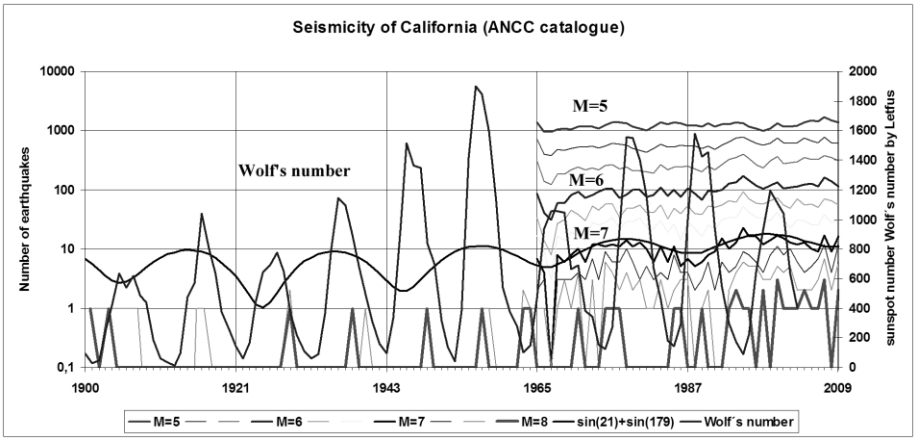

Fig. 4.37: Seismicity of California and solar activity.

We made the frequency-magnitude (G-R) distributions with the step of magnitude 1/3 of magnitude for all of the earthquakes greater than M=7.66 since 1900 and for all earthquakes greater than M=5 since 1965, we used a step of one year (see Fig. 4.37). The curve with the best fit for seismic activity with events with magnitudes equal or greater than M7 can be described as the sum of sinusoids with 21 and 179 year long periods. The

approximation fits very well. The regression coefficient r=0.73 and the relationship can be described by formula

$$\log N_7 = 0.035\,(4.5 \sin((2\pi\, t\, /21) + 5 \sin(2\pi\, t/179) + 10) + 0.25 \qquad (4.7)$$

where N_7 is the number of seismic events with $M \geq 7$ and **t** is time in years. It is seen that for both periods 21 and 179 years the weights are nearly the same.

These periods are connected with solar activity and with the 'Van' period of similar positions of planets (Jose 1965), starting on the year 1924.

It is interesting that the maximum of seismicity in California corresponds with the maximum of solar activity during even solar cycles and the minimum of seismicity corresponds with the maximum of solar activity during odd solar cycles.

If the seismicity is influenced by solar activity in the Hale cycle and 179 year long cycle, when the variations of solar energy that reached the Earth are in the order 0.1% (Willson & Hudson 1991), then the seismicity would be much more affected by climate changes of Milankovich cycles (Milankovich 1930) (17,000-22,000 years of precession of the equinoxes, 41,000 years of wobble in Earth's orbit and 100,000 years of eccentricity). Such Milankovich cycles have a big impact on the climate on the Earth (Petit et al. 1999), however, we are not able to test the influence on seismicity. We have only the possibility of testing much longer climate changes by orogenesy. If we supposed that during the orogeny period the seismic activity is higher, then we could compare orogeny periods with global climate changes (Veizer 2005, Royer et al. 2004, Zachos 2001, Scotese 2003) (see Fig. 4.38).

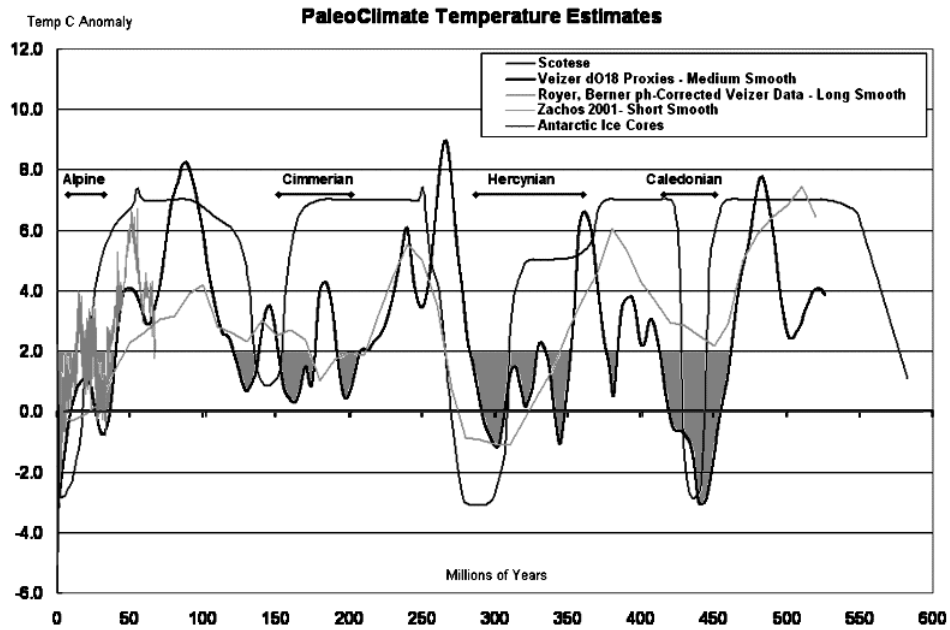

Fig. 4.38: Comparison of paleoclimate temperature estimates and orogeny periods (compiled by Post & Illis 2009).

It can be seen that all of cold climate periods correspond with the orogeny periods. The depth of cooling is proportional to the intensity of orogeny. The main orogeny periods, Caledonian, Hercynian and Alpinian, were observed during cooling periods, when the temperature was under 0 C. On the other hand the Cimmerian orogeny (sometimes called only as a orogeny phase) did not have global influence and the global temperatures did not drop below zero.

4.9. Influence of Atmospheric Pressure Changes, Snow Cover and Floods

In addition to tides, LOD, and temperature and climate variations there are many other earthquake triggering mechanisms such as static or dynamic transfer generated by distant earthquakes (Hill et al. 1993).

Similarly like ocean tides, the hurricanes, large cyclones and/or anticyclones can trigger earthquakes (Gerstoft et al. 2006, Holub et al. 2008) by the deformation of the Earth's surface. It is possible to evaluate the magnitude of the deformation of the Earth's surface in the case of cyclones and/or anticyclones. We can use the Green's spherical functions (Farrell 1972) and calculate that atmospheric pressure variations which can reach 50 hPa and induce deformation of the solid Earth in centimetres. This deformation is less than that caused by solid Earth tides. The horizontal deformations can be induced too, as was detected by VLBI (Petrov & Boy 2003, Estermann et al. 2003).

However there are not any observations of major earthquakes being triggered by air pressure variations. 'Slow earthquakes' or microseisms triggered by hurricanes have been observed (Liu et al. 2009, Holub et al. 2008).

Snow cover (Estermann et al. 2003) and floods (Bevis et al. 2005) have a stronger influence on earthquake triggering than atmospheric pressure. For example, the seasonal fluctuations of water cover of the Amazon River system (with the height of 30 m) induce deformation of the solid Earth in the order of 5 cm in vertically and 1 cm in horizontal direction, which is comparable with the Earth tides, but on the much longer time scale.

4.10. Conclusion of Chapter 4.

We analysed in this Chapter 4 various possible earthquake-triggering mechanisms. We showed that seismicity, on various scales from global down to local, is influenced by exogenous factors such as tides, temperature variations on the Earth's surface, climate changes, and gravity related forces associated with Solar System bodies. Solar storm activity has an influence on seismicity as well. Air pressure variations, precipitation, distant earthquakes and human activity have weaker but still observable influences.

It was shown that there is not just one dominant triggering mechanism. All of the earthquakes triggering forces are working together, and at different times they can have greater or lesser impacts on seismicity.

The seismic response to external forces is not simple, because the rock mass is itself not simple. That is why two or more different responses can be observed during a single earthquake triggering cycle. For example, if there were two or more faults with different orientations in the massif, the Coulomb criterion (4.5) would be fulfilled for each fault during different phases of the tidal cycle. Sub-vertical faults will be predisposed for slip during high tides in contrast to sub-horizontal faults, which will be predisposed for slip during low tides independent of their orientation. On the other hand, the same reaction of the massif can be observed in the case of triggering by two distinct triggers, for example, the gravity of Sun has the same diurnal period as solar irradiance.

5. VERTICAL STATIC PENDULUM

As our research has shown (see Chapter 1.2), if we want to predict earthquakes, direct or indirect measurements of the stress state of the rock mass are necessary. The theories and mathematical models are incomplete and in all cases they only approximate the real world.

The analysis of seismicity showed that in many cases, the seismicity itself gave us the information about the critical state of rock mass too late to predict the earthquakes. Other methods, like water level in wells or electromagnetic methods, are tied with the stress state in the rock mass. However, the noise and disturbances make the detection of that critical state uncertain. From this point of view the deformometry methods would be right for this purpose. The measurement must be exercised in underground conditions, outside of natural or artificial noise and outside temperature or other variations. The sensitivity of such measurements must be better than 10^{-7} strain or 0.1uRad to detect the deformations one order less than those induced by tides or thermoelastic waves. The up-to-date tiltmeters or strainmeters can detect such deformations; however, only in a few cases were the anomalous tilt or deformation preceding the earthquakes detected. Why?

One of the possible reasons is that there is insufficient measuring of the components of strain tensor or filtering of "disruptive effects" or choice of "optimal" conditions of measurement to produce data similar to theoretical, as possible. If we bear in mind that the tectonic stress has mainly subhorizontal principal components (Havíř & Špaček 2004), we can suppose that most of the deformations made by this tectonic stress will be observable with the deformation of a plumb line namely by rotation, by strain, or by layering (see Fig. 5.1).

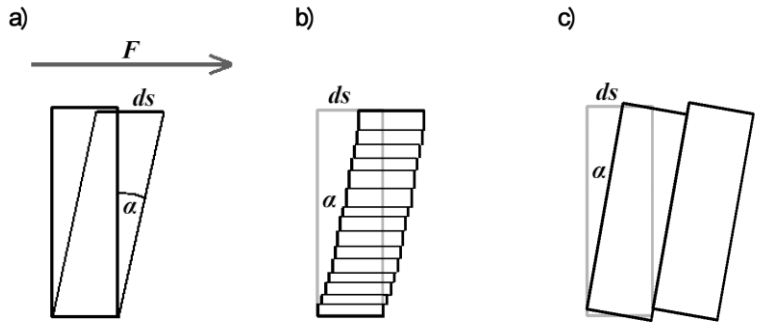

Fig. 5.1: Typical examples of massif deformation due to tectonic stress: **a)** strain and rotation, **b)** layering, **c)** pure rotation (vertical cross-section).

If we measure the tilt using a tiltmeter that is installed on the horizontal plane we can measure only anomalous tilt in the case (c) in Fig.5.1, but not in the cases (a) and (b). However, the most common cases of deformation are cases (a) and (b) on the Fig. 5.1, when the block of rocks has its lower end fixed among other block and its free end is on the surface. All three cases of deformation can be measured by one apparatus, which will measure the deformation *ds* in the horizontal plane or angles of tilt of the plumb line $\alpha_x = \delta z/\delta x$ or $\alpha_y = \delta z/\delta y$ (see Fig. 5.1).

The second reason, why the deformations of massif, evoked by tectonic stress, could not be observed, was that the position of the measuring apparatus was incorrect. The emplacement of apparatus into so-called 'tectonic shadows', i.e. into the places behind the distressing space, makes the correct measurement of tectonic stress impossible. For example, if we will install the apparatus, which can measure the deformations of the horizontal tube, between points A and B (see Fig. 5.2) the measured values *ds* would be greater than in the case of measurement of values *ds´* between points C and D, because *ds*>>*ds´*. The measured value *ds* will depend each time on the geometry of measurements and the direction of the anomalous forces.

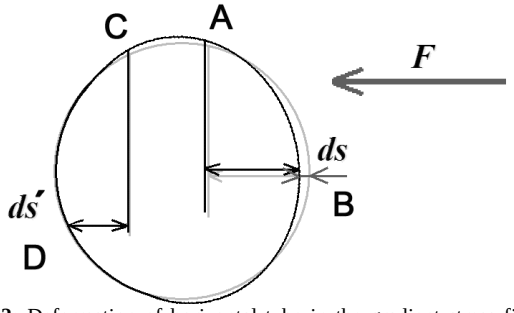

Fig. 5.2: Deformation of horizontal tube in the gradient stress field generated by horizontal stress.

The result of our analysis is that measurements of movement of one of the walls of the underground chamber or cave dome, with respect to the plumb line, is optimal for indirect measurement of tectonic stress variations. That is why we suggested, for the indirect stress measurement, a new type of apparatus based on the vertical static pendulum (Neumann 2007). The actual position of the emplacement of the pendulum will arbitrate between preferred directions and sensitivity of the tectonic stress. A similar situation will be in the vicinity of major tectonic faults, which manages the orientation of the principal component of the stress tensor (Staš & Souček 2002). Measurements in the vicinity of faults will prefer the detection of forces in the same direction as the direction of faults, and those measurements will be not adequate for the assessment of direction of principal component of the stress tensor.

As determined in Chapter 3, those measurements are needed to study the real behaviour of the Earth's crust. This chapter describes a new original measurement device used for the measurements. The measurement device description is divided into the following parts:

- Physical principles
- Technology and functionality of the device
- Measurement system
- Deployment

5.1. Physical principles

The measurement device is based on a simple physical principle. It is a vertical static pendulum. The pendulum weight (bob) is made from electro magnetically neutral material. It is not a conductor or an insulator and it has minimal permitivity and permeability. The weight is hung on the pendulum rod and the swing attenuator dampens its movement.

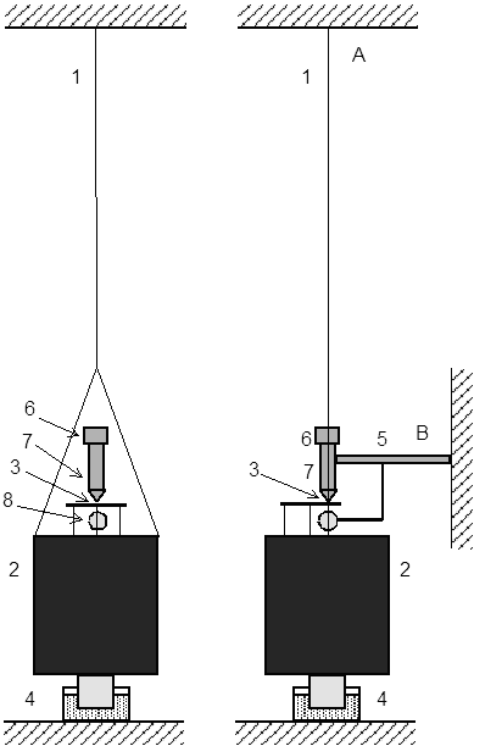

Fig. 5.3: Scheme of static vertical pendulum clinometer (1- suspension, 2- mass, 3- pattern, 4- oil damper, 5- camera suspension, 6- camera, 7- microscope, 8- light).

An optical sensor that is in the horizontal plain measures the position of the pendulum weight relative to its surroundings. The light beam that is used is perpendicular to the pendulum movement plain.

The camera takes pictures, which are then transferred to an on-line computer and processed. The result of the image processing is stored in the raw data form. This raw data is then transferred to the central computer, where it is transformed and processed.

5.2. Technology and functionality

Three technologically different generations of the pendulums have been developed (Neumann 2007). The last one is described in the following text.

The weight was made from concrete with the weight of about 5kg. A minimum amount of metal components were used. The swing attenuator was filled with heavy lubricating engine oil. The pendulum rod was made from steel wire with a diameter of about 1mm (according to local

conditions). The sensor is a digital camera with a microscope objective lens. Optical magnification has been setup by the lens selection with respect to local conditions. The light source is a monochromatic LED diode.

A very important part of the weight position measurement subsystem is the micro-raster. It is specific pattern made on the glass backplane. The pattern has been designed to support the error free functionality of the evaluation algorithm. It supports a wide range of optical magnification of the sensor. The specific irregular and non-repetitive pattern has been developed to support a unique acquired image in any position.

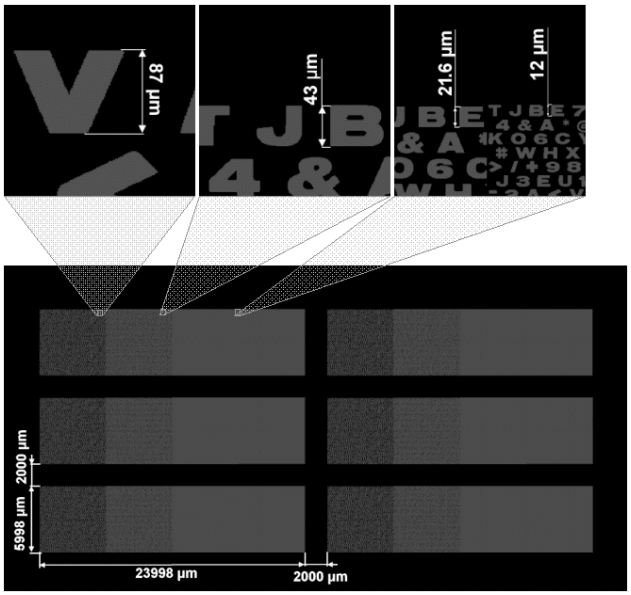

Fig. 5.4: Pattern used in the measurement by pendulum.

The computer, with specific evaluation software, is the part of the measurement device that captures the micro-raster image by the micro-camera and calculates relative image displacements with respect to the reference image. A low power consumption computer and USB digital camera have been used.

The camera resolution was usually setup to 800x600 pixels. The square cutout 600x600 pixels or 512x512 pixels was used for the following processing.

The acquired image is numerically filtered to its contour view. The acquired contours, together with stored reference images contour, are transformed into the position difference in X- and Y-axes. Modified two-dimensional Hough parametric transformation algorithm are used.

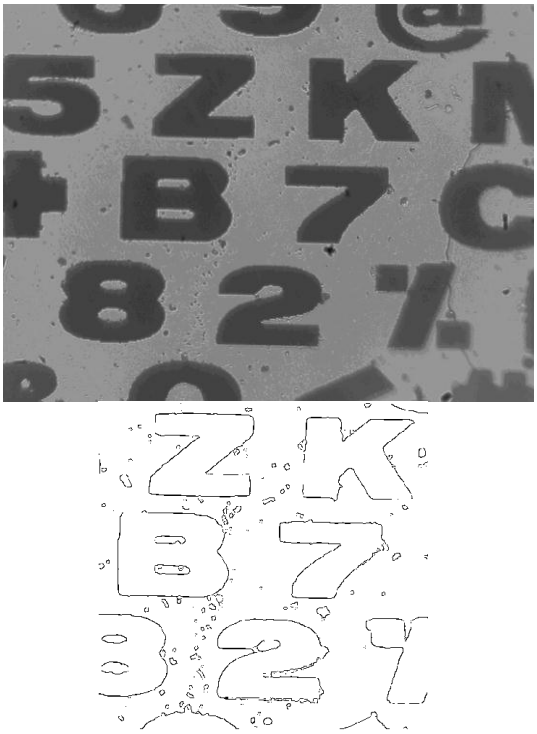

Fig. 5.5: Acquired image and contour view examples.

The result of repeated digital image filtering is a time series of relative displacements in two orthogonal axes, which are calibrated in pixels (optical elements of image area) relative to the sensor orientation.

The sensitivity of the measurement device was setup in the range of about 2μm/pixel to 0.07μm/pixel in different localities. The sensitivity is not the technology maximum; it was selected as the optimum between sensitivity, measured displacements, short period noise, and measured displacement value range.

The digitalized optical cut-off area has a limited size (600x600 or 512x512 pixels). Adaptive algorithm, using automatically captured reference image, is used in the case when the pendulum displacement is greater than the size of the captured optical area.

The length of the pendulum rod has been from 1.0m to 36m approximately, depending on the specific situation in the locality.

The basic measurement device calibration is geometrical and absolute. Optical image resolution was calculated from the sampled image size with a known size micro-raster pattern. The pendulum length was measured directly in every locality. The micro-camera objective lens optical features and camera sensor size were considered a constant. Calibration accuracy was estimated better than +/-10%. The global pendulum sensitivity was between 150nRad/pixel and 15nRad/pixel. The sensitivity had to be setup with respect to the local conditions in the place of measurement. Sampling speed is limited by the CPU speed of the computer used. The image transformation is a CPU speed intensive task. It was recognized that a 10s sampling period was adequate to the measurement needs. The using of low power consumption computers was able to reliably support the 10s samplings.

5.3. Measurement system

The measuring system consists of separated measurement devices placed in specific locations, and a central system. The measurement device was adapted to the specific local circumstances, namely to the power supply conditions and Internet connection possibilities. The typical measurement device consists of two computers. The first one deals with making measurements (as described above) and is placed close to the pendulum underground. The second one is placed on the surface to support Internet connectivity.

The cable between both computers is used typically to enable communication between computers and to supply power to the measurement computer. A very long cable is usually needed in real condition; therefore specific electronic adapters had to be used to support the long cable communication and the power transport. The communication computer was connected to the Internet according to local possibilities. GSM modem supporting only a low speed Internet connection had to be used in localities where no wired connection was available.

Both computers are programmed to communicate with the central system in real time. The raw measured data is transferred to the central

system. The communication computer reads commands from the central system and writes status information to the central system as well.

The raw measured transferred data from all measured devices are processed by the central system on a daily basis.

The central system automatic data processing includes transformation of raw data into physical coordinates, calculation of averages and variations (30min and 3min) and transforming into the form of time series and graphs. The calculated results can be displayed remotely by a standard web browser and can be used for further analysis. The central system is used for system management as well. It receives status information from all measured devices and evaluates technical parameters every hour. The results can be used for quick overall information from all measurement devices and for a more detail view of individual devices. The measurement system enables remote control of the measurement devices including operation support and the ability to focus the camera remotely.

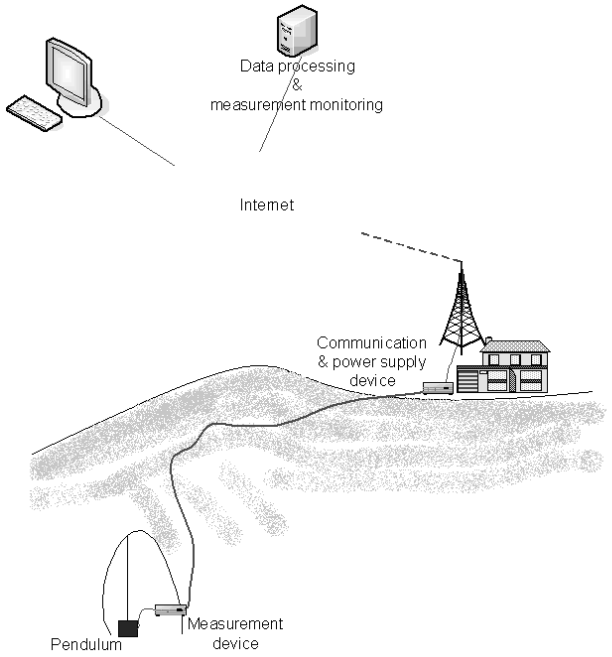

Fig. 5.6: Measurement system - principal scheme.

Kalenda, P., Neumann, L., et al. Tilts, Global Tectonics And Earthquake Prediction, SWB 2010, London.

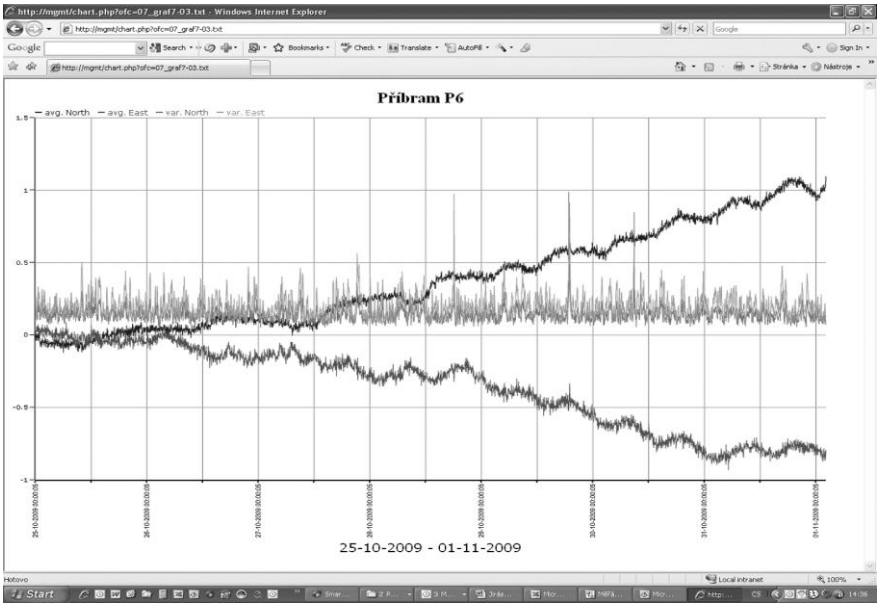

Fig 5.7: Example of processed measured data in one-week time window.

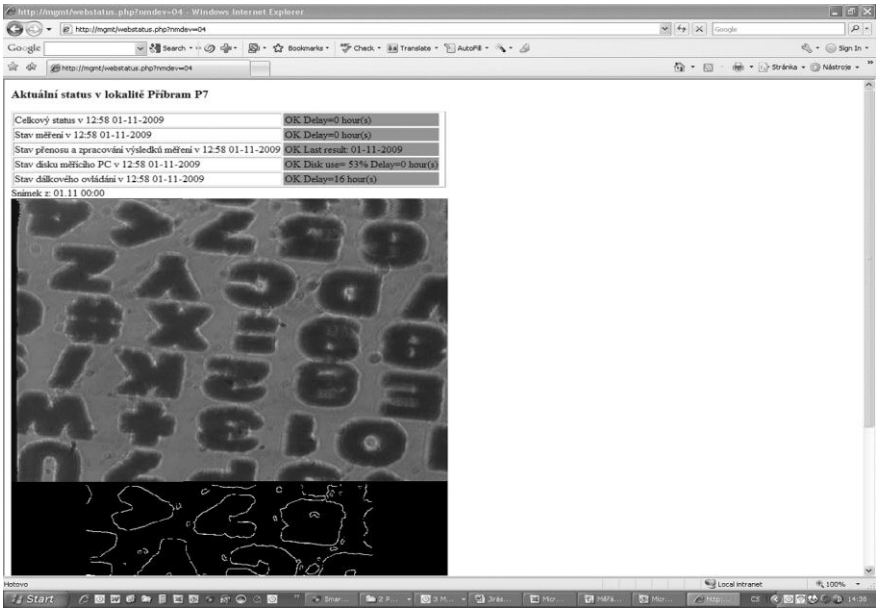

Fig 5.8: Example of status information of one measurement device.

5.4. Deployment

A vertical pendulum is a highly sensitive device. It can react to traffic, walking people, wind, drought, changes in humidity and temperature; therefore it needs an insulated chamber or location protected from people not connected with the research. We found optimal places in the old inclined gallery Prokop in Příbram abandoned mines, with chambers and branches, where only highly scientific instrumentation is in operation at present (Skalský 1963, Skalský and Pícha 1965), and only operators are allowed to enter. A suitable environment will be found in cave No.13C in Moravian Karst, which is closed to the public.

Ten pendulums were in operation in Central Europe at the end of 2009 (see Fig. 5.9 and Fig. 6.1) and Table 3. For the detailed map of pendulums in operation see Fig. 8.1.

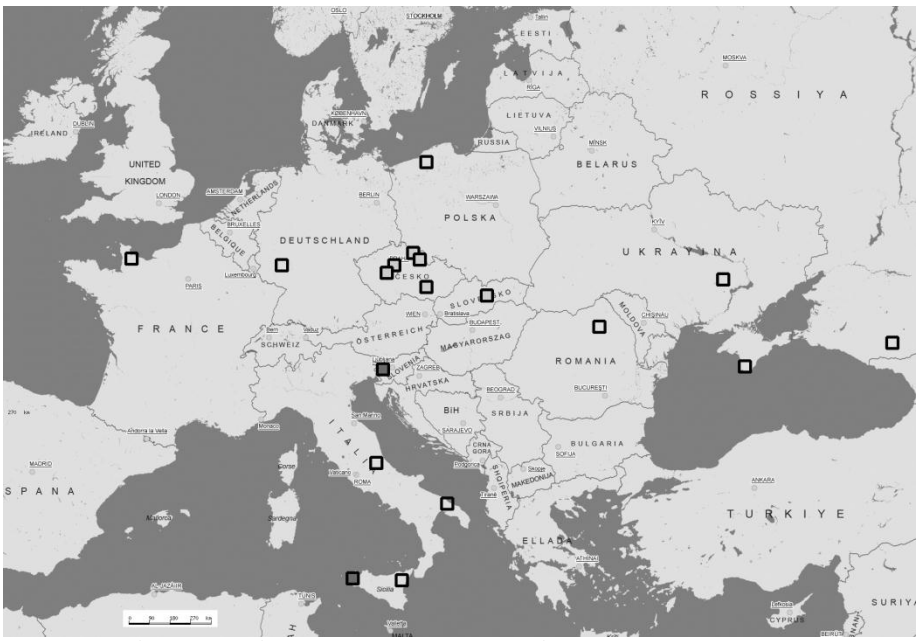

Fig. 5.9: Map of dislocation of pendulums – stage on the end of 2009
grey squares – in operation, dark – installed but not in operation, open – planed.

Table 3 Parameters of pendulums in the underground

sign of Pend.	locality	in opeartion since	end of operation	latitude	longitude	depth [m]	length [m]	sensitivity nRad/pix	azim X	instalation position
P1	Příbram	9.2.2007	1.11.2007	49.68601 N	13.99722 E	1	1.03	346	225	at NNW side of tube
P1a	Příbram	9.10.2008		49.68601 N	13.99722 E	1	1.02	275	225	at NNW side of tube
P7	Příbram	17.5.2007		49.68515 N	13.99288 E	96	3.63	82	350	at NE side of chamber
P6	Příbram	20.1.2009		49.68561 N	13.99416 E	65	2.00	95	45	S side of road
13C	cave No.13C M. k.	3.11.2007	20.9.2008	49.39724 N	16.77243 E	30	30.49	12	255	N side of abyss
13Ca	cave No.13C M. k.	19.10.2008	5.3.2009	49.39724 N	16.77243 E	30	30.49	25	255	N side of abyss
13Cb	cave No.13C M. k.	4.4.2009		49.39724 N	16.77243 E	30	30.49	27	255	N side of abyss
Lub	Lubeník Slovakia	25.8.2008		48.64934 N	20.17434 E	200	10.25	41	27	SE side of schaft
S1	Skutina, Sněžné	28.3.2009		50.35501 N	16.29112 E	3	36.55	18	315	N wall of fortress schaft
D2	Skutina, Sněžné	3.10.2009		50.35501 N	16.29112 E	3	17.88	56	315	N wall of fortress schaft
Ida	Ida mine M.Svat.	1.4.2009		50.53289 N	16.08433 E	200	4.56	45	142	NE side of chamber

6. PENDULUM MEASUREMENT RESULTS – TILTS

The first measurements with a vertical static pendulum started in a block of flats in Prague in 2000 (Neumann 2005). This measurement showed that the main deformation of the building is in connection with the Sun irradiation of the building's walls (insolation). On cloudy days the tilt of the building was less than during sunny days. The pendulum tilt reacted very quickly to the change of the Sun's radiation caused by clouds.

The first underground measurement started in Prokop mine in Příbram on February 2007 (pendulum P1 ca. 1 m below the surface) (see Fig. 6.1). Underground pendulums, which have been in operation since the beginning of 2007:

- P1 in Příbram (1.05 m long, 1 m below the surface)
- P6 in Příbram (2 m long, 65 m below the surface)
- P7 in Příbram (3.6 m long, 96 m below the surface)
- 13C in the cave No. 13C in Moravian karsts (30.5 m long, 30 m below the surface),
- Lubeník (10 m long, 200 m below the surface)
- Skutina (36.5 m long, in the fortress from the surface down)
- Ida mine (4,5 m long, 200 m below the surface).

Besides underground pendulums, there is in operation a pendulum in a block of flats L2 in Prague (2 m long, 20 m above the surface). This pendulum and additional sensors are controlled mostly by the external parameters such as insolation, wind, temperature, and air pressure, which can influence the surface and/or rock mass deformation.

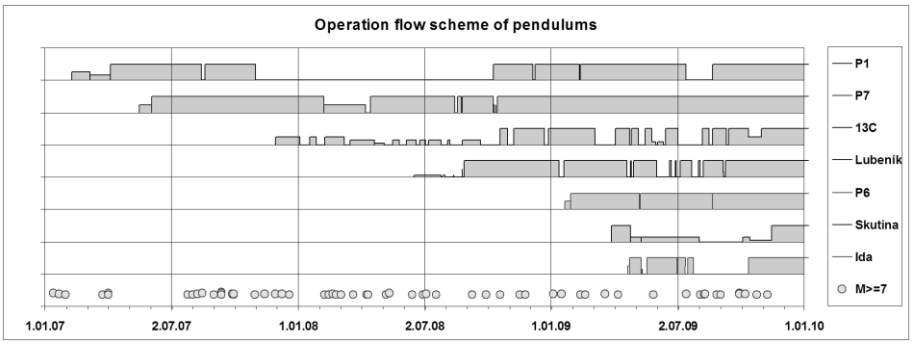

Fig. 6.1: Operation flow scheme of underground pendulums.

All of the results of measurement obtained from surface and underground installations show different deformations of objects on the surface and of rock mass underground.

After a pendulum is installed there is a period during which stress is relaxed in the pendulum's cable and the suspensions of the cable of the pendulum and camera. This deformation development can be described by the equation

$$d = d_o \exp(-k(t-t_o)) \quad , \qquad (6.1)$$

where $\boldsymbol{d_o}$ is representing decompensated deformation, which was caused by changes of stress in the surrounding area of the pendulum's suspension and by change of strain of the pendulum's material (see Fig.6.2). The constant $\boldsymbol{k}$ determined by elastic properties of hanger material and of rock in the area of points of suspensions A and B (see Fig. 5.3). The constant $\boldsymbol{t_o}$ is the time of manipulation with the pendulum when the stress state in the area of suspension of the camera and cable was changed. Such stress relaxation is clearly visible on Fig. 6.2 between May 17, 2007, when the pendulum was re-installed, and June 10, 2007 or in the Fig. 6.3 between April 15, 2008 and May 1, 2008.

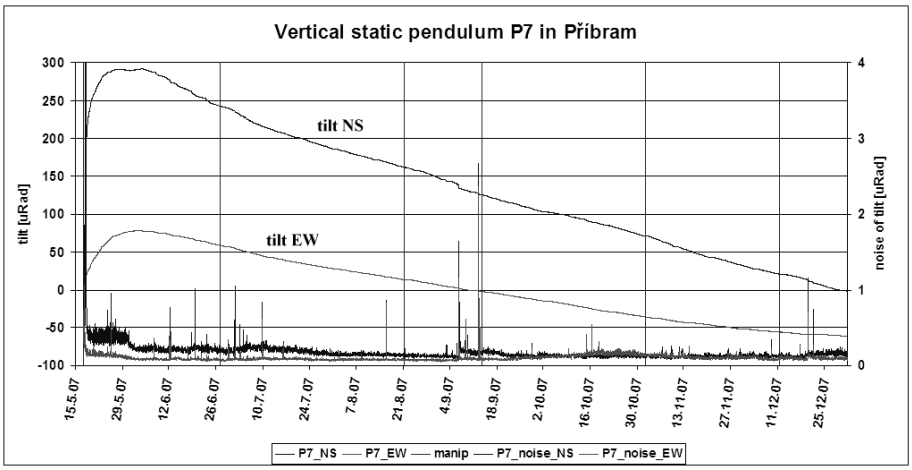

Fig. 6.2: Development of tilt and noise of pendulum P7 in Příbram (vertical lines mark the time of small manipulation with pendulum, i.e. focalisation of optics). Tilt is defined as an average tilt during 30 minutes and noise is defined as a variation of tilt in a period of 30 minutes.

The measurement of deformation is not disturbed by this additional stress relaxation of the pendulum after a couple of weeks or months. The measured deformation is fully dependent on changes of external stress in the rock mass between points of suspensions A and B. The length of measuring a base between points A and B and their geometry in the chamber determines what reaction of the massif on the external stress field will be. If the length of the measuring base is longer, the results of deformation will be less sensitive to the geometry in the area of points A and B.

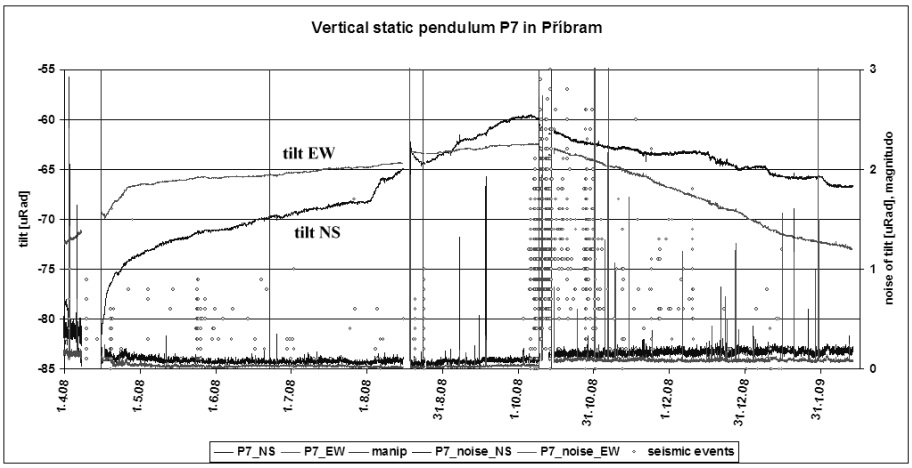

Fig. 6.3: The tilt (upper curves) and noise of tilt development (lower curves) on station P7 in Příbram and seismicity in Nový Kostel seismic swarm area, registered by local network Webnet (Horálek, Fischer 2008).

It is possible to define the periods, when the tilt development was changed radically on the mid-term scale. For example, pendulum P7 in Příbram changed its tilt development around August 3 and October 1, 2008 (see Fig. 6.3). The next big changes of tilt development were observed at the turn of 2008 and 2009. One can see the reaction of the massif on the increasing of stress in the beginning of October 2008 by the increasing of seismicity in the seismic swarm area in Western Bohemia (Horálek, Fischer 2008).

On a short-time scale we can observe semidiurnal variations of tilt caused by earth tides (see Fig. 6.4). The amplitude of tilt varies in time and it is different in both directions (NS and EW) compared with each other or

compared with theoretical values of tilt according to the semielastic model of the Earth's lithosphere by Wahr-Dehant-Zschau (Skalský 1991).

Both components of tilt in the directions NS and EW are different, especially on the pendulum P7. This behaviour of the pendulum is probably associated with the geometry of the emplacement of the pendulum – the upper suspension is mounted in the roof of chamber and the pendulum is hanging along the northern corner. That is why the pendulum is sensitive especially on the northern components of stress (see previous chapter). If we analyse the spectrum of pendulum movement in both directions then we can see that the diurnal (non-tidal) component is prevailing in a NS direction contrary to the semidiurnal component, which is visible in an EW direction (see Fig. 6.4). The ratio between observed amplitudes and theoretical tidal amplitudes varies between 0.5 to more than 20 (see for example Fig. 10.10). The sensitivities of other pendulums, which are installed in different conditions, are different. For example the pendulum P6, which is installed on the southern side of the mining road only 60 m from pendulum P7 is almost insensitive to the changes of the NS components of stress. And both tilt variations are comparable with theoretical values (see Fig. 6.5).

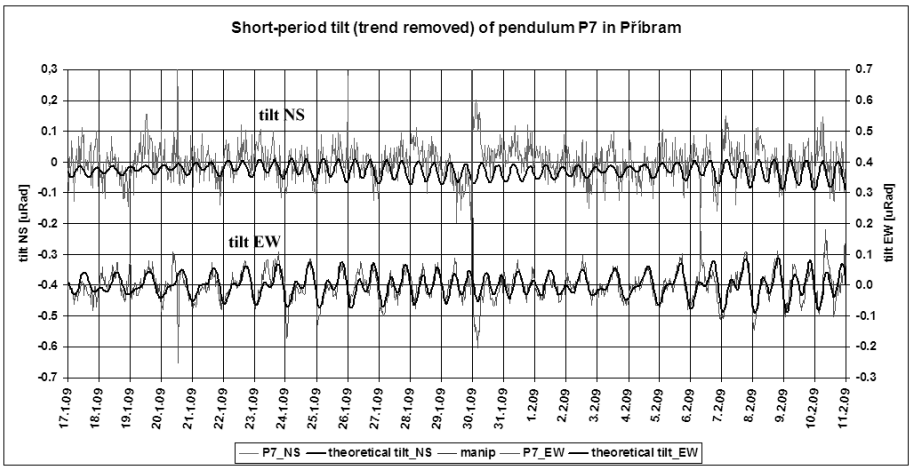

Fig. 6.4: Short-period tilt (trend removed) of pendulum P7 in Příbram.

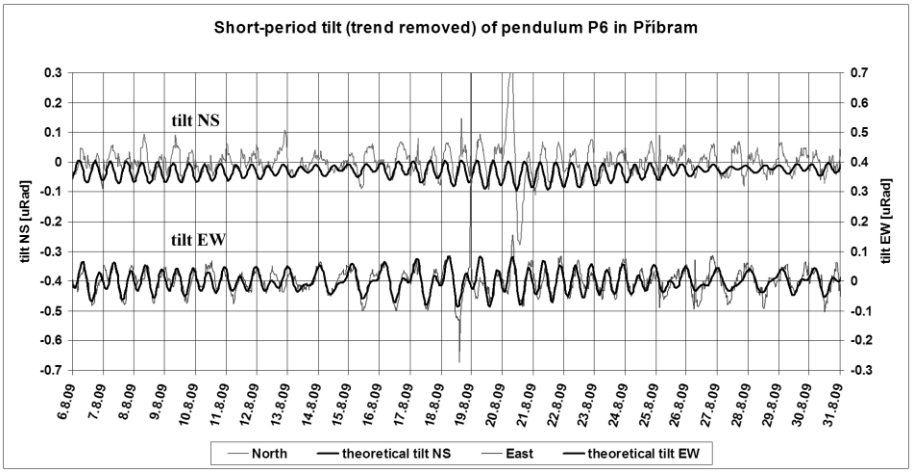

Fig. 6.5: Short-period tilt (trend removed) of pendulum P6 in Příbram.

When the primary data (movement of the pattern on the camera screen), measured with a sampling period of 10s, with an accuracy of 1 pixel of picture are analysed, the various forms of reversible or irreversible deformations in the area of the pendulums are visible.

The diurnal periods of tilt are clearly visible on the pendulum P1 at Příbram, which is installed only 1-2 m below the surface (see Fig. 6.6a, b). Such diurnal waves are caused mainly by insolation of the Earth's surface (see chapter 9.3 or Neumann 2007). In the afternoon, when the surface temperature is the highest, the deformation of the rock mass in the area of the pendulum becomes irreversible (see Fig. 6.6b). Such diurnal waves were observed on pendulums P6 and P7 too, although pendulum P6 is installed in the distance 120 m from pendulum P1 at a depth of 65 m below the surface and pendulum P7 is installed 180 m from the pendulum P1 at a depth of 96 m below the surface (see Fig. 6.7). The amplitudes of diurnal waves on pendulums P6 and P7 are much smaller than on pendulum P1.

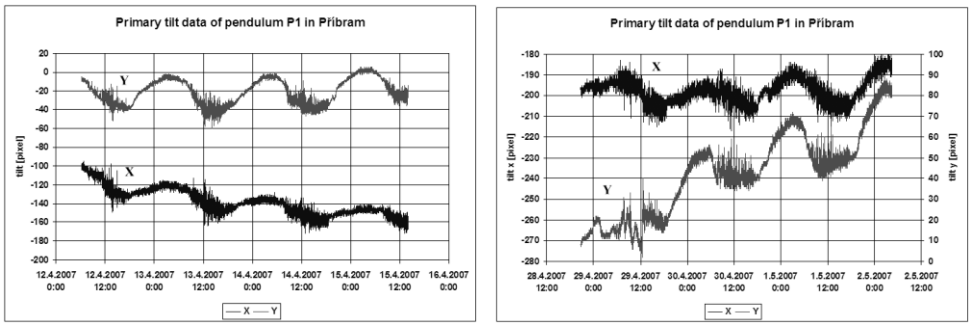

Fig. 6.6a, b: The diurnal variation of tilt on pendulum P1 in Příbram.

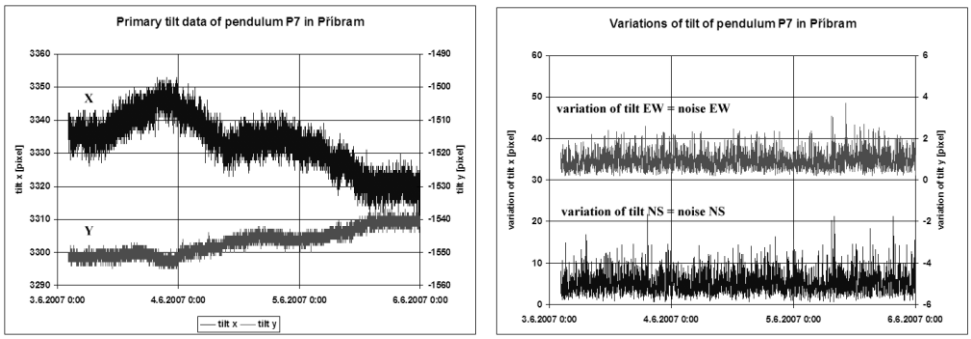

Fig. 6.7a, b: The diurnal variation of tilt and noise on pendulum P7 in Příbram.

The most often detected irreversible deformations are creep (see Fig. 6.8a, b), microearthquakes (see Fig. 6.9a) or silent earthquakes (see Fig.6.9b). In the case of creep, the movement or deformation lasts from minutes to hours. The movement has nearly the same velocity for very long times. In the case of silent earthquakes the process lasts minutes and sudden quick movement changes pure slow creep many times. In the case of microearthquakes the process is very quick and the deformation is observed between two samples of images, i.e. it is shorter than 10 s, but the energy of such quakes is so small that it is not detectable by any seismometers or geophones. Only in the case of the energy released by many such small microearthquakes or silent earthquakes, the tremors or silent slip events (SSE) are detectable by increases in noise levels (Dragert et al. 2004, Ito et al. 2007, Bachmann 2007, Voisin et al. 2008). During the period of observation, no local earthquake from the area of Prokop mine in Příbram

was observed. The reason is simple. This mine has not been in operation for a very long time (since the first half of 19th century) and the mining-induced deformations have already relaxed.

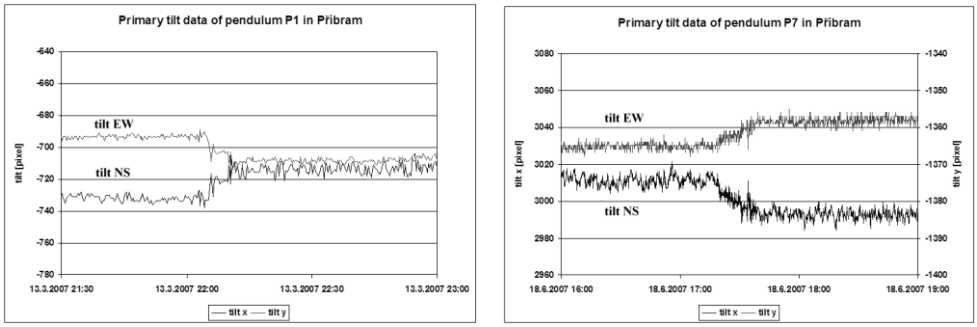

Fig. 6.8: Creep, observed on pendulums P1 and P7 in Příbram.

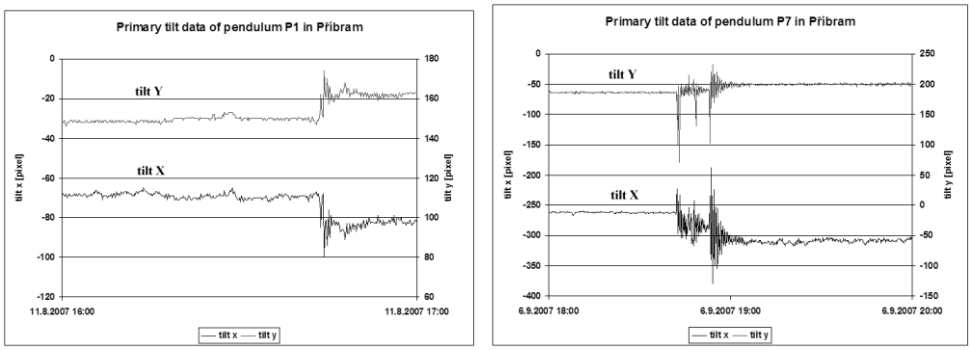

Fig. 6.9: Microearthquake and silent earthquake, observed on pendulums P1 and P7.

The movements, generated by local, regional or teleseismic earthquakes were observed on all pendulums. Sometimes, coseismic deformations were observed, which were caused mainly by surface waves of big earthquakes, i.e. in the case of the Sumatra earthquake on September 12, 2007 (M=8.5) (see Fig. 6.10 and 6.11).

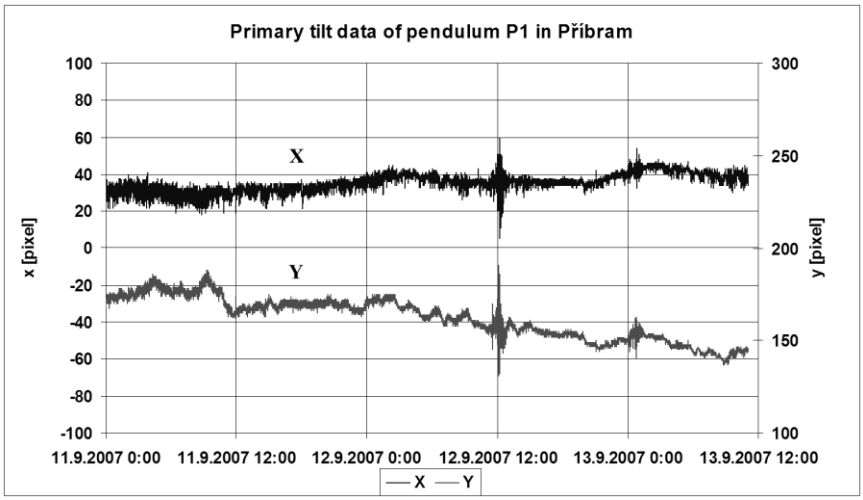

Fig. 6.10: Seismic waves registered during Indonesian earthquakes on September 12 and 13, 2007 (M=8.5 and 7.9) by pendulum P1 close to the surface.

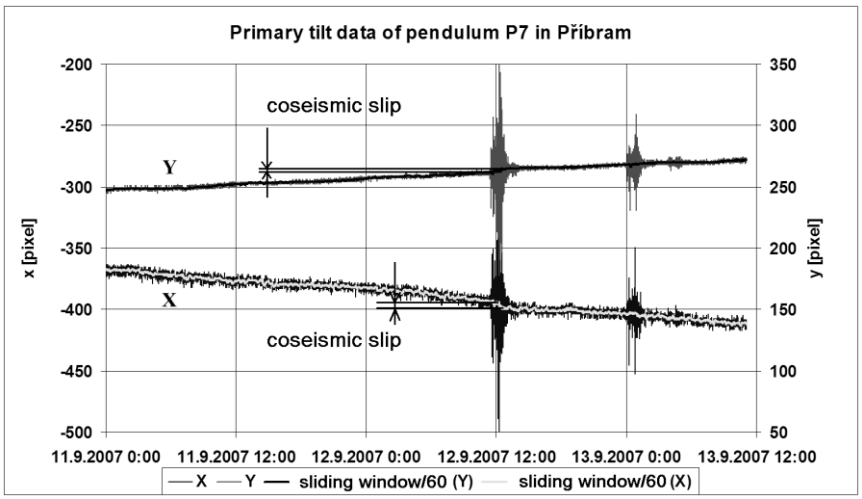

Fig. 6.11a: Seismic waves and coseismic slip registered during Indonesian earthquakes on September 12 and 13, 2007 (M=8.5 and 7.9) by pendulum P7 (96 m below the surface),

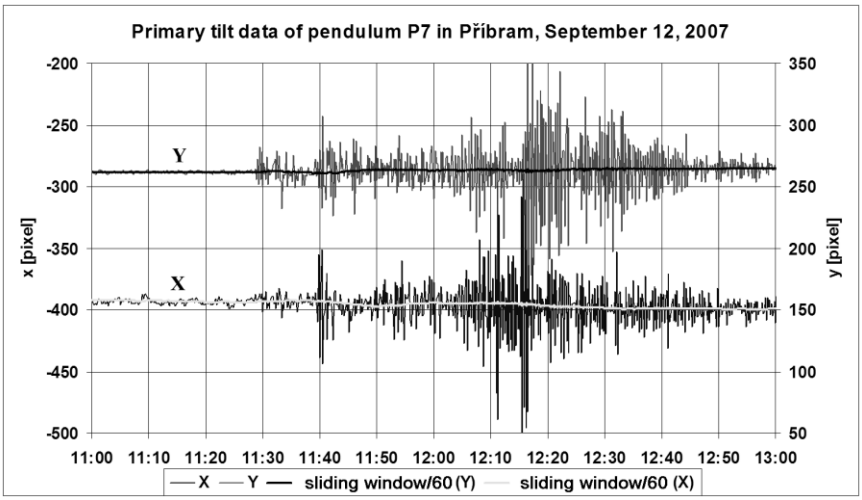

Fig. 6.11b: Detail of seismic waves and coseismic slip registered during Indonesian earthquakes on September 12, 2007 (M=8.5) by pendulum P7 (96 m below the surface).

There are visible diurnal periods of movements of the massif before, as well as after, the earthquake on both pendulums P1 and P7. The coseismic slip can be easily seen with pendulum P7. But, due to high noise and high deformation of the surface of the coseismic slip, it is not visible on pendulum P1. We can analyse in what part of the seismic signal the main coseismic slip started. On Fig. 6.11b it can be easily seen that the first part of coseismic slip started during the time when the S-waves arrived (after 11:40). And the second part of the coseismic slip started after the Love waves arrived (after 12:15). We can analyze the directions of the movement of the massif (see Fig. 6.12a-d). The movement of the massif (particle motion) during periods of S and Love waves was the same as the general movement of the pendulum during the periods of increasing stress. This is why the coseismic slip was observed especially during these periods of incoming S and Love waves (see Fig. 6.11b, 6.12c and 6.12d) and its direction was the same as the direction of general movement.

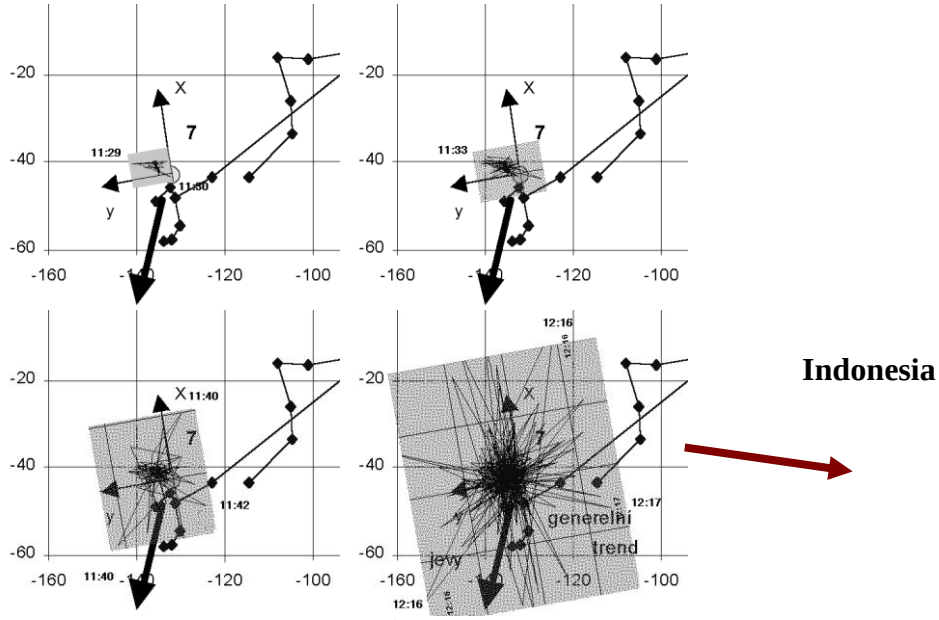

Fig. 6.12a-d: Particle motion diagram of pendulum P7 during **(a)** Pn phase, **(b)** Pg phase, **(c)** S phase, **(d)** surface waves phase. The direction of the general trend of pendulum movement is marked by the thick black arrow. The back azimuth to Indonesia is marked by the red arrow.

The pure rotation anomalies are sometimes observed on all of the pendulums, but these anomalies have never been observed at the same time on two or more pendulums (see Fig. 6.13). Due to small attenuation of torsion, the period T=38.5 s on pendulum P7 can be easily seen for almost 20 minutes. We are not able to interpret their origin at the present time.

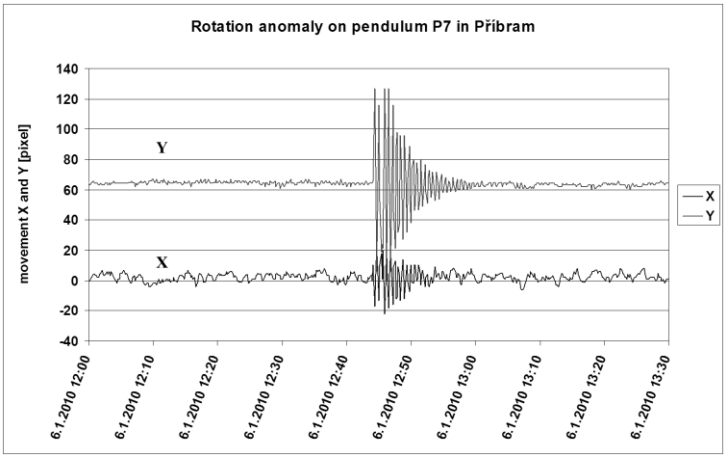

Fig. 6.13: Pure rotation anomaly registered on pendulum P7 in Příbram.

7. INTERPRETATION OF PENDULUM MEASUREMENT

7.1. Interpretation of Anomalous Stress Periods

The estimation of the stress tensor in the area of the pendulum is not as easy as it looks. This is because it is not clear what type of deformation is caused by increasing stress, and what deformation is caused by decreasing stress and the massif relaxation or by only rotation of the axis of the principal stress component. Blocks will be inclined to the north when the force ***F*** increases and its direction is from south to the north because the blocks of Earth crust can be regarded as a beam with one fixed end in the mantle and one free end on the Earth's surface (see Fig. 5.1). On the other hand, if the force ***F*** decreases and its direction is oriented to the north, the blocks will incline to the south according to Hook's law

$$\sigma_{ij} = \sum_{kl} c_{ijkl} \varepsilon_{kl} \tag{7.1}$$

where ε_{kl} is the strain, c_{ijkl} is the component of elastic modulus and σ_{ij} is the component *ij* of stress.

In the real environment of the Earth's crust, the ideal beams with one fixed end are not present and individual blocks of the Earth's crust react individually to increasing stress by individual deformation, rotation, and movement. These are defined by the local geometry of a block's contact with other blocks, by stress transfer between blocks, and by the physical parameters of the rock mass and the faults between blocks. This results in the apparently chaotic and opposite movements of blocks with various directions and amplitudes (Stemberk et al. 2003, Briestenský et al. 2007a, Briestenský & Stemberk 2007b).

How can we determine which deformation matches the increasing stress, and which deformation matches relax time and decreasing stress? It is possible to determine this with the help of irreversible deformation. When the stress in the rock mass increases, Hook's law holds until the strength limit. When the stress is greater than the strength limit of the softest parts of the rock mass, the creep of the massif occurs, the seismic noise increases and the deformation becomes irreversible. There are rose diagrams on Fig. 7.1 of directions of tilt, which were measured during one hour long intervals between point A of the suspension of pendulum and point B of the suspension of the camera.

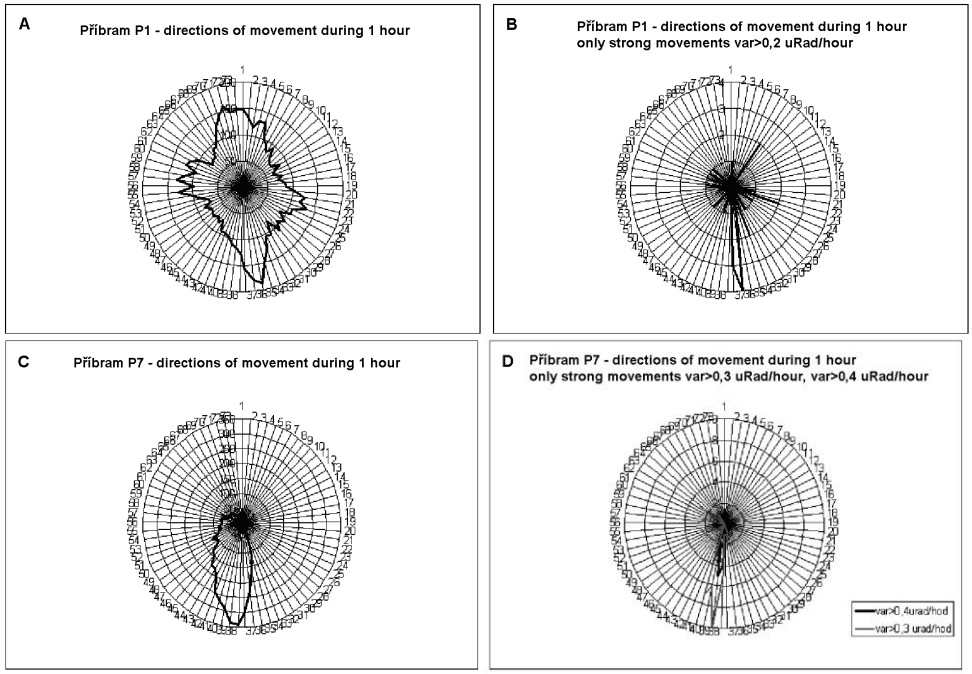

Fig. 7.1: Directions of movement of a pendulum during one hour.

The prevailing directions, measured on pendulum P1 are in directions NNW, SSE, WNW and ESE (see Fig. 7.1a). If only the largest movements are summarised, the prevailing directions are only to SSE (see Fig. 7.1b). The general direction of pendulum P7 was to the south (see Fig. 7.1c), which is the same as during the largest movements (see Fig. 7.1d). Generally speaking, the direction to the south (SSW – SSE) is the direction of the principal component of the stress tensor in the horizontal plane in Příbram during the observed period.

A second method for determining the period of the increased stress in the area under study involves the monitoring of microseismicity. The microseismicity generates seismic noise, which can be measured by variations of differences between actual positions of the pendulum and the central (average) position, i.e. the 'noise' of the pendulum (see Figs. 6.3, 6.6, 6.7 and 7.2). During 2007, both pendulums P1 and P7 in Příbram showed the same periods of increasing noise. The noise measured by

pendulum P1 closer to the surface is higher than the noise measured by pendulum P7, which was deeper. The largest amount of noise was observed during the first half of September 2007 (marked by No.4 in the Fig. 7.2).

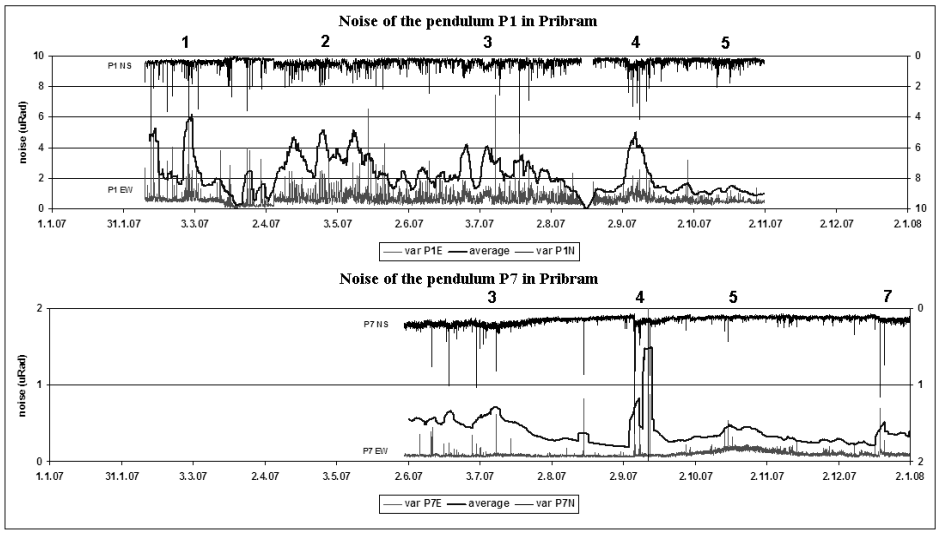

Fig. 7.2: Development of noise (tilt variation) registered by pendulums P1 and P7.

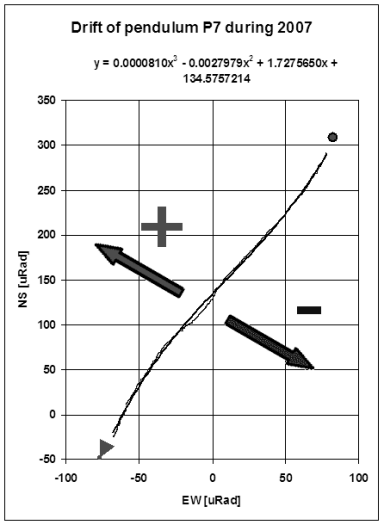

Fig. 7.3: Secular drift of pendulum P7 between June 1 and December 31, 2007.

A third method for identifying periods of increasing stress involves measuring the anomalous drift. The normal drift of pendulum P7 in Příbram is in N-S direction. If we want to find the periods of anomalous stress in the E-W direction we can interpolate the normal drift by the simple polynomical curve of as a minimal order as possible. We used the tilt data between June 1 and December 31 and we interpolated the drift of the pendulum in the horizontal plane by a polynom of the 3rd order (see Fig. 7.3). The residuals between interpolated curve and measured curve show that the anomalous tilt to the west is accompanied by increasing noise. We can conclude that

the anomalous tilt of the pendulum to the west is due to an increase of stress from the east. The largest anomaly preceded the most powerful earthquake during the observed period on September 12, 2007 in Sumatra (M=8.5) followed by aftershock on September 13, 2007 in Sumatra (M=7.9) (see Fig. 7.4). This anomaly started on September 6 after a fairly powerful earthquake in Taiwan (M=6.2). And the maximum of anomalous tilt to the west was observed around September 12. After the mainshock, the anomalous tilt to the west stopped and the relaxation period started after October 1, 2007.

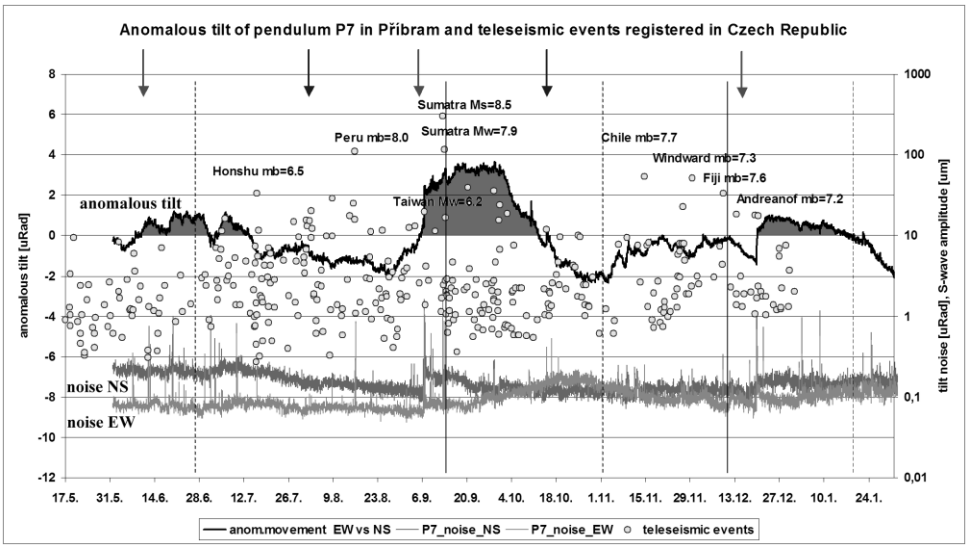

Fig. 7.4: Anomalous tilt of pendulum P7 in 2007, perpendicular to the secular trend.

Two other anomalous periods between June 5 and July 12, 2007, and December 20 and January 15, 2008 were accompanied by fairly powerful earthquakes in Honshu (M=6.5) and in the Andreanoff Island area (M=7.2). On the other hand, three strong earthquakes in Peru (M=8), Chile (M=7.7) and the Windward Islands (M=7.3) were observed during the 'relaxation' period of our lithosphere plate and no anomalous noise and westward tilt was observed.

A fourth way of identifying the period of anomalous stress involves learning how to recognize the massif response to external forces. It is best to use tides here because they are easily computed for any location on the Earth. We can compare the time course and amplitude of measured tilt and computed tilt in both perpendicular directions NS and EW (see Fig. 7.5).

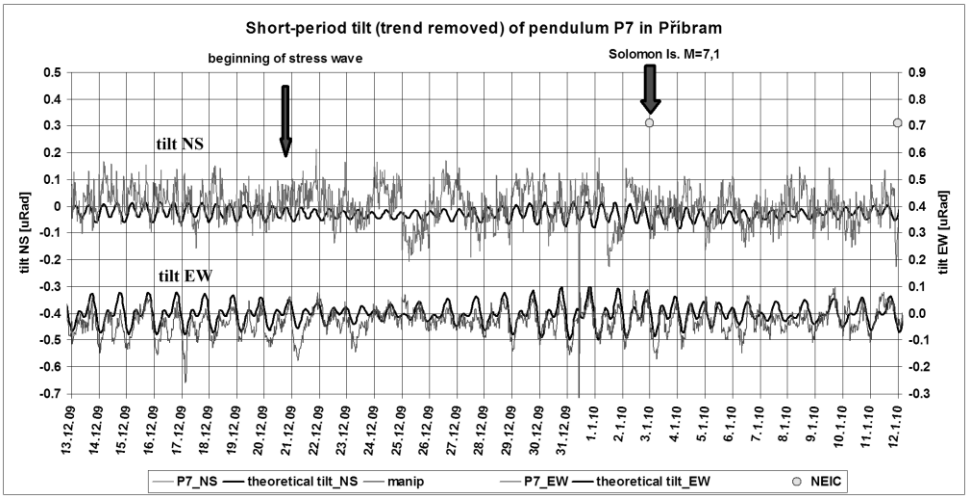

Fig. 7.5: Comparison of measured and computed tilt in NS and EW directions.

During the periods of increasing stress the pores and microcraks are closing in according to the simple models of preparation stages of earthquakes (for example Mjachkin et al. 1974, Rikitake 1976, Bolt 1988, Sobolev 2003). At that time the attenuation coefficient of the seismic waves is dropping and the response of the rock mass to external forces, like tides, increases. We can observe that the amplitudes of measured tilt are greater than the theory predicts (see Figs 6.5, 7.5, 10.10 and 10.16).

7.2. Interpretation of Principal Component Directions

At any time it is possible to evaluate the direction of the principal component of the stress tensor, which is not constant. Instead, it varies in time according to the actual collision of blocks or of entire lithosphere plates (see Fig. 7.6).

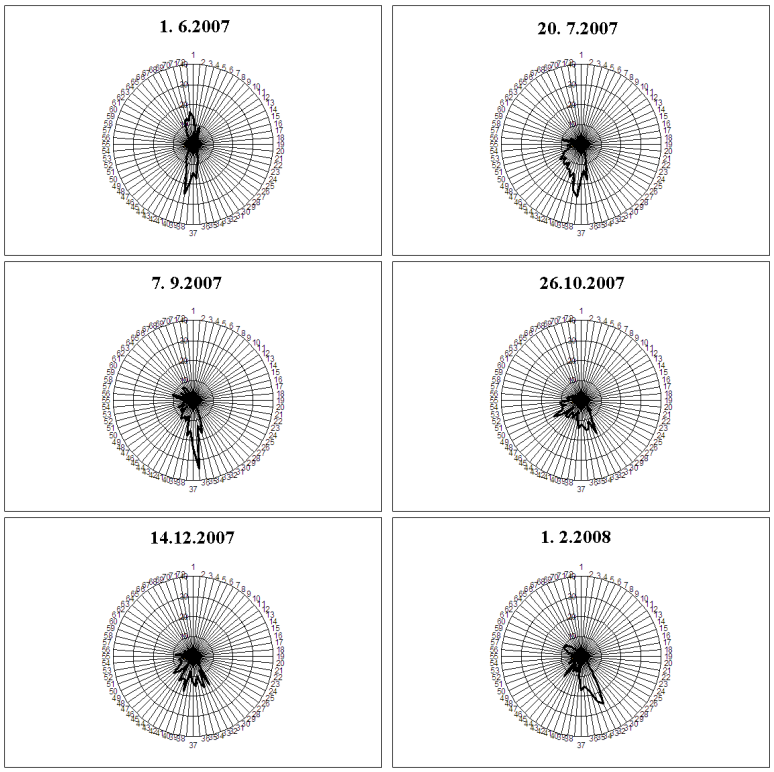

Fig. 7.6: Rose diagrams of 1-hour tilt directions summarised one week on pendulum P7.

We observed that the direction change of general tilt of pendulum P7 was more than 30 degrees from S to SSE during a period of 6 months in 2007. However, sometimes there were periods during which the perpendicular - subsidiary - direction WSW of tilt was more frequent than the principal SSE direction (see Fig. 7.6 - October 26, 2007).

We can observe the wobble of all pendulums and evaluate the prevailing direction of movements or sudden steps, or the directions of polarizations of periodic tilt. We can see on the Fig. 7.7 that the first anomalous tilt of the pendulum in the Ida mine was on January 27 in the NEN direction. Then the chaotic phase started where there was no prevailing direction of tilt. The second sudden tilt was in the WNW direction on January 30. The last phase showed the polarization in NE-SW direction until February 2, 2010. We can

estimate that there are two independent perpendicular directions, which are opposite to each other. The first is from the SW and the second is from the SE.

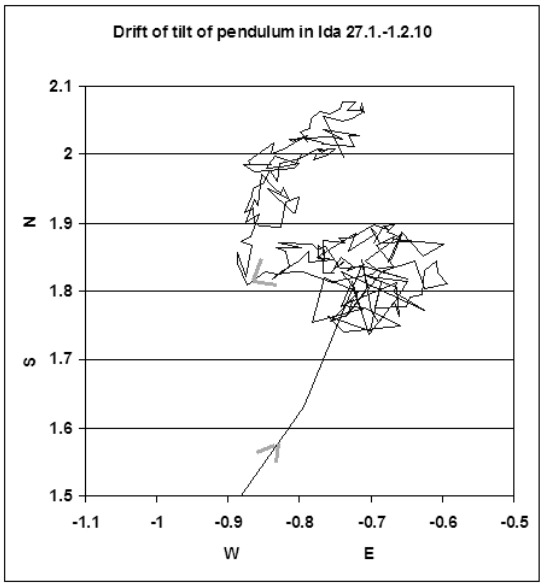

Fig. 7.7: Wobble of the pendulum in mine Ida between January 27 and February 1, 2010.

7.3. Interpretation of Observed Tilt Waves and Their Periods

There are numerous periods in the spectrum of tilt. Periods shorter than one half day are mostly associated with seismic waves that are generated by local (see Fig. 6.6) or distant sources (see Fig. 6.11).

Semidiurnal periods are generated by tides. However, the ratio of observed amplitudes and theoretical ones varies in time (see for example Figs. 6.4 or 6.5). We can extract the development of amplitudes of most important tidal and non-tidal periods in time (periods 24:00 and 12:42 hours) (see Fig. 7.8). We can see that there are periods with dominant non-tidal diurnal period (April – September) and other periods with dominancy of tidal semidiurnal period (January – February and November – December 2008).

If we analyse the periods, when non-tidal periods were dominant in the spectrum of the NS component of pendulum P7 (compare Figs. 7.8 and 8.2), we can see that such periods respond with the 'relaxation' phase of the stress field (see Chapters 7.1 and 7.2). Nevertheless catastrophic earthquakes with M>7.5 were observed in that period. The most powerful was the Sichuan earthquake on May 12, 2008 (M=7.9), with its epicentre far from where the Eurasian plate contacts other plates. On the other hand, the most powerful earthquakes that were observed during periods with dominant tidal periods in the spectrum on pendulum P7, were at the contacts of ocean lithosphere plates with our Eurasian lithosphere (Indonesia 2008, Sumatra 2009).

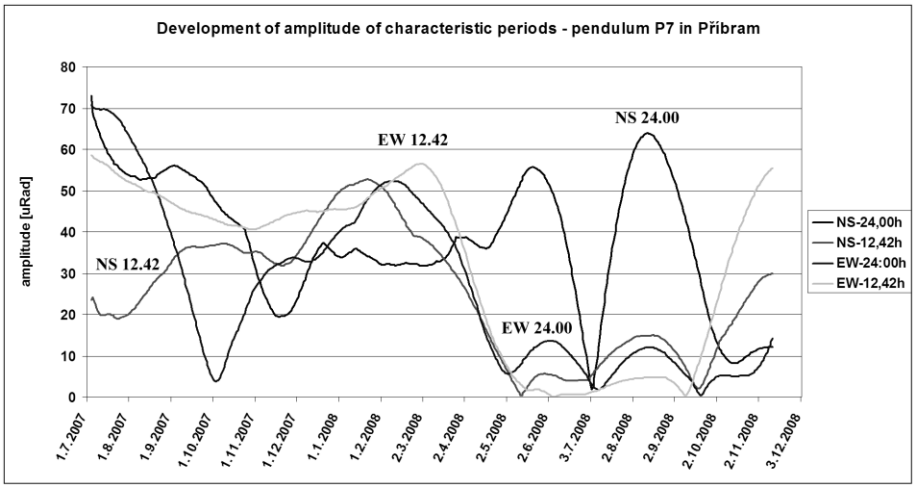

Fig. 7.8: Development of amplitude of characteristic tidal and non-tidal periods.

The development of amplitudes of tidal or non-tidal periods in the spectrum of tilt provides us with information regarding the mechanisms that are generating the stress changes, and where the stress concentrator is probably located. If the diurnal non-tidal periods are observed, then the main mechanism is probably generated by solar irradiation of the continental crust (see Chapter 3.5). If the semidiurnal tidal periods are mostly observed in the spectrum of tilt and their amplitude is higher than a

theoretical one, the collision between oceanic and Eurasian plates is the mechanism responsible for such tectonic stress generation.

In contrast to the circadian periods, longer periods (days or weeks) were observed (see for example Figs. 7.5, 8.2 or 10.16). Such periods were observed mostly before very powerful earthquakes. We referred to them as 'stress waves'. C. Doglioni (1993) or E. Khalilov (2009) called them 'tectonic waves'. Their time of occurrence and their behaviour indicates that they are being generated near the focus area of future mainshocks, when the asperities are destroyed. The destruction, however, need not be by seismic events. It can be by creep, silent earthquakes, tremors (see Fig. 6.8), or micro earthquakes (see Fig. 6.9). The 'stress waves' can also show pulse character (see Fig. 10.17 or 10.19).

The longest observed periods have lengths comparable with one year. The almost three-years long measurement of pendulum P7 in Příbram showed that the general tilt from spring to autumn was towards the north (relaxation period) and the noise was smaller than during winter, when the tilt was generally towards the south (compression period) (see Fig. 8.2). This annual drift of the pendulum in Příbram was opposite to that observed in Grotta Gigante near Trieste (Zadro & Braitenberg 1999, Braitenberg et al. 2006). The development of the variation of tilt (noise) was in agreement with the development of microseisms during one year (Zátopek 1941, Kárník & Tobyáš 1961). Such an annual cyclic development of tilt and noise of pendulums can show on the mechanism of their generation by a thermoelastic wave with an annual period as described by Hvožďara et al. (1988). However, diurnal thermoelastic waves amplitudes are orders higher, because annual thermoelastic waves penetrate much deeper than diurnal thermoelastic waves.

8. COMPARISON OF PENDULUM MEASUREMENT WITH OTHER METHODS

It is necessary to compare the results of measurements with other methods to describe the stress state with greater clarity and detail, because no one method can describe the reality of its complexity and our deformometry method, based on the measurement of only two parameters. We compared our pendulums tilt data for the 2007-2009 period, discussed in Chapter 7, with other methods. We used the year 2007 because no other year was covered by a number of methods. We used the data from 3D crack gauges that were installed on active faults in caves in the Bohemian Massif (Briestenský et al. 2007a), data from water level measurement in wells in Eastern Bohemia (Stejskal et al. 2007), strainmeter data from Vyhne, Slovakia (Brimich 2006), and data from an absolute gravimeter on Pecný (Pálinkáš 2006, Pálinkáš et al. 2008) (see Fig. 8.1). We used the data from two seismic areas – Nový Kostel seismic swarm area (Horálek & Fischer 2007, Zedník 2007), and the Police basin (Zedník 2007).

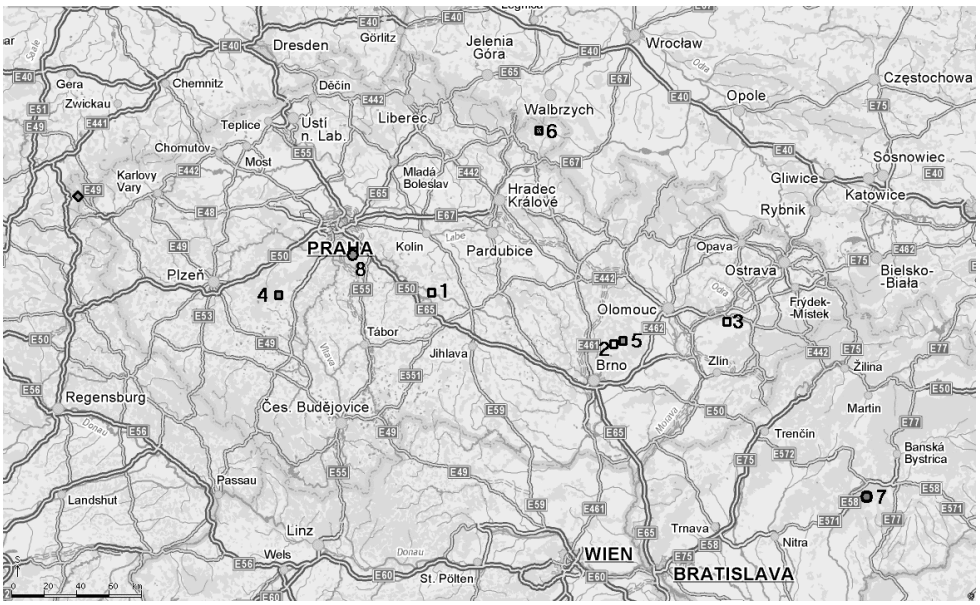

Fig. 8.1: Instrumented localities and boreholes.

3D crack gauges – light squares (1-Šeptouchov, 2-Pustožlebská, 3-Zbrašov); vertical pendulum clinometers – red squares (4-Příbram, 5- cave No.13C); boreholes – dark squares (6-Police Basin); strainmeter – blue circle (7-Vyhne); rhombus (Nový Kostel seismic zone), absolute gravimeter – red circle (Pecný).

8.1. Comparison with Tiltmeters and Tidal Stations

The tiltmeter, installed in Grotta Gigante near Trieste in 1959 (Marussi 1959), measures parameters that are similar to the ones measured by our vertical static pendulum. However, it is based on the horizontal pendulum principle and only the long vertical baseline is comparable. Its registration was analogous with 1 hour sampling until 1996, which has been reduced to the rate of 1 sample per day after application of a low-pass anti-alias filter (Breitenberg et al. 2006). Actual data, sampled with frequency 25 Hz (Breitenberg 1999), was not available to us and so we compared our data with only the general annual variations of tilt. The tiltmeter in Grotta Gigante shows periodic annual motion in the NE-SW direction with maximum tilt in March – April (ENE) and in October – November (WSW). Such tilt motion has the same phase as was observed on pendulum P7 in Příbram (see Fig.8.2). However, there is a problem in that the two motions are in opposite directions. That might be associated with the geometry of pendulum P7, which hangs in the northern corner of chamber in Prokop mine in Příbram (see Fig. 5.2).

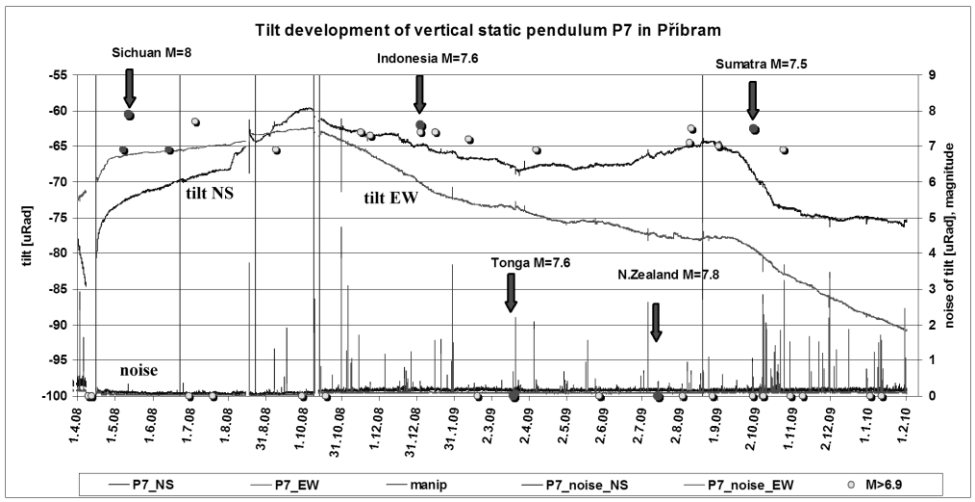

Fig. 8.2: Tilt development of vertical static pendulum P7 in Příbram in 2008 and 2009 and strong earthquakes with M≥6.9.

8.2. Comparison with Strainmeters and Water Table Levels

Horizontal strainmeter, installed in granite rocks in the gallery of St. Anthony of Padua (Hvožďara et al. 1988), would have to react to horizontal stress changes in a similar way as a plumb line measured by vertical static pendulums. When we look at the results of measurements in Vyhne during 2007 (Brimich, pers. comm.) (see Fig. 8.3) we can see that the strain has similar annual motion as the tiltmeter in Grotta Gigante or pendulum P7 in Příbram with extremes of strain in March (compression) and in October – November (extension).

Strainmeter 'noise' defined as the difference between two subsequent values of strain shows the same annual progress as microseisms with its maximum in the beginning of winter and its minimum in the beginning of summer. It shows that during the winter (period of rock mass extension), the strength limit is reached in microscale, which generates the microcracks, creep or microseisms. The noise is higher during periods of coming seismic waves as well (see the vertical abscises on the Fig.8.3), or, it can form groups with slow increasing and decreasing of its amplitude. The periods of increasing noise can be interpreted as periods of higher stress than average (as for example in the period from September 1 to October 5, 2007).

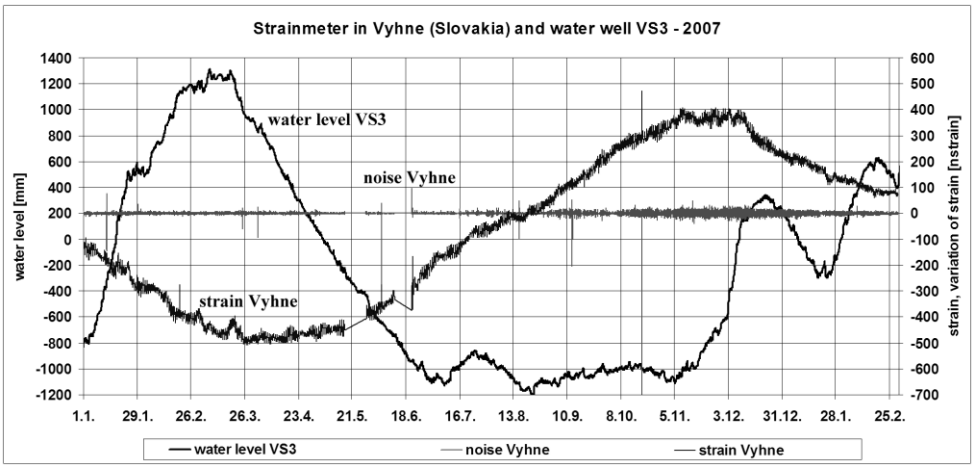

Fig. 8.3: Strain in Vyhne and water level in well VS3 development in the year 2007.

A second possible way to identify periods of increasing stress in the rock mass by strainmeter (in addition to noise analysis) is to look for periods of higher than average strain in the sense of its dilatancy. We did not find many periods like that during 2007 because most of the anomalous strain periods showed the extensions of the rock mass rather than compression (for example around January 21, March 2, March 20, 2007). The periods between August 21 and September 20 and days around November 11, were periods of higher stress than average, when the actual development of strain diverged from the smoothed sinusoidal annual development of strain.

If we suppose the rock having Young's module $E = 3x10^4$ MPa, then we can assess that the stress in the areas varies during one year by about 30kPa on the basis of the annual motion of strain with a peak-to-peak amplitude of 1 μstrains. Such variations of stress are enough to cause some parts of rock mass to exceed their strength limit during winter and during increasing tectonic stress periods.

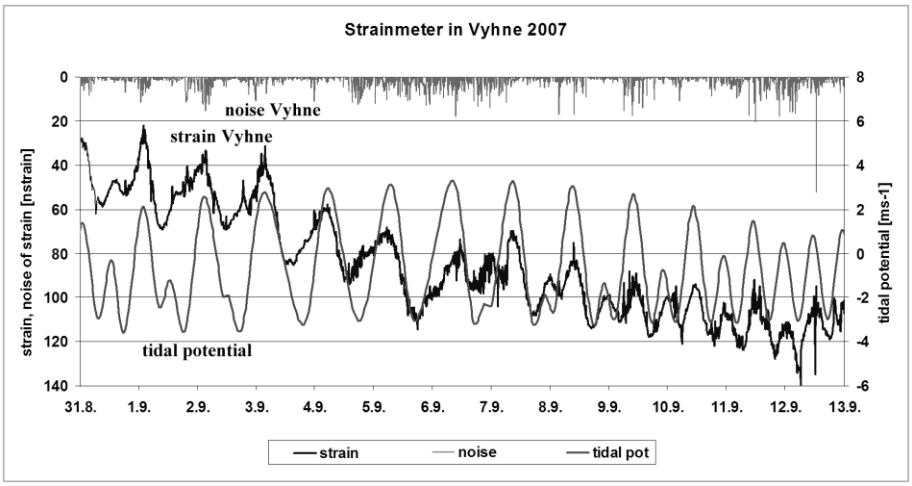

Fig. 8.4: Development of strain in Vyhne in September 2007.

If we compare the development of strain with the theoretical development of tidal potential on a short-time scale (see Fig. 8.4), we can state that they are similar with a high coefficient of correlation. In the vicinity of the gallery of St.Anthony of Padua the diurnal strain variations are between 20 and 50 nstrains, with corresponding variations of stress on

the order of 1 kPa. Such stress variations cannot lead to faulting, but it can produce micro deformations of the rock mass, creep, and microseisms triggering during higher stress periods. This can easily be seen on Fig. 8.4 with the development of noise, which has the same periods as the tides (periods from September 1 to September 3 with maxim around midnight and between September 8 and September 12 with maxim around noon).

Water levels in the wells VS-3 and V-34 in Eastern Bohemia have been monitored for more than 2 years. The precision of these water level readings is 1 mm and the sampling period is 10 minutes (Stejskal et al. 2007) (see Fig. 8.1). The water levels show significant annual variations (see Fig.8.3). We choose for our next analysis only the well VS-3, because the water levels in wells VS-3 and V-34 show similar development. The reaction on the external forces was higher for VS-3 than the reaction of well V-34, which does not show any similar anomalies making it suitable as a reference object for monitoring of water level variations that can be considered independent of natural hydrological regime (see Fig. 8.3). The atmospheric pressure effects were compensated according to Rasmussen and Toll (2007). The rainfalls caused an increase in water level in VS-3 on January 19, March 2, July 10, August 21 and especially December 3, 2007. Probably such rainfall triggered at least the first two of three anomalous changes in the underground water level in the borehole VS-3, which had been registered during the year of 2007 (see Fig.8.3 and 8.5). The anomalies are of a sudden jumping character known from earlier years of monitoring. Similar variations are absent in the well V-34 and any coincidence with other outer climatic and hydrological factors can be, therefore, excluded. A more detailed description of observed anomalous water level variations can be seen with the following:

- *11.07.2007, between 11:00 and 15:00 hr UTC*. Sudden jump in GWL by 57 mm was registered.
- *23.08. – 24.08.2007, between 22:00 and 02:00 hr UTC.* Sudden jump in GWL by 72 mm was registered.
- *6.09. 2007, between 05:00 a 16:00 hr UTC.* Sudden jump in GWL by 56 mm was registered. Increase was considerably slower compared to previous cases and developed during 11 hrs.

The anomaly, registered on September 6, could have been triggered by rainfall or by tectonic stress increase.

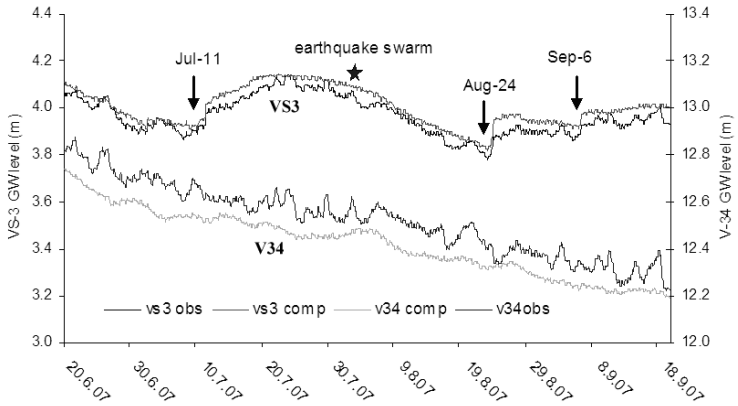

Fig. 8.5: Underground water level variations in boreholes VS-3 a V-34.
Anomalous changes in VS-3 are marked with arrows and dates; obs - direct observation, comp – direct observations compensated to exclude the effects of atmospheric pressure.

The annual development of water level has nearly the same cycle as the rock mass strain in the Vyhne. In the time of the compression of the rocks the water level showed that the reservoir was compressed and the water level was rising. In the time of dilatation of rocks the reservoir was extended in its volume and the water level in the well was getting lower. This annual variation of water level in the order of 2 m showed that the pressure in the reservoir changed in the order (range) of 2 kPa.

8.3. Comparison with Crack Gauge TM71

Long-term monitoring of rock massif deformations is currently being performed with the use of a 3-D **crack gauge TM71** (CS Patents Nos 131631 and 246454, author Košťák, B. – Inst. Rock Structure and Mech, Czech Ac. Sci) in many places in Central Europe (Stemberk et al. 2003). For our next analysis we used only crack gauges that had been placed in the caves in the Czech Republic (see Fig. 8.1):

Cave Šeptouchov – A crack gauge TM71 was installed in a lenticels body of crystalline limestone found in a paragneiss complex at a depth of about 15 m under the surface (Homola, 1952, Skřivánek 1972, Cícha,

1991). Major tectonics in the cave is represented by NNW-SSE striking faults. One of them is instrumented.

Cave Pustožlebská – A crack gauge TM71 was installed on Macocha Fault (NW-SE) in Vilémovice limestone strata (Kadlec et al. 2001) at a depth of about 110 m under the surface.

Cave Zbrašov – There are three crack gauges TM71 installed in this aragonite lime cave on a NW-SE fault (Kadlec et al. 2001) in Devonian limestone about 50 m under the surface.

The deformations are registered as displacements on rock massif dislocations. The instrument works on the principle of mechanical-optical interference and has a sensitivity in the range of 0.05 to 0.0125 mm in all the three Cartesian co-ordinates in space. Sensitivity to rotation is $3.2\ 10^{-4}$ rad. In case of hard rock massif the instrument is mounted with the use of thick wall steel tubes ∅ 40 to 60 mm into core runs made to sidewalls of the selected dislocation. The core runs of depths of 300 to 500 mm of solid rock are adapted to local conditions. The instruments are then installed between two tube consoles fixed in the core runs (Stemberk et al. 2003).

Making measurements involves making a photocopy of the interference picture using a special paper or a digital camera.

Four anomalies of displacements (signed 1 – 4 on the Fig. 8.6) were recognised during 2007 (Stemberk et al. 2008). On the other hand, when speaking about anomalous displacements we refer to those that have been observed in previous years.

In the Šeptouchov Cave, interval Nos. 1 and 2 produced sinistral displacements, which represented lifts of the NE block with respect to the SW block. The lifts reached about 0.2 mm combined with compression on the fault. At the same time Pustožlebská Cave indicated dextral displacements of 0.04 - 0.05 mm with the NE block subsidence in respect to the SW block. Both caves produced fault compressions of 0.05 – 0.15 mm. In the same intervals Zbrašov Cave registered sinistral displacements of 0.02 mm combined with lifts of the NE block in respect to the SW block by 0.13 mm and 0.02 mm, respectively.

During the interval No. 3 all of the gauges registered vertical displacements principally, i.e. subsidence of the NE block with respect to the SW block. The subsidence in Šeptouchov was 0.36 mm, and in

Pustožlebská 0.11 mm, while the opposite was found in Zbrašov. In detail: gauge Zbrašov3 - 0.42 mm and gauge Zbrašov1 - 0.27 mm. All of the gauges registered extensions 0.01 - 0.1 mm. Besides this, the rotational movements 0.03 - 0.04 grad were observed during these interval at all of the cave measurement points in horizontal and vertical planes.

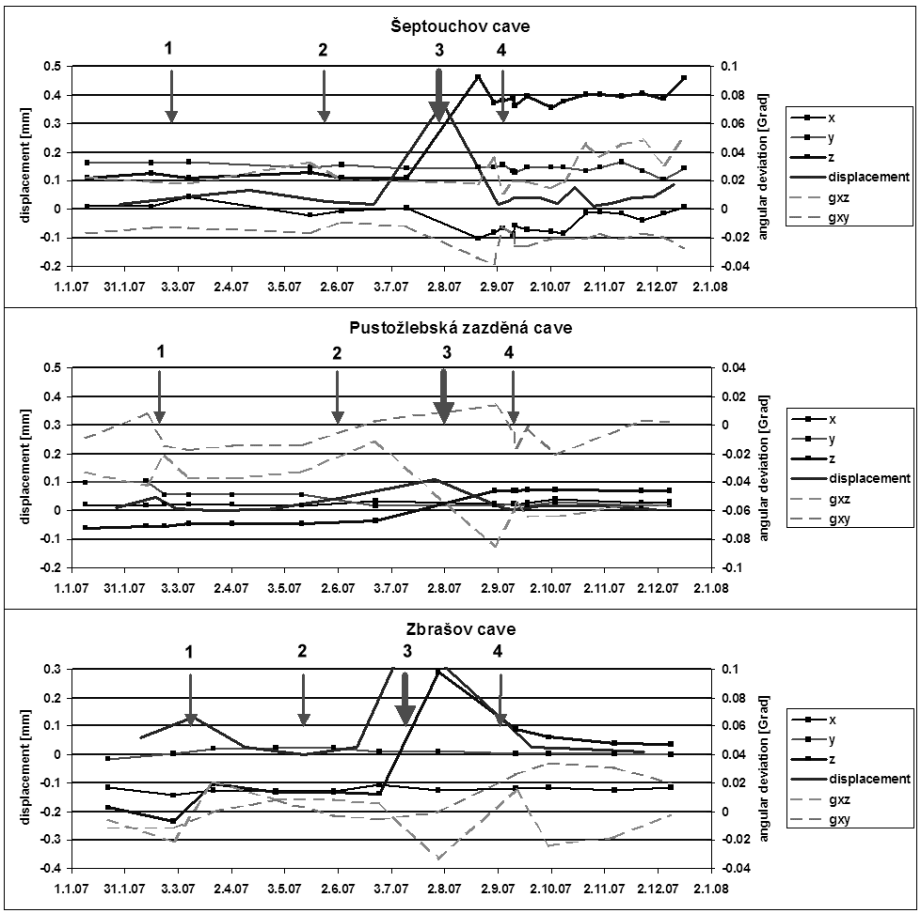

Fig. 8.6: Deformations and displacements registered on faults in caves by the gauge (according to Stemberk et al. 2008).

The interval No. 4 provided special S-like (Shanov 1993) movements of amplitudes 0.01 – 0.03 mm with the exception of Zbrašov.

8.4. Comparison with Absolute Gravimeter

The absolute gravimeter SG-050 has been in operation on Pecný since 2007 (Pálinkáš et al. 2008). Temperature, atmosphere pressure, precipitations and soil humidity are measured in parallel with gravity to correct the gravity data on these external-perturbing influences. An annual variation of gravity was detected by analysing a series of gravity measurements by FG5 absolute gravimeter between 2001 and 2005 (Pálinkáš & Kostelecký 2005). The amplitude of this annual gravity variation is 27 nms^{-2} and the maximum gravity value appears at the beginning of March. To explain seasonal variations in gravity, effects of the ground water level and soil moisture have been computed. After applying corresponding corrections, the dispersion of the reduced gravity series decreased by about 45 %.

This annual drift in the gravimeter readings corresponds with all the other methods: tilt measured by pendulums, strain in Vyhne, and the water level measured in Police Basin.

The data from supraconducting gravimeter SG-050, sampled in 5-minute intervals, was corrected for atmospheric pressure variations and tides. Although the short-period variations of atmospheric pressure were compensated optimally, the long-period variations of atmospheric pressure can easily be seen in the residual gravity data (see Fig. 8.7). Rheological features of the rock mass can cause such imperfect compensation, mainly due to anisotropy. In spite of such imperfect compensation for the external influences, the anomalous variations of gravity are visible with the residual gravity data. The largest anomaly can easily be seen from September 6 to October 12, 2007.

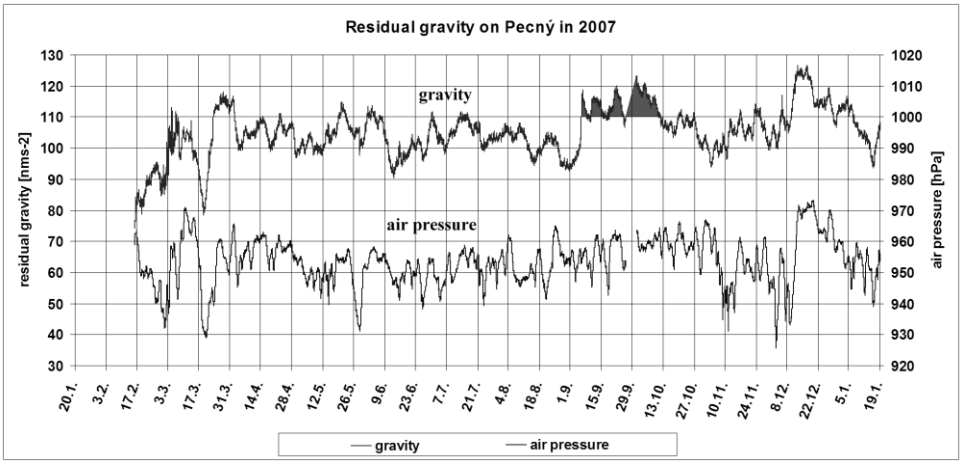

Fig. 8.7: Development of residual gravity on absolute gravimeter SG-050 on Pecný.

8.5. The common result from comparison of various methods in 2007

Generally, the results acquired with the use of all the methods in question show that the Central European stress field bears a uniform character and all the instruments installed at places, even hundreds of kilometres apart, may identify its parallel changes. The reactions will be different and dependent on the method used.

Regarding the year 2007 as a whole, one can observe some yearly cycle in superficial Earth zones. It is best observed with the Vyhne strainmeter data. At the beginning of the year it appears with compression and later in the year with extension followed by increased noise (see Fig. 8.3).

Individual short-term stress changes (impulses) can be identified in this yearly cycle. Changes have different characters in different sites and devices. Recorded stress changes are observable from a few days to about one month. Only devices with a quasi-continual record register shorter changes with durations of several hours, which largely coincide with seismic waves radiating outward from far earthquake foci (e.g. Sumatra, September 9th 2007, Ms = 8.5). Longer periods of stress changes, described subsequently, can be recorded by a majority of the devices and

local seismicity in the Western Bohemia seismic swarm area (Horálek & Fischer 2007, Zedník 2007) (see Fig. 8.8):

Event 1 - *second half of February until the beginning of March 2007.*

Crack gauges in all localities indicated a side movement with compression. This correlates well with the maximum of increased noise on pendulum P1 in Příbram on February 14 and March 2, 2007, as well as with increased movement to S, which indicated stress increase. Groundwater level indicators in Police Basin indicated maxima on January 1, February 2 and March 15, 2007. Simultaneously, the Nový Kostel observatory reported one of the most extensive seismic swarms of 2007 with maxima on February 9 and February 16, 2007 (M=2.1).

Event 1a – *second half of May until the beginning of June* 2007.

This stress impulse was of lower intensity and produced low displacements with compression on gauges in Šeptouchov and Pustožlebská caves. Pendulum P1 indicated moderate relaxation in the massif. At the time of maximum gauge reactions (May-June), only large solitary seismic effects were observed (May 21 and June 7, 2007) at Nový Kostel with magnitudes up to 2.5.

Event 2 – *second half of June until the beginning of July 2007.*

In this period the pendulums marked the start of side compression from E (from June 11, 2007) with maximum side compression and maximum anomalous deformations (June 21 and July 4, 2007). A larger seismic swarm was indicated in the Nový Kostel area (June 20 until June 24, 2007). No anomalous movement of groundwater level was observed before July 11, 2007.

Event 3 – *the end of event 2 (second half of July until the beginning of August 2007).*

This is a period of the most extensive movements on 3-D gauges in all the caves. They showed coincident extensions and vertical movements on investigated fault fractures, which indicated a decrease in horizontal stress. Such a decrease in horizontal stress was indicated on all pendulums, both in

the decrease of noise and the relative relocation to N, i.e. against the normal stress field. At that time the water level indicator V-34 showed a maximum groundwater level increase. This was connected with increased rain precipitation from June 22 to July 10, 2007. Another seismic swarm was registered at Nový Kostel on August 8, 2007. Additionally, several days before that, on August 3- 4, 2007, the most extensive seismic swarm in the Police Basin was registered.

Event 4 – *the beginning of September 2007.*

This stress wave produced the most exotic movements, i.e. dissimilar to previous ones, as well as maximum rotations on gauges (Šeptouchov Cave). The pendulums showed a uniformly anomalous stress increase with relocations to S and W. Such movements began with the observations of August 27 until September 3, 2007. Deformations reached maxima between September 7 and September 20, 2007. The Vyhne strainmeter showed increased noise with maxima between September 6 and September 12, 2007, i.e. just at the time of a Sumatra earthquake. The event might have initiated even the small seismic swarm recorded in Nový Kostel from September 12 with maximum on September 21, 2007. Abrupt changes appeared in groundwater level data in the Police Basin Well VS-3 (August 24 and September 6, 2007). This stress event was the most extensive in the year 2007. It was observed with almost all of the instruments including the absolute gravimeter on Pecný and might be connected with the Sumatra earthquake, Ms=8.5 indicated on Fig.7.4.

Event 4a – *a short event round October 19, 2007.*

A stress wave was registered on the Šeptouchov gauge. Noise also increased on pendulum P7 in Příbram and in Vyhne. Extensive solitary events also appeared at Nový Kostel. However, pendulum movements did not show any special inclinations, i.e. neither to S nor to W, which often indicates tectonic pressure from N or E, respectively.

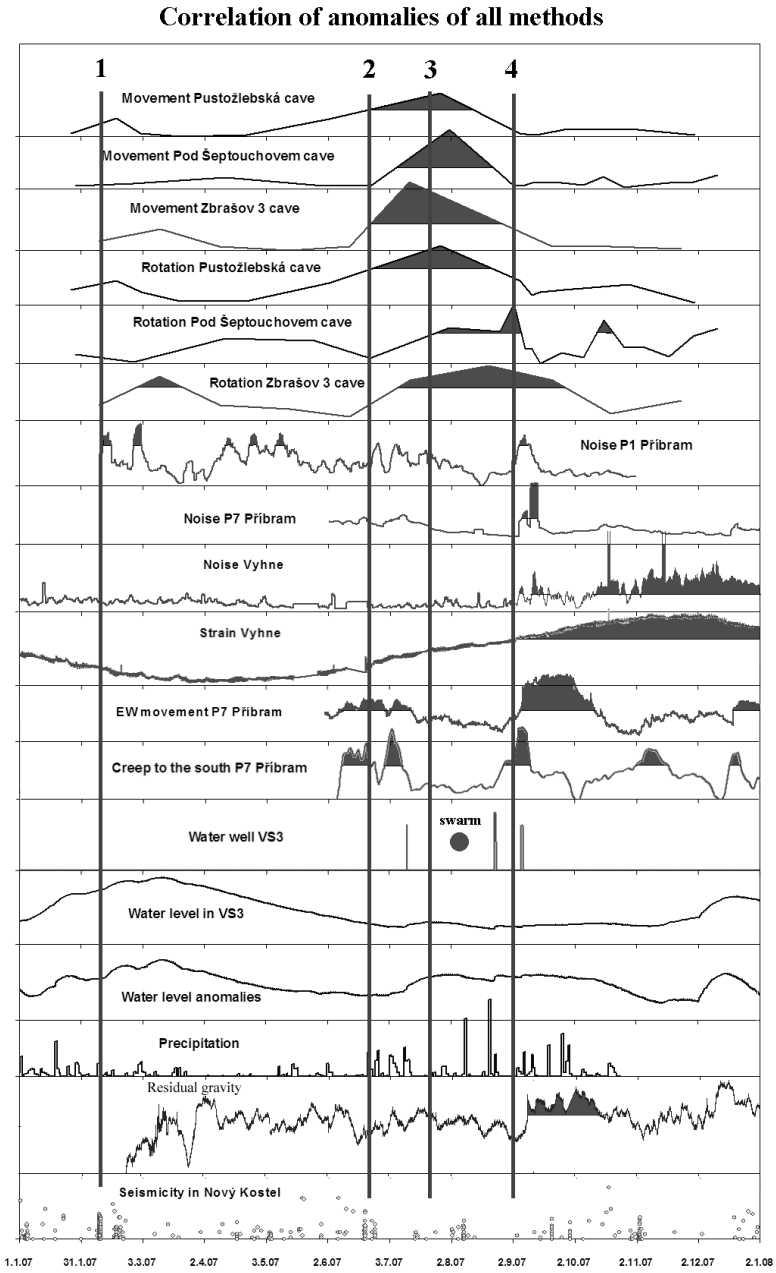

Fig. 8.8: Correlation of anomalies of all methods.

Generally, it is possible to say that, on the basis of the comparison of several methods, all of them show the same annual periodical variations of stress with its maximum in winter and its minimum in summer. All of the methods were able to detect anomalous periods of increasing or decreasing stress in the general stress field. The anomalous periods of stress varied from several days to several weeks. Some of the stress anomalies appeared in the form of peaks or short pulses that had durations of several days.

The horizontal movement on faults manifested in the increasing stress. In contrast, the vertical movement of normal faults accompanied decreasing stress. Vertical static pendulums were able to detect the anomalous periods of stress through the detection of anomalous tilt and increases in noise. The gravimeter data showed that in the periods of increasing stress, detectable increase in gravity was observed, which could be the result of increasing density of the rock mass.

The most significant anomaly was observed in connection with the nucleation stage of the catastrophic earthquake that occurred in Sumatra on September 12, 2007 (Ms=8.5). There is a question regarding to what extent the maximum stress wave registered in 2007 could be affiliated with that catastrophic Sumatra earthquake of 12.09.2007, M_s = 8.5. Regarding the noise analysis of the Příbram pendulum inclinometers, the wave originated around the date of September 6, 2007 when the Taiwan earthquake (Mw=6.5) occurred, with foreshocks appearing from September 3, 2007. This would indicate a global tectonic lithospheric plate process.

No single period of increasing stress was observed before major earthquakes that occurred in the South America lithosphere plate. In contrast, major earthquakes were observed during the relaxation periods (decreasing stress periods) in Central Europe.

It is possible to predict earthquakes, placed on one lithoshere plate, when this plate is monitored using deformometry and other methods.

9. MECHANISM OF PLATE MOVEMENT, EARTHQUEKS PREPARING AND TRIGGERING MODEL

Choosing the systematic attitude for earthquake prediction and not only ad-hoc from case to case, we must try to determine: what processes take place before the earthquake, what type of forces are involved, what the triggering mechanism might be, what the strain stage looks like, and what is taking place in the rock layers that are disrupted during the earthquake. So we need to create a theory model for what processes are involved and how the energy is released. Measured data should always be compared with the proposed theory model. That will help us interpret the data, as the theory model will provide us with a guide for explaining the observed phenomena.

9.1. Westward drift of lithosphere plates

Today the fundamental dispute is about whether the movement of lithosphere plates is caused by mantle convection drag, or if the plates move because of other, still unexplained, reasons. If today's science wants to deny the possibility of the movement of plates by external forces, it only uses the weakest exogenous forces like the earth or ocean tides, Eötvös force (Eötvös 1913) and the differential rotation of the Earth spheres. It 'refutes', numerically, the ability of exogenous forces to cause the movement of the plates. And so it wants to confirm that convection cells in the mantle must cause the drag of plates. Unfortunately, the convection cells in the mantle have not been detected by anyone using any of the available methods. And nobody has confirmed that the convection currents in the mantle drift the lithosphere plates. These convection cells in the mantle and other mechanisms are still only hypotheses and are at the level of theoretical models (Tosi, 2007). Anderson and Dziewonski (1984), Anderson (1988) and Dziewonski and Anderson (1984) pointed to the fact that the relatively hot areas in the upper mantle at depths of 200-400 km do not correspond to the area of the molten material in the convection cells.

Jeffreys proved that in theory, the viscosity of convection streams driven by thermal convection would be so high that the streams would be quickly stopped.

Scaler (2003) showed that the stress of lithosphere plates in the so-called 'triple points' where the three boards meet, is quite different from the idea of tension or pressure caused by convection streams in one direction.

According to Kery and Vine (1996) the height of the geoids above the reference ellipsoid does not agree with the presumption of the output of magma in convection currents in the areas of mid-ocean ridges and rifts. Pratt (2003) published many other arguments in his review work. These disagreements led Owen (1983) to submit a theory of the expanding Earth, which explains observed discrepancies in the alternative way. Only recently, the development of satellite geodetic observations has enabled to us to demonstrate an exact mutual movement of the lithosphere plates against each other (DeMets et al. 1990). There is no room for interpretation for theories of the expanding Earth or surge tectonics (Mayerhoff et al. 1996).

The global westward drift of the plates has been detected from a fixed Antarctic plane reference frame (Bostrom 1971, Knopoff and Leeds, 1972) and from a hot-spot reference frame (Richard et al. 1991; Gordon 1995). A recent measurement of the movement of lithosphere plates by means of GPS shows that global distribution of the plate velocities and seismic activities tends to decrease towards the poles (DeMets et al. 1990) (see Fig. 9.1).

The westward drift of the oceanic crust and of the lithosphere plates therefore exists. But until now no mechanism for their movement has been found.

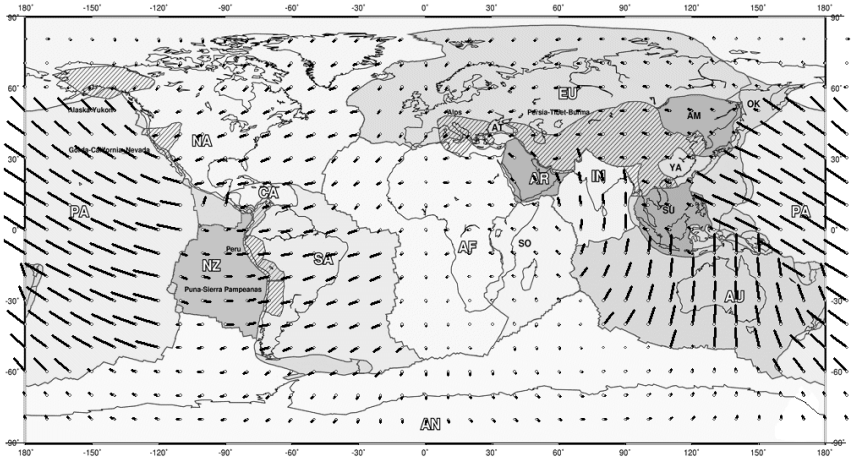

Fig. 9.1: Relative drift of lithosphere plates with respect to all hot-spot frame (map DGFI).

First, we will describe what the hot-spots are and what their properties are. That will consequently help us to elucidate the relation and mutual lithosphere movement against the mantle and also different lithosphere plates against each other.

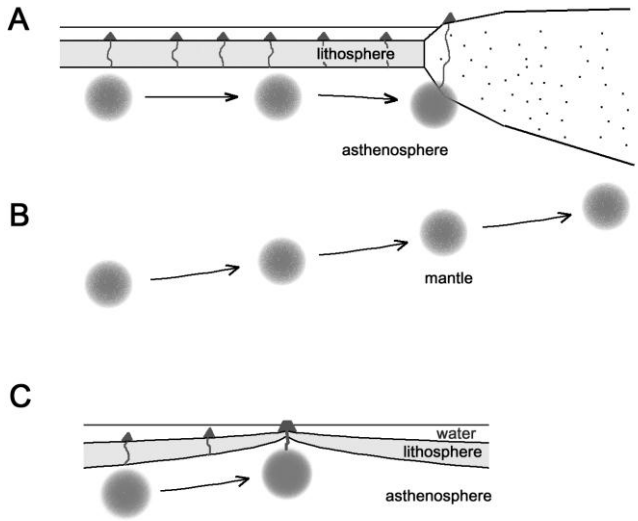

Fig. 9.2: Relative motion of hot-spots with regards to the lithosphere.

Hot-spots are warmer regions in the mantle with lower densities than average. They partly or fully melt their surrounding mantle and ascend until they strike the solid lithosphere (see Fig. 9.2 A,B). The shallow origin of hot-spots is evidenced by Doglioni et al. (2005).

'Melting through' the crust only occurs where volcanoes are created, because the solid lithosphere prevents the hot-spots from moving further upwards. The chain of volcanoes is created on the surface, because the overlying crust moves against the hot-spot and the hot-spots are surrounded by the asthenosphere against which they do not move. Among the most well known is the Emperor-Hawaii volcanic chain or the Yellowstone. If we compare trajectories of hot-spots marked by these volcanoes and date them, we find that many of them show very similar velocities of hot-spot movement against the lithosphere, as it is e.g. in most of the Pacific plate hot-spots. An explanation could be that all those hot-spots are 'anchored' in the mantle above which the lithosphere moves with the same speed (Doglioni 1993).

However, some hot-spots have lower velocities of their apparent movement. And others do not move against the surface at all. The common

feature of these hot-spots is that they are either placed below the thin lithosphere, especially below the rift zones (see Fig. 9.2c), or they drifted until they were caught below the thicker continental shelf (see Fig 9.2a). Typical examples of the hot-spot capture in the middle of the rifts are e.g. Iceland or Galapagos (see Fig. 9.3a,b). Some deeper hot-spots in the mantle, which did not ascend sufficiently high, could continue moving even beneath the continents (e.g. Yellowstone hot-spot) (see Fig. 9.2b), where they were consequently captured in some of the traps, for example the hot-spots in East African Rift.

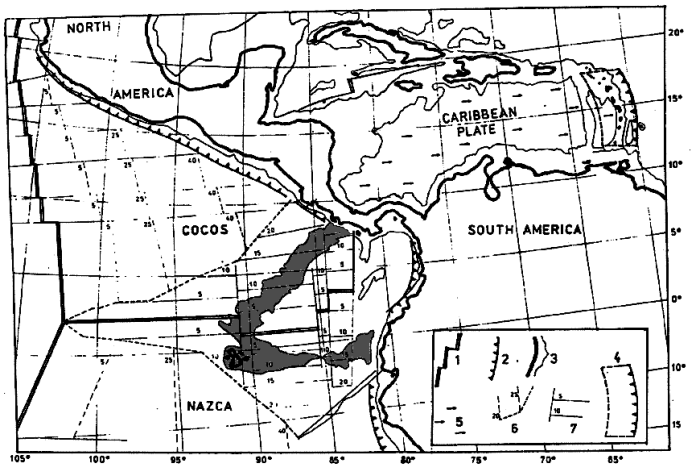

Fig. 9.3a: Hot-spot Galapagos depicted on crossing of two rifts with two volcanic chains: 1 – rifts, 2 – subduction, 3 – shoreline, 4 – subduction zone and schematic contour of submerged plate, 5 – direction of mantle flow, 6 – izochrones (Hey and Vogt 1977).

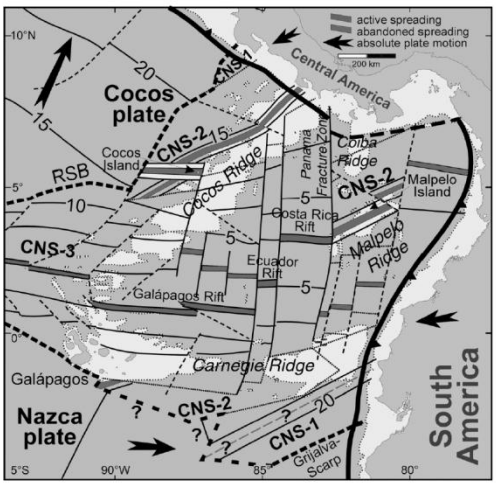

Fig. 9.3b: Hot-spot Galapagos captured on the crossing of two rifts with two volcanic chains (Meschede & Barckhausen 2000).

It is possible to state that hot-spots, together with the mantle, can easily move against the lithosphere when it has a sufficiently flat bottom. They can move even more easily in cases where the thickness of the lithosphere thins in the eastward direction towards the mid-ocean rift. In other words, the hot-spot tracks can be created only if the directions, where the lithosphere is flat or thins, are in agreement with the direction of

the possible hot-spot movement. Any other hot-spots will move only with a smaller velocity than the mantle relative to the lithosphere, down to zero velocity (Ostřihanský 1997).

Correlation of 'quick' hot-spots trajectories, even over large distances, shows that not only does the lithosphere retains its geometric shape but also the same is true for the asthenosphere and the mantle beneath. This means that there are not streams with different velocities of movement against their environments, but the opposite. The asthenosphere and upper mantle are in comparison to other parts of the mantle 'relatively static' and only the lithosphere moves above them. For this reason hot-spots can be used as a reference frame for the estimation of actual movements of plates. This frame is then bound to the Earth as a whole supposing that similar 'slippages' as those between the lithosphere and the mantle can exist as well as between the mantle and the core, and the core and the internal core (Scoppola et al. 2006).

The frame of shallow, relatively fast moving hot-spots, was chosen by Doglioni et al. (2005) for the analysis of the relative velocities of the lithosphere and the mantle. Their result shows that all plates move to the west with respect to the mantle including the Nazca plate, which we used in our previous study as a suitable reference frame with small or no movement (Ostřihanský 1997). With this frame the Antarctic lithosphere plate moves as well, although it was used as the reference frame by Knopoff & Leeds (1972), however, its speed is small (Crespi et al. 2007). So, the conclusions of all these works are similar.

The conclusions of all of the studies that the lithosphere moves in a westward direction above an immovable mantle can also be demonstrated by the examination of **other effects**:

- asymmetry of subduction zones,
- geoids height,
- Euler´s poles of lithosphere plates.

As the oceanic crust grows in rifts on both sides, the westward drift creates an asymmetry of rifts not only by the topography but also by physical parameters of a new crust (Doglioni 1993, Panza et al. 2009, Husson et al. 2009) (see Fig. 9.4). The proposed east-west coupling is also supported by the observed melt production under the East Pacific Rise,

which is asymmetrical towards to the west (MELT 1998; Toomey et al. 1998). The eastward propagating density deficit in the asthenospheric mantle from the rift zone could account for this asymmetry and explain the results of mantle tomography (Dolgioni et al. 2003).

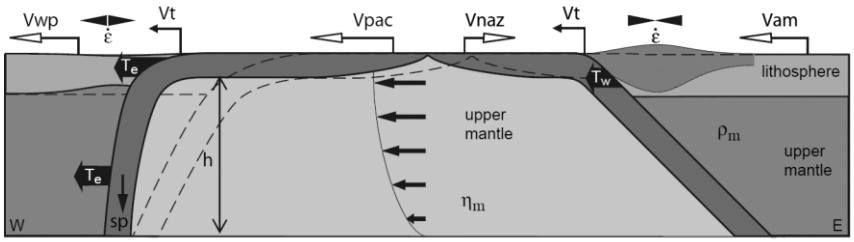

Fig. 9.4: Kinematics of the Pacific domain. Black and grey arrows indicate trench and plate velocities in the hot-spot reference frame, respectively (taken from Husson et al. (2007) and modified).

Not only the oceanic rifts, but the rifts on continents have important different geodetic and petrologic characteristics on both sides (Doglioni et al. 2003). The accumulations of masses against the direction of lithosphere movement are distinctive, therefore they are placed mostly on the eastern (NE, SE) wings of rifts.

Also subduction zones on both sides of the ocean have quite different characters (see Figs. 9.4, 9.5 and 9.6). The subducting plate has a characteristic shape. On the western margins of the oceanic subducting plate the dip of its merging is bigger than on the eastern margin. And very often its fracturing and repeated merging occurs, occasionally not under the continental lithosphere, but under the new oceanic crust during the formation of back arc basins (see Model 2 on Fig. 9.5). Sometimes even a total separation of the broken and merged part of the oceanic lithosphere occurs, which then seemingly returns back beneath the merging plate. It is remarkable that back arc basins do not exist in subduction zones dipping towards the east. If they had existed they would have been overridden by westward moving continents (see Model 3 on Fig. 9.5). In all cases liquefaction and liquidation of the oceanic crust occurs upon its contact with the neighbouring plate or with the older remnants of the oceanic plate. In the case of Model 2, the liquefaction and liquidation of the oceanic crust occurs even on both sites at the same time (more details in Ostřihanský 1997).

Kalenda, P., Neumann, L., et al. Tilts, Global Tectonics And Earthquake Prediction, SWB 2010, London.

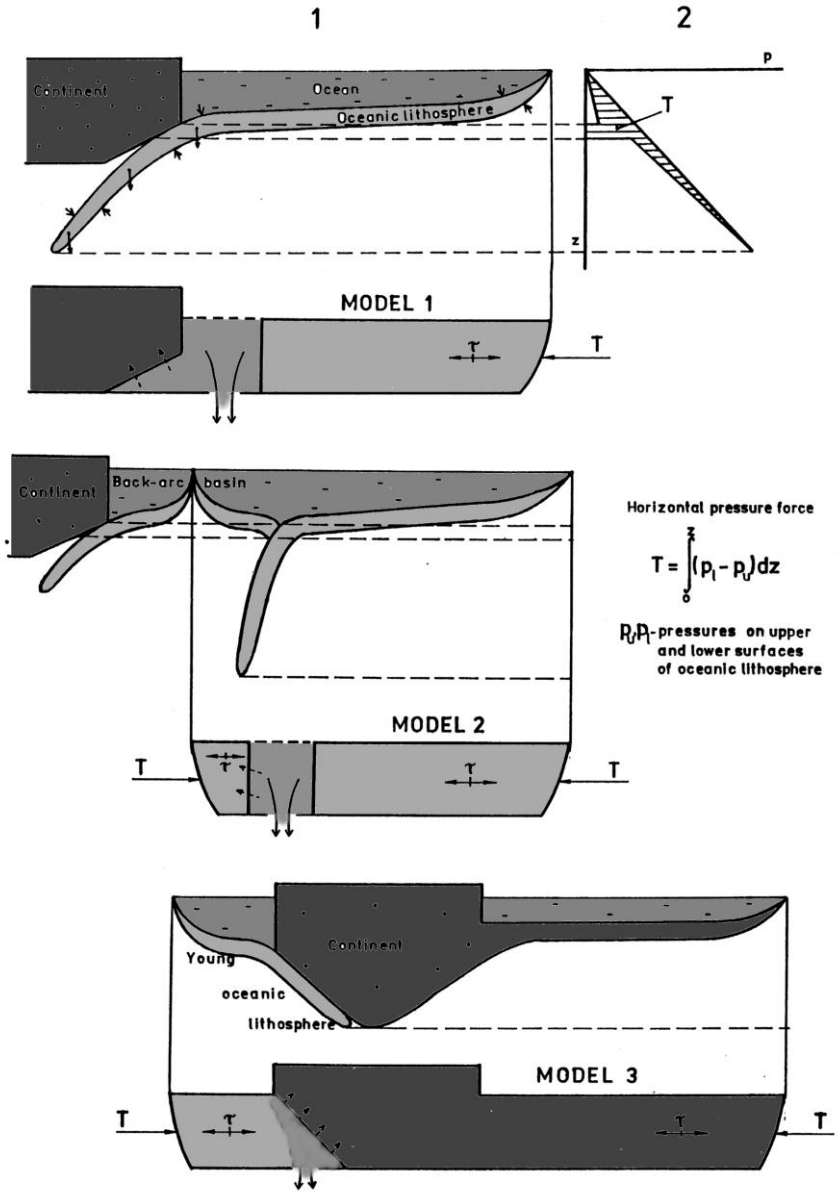

Fig. 9.5: Models of liquidation of oceanic lithosphere. (Ostřihanský 1997) Arrows mark the direction of prevailing stress and friction.

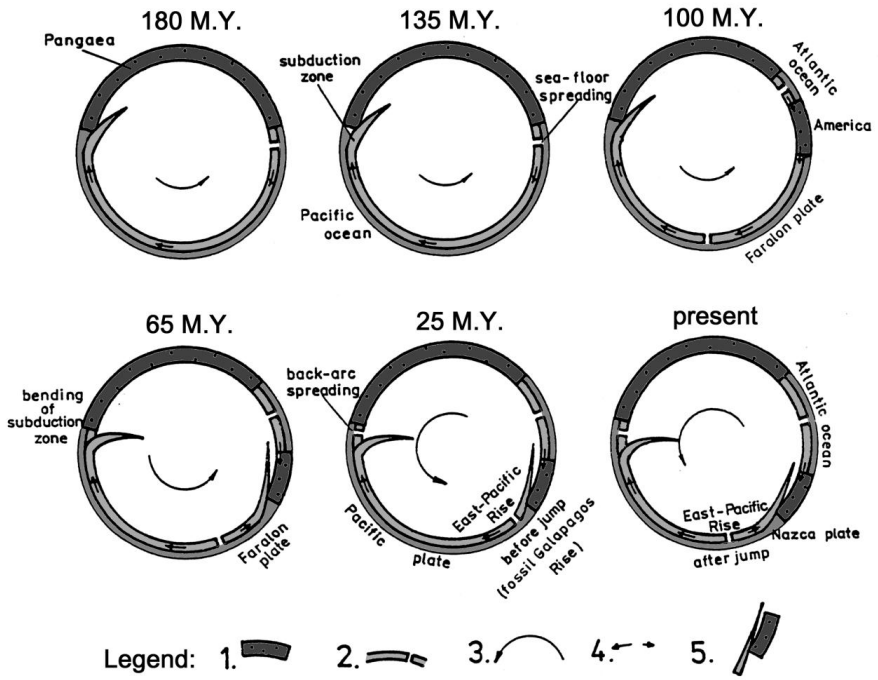

Fig. 9.6: Development and asymmetry of plates (north pole view). 1- continental lithosphere, 2- oceanic lithosphere with mid-ocean ridge, 3- direction of the mantle rolling beneath the lithosphere, 4- motion of oceanic plates with regards to stable Pangaea, 5- subduction of oceanic lithosphere beneath the continent (Ostřihanský 1997).

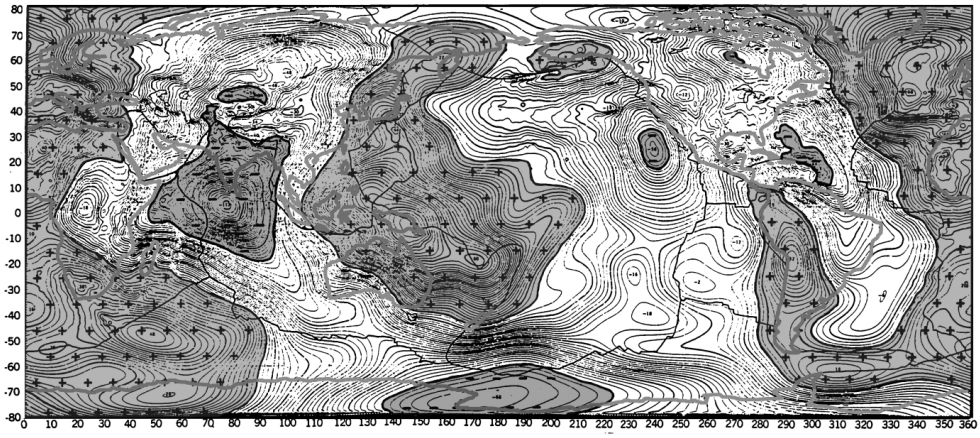

Fig. 9.7: Heights of geoid (modified according to Marsh et al. 1988). Orange – margins of continents, black – margins of lithosphere plates, filled +10 m and –50 m isolines (see colour pages too).

Heights of the geoide present an important guide regarding the character of the mechanism of lithosphere plate movement (Marsh et al. 1988, see

Fig. 9.7). They show where surplus (positive anomaly) and lack (negative anomaly) of masses are situated. Positive anomalies agree with regions where, to a large extent, the oceanic lithosphere is assimilated (north and west of the Circumpacific ring (the Ring of fire) or the western margin of the South American plate). Additionally, the western rim of the Eurasian and African plate shows positive anomalies in spite of the fact that no oceanic crust subducts beneath them. In contrast, the largest negative anomaly is situated in the 'furrow' behind (SSW of) India and at the eastern rim of the Pacific plate.

However, we shall now try to determine what the absolute velocity of the different lithosphere plates is. We shall take into account the results of plate movements in the frame of quick hot-spots of the Pacific plate and then we will see that an apparent movement of the lithosphere plate against the mantle is not in accordance with the Earth's equator. The plain of rotation of the crust against the mantle has an evident incline roughly of 23°, with Euler's pole of rotation approximately (56°S, 137°E) (see Fig. 9.8 and 9.9).

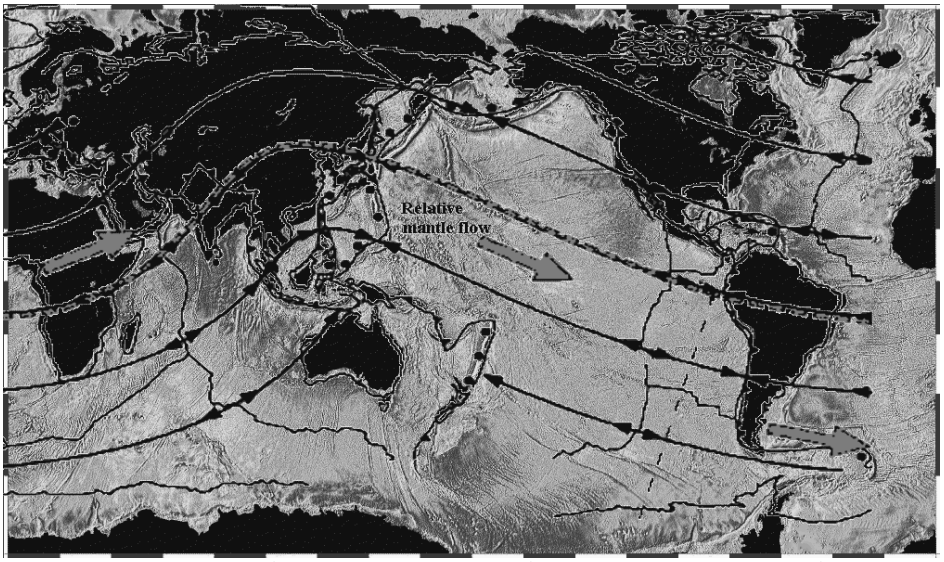

Fig. 9.8: Relative mantle flow according to lithosphere frame (Doglioni 1993) and map of gravity anomalies in oceans measured by satelite alimetry (Sandwell and Smith 1997) (see colour pages too).

When Crespi et al. (2007) calculated what the common movement of all lithosphere plates against the mantle was, they obtained the same results. As a curiosity, let us add that the south magnetic pole is not very far from the Euler's pole of all the lithosphere plates in total (NetRot on Fig. 9.9). However, we shall not discuss here the possible connections between them, as described by e.g. A. Rousseau (2005), or look for the sources of the magnetic field.

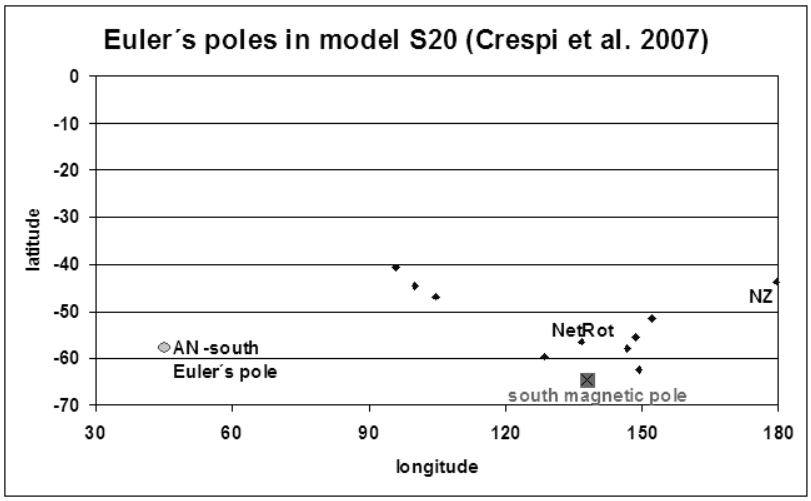

Fig. 9.9: Euler´s pole of rotation lithosphere plates (according to Crespi et al. 2007).

Comparing the mantle flow and gravity anomalies in the oceans measured by means of satellite altimetry (Sandwell and Smith 1997) (see Fig. 9.8), we can see that distinctive transform fault lines are in most cases parallel to, or only gently diverted from, the movement of the plate. On the contrary, most of the rift regions and oceanic arcs are perpendicular to the direction of the movement. All of this corresponds to the idea of the direction of stress in them. The most surprising finding is reached by comparing the movement of the mantle flow with the movement of the Indian plate during the time span from 80 M.y. to 40 M.y (Scotese 2003). We can see that they almost did not move against each other or that the movement of the Indian plate was small, and relatively in a more northward direction, in comparison with today's mantle 'flow'. From that, it follows

that the asthenosphere does not move. Instead, the lithosphere plates move against the immobile mantle and asthenosphere. Admittedly the relative motion is the same. However, the sense of movement and tectonic processes is quite different. Instead of the active 'departure' of the Indian plate from Africa we have here the passive tearing apart, which is more wedged and braked in the mantle. It is possible to date the onset of this tearing apart by means of the velocity of growth of the oceanic crust on the southwest rim of Africa, which changed roughly 90 M.y. ago (Somoza 2008), or by the change of the tectonic regime of South America ca. 80 M.y. ago (Favela and Anderson 1999). In the same way, instead of the impact of the Indian plate onto Eurasian plate, we have here the impact of Eurasia plate onto the Indian plate which stands on the mantle.

Already in 1993, Doglioni has written about why lithosphere plates have different velocities. The reasons are: a) thickness variations in the lithosphere plates (mostly continental plates), b) variations in the density of the asthenosphere and c) variations in the lateral viscosity of the asthenosphere. The eastern part of the African plate and the Madagascar microplate have, therefore, a higher friction with the mantle than the remaining part of the African plate, which was probably one of reasons for their tearing apart. The Antarctic plate has been as stable as the Indian plate, which is manifested by a small movement in the direction towards the South American plate and away from the Australian plate (Crespi et al. 2007). Only on its rim, which is closest to the equator of lithosphere rotation at the Scotia Sea (relative latitude ca. 60°), can we find effects of plate tectonics with subduction of the oceanic lithosphere beneath the island arcs (see Figs 9.10a,b).

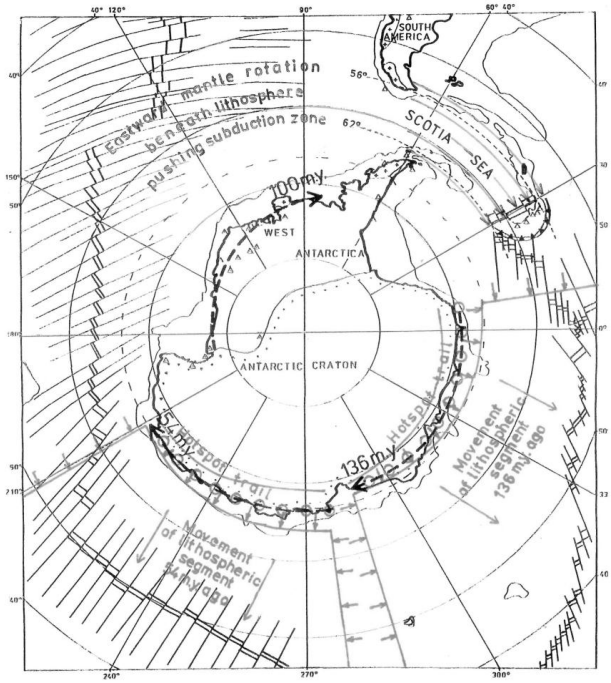

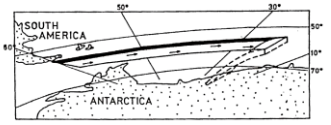

Fig. 9.10a: Rotational and equatorward movement phenomena in Antarctica. Meridional mid-ocean ridges reaching deeply into polar region created favourable conditions for the movement of released segments separated from the remaining part of Antarctica by the equator ward Eötvös force 136, 100, and 54 M.Y. ago. Red marks the lithosphere segments and the action of the ridge-push force. The Scotia Sea basin situated exactly between the 56^0 and 62^0 parallels represents the most convincing rotational phenomenon on the Earth (Ostřihanský 1997). The mid-ocean ridge position according to Heezen and Tharp (1985).

Fig. 9.10b: Lithosphere cut-out created by pushing of the subducted slab by mantle 'flow' (Scotia Sea basin).

On February 27, 2010 an earthquake occurred at Maule, Chile. The following GPS measurement showed that the American plate moved westward over the subducting Nazca plate, which was liquidated during westward movement of the overriding continent. In this way, the no longer existing back arc basins of the eastern side of Pacific, were destroyed. Although they had been present, they were overridden by the westward moving continent (MODEL 3 – see Fig. 9.5). The image of the University of Hawaii shows that the whole southern part of the continent moves westward with the greatest movement on the Pacific shore where the continental material was compressed. As the Nazca plate dropped, the South American plate was released and the city of Concepcion jumped westward by 10 feet (Mason 2010). The Nazca plate is one of the most stable plates in relation to the mantle. The Galapagos hot-spot had been formed before the creation of the sea-floor spreading separating the Nazca and Cocos plates. As the tearing apart of the plate proceeded from east to west the magma of Galapagos hot-spot fed the sea-floor spreading opening and in this manner

and the double hot-spot track was created (marked on Fig. 9.3a by red colour).

Considering the immobility of the mantle and anchoring of the Indian plate in it before its collision with Eurasia, we can form a mental picture of how today's gravity anomaly, with a minimum on the south from India, was created (see Fig. 9.7). The material below Eurasia, which was situated in the band of collision, should relatively 'by-pass' the Indian plate. This material had not completely liquefied and its viscosity was relatively high. Therefore, this material had a problem to 'flow' to the space behind India and today we can observe a lack of mass there. The length of the negative anomaly behind India corresponds to the intensity of the lithosphere plate movement against the mantle in the period of the last ca. 30 M.y. The collision of India and Eurasia started ca. 38-45 M.y ago by accretion of island arcs (Scotese & Golonka 1992, Scotese 2003) when blocks of the continental lithosphere were still 12° away from one another. Also gravity anomalies on the bottom of the Indian Ocean (Sandwell & Smith 1997) (see Fig. 9.8) have a distinctive linear character and they resemble the lateral moraines of icebergs created by passing the nunatak. Such details are visible on the volcanic chains or on the mutual movement of the Nazca and Cocos plates (Hey & Fogt 1977, Meschede & Barckhausen 2000, Bohannon & Geist 1998). This supports the idea that the direction of movement of all lithosphere plates was changed after the main collision of both continental crusts of Eurasia and India ca 27-23 M.y. ago. At the same time other events occurred. Tectonic events were visible on the North American plate (Ward 1991, Bohannon & Geist 1998, Shawe 2001), the direction of the apparent movement of the Emperor-Hawaii chain changed during the time when Midway island was created (Brent et al 1997), and the rejuvenation of continental hot-spots under the contemporary lithosphere extension occurred (Favela & Anderson 1999).

Thus the westward drift determines how the following deformations will spread. If some asperity occurs inside the rock mass or on the fault plane and stops the movement, then 'in front of it', and therefore against the direction of the crust movement, the stress will increase till the asperity fails. On the other hand, 'behind it', and therefore in the direction of the crust movement, we shall observe the lower stress until the asperity fails. If the asperity is larger, then we can expect a longer period of anomalous

stresses and the release of a larger portion of energy than in the case of a smaller asperity.

After the asperity failure, the deformation 'wave' will move to the west in accordance with the westward drift. And therefore, the aftershocks will occur on the wave crest worldwide. The stress drop in the direction of the main principal component of stress tensor in the area to the east of asperity can lead to the aftershock sequence due to stress changes. This frame of transfer of deformation and/or stress, in accordance with the western drift, will be valid not only for one lithosphere plate but, on the global scale. This can be seen in a series of the largest earthquakes which occur worldwide after a long period of quiescence (Sieh et al. 2008).

It is possible to summarize that the movement of particular plates on the asthenosphere determines the mutual movement of continents against each other and against the oceanic plates. The speed of their movement depends on their friction with the mantle. We shall try to describe the reason for the movement in the following chapter.

9.2. Energy sources and possible mechanisms of plate movements

When in 1912 Alfred Wegener published his theory of continental drift (Wegener 1912), hardly anyone believed that continents could 'float', recede from one another and collide with others creating mountain belts. At the time of his death in 1930 his theory had not been accepted. In fact, conferences were organized to find arguments against this theory. A. Wegener, himself, considered that the mechanism of movement of the lithosphere plates could be generated by the centrifugal force generated by the rotation of the Earth. It proved to be a wrong assumption and this mechanism was refused at the conference in 1928. Since the mechanism of movement of plates was not recognised and clearly explained, the whole theory of continental drift was refused at that time.

Only at the end of 50s and 60s did the theory of continental drift become accepted based, in particular, on the study of oceanic magnetic anomalies (Gregory et al. 1960, Vine & Mathews 1963, Vine 1966), and on seismicity, which pointed to Wadati-Benioff zones where the underriding of oceanic lithosphere beneath continental plates occurs.

Arthur Holmes considered that the convection currents in the Earth's mantle, driven by thermal convection and heat transfer from the Earth's

interior, move the lithosphere plates. This explanation of continental plate movement is generally accepted today in spite of the fact that until now there has not been any heat source, which could explain this convection mechanism (Garai 2007). The most probable, and therefore generally accepted energy sources, being proposed these days are: Remaining heat after the Earth's accretion in the first stage of its formation (Kachlík & Chlupáč 1996), gravitational separation of the Earth's material (Ricard et al 1991, Scoppola et al. 2006), heat generated by the radioactive decay of certain elements (Holmes 1939), tidal friction (Munk 1998), and change of the angular momentum of the Earth (Garai 1997, Doglioni 1993, Doglioni et al. 2003, 2005, Rousseau 2005, Crespi et al. 2007).

We will now estimate how big the endogenous sources are. First of all we will study the heat, which is produced by **radionuclide decay**. The heat released by radionuclide decay in the Earth's interior can be estimated on the basis of the occurrence of radioactive elements. In nature radionuclides occur in several groups.

Among the most widespread elements the radionuclide ^{40}K, which represents 0.019 % atoms of potassium, is the only important factor. Potassium belongs to the principal elements in most of the Earth crust rocks although in the mantle, it is usually only in trace amounts. A greater part of potassium ^{40}K changes to calcium ^{40}Ca and a smaller part by electron capture to argon ^{40}K, which has a considerable importance in geochronology. In the geological past also ^{26}Al was important, but it has now totally decayed. Next there are the nuclides as ^{14}C or ^{3}H (tritium). They are created by the effect of cosmic irradiation or by human activity and owing to their short half-lives they cannot act in the Earth's interior.

The second important group of radionuclides consists of the decay series $^{238}U \rightarrow ^{206}Pb$, $^{235}U \rightarrow ^{207}Pb$ and $^{232}Th \rightarrow ^{208}Pb$ (in geological past also the 'neptunium' series). Uranium and thorium rank among the least abundant elements in the Earth. Nevertheless, their average contents are relatively higher in the Earth's crust. Uranium and thorium and most of the by-products of their decay series (radium, radon and polonium are the most known) are elements that have no stable isotopes. In the decay series the so-called radioactive equilibrium can be quickly set up (in the geological time) when any intermediate decay product increases with the same speed as it decays. The radioactive equilibrium is established under the condition that

no by-product is separated (by chemical way or the gas radon escape). The radioactive equilibrium is established most slowly in the 238 uranium series (about one million years) and the most quickly in 232 thorium series (about 70 years). Intermediate decay products with the shortest half-lives are very intensive radiators, but they occur in very small amounts. The $^{238}U/^{235}U$ ratio in natural uranium is presently about 138, but in the past it was higher because ^{235}U decays more quickly.

The third group of radionuclides creates mostly minority isotopes of trace elements, mostly, with very long half-lives of decay (always over 10^{10} years). Many of them (particularly ^{87}Rb) are used in isotope geochemistry. Some of these elements have the radioactive energy output comparable to potassium or even higher. But in nature, their radioactivity is not as significant as that of other radionuclides (rubidium mostly occurs as trace admixture for potassium, samarium is mostly accompanied with thorium, lutetium by uranium etc.).

The fourth group of radionuclides involves only short-lived radioisotopes (in geological time!), including elements whose natural occurrence is negligible at present (technetium, promethium, astatine and transurans), as well as the already mentioned ^{26}Al. These radionuclides were important only in the Earth's early history because their pool is not replenished (in contrast to radium etc.) by decay of long-living isotopes.

So, despite a large number of existing radionuclides, the vast majority of nuclear energy is released by the ^{40}K and the decay series of ^{232}Th, ^{238}U and ^{235}U. Neglecting other radionuclides in the calculations of 'radioactive heat production' (Rybach, 1976)[1] has its practical justification - mostly they are elements whose concentration in rocks is usually low and more difficult to analyze.

Until now, the most often used calculation of the heat production by radioactivity has been the following:

$$RHP=\rho(9.52C_U+2.56C_{Th}+3.48C_K)10^{-5}, \quad (9.1)$$

(RHP in $\mu W\ m^{-3}$, density in kg/m^3, K concentration in mass %, U and Th in ppm; the calculation also includes by-products in decay series under the presumption of radioactive equilibrium).

[1] [1]According to already published opinion of one of the authors (Procházka, 2008, 2009) there could be an important overestimation of radioactivity heat production due to neglecting of radiochemical processes.

Considering the average contents of these three elements in continental crust rocks and in oceanic crust and mantle rocks, we can estimate the heat production in representative rocks and then calculate the contribution to total heat flow of major geological units. Today's estimations of heat production are not basically different from those, which were published already in the 80s. E.g., Keith (1993) presents the following values of radioactive heat production (taken from Parsons & Richter 1981, Jochum et al. 1983, O'Nions 1987);

- Least-contaminated oceanic peridotite 1.5 pW/kg
- Upper crust (granodiorite) > 450 pW/kg
- Lower crust (pyrox. granulite) > 150 pW/kg
- Estimated whole Earth heat productio 4.8 pW/kg

If we summarise the total produced energy of rocks over the whole volume of the Earth, the total produced energy per year would be 2.5-5x10^{20}J (Keith, 1993). According to one of the latest models of the Earth's composition we obtain these values (see Tab. 4):

Table 4. Average K, U and Th concentrations (in ppm) in the Earth's body (Allégre et al. 2001) and total radioactive heat production from these values according to Rybach (1976) (total Earth density 5515 kg/m^3).

K	U	Th	total output (μW / m^3)	total planet output (W)	radio. energy production (J/year)
171	0.0144	0.051	0.018	$1.95 . 10^{13}$	$6.15 . 10^{20}$

Almost one half of this heat is produced in the crust. However, as is evident from the measured heat flows above rifts and continents, the greatest part of energetic flow corresponds to relatively narrow zones of the rift's vicinity and continent margins (Keith 1993) and is not in accordance with radioactive distribution.

On the contrary, seismic profiles crossing the Atlantic Ocean clearly show the isolated distribution of thermal anomalies which cannot be explained by thermal convection (Anderson and Dzievonski 1984, Anderson 1988). In addition, the heat released from radionuclides, which

are concentrated in the crust, cannot rotate presumable convection cells in the mantle.

If we compare the total output of radioactive energy production with the total energy of all volcanoes and earthquakes on the Earth during one year, which is approximately 10^{22} J/year (Brázdil et al 1988), we can state that it is not enough for the proposed mechanism of convection cells.

Tidal drag as a mechanism for displacing the lithosphere has been proposed to explain the observed westward drift (Bostrom 1971, Knopoff and Leeds 1972). Jordan (1974) discredited this proposal demonstrating that the viscosity, which would allow decoupling between the mantle and the lithosphere, should be lower than 10^{11} Pa s. The present day viscosity estimates for the asthenosphere are much higher ($3x10^{16}$-10^{20} Pa s) (Garai 1997, 2003, Vergnolle et al. 2003). Hirth and Kohlstedt (1996) calculated a variable viscosity profile (with mean viscosity values as low as 10^{18} Pa s) for a melt-free oceanic lithosphere. Mei et al. (2002) calculated, for the asthenosphere of a mantle wedge resting above a subducting plate, a very rough viscosity profile. The viscosity of the mantle wedge can vary by ~3 orders of magnitude (between $<10^{16}$ Pa s and $>10^{18}$ Pa s) over a depth span of 60 km, due to the combined effects of water and melt weakening. In summary, asthenospheric viscosities from numerical modelling are in a reasonable range between 10^{17} and 10^{20} Pa s. The viscosity of the lower mantle is constrained to ~10^{21} Pa s (Vermeersen et al., 1998).

Such viscosities are too high for movement of the continents.

The **tidal friction energy (dissipation**) is approximately $1.6x10^{19}$ J/year (Denis et al. 2002), or one order higher $1.1x10^{20}$ J/y (Varga et al. 2005), or $1.2x10^{20}$J/year (Munk 1998). This is 1-order greater than the energy of one medium volcanic eruption (10^{19}J (Grygar 1994)), but still two orders less than energy of all of the earthquakes on the Earth per year (Brázdil et al. 1988). In addition, the tidal friction acts mostly in the Earth's surface layers and oceans as has been shown, for instance, on the Earth's nutation. So, the tidal friction also would not be able to generate the necessary convection currents.

The 'by-product' of tides, i.e. **the change of the Earth's rotation**, i.e. variation of the length of the day (LOD), can be considered. But even here

the energy dissipation is in order of $4x10^{20}$ J/year (e.g. for 14-days wave) as was shown in chapter 3.2. This energy is larger then tidal friction, but it is not sufficient to cover the energetic dissipation of all earthquakes and volcanic activity. On the other hand, changes in the Earth's rotation give priority to the differential rotation of different layers and particularly to the movements between the lithosphere and the mantle over the asthenosphere as many authors have proposed (Keith 1993, Doglioni 1993, Ostřihanský 1997, Garai 1997, Smith & Lewis 1999, Doglioni et al. 2003, 2005, Scoppola et al. 2006, Crespi et al. 2007 and others).

We can see that none of the supposed energy sources can cover all the energy needs of the proposed mechanisms based on thermal convection cells.

However, on the Earth (more exactly above the Earth) there is yet another important energy source. It is the **solar irradiation**. The solar energy, which reaches the Earth, is 5.10^{24} J/year (Abbot 1911). The amount of energy is high enough to deform the entire Earth and to melt all of the rocks in all of the volcanoes on the Earth. But we need to show how this energy is changed to the movement, which drifts the continents. This will be explained in the following chapter.

9.3. Thermoelastic waves

We have been measuring the tilt of buildings by pendulums since 1998 (Neumann 2007). The first underground pendulums were installed in 2007 in Prokop mine in Příbram, Czech Republic at the depths of 1 and 96 m below the surface (Kalenda et al. 2009). Eight underground pendulums have been installed in Central Europe up until 2010. All of them showed mechanisms, which are able to start and support the continental drift – thermoelastic wave in company with ratcheting.

The tilt of the building on the surface is directly tied to solar irradiance and air temperature. And it has a mostly diurnal (circadian) period (see Fig. 9.11). The tilt of the building in the N-S direction starts immediately after an increase of external air temperature. On the other hand, the tilt of the building in the E-W direction varies mostly with solar irradiance. The

relationship between them is very close. The amplitude of the tilt depends on the energy reaching the surface of the wall. The tilt is minimal during cloudy days. Maximum tilt is observed during sunny and clear days, when dust in the air is minimal and the difference between temperatures in the day and in the night is maximal.

As the delay between the beginning of tilt of the building and beginning of sunshine is very small (less than 5 minutes), other mechanisms than thermal wave propagation from the surface, deep to the wall, must exist. Maybe, the energy transfer from irradiance to the wall passes deeply inside the mass and not only on the surface. The decay of the tilt in both directions is much slower then the increase. And it starts immediately when the sun is hidden behind clouds, or at the moment of sunset.

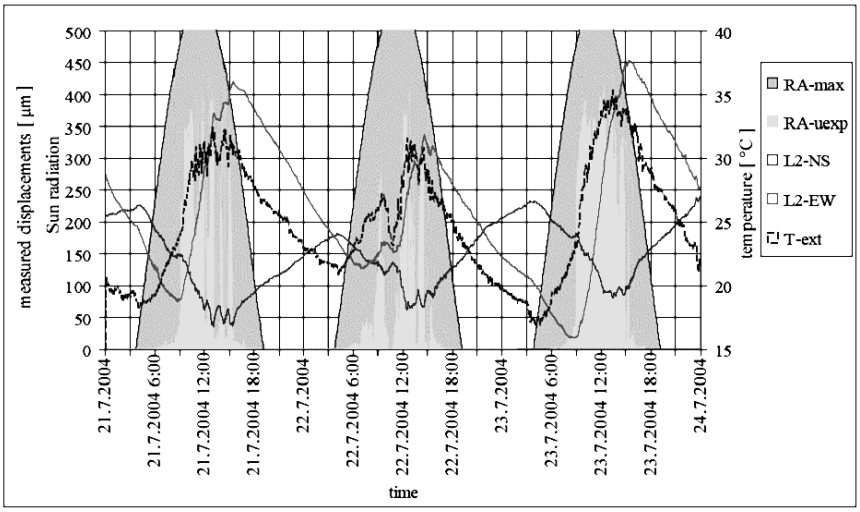

Fig. 9.11: Tilt of building due to temperature and solar irradiation
RA-max – theoretical maximal solar irradiance, RA-uexp – observed solar irradiance, L2-NS and L2-EW – tilt of pendulum L2 in NS and EW directions, T-ext – external temperature (see colour pages too).

If we measured, by pendulum, the tilt of the tunnel 1 m below the surface in Prokop mine, the results were the same or similar as on the surface (see Figs. 6.6 a,b). Clear diurnal periods of tilt were visible and their amplitudes depended on the solar irradiance of the Earth surface. The maximum deformation and the maximum of noise (variation of tilt around the average position) was observed in the afternoon (12:00 – 14:00) at local time depending on the weather and sunshine. It has been shown that the

circadian tilts of the gallery are in order 10 uRad. The course of tilts was asymmetric with the quick deformation before noon, and a slower deformation in the afternoon hours. The deformations sometimes became irreversible during very sunny days (see Fig. 6.6b).

The diurnal period of tilt was visible at the depth of 96 m in Prokop mine as well (see Fig. 6.7a). And even the noise had a diurnal period (see Fig. 6.7b).

In 1968-1969 Melchior and Skalský (1969) measured tilts in the mine in Březové Hory (in Příbram) by tiltmeters (horizontal pendulums) at the depth 1300 m below the surface. They found that also at these depths the circadian wave was observable, and it had 4 – 10x higher amplitudes than it should have according to tidal theory. This proved that the circadian thermal wave generates the thermoelastic wave, which propagates from the site of insolation (surface) to all sides and to the depths. This thermoelasic wave has the same phase as the thermal wave in close-to-surface layers, therefore, its maximum stress was in the afternoon between 12:00 and 14:00 LT. This thermoelastic wave was theoretically described by Hvožďara et al. (1980), and in this book in chapter 3.5.

The circadian thermal wave reaches only to the depths ca 15 cm (Mareš 1984) according to the relationship

$$\vartheta(h) = \vartheta_0 e^{-h\sqrt{(\omega/2a)}} \cos(\omega t - h\sqrt{\omega/2a}) \qquad (9.2)$$

where **h** is the depth below surface, **ω** is the angular frequency of cyclic change, **a** is the coefficient of thermal conductivity according to relation

$$a = \lambda / c\rho \quad , \qquad (9.3)$$

where **λ** is the thermal conductivity, **c** is the specific heat, and **ρ** is the rock density. Nevertheless, the thermoelastic wave, which is generated by the thermal wave, spreads over a long distance as was observed before the Wenchuan earthquake (see Chapter 10). As the amplitude of the circadian thermoelastic wave is not large, the annual thermoelastic wave was observed on the strainmeter record in Vyhne (Slovakia) first and interpreted correctly by Hvožďara et al. (1988) (see Fig. 8.3).

This annual wave was observed on most of the deformometer and tiltmeter measurements – in Grotta Gigante (Braitenberg et al. 2006), on water levels (see Fig. 8.3) (Stejskal et al. 2007), and also on the absolute gravimeter on Pecný (Pálinkáš & Kostelecký 2005, Pálinkáš & Kostelecký

2008). All instruments show that the extremes of deformations in Central Europe occur around March – April and around September – October (see Fig. 8.2). The level of noise, both on strainmeters and our pendulums, show that the noise is largest from October to March, i.e. in winter. We interpret such winter periods as periods of increased stress. Why is the maximum stress in the rock mass not during the summer, when the surface temperature is highest and when rocks expand? The answer is easy: It depends on the propagation speed of the thermal wave to depth. The thermal wave propagates to depth of ca. 15 cm during one day, which causes the expansion of a thin rock layer only. The coefficient of thermal conductivity ranges for common rocks and soils in interval a = 7. 10^{-7} to 22.10^{-7} m^2s^{-1} and so during one half year, the thermal wave propagates to the depth ca. 10 – 12 m according to the relationship (9.2) (see Fig. 9.12a-d).

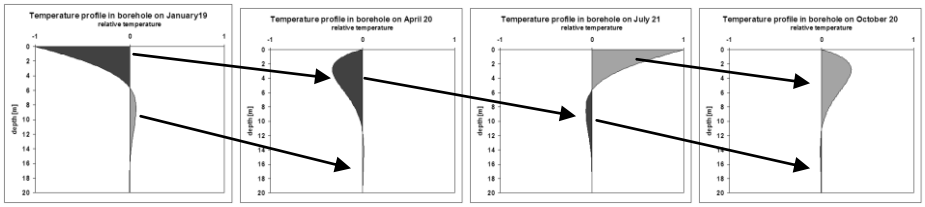

Fig. 9.12: Theoretical temperature profile in the borehole.

This thermal wave increases the rocks volume that consequently evokes in surrounding rocks the thermoelastic wave. Its size is directly proportional to integral

$$\varepsilon \approx \int_0^R \alpha \Delta \vartheta(h) dh \quad , \tag{9.4}$$

where **ε** is the lateral strain, **R** is the Earth's radius, **α** is the thermal expansibility of rock, $\Delta \vartheta(h)$ is the difference between long-term medium and instant temperature at a given depth, and **h** is the depth. Already from figure 9.12 it can be seen that at times, when the temperature on the surface is maximal (on July 21), this integral is not maximal even in those cases where undisturbed and isotropic rocks reach the surface. This integral is maximal at the end of August (see Fig. 9.13). Taking into account the weathering of the real crust on the surface, which declines exponentially to the depth, we can observe that the integral (9.4), i.e. the relative size of

thermoelastic wave, will have its maximum in September or as late as October. Considering yet more weathered crust on the surface, then the maximum of the thermoelasic wave would shift into winter months, which we observed. By the thermal wave propagation at greater depths of unweathered rocks and their thermal expansion, we can explain both the maximum rock extension on the strainmeter in Vyhne in November 2007 (and always in the beginning of winter in following years), and also tilt changes of the pendulums in Grotta Gigante, in Příbram and elsewhere. It is interesting, but logical, that at the time of rock extension at greater depths the pore spreading occurs in shallow depths and ground water dropping down is observed.

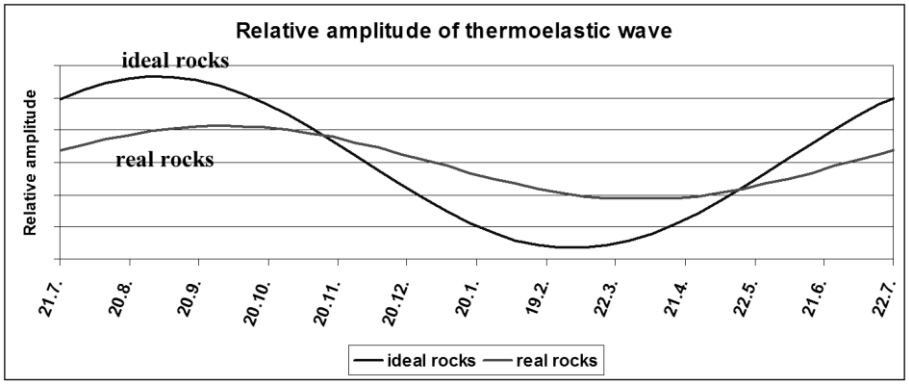

Fig. 9.13: Relative amplitude of the annual thermoelastic wave in unweathered and real rocks.

From this point of view, the close-to-surface parts of rocks can be divided into two layers:

- The upper weathered layer, which does not participate on stress genesis and transfer. More exactly its share of genesis and transfer of stress is negligible. However, this layer is able to transfer the thermal wave to the depths. This layer can serve as a source of ratchets (see further).
- The lower layer of the unweathered rocks, is able to expand thermally and is able to transfer the shear stresses to deeper parts of the Earth.

From the seismic and thermoelastic point of view, we shall further consider that this compact layer is the first close-to-surface layer and we shall investigate its behaviour in the annual cycle. On the base of measurements we know that this layer is the most extended in winter and

generates the largest pressures in horizontal direction and shear stresses in vertical direction against underlying layers, which have lower than average temperatures, because there are thermal waves advanced from the previous winter (see Fig. 9.12). As the temperature in the underlying layer is lower than temperature in the overlying extended layer, on contact between them, shear movement occurs and the subvertical cracks in the underlying layer will tensily open. The reverse process will occur in summer when the overlying layer has lower temperature than average. This upper layer will shrink and the subvertical cracks will open, in which the material from surface will fall by gravitation. The underlying layer will have higher temperatures than average and this layer will thermally extend, so that interface shear movements between layers will occur against the overlying layer, but in reverse direction than in winter.

This process, described above, is valid for all thermal cycles either in diurnal, annual or climatic cycles or in their superposition. Therefore, the larger effect of annual and circadian cycles will be observed after the period, when the larger temperature variations than average dominated the Earth and vice versa. What will be the probable amplitudes of these cycles? Considering that for the short-period diurnal cycle, the thermal wave will reach a depth of only 15-30 cm and during the annual cycle the thermal wave, with roughly the same temperature difference on surface, will reach a depth of 15-30 m, then it is obvious that the integral (9.4) will be in the case of annual cycle, orderly higher. By measurement with the strainmeter in Vyhne, Slovakia (see Fig. 8.3) and with pendulums in Příbram (see Fig. 8.2) it was found that the rates of amplitudes in diurnal and annual cycles vary between values 1:15 – 1:100. Roughly, at the same rate the strain rate in rocks varies in the course of both cycles. So, in case of circadian cycles the stress will only rarely reach the limit of strength of undisturbed rocks (compare Fig. 6.6a and 6.7a) and therefore also the noise in deeper parts of the massif does not have distinct circadian cycles, in spite of the fact that even this can be followed (see Fig. 6.7b). On the contrary, in close-to-surface weathered rock layers, the diurnal cycles have a basic importance.

We can estimate the amplitudes of stress or deformations in the far field, which are generated during various cycles on the Earth's surface according the integral (9.4). The depth, which is penetrated by thermal wave, is evaluated for the phase shift π in relation (9.2) (see Fig. 9.12b).

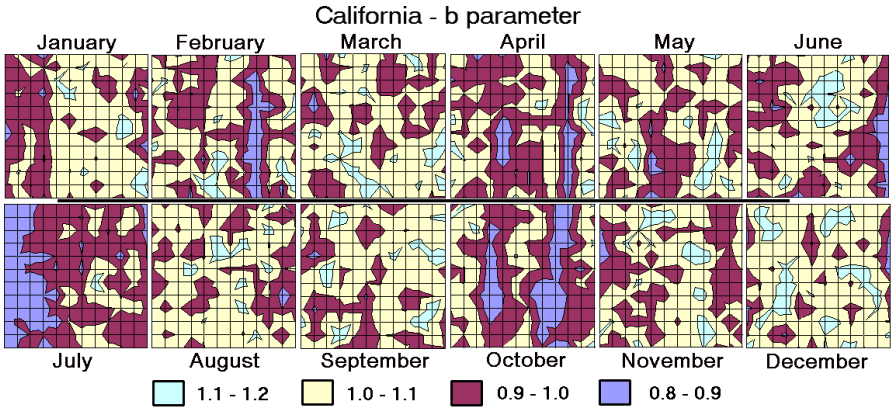

Fig. 4.22 Parameter **b** of G-R distribution of California earthquakes in 3-D phase space

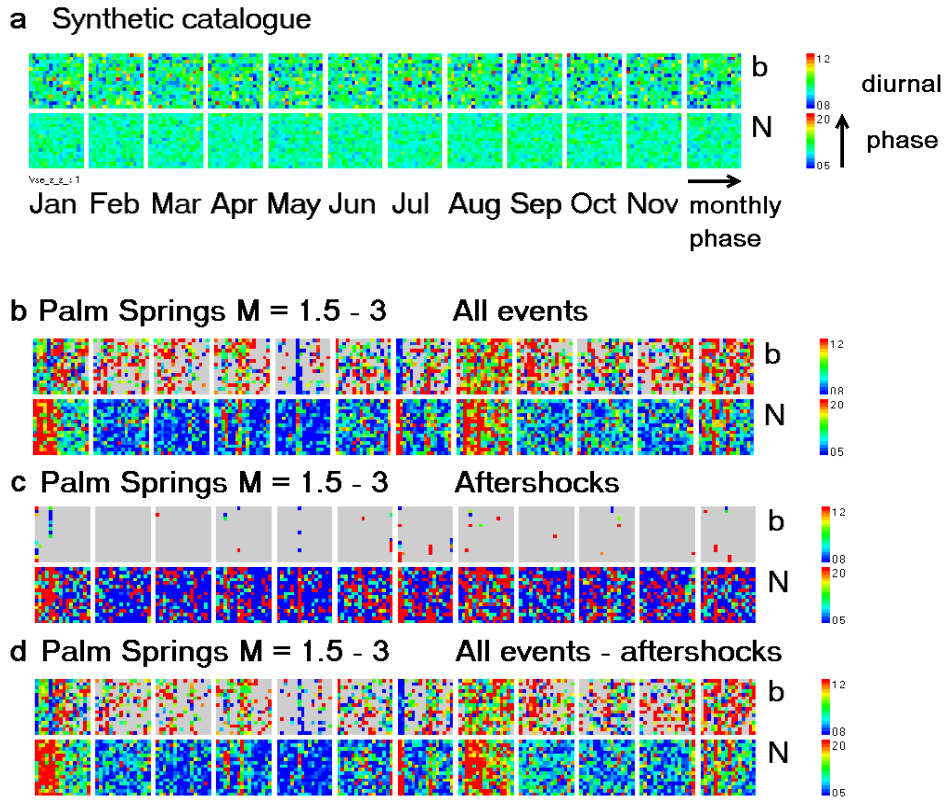

Fig. 4.23 Parameter b of G-R distribution of Palm Springs earthquakes in 3-D phase space. a) Synthetic catalogue, b) Palm Springs catalogue m = 1 – 3, in period 1980 – 2004 - all events, c) aftershocks, d) mainshocks.

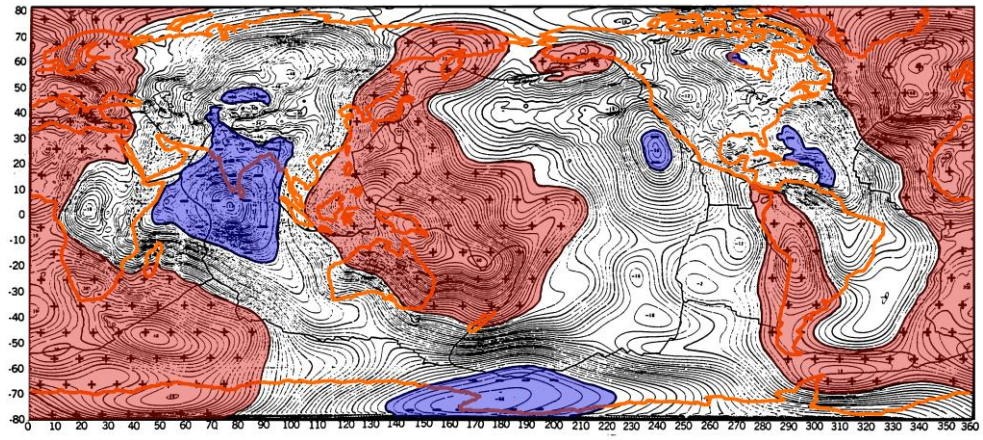

Fig. 9.7 Heights of geoid (modified according to Marsh et al. 1988). Orange – margins of continents, black – margins of lithosphere plates, filled +10 m and –50 m isolines

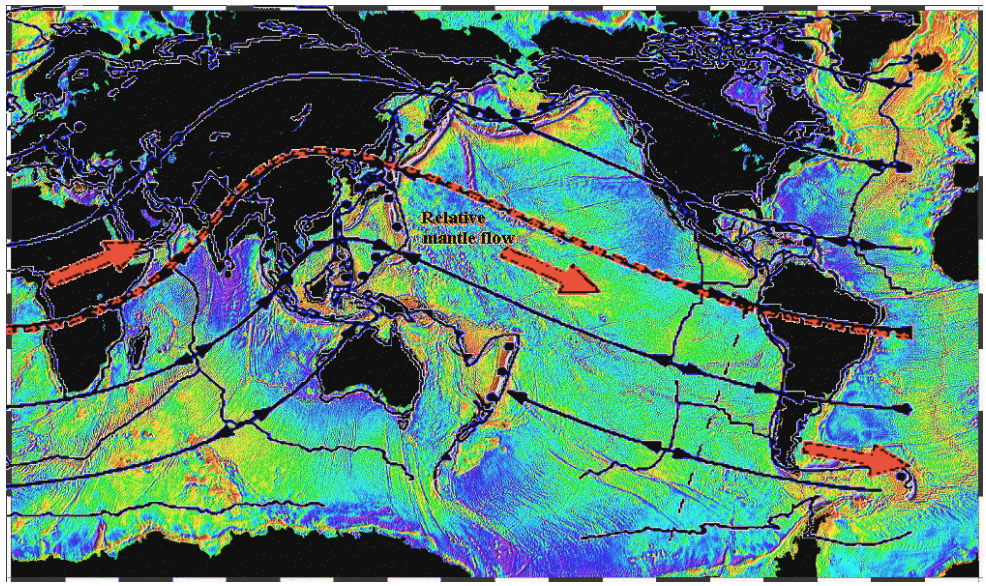

Fig. 9.8 Relative mantle flow according to lithosphere frame (Doglioni 1993) and map of gravity anomalies in oceans measured by satelite alimetry (Sandwell and Smith 1997)

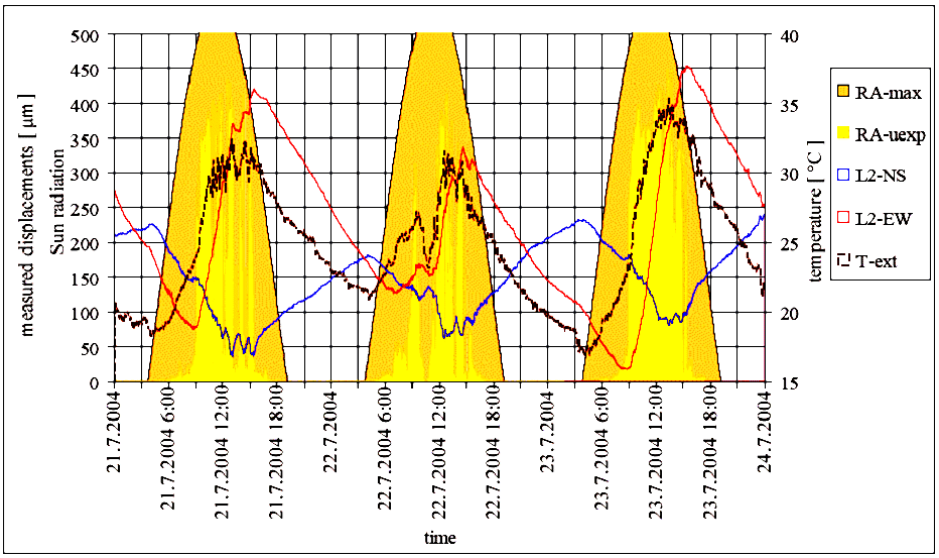

Fig. 9.11 Tilt of building due to temperature and solar irradiation

RA-max – theoretical maximal solar irradiance, RA-uexp – observed solar irradiance, L2-NS and L2-EW – tilt of pendulum L2 in NS and EW directions, T-ext – external temperature

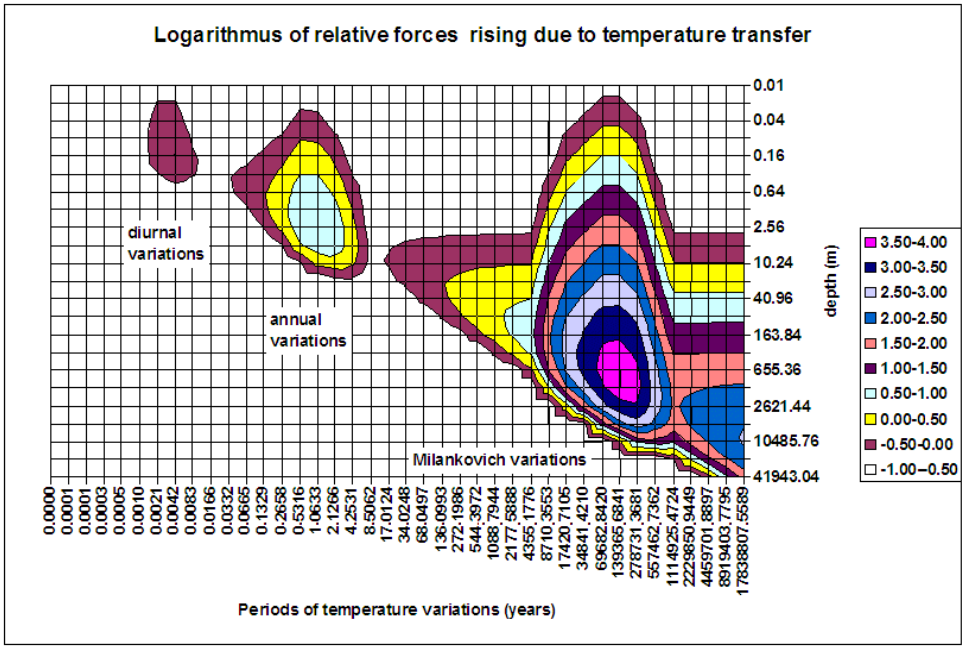

Fig 9.14 Logarithm of relative forces excited by temperature variations of the Earth surface, which penetrates depths depending on their periods

Kalenda, P., Neumann, L., et al. Tilts, Global Tectonics And Earthquake Prediction, SWB 2010, London.

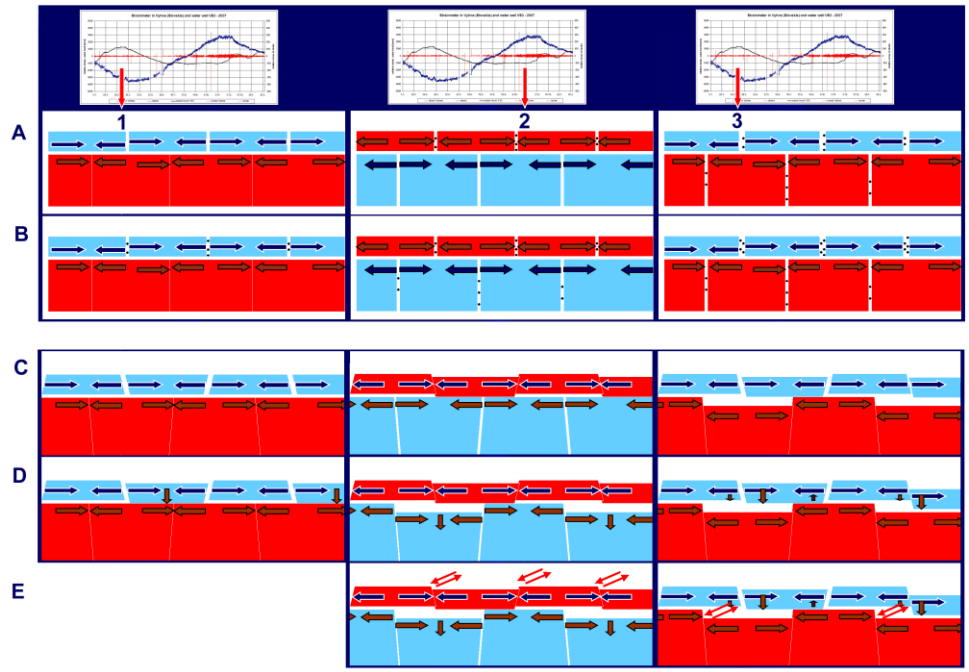

Fig. 9.15 Principles of ratcheting and movement mechanism of tectonic plates

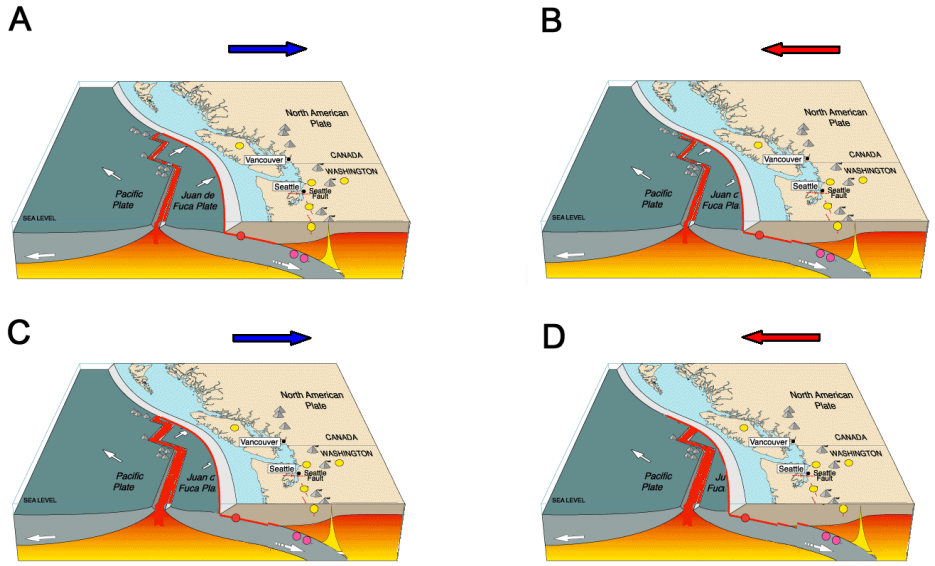

Fig. 9.16 Mechanism of movement of lithospheric plates (blockdiagram by Wikipedia, modified)

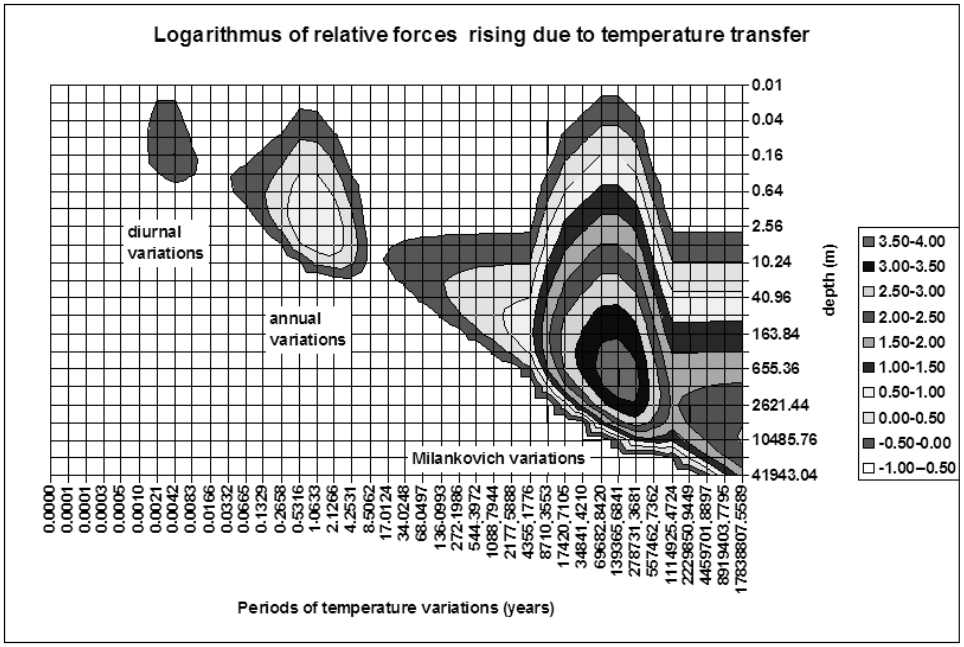

Fig 9.14: Logarithm of relative forces excited by temperature variations of the Earth surface, which penetrates depths depending on their periods (see colour pages too).

We have confirmed that the relative stresses generated by annual cycles are up to 2 orders of magnitude higher than stresses generated by diurnal temperature variations, as was shown in our measured data. So, we can confirm that the theoretical estimation of their rate, which the thermoelastic model predicted, is correct. As we know, that in the case of the annual cycle, the stress in solid rocks in winter approaches the strength limit of the weakest components, we can claim with certainty in the case of thermal variations given by Milankovitch cycles (Milanković, 1930) - excentricity ca. 100.000 years, axial tilt (obliquity) ca. 40.000 years, and precession ca. 22.000 years, the stress will overcome the strength limit of all rock components and therefore will never reach the magnitude of 4.5 orders higher than for diurnal variations and of 3.5 orders of magnitude higher than annual variation as the theoretical model predicts (see Fig. 9.14). It is only a theoretical image of how big these stress variations could be in the case of

the strongest rocks, but in case of real environments the stress values reach only the values comparable with the strength limit in upper part of the crust to the depth ca. 2-5 km.

If we consider larger periods of climatic variations than Milankovitch cycles, then the thermal wave would affect the whole thickness of the Earth's crust and the faulting could be observed during 'winter' (during the cold period of climatic cycle). It is visible on Fig. 4.23 that all of important orogeneses on the northern hemisphere passed during the cold periods of the observed longest climatic cycles. Their principle can therefore be identical with the plate movements in the diurnal, annual and Milankovitch cycles.

9.4 Ratcheting and lithosphere plates movement mechanism

Diurnal, annual and longer temperature variations on the Earth's surface, as it has been shown, lead to rock deformations. But, how could these cyclic changes lead to the permanent, irreversible deformations and the unilateral movement of lithosphere plates in the westward direction against the mantle? The answer is simple: By ratcheting. This mechanism was first described by James Croll on the asphalt buckling (Croll 2005, 2006, 2008) or on the periglacial morphologies (Croll & Jones 2006, Croll 2007a, 2007b). The results were applied to the Earth's layers. And a new hypothesis of plate tectonics, based on ratcheting and Milankowich cycles, was published (Croll 2007c).

Let us look for an explanation in the process of thermoelastic wave generation itself and ratcheting according to the results of our measurement.

Let us suppose that we have only two layers of rocks where the thickness of the upper layer is comparable with one half of a wave length of the annual thermal wave (e.g. ca 12 m) (see Fig. 9.12), and the second layer forms the lower half-space (see Fig. 9.15).

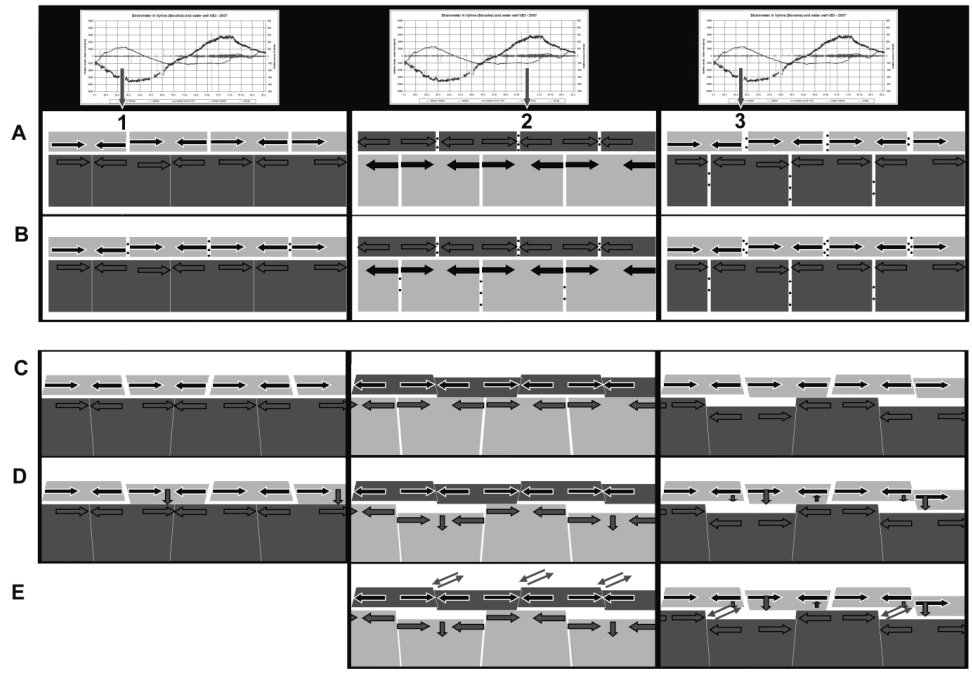

Fig. 9.15: Principles of ratcheting and movement mechanism of tectonic plates (see colour pages too).

In the spring, when the cold wave reaches the upper unweathered layers, it dilates them (see Fig. 9.15, column 1, row A). Below this layer, the warm half-wave from previous summer occurs and relatively extends these layers. The deformation (extension) is transferred also to the upper layer by sliding friction between both layers. And so, open cracks can originate. Any material can move to these cracks, mostly brought by water from the surface (soils and sands) or by gravitation (stones, blocks of rocks on faults) (see Fig. 9.15 column 1, row B). At the end of summer and the beginning of winter, when the warm half-wave reaches to undisturbed layers, it expands them (see Fig. 9.15, column 2, row A). However, the ratchets occur in this upper layer, which were filled six months before. By temperature expansion and sliding friction with the layer situated beneath, cracks open again, into which ratchets can fit from the layer situated above (see Fig. 9.15, column 2, row B). The whole process is repeated the following year only with the difference that in both layers the ratchets occur in cracks, which prevent the layer dilatation to the same position as the year before. However, the rock,

as a whole, will consequently extend (see Fig. 9.15, column 3, rows A and B).

If we suppose that the faults and cracks have all of types of dips (not only subvertical), the blocks of rocks themselves can act as ratchets. In spring, the upper layer will cool again (see Fig. 9.15, column 1, row C) and the block subsidence will occur against other blocks because the normal friction on faults will decrease (see Fig. 9.15, column 1, row D). On the contrary, the expanded blocks will not be able to get themselves into the original position during the winter (see Fig. 9.15, column 2, row D), and they will be forced to find other positions with horizontal shifts among blocks given by crack and faults orientation against principal component of stress (see Fig. 9.15, column 2, row E). The whole cycles will be repeated in spring but with the difference that blocks are already not in their original positions. And both horizontal and vertical movements originated among them (see Fig. 9.15, column 3, row D).

Therefore, in winter, we shall observe mostly pressure stress because the upper decisive layer is heated (see Fig. 9.15, column 2) and in summer we shall mostly observe tension stress with vertical block movements (column 3). Exactly such general movements were observed in 2007 on most of the dilatometers on faults and on pendulums (see chapter 8).

This described ratcheting mechanism is valid for the continental crust, which laterally grows in this manner. Since the Precambrian era, the area of all continents more than doubled (Rollinson 2008). This enlargement of the continental crust was made up of material derived from the upper mantle rocks during the entire period (Foley et al. 2003). The movement of oceanic crust is different, but the principle is the same as the ratcheting mechanism on continents.

Using the example of the Juan de Fuca plate, we will show how such a mechanism operates on the continental and oceanic crust interface. In the same way as in the previous case of the ratcheting mechanism within the continental crust, the cold thermal wave reaches unweathered continental rocks in the spring and dilates them. The continental crust pulls the lower layers including the subducted oceanic crust (see Fig. 9.16A). The weakest area, with the lowest strength in pull is, in this case, the ocean rift which opens and magma from the asthenosphere fills the released space.

In winter, when the continental crust is most dilated, the compression of the oceanic rift occurs, but because the solidified magma ascending there in the previous period prevents it from fully closing, the rift will not move to its original position. Instead, higher stress will be transferred to both parts of the oceanic crust (See Fig. 9.16B). The Pacific plate will be, therefore, forced to move westward (only by contribution of the NA plate and the rift mechanism of the Juan de Fuca plate) and, on the contrary, the Juan de Fuca oceanic plate will be forced to push underneath the continental crust because stress, which can overcome the slide friction on the area of contact of the oceanic and the continental crust, is lower than the compressive stress evoked by thermal extension of the rocks. We can estimate the size of this stress from the strain measurement in granites at a depth of ca. 100 m beneath the surface (Brimich 2006). If we suppose the effects of 10 K change in temperature at depths in the order of 20 m (layers, penetrated by annual thermal wave) and a rock having a coefficient of thermal expansion $3x10^{-5}$/K, then a strain of 300 μstrain, which if fully restrained in a rock having E = $3x10^4$ MPa, would induce a horizontal (in-plane) stress of 9 MPa in the seismogenic depths. This is significant even compared with the 240 MPa vertical stress at a depth of 8 km!

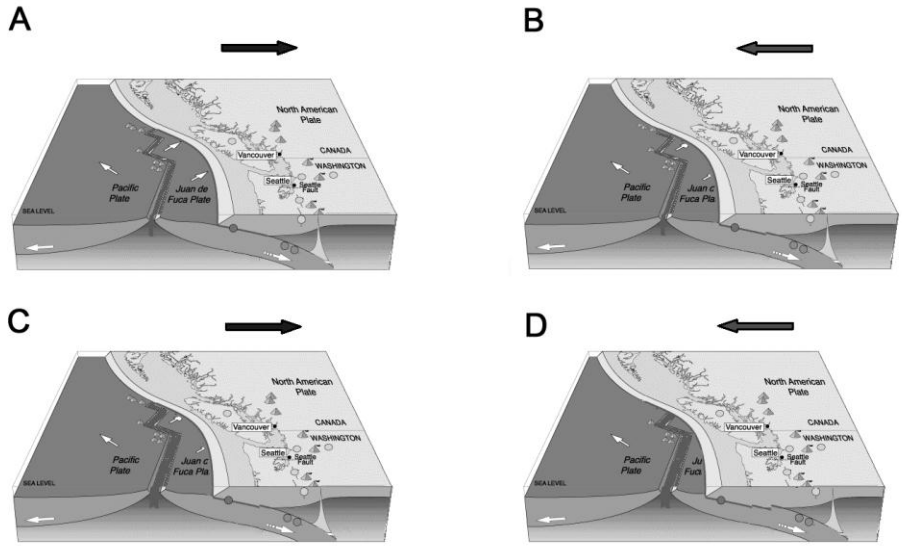

Fig. 9.16: Mechanism of movement of lithospheric plates (blockdiagram by Wikipedia, modified) (see colour pages too).

In the second year when the dilatation of the continental crust occurs, the rift zone is opened again and is filled by next magma, which solidifies on both sides of the rift on the Pacific and on the Juan de Fuca plates. The entire cycle will be repeated as far as the full subduction of the whole rift occurs. And the Pacific plate will start to subduct, but more slowly. At the same time as the subducted Juan de Fuca plate shifts, the magmatic chambers will shift further eastward (see Fig. 9.16 D).

The measured shifts of the North America plate show that the permanent shift of the oceanic crust against the continental crust does not occur only in an annual cycle and that the dilatation and extension of rocks in the diurnal cycle is sufficient for their mutual movement (Dragert et al. 2004, Royle 2006, Brudzinsky & Allen 2007). In the Cascadia subduction zone the continantal crust is compressed by the oceanic crust of Juan de Fuca plate relatively eastward by ca. 10 mm/year and approximately every 13-16 months the accumulated stress is released with abrupt movement of continental crust westward by ca. 5 mm, that is accompanied by tremors e.g. in the Victoria area (Dragert et al. 2004). Other regions of Cascadia have different regimes of triggering tremors with the quasi-periodicity of 10-18 months (Brudzinski & Allen 2007). Under tremors and earthquakes, the ratchets are not formed by shifting plates, but only by already accumulated stress releases. For this, the triggering mechanism can be different from the mechanism leading to accumulation of energy. In

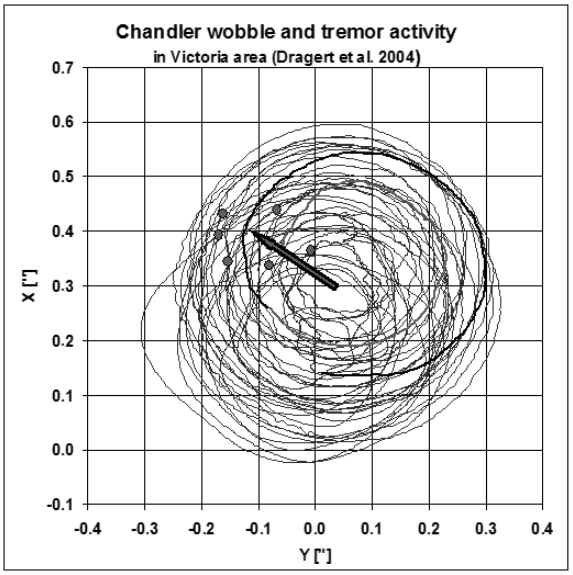

Fig. 9.17: Polar wobble in the time of tremors in Victoria area in Cascadia (Dragert et al. 2004).

case of the Victoria area the Earth's nutation was one of triggering mechanism, so tremors were triggered mostly in one phase of the Chandler period (see Fig. 9.17).

The underthrusting of the plates in the Cascadia subduction zone shows that the ratcheting mechanism had occurred already in diurnal cycles. As the measured strains at a depth of 100 m below surface show, the circadian variations have a size of 20 nstrain (see Fig. 8.3). Considering the east-west size of the North American continental crust ca 6000 km, then the total extension of the continent can be up to 0.12 m, from which one half falls on the western coast and the other half on the eastern coast. So, theoretically, the rifts could open in the order of 1 cm daily. Of course, the larger part of dilatation and extension is consummated for elastic deformations, but the part of diurnal dilatation opens the rift and the smaller part of this free space is filled by magma (ratchet). In spite of that, it is sufficient that the rift is opened, on average, for 0.1 mm and filled by ratchets. Therefore, the observable movements of oceanic crust for ca. 30-40 mm/year would occur, if only 1 % of the total diurnal variation were changed into the non-elastic deformations (Scoppola et al. 2006).

The same mechanism, as in the case of Cascadia subduction zone, was observed in Mexico with dilatation of continental crust, evoked by increments of stress in the continental crust ca. 15 cm/year, abrupt jumps roughly 50 mm (Payero et al 2008), or in New Zealand with dilatation of the continental crust ca 15 mm/year and jumps roughly 20 mm (Douglas et al. 2005).

It is necessary to explain why the preferred western movement of the plates and the western drift occur, when the dilatation of rocks acts on both sides of the continental plate equally. Most of exogenous mechanisms evoking Earth's crust deformation have a westward drift (irradiation, tides, LOD, and direct gravitational action). This is caused by the Earth's rotation around its axis and by the position of two main bodies – the Sun and Moon. Looking in more detail at the effects of these mechanisms, we can see that their action is asymmetric with quick increment of forces and stresses in front of the 'wave' and slow reverberation in the tail (see Fig. 6.6, 9.11). This asymmetry leads to the effect that rock properties will apparently

change according to the increment of forces. The rocks will appear more rigid for the quick increment of forces then for the slow subsidence. So, in the front of the wave the rock will be more deformed over a greater distance then it will relax on the tail of the stress wave. The most asymmetric effect was measured with the diurnal variation of insolation and therefore this mechanism is probably the decisive mechanism for the westward drift. The smaller effect, but not negligible, will be produced by the Earth's tides and mainly by the ocean tides, which drift water masses in a westward direction.

9.5 Discussion of thermoelastic and ratcheting model of the movement of lithosphere plates

The proposed model of lithosphere plates movement is driven by thermoelastic waves, generated above all by Earth's surface irradiation. This proves to explain the different velocities of lithospheric plates movement against the mantle and in many cases against each other. Taking into account the model of the real Earth as it is theoretically outlined in chapter 3.5 and modelled in chapter 3.6, we can see that the oceanic plates between two large continents are moving very quickly. Adding dilatability of Eurasian and South American plates in their largest dimension, we can see that the Pacific plate, which is situated on their connecting line, will shift, theoretically, with the highest speed against the mantle, which has been confirmed by measurement (Fig. 9.1). Smaller oceanic plates anchored between the Pacific plate and both Americas plates (Juan de Fuca and Nazca) have relatively small speeds of movement against the mantle, similarly to Galapagos block (between Nazca and Cocos plates).

The movement velocity of the continental plates is distinctly lower compared with the oceanic plates. Many of them move against the mantle with only negligible velocities (Antarctic plate, Indian plate) or with small velocities (Australian plate). A dependence of velocity of the plates on the depth of their roots has been observed. Continents with deeper roots have lower velocities of movement against the mantle. In the case of deeper roots, a lot of friction originates, which the mechanism of western drift has to overcome.

This theoretical model of plate movement and the ratcheting mechanism also explains the contemporary direction of the plate movement, which has not exactly the western direction but the plane of equator inclines against the geographical equator by ca. 32° (Doglioni 1993). Connecting the sites with the highest irradiation of all continents in summer with the sites of highest insolation of all oceans in winter, we can find that the equator of lithospheric plates movement passes through both points. This determines the largest deformation of the main continental surfaces on the Earth, and therefore the deformation of Eurasia and Africa. Performing the same analysis with the Australian, Antarctic and South American plates we can find that the dilatability of these continents determines the direction of movement of these plates, with the difference that the larger area of Eurasia and Australia dominates the whole movement of Antarctica in the direction to the Americas.

This theoretical model also shows that important mechanisms – thermoelastic wave, gravitational effects, tides and change of Earth's rotation velocity have synchronous action with western vergency because their periodicity is determined by Earth's rotation and its position against the two most important bodies – Sun and Moon. This effect is not symmetric on the west and the east. Tides and LOD contribute to the decrease of friction and for the increment of shear stress between the crust and the mantle. Also, the direct role of pressure in magma is not negligible as it is possible to observe e.g. on tidal periods of permanently active volcanoes in rift zones – open gates to the Earth's interior (Tazief 1975).

The outlined model shows how and where the energy is consumed and accumulated in rocks in thermoelastic waves. The regions, where the greatest changes of elastic energy into seismic energy occur, are the fragile and shallow regions, which are where the plates contact. The one exceptions is the deep Wadati-Benioff zone, where one solid lithosphere plate submerges beneath another one. And both friction and its dissolution and fracturing occur. In sites with lower viscosity, instead of earthquakes, only silent slip earthquake (SSE) or tremors occur. Their analogy occurs also on the contact of the lithosphere bottom with the mantle. There the thermal energy will be released everywhere giving origin to volcanoes of island

arcs, mountain belts and rifts. On the other hand, the smallest energy release will be observed in sites of low friction of oceanic and continental plates with the mantle.

The outlined theoretical model of movement mechanism of lithosphere plates can be verified by the development of continents since Precambrian age.

The most interesting question from the geology of the Precambrian age is: Why are not the linear orogens of the Archean age known? This fact, together with the high age of most of continents, is generally accepted as a proof that the plate tectonics started during Proterozoic, or perhaps as late as the Upper Proterozoic age.

Comparing basic factors, which can cause the hypothetic convection currents, we can show that in the first periods of the Earth's development their effects were greater than today. Remaining heat after the Earth's accretion was higher; radionuclides were less concentrated in the crust and they were more abundant, the Earth was less stratified than it is today, tides were higher and also the speed of the Earth's rotation was higher. Qualified estimation of remaining heat states that 2 billion years after the Earth's origin, the remaining heat had been at least 4x higher than today. Radionuclide heat production 2 and 4 billion years ago gives the Table (5).

Table 5. Relative amounts of main radionuclides and decay series (the same ratios are valid also for by-products) at the present time, two and four billions year ago and total production of radioactive energy by them (calculation according to Rybach (1976), contents of K, Th and U in the Earth body for present time according to Allegre et al. (2001)) with correction for changing uranium isotopic composition. Owing to the probable considerable importance of today's already extinct radionuclides the production of radioactive energy in Archaic was apparently much higher.

radionuclide (series)	^{40}K	^{232}Th (series)	^{238}U (series)	^{235}U (series)	output (K+Th+U)
present time	1.0	1.0	1.0	1.0	1.0
2 billion years ago	2.9	1.1	1.4	7.2	1.7
4 billion years ago	8.4	1.2	1.9	51.4	4.0

Similar to the radionuclide heat production and Earth's accretion, the tidal effect was higher in Proterozoic age, as can be seen on the base of rythmits, which were analysed by Williams (2000). In Upper Proterozoic age (~620 M.y.) the Moon was at the distance of ca. 0.965 **a**, therefore almost the same as today, but in the Lower Proterozoic age, 2 billion years ago, its distance was 0.6-0.9 **a.** Tides at that time were 1.44-4.5x higher than today (**a** = large semiaxis of Moon's orbit). Also the Earth rotation was, in the Archean age (Lower Proterozoic?), approximately 1.5x faster than today, and one solar day was ca 17 hours long (Williams (2000).

In contrast, the temperature on the Earth's surface was, soon after its creation, comparable with the present time. The existence of sea sediments with an age of about 4 billion years is witness to this. The temperature difference between the lower mantle and the surface was therefore incomparably higher than at the present time because the temperature of mantle was higher. Also the viscosity of the lower mantle was lower. This means that possible convection cells in the mantle, if they existed, should have been far more powerful in the Archean age and in the Proterozoic age.

As it can be seen, not one of mentioned mechanisms (radionuclide heat, Earth's accretion, tides) moved the continents during the Archaic age, although they were much stronger than today.

Trying to have a look on the mechanism of lithospheric plates movement through the prism of thermoelastic waves and the ratcheting mechanism, we have several explanations why in Archean age, collisions of continental lithospheric plates could not occur, although the plate movement itself occurred.

The main factor of movement is the dilatation of continental plates and their interaction with ocean lithospheric plates. In the Archean age, the area of continents was a half that of today's (Rollinson 2008), and the magnitude of interaction of continental plates was in half or smaller. In addition to this, we suppose that the continent was not decayed into a number of blocks and therefore we suppose a simple interaction between one continent and several ocean lithosphere plates, which on the western coast of the continent submerged beneath it in the same way as today, forming far smaller

mountain ranges than today's Alps or Cordilleras. On the eastern coast of the continent, the island arcs were created the same as today (see Fig. 9.6, compare Scotese 2003).

The Earth's climate seems to be yet a more important aspect. In the Archean age, the climate was far warmer and almost changeless. The atmosphere in the Archean age and even in most of the Proterozoic age was, in comparable with today, distinctly reductive and richer in carbon dioxide (CO_2) (Berner 1991). In modern times, CO_2 has been removed from the atmosphere by natural processes because volcanism cannot compensate the sedimentation of carbonates and burying of organic carbon. As the mechanism of continent movement utilizes the difference of rock dilatation by changes in their temperature, no distinctive deformations of continents and no great movements of oceanic plates occurred at that period. The same reason for the absence of plate tectonics can be seen in the case of Venus where, owing to the greenhouse effect, the difference of temperatures on the day and on the night side of the planet is negligible. It seems that observable orogeneses coincided with cold climatic periods on the Earth, when the content of water vapours and CO_2 in the atmosphere probably radically decreased and the temperature differences between day and night and between summer and winter increased (see Fig. 4.23).

The next necessary, but not sufficient condition for plate tectonic origin, is the presence of two or more types of plates with different materials of different dilatability, strength and plasticity. In cases when the lithosphere is so strong that distinctive temperature changes could not divide it into plates and move them, we could observe only cyclic deformations and possible cracking as it is in the case of Moon. There, moon-quakes occur with period of ca. 27.5 days, consistent with the Moon's orbital period. In the case of one type of rock, as it is e.g. on Jupiter's satellite Io, we can observe a distinctive volcanic seismic activity generated by tides (Strom et al. 1979). Similarly on Neptun's satellite – on Triton – we can observe ice volcanoes also generated by tides (McKinnon & Kirk 2007). The tides are able to generate sufficiently large amounts of energy to initiate ice-volcanism in both cases, however no plate movement against deeper layers occurs, probably due to an absence of thermoelastic waves and the absence of more homogenous material on the surface of both satellites.

The ratcheting mechanism leads to diagenesis namely of sedimentary rocks. As the ratcheting mechanism itself does not lead to the continental crust division but uses only already prepared faults then an independent question seems to be: What did cause the initial fracturing of the continental (Rodinia) and/or oceanic lithospheres into small blocks? We assume that one of the mechanisms, which could lead to the division of the continental plate into smaller pieces, could be a large asteroid impact.

From the point of view of this new global tectonics theory, the most important changes from Archean age to the present can be summarized:

1. The denser atmosphere of the Earth, which was many times richer in carbon dioxide, caused the temperature variations that were far less distinctive than at present. From this point of view it is reasonable to suppose that there has been a long-term trend of increasing intensity of periodic deformations of the lithosphere (and according to the new global tectonics also movements of lithosphere plates).
2. In contrast, the energy contribution of the tidal forces, Earth's primordial heat (from accretion) and radionuclide heat – not only relative but also absolute – to the geological processes, has decreased in time.
3. The origin of dry-land plants and soil (worldwide in Silurian or at the latest in Devonian) meant not only erosion suppression, but also apparently partial suppression of periodic temperature variations and successive surface deformation. This could be an explanation why the plate tectonics, in spite of the continuing long-term weakening of the greenhouse effect, was not expressively 'accelerated'.
4. The distribution of continents whose reconstruction is however, for the Precambrian age, very uncertain, would probably have a considerable importance for possible effects of thermoelastic deformations.

Our theory makes it possible to explain the non-existence of plate tectonics in the Archean age, supposing that more equalized temperature - a consequence of strong greenhouse effect -was more important than the stronger tidal action and the quicker erosion. Verifying correctness of this assumption is, according to author's opinion, the theme for the next

research, and probably will not be possible without considerable extension of still fragmentised data about most of the Precambrian period.

9.6 The preliminary earthquakes preparing and triggering model

The preliminary earthquakes preparing and triggering model (EPTM) has been formulated. We suppose, this is only the preliminary model and that it will become more accurate in the future. Therefore, any of the future earthquake predictions will not give us the answer if the precursors will be found, but whether they are correctly interpreted by means of this model, providing the earthquake prediction enables us to verify the suggested model and data interpretation in its frame. The earthquake prediction is not a test of measurement quality.

Description of the model:

1) Tectonic stress generation

Many cyclical processes exist on the Earth's surface, which cause its deformation (thermoelastic waves, tides, air pressure variations, variations of the revolution of the Earth, direct gravity influence of planets – see Chapter 3). Most of the processes have the western drift, based on the revolution of the Earth around its axis. Although these processes cause the changes of stress in the order of kPa, all of them contribute to the process of energy accumulation in rock mass. However one of them – thermal extensions of the rocks – is able to increase the stress in the order of Mpa. It is not able to move the lithosphere plates itself. How can it be that this energy accumulation proceeded and how can it be that the lithosphere plates moved?

Non of the deformation processes are reversible because there is one important mechanism – ratcheting (see Chapter 9.4), which causes the irreversibility of the deformation and continual increasing of accumulated energy in the rock mass. The nonlinear irreversible process (ratcheting) can exist everywhere in the rock mass. In this way, the continents are spreading out all the time because the ratchets fill the free space in the faults, cracks or micro-cracks. This ratcheting is important in the case of the system, when

the oceanic crust is between two continents. In this case, the ratchets (new lavas) fill the free space in mid-ocean rifts, which causes relative quick spreading of the ocean crust on both sides from the rift zone and the expanding of the ocean between two continents. If the expansion of rift is greater than the space of the ocean between continents, one or both sides of ocean crust are pushed down under the continental shelf.

This ratcheting is acting on all discontinuities on all of scales on the Earth, beginning with the crystal structure, micro ruptures, through the scale of rock mass blocks, up to the global-scale faults, lineaments and rifts. This ratcheting is able to collect the small increments of deformation during long-time period into a huge deformation or sudden slip of fault as an earthquake.

As the movement of massif is asymmetric (compare Figs. 3.7a and 6.6a or 9.11), the strength limit is exceeded and accompanied mostly by westward movement and less by the eastward movement. This causes the westward drift of the continents against mantle, which is in accordance with the western movement of the deformation 'waves' on the Earth's surface (see Chapter (9.1). The drift of lithosphere movement follows the direction of dominant diurnal extension of the continents (see Chapters 3.6 and 9.1).

The ratcheting process itself cannot generate stress in the rock mass. It increases the size of the rock mass in the horizontal plane, but the Earth's surface is constant. The trend of the increasing of the size of the rock mass in the horizontal plane against the other masses on the constant surface of the Earth creates continuous stress and deformations.

2) Stress redistribution mechanisms – asperity model

The deformations, that probably precede big earthquakes, could be described on the basis of the model of the earthquakes focus. The asperity model (Wyss et al. 1981) appears to be the most plausible model, which shows that the movement between the wings of the fault starts at the time when the asperity, which inhibits the movement, is going to break. The size of the asperity determines the accumulated energy and the accumulation period. The bigger the asperity then the bigger the earthquakes and the longer the time of destruction (seismic cycle). Several different asperities can be on one fault or in one focus area and they will decide the

development of the future EQ focus in time and the development of the release of energy.

The asperity model shows (Wei 2007) that in the gradually increasing stress field (the consequence of tectonic movements), no precursors can be observed during the first stage, the energy accumulation phase. This period can last tens, or even hundreds of years depending on the size of the asperity and the velocity of the tectonic movement.

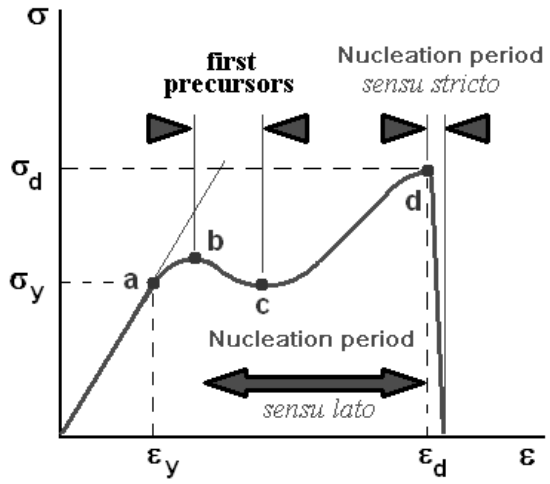

Fig. 9.18: Definition of nucleation period: a – proportional limit, b – upper yield limit, c – lower yield limit, d – failure limit, (σ_y, ε_y) – deformation on the proportional limit, σ_d – tensile strength, ε_d – tensibility.

The point **a** - proportional limit - (see Fig. 2.1 or 9.18); when the stress is approaching the strength limit, the higher strength of asperity appears and the deformation rate decreases. Sun Wei (2007) called this phase 'deadlock'. At this moment the destruction of smaller asperities starts and the main portion of stress concentrates around the main asperity. The outward behaviour of the massif is chaotic – the disturbances of deformation are observed at the time of the destruction of smaller asperities. This period could lasts from days to months depending on the size of the main asperity, until the point **b** is reached (upper yield limit) (see Fig. 2.1 or 9.18), when the destruction of the main asperity starts. The apparent stress relaxation prolongs until point **c** (lower yield limit), which takes from few days or weeks. The quickest phase of the nucleation period *s.l.* (the transient stress-hardening) starts from point **d** (failure limit), when the movement on the fault plane (nucleation period *s.s.*) begins. The period of the transient stress-hardening lasts from hours to days.

The whole process of the energy accumulation to the massif destruction is not observable by apparatus. The first precursors appear during the

second stage (phase) around point **b**, when the smaller asperities are broken. The rate and meaning of the deformation changes in the massif surrounding the main asperity is changing at the same time. Then the nucleation phase (stage) *sensu lato* starts. Its time period, with the respect to the asperity size (proportial to earthquake magnitude), can be described for average tectonic settings by the equation (2.4).

We can see that the 'stress waves', which are generated around the main asperity before its destruction, will last from days to months. Such periods are not observable by standard wide-range seismic apparatus (see Fig. 9.19). Only static apparatus, i.e. gravimeters, deformometers or tiltmeters with the non-compensated base, could be used to observe these deformations.

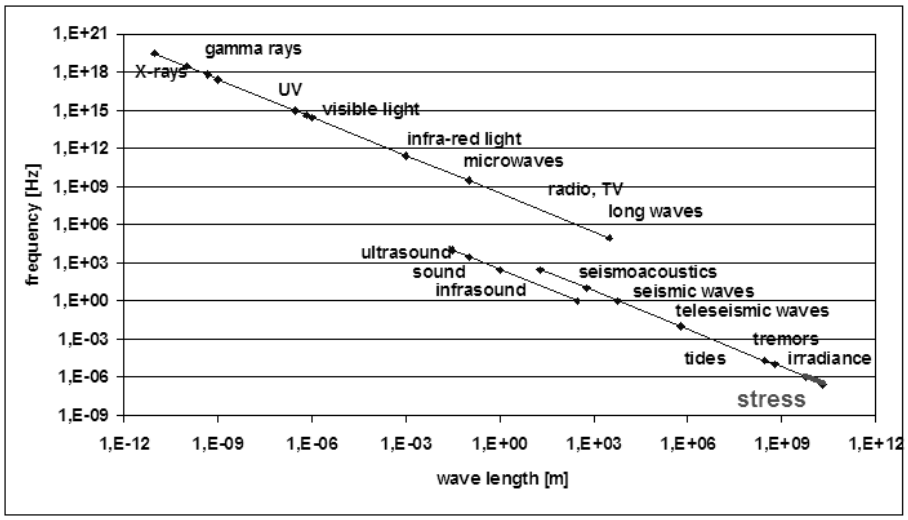

Fig. 9.19: Spectrum of E-M waves, sound waves in the air and waves in rocks.

As the wavelength of the 'stress waves' is longer then the Earth's circumference, the attenuation of these waves is a relatively small depending on the number of contacts between lithosphere blocks (number of faults) and their openings.

The movement of 'stress waves' is in accordance with the western drift mostly to the west from the asperity.

3) Triggering of earthquakes

The small increment of stress can trigger the mainshock when the stress state is approaching to the strength limit of the rock mass (point **d** on the Fig. 2.1). This is the reason why any of the exogenous or endogenous mechanisms can trigger the earthquake, as is shown in Chapter 4.

The most important triggers of earthquakes (and mechanisms of deformation of the Earth) have diurnal periods as shown in Chapter 3. The number of earthquakes, which are triggered by mechanisms with diurnal period is 3 to 5 times larger, than the number of earthquakes triggered by tides or changes of the revolution of the Earth (LOD) (see chapters 4.1, 4.7 and Kalenda et al. 2006). Today we assume that the diurnal period of deformation of the Earth is mainly connected with the thermoelastic wave, generated by solar irradiation of the Earth's surface and thermal variation of the rock mass. However, many other mechanisms have diurnal periods too (see Chapter 3). The thermoelastic wave itself has longer periods, which generate larger deformations of the Earth's crust – annually (see Fig 8.3), Milankovich periods (see chapters 4.8 or 9.3), or climate periods (see Chapter 4.8 and Fig. 4.38). The stress in the rock mass is greater than the strength limit of the rocks during such long-period variations (see Fig. 9.14).

The second most important mechanism appears to be tides with periods of 18.6 years (Moon nodal period), Moon perigee period of 4.425 years (see Chapter 4.2, by its annual or semi-annual variations (see Chapter 4.4) and by fortnightly, diurnal and semi-diurnal variations (see chapters 4.3 and 4.4).

The direct influence of tides on the deformation of the Earth (and triggering of earthquakes) is covert by the complementary mechanisms of tides – the changes of Earth's revolution – LOD (see Chapter 4.5), because its action is the biggest at the time of the minimum action of tides (see Chapter 4.4). This mechanism supports the layering, the inter-layers deformations and movement of lithosphere plates on the asthenosphere (see Chapter 9.1).

The polar wobble plays a similar role as the LOD parameter (see Chapter 9.4), because it deforms the whole Earth and it supports, mainly, the interlayer movement.

The other trigger mechanisms, like earthquakes, have a smaller radius of influence than above-mentioned mechanisms, because seismic waves have greater attenuation than 'stress waves'. The only exception to this rule is the opposite side of the Earth, where the amplitude of seismic waves increases (due to the spherical shape of the Earth). The amplitude could be comparable with their amplitude in the vicinity of the focus of the triggering earthquake.

Other triggers of earthquakes (floods, air pressure anomalies, hurricanes, precipitations and human activity – see Chapter 4.9) seem to be less important.

It should be noted that the influence of different triggers could vary significantly in different places and at different times. The spatial dependence can be caused by irregularity of the rock mass material in different places. And and time dependence can be caused by the memory effect (hysteresis) of the ratcheting process.

4) Precursors of earthquakes

As it was shown on the asperity model (see Chapter 2.1), the various kind of precursors occur at the beginning of the nucleation stage *s.l.* (point **b** on the Fig. 9.18), because smaller and weaker asperities in the vicinity of the main asperity are destroyed before the main asperity. At that time the main asperity becomes the main stress concentrator and the disproportion between main asperity (hardening) and it's surrounding (softening) increases. This process was described and observed in laboratory conditions by F.Freund et al. (2006).

The precursors could be divided into three categories:

- local (radon anomalies, gas anomalies, earthquake clouds, infrasound, local deformations, ion, thermal anomalies, …)
- short-range (electromagnetic field, ionosphere, water level, tilt, gravity, animal behaviour anomalies, …)
- worldwide (stress field, Earth's axis movement (Chandler wobble), LOD, global electromagnetic field, …).

All of the precursor anomalies need not strictly fall to their categories and overlap. The area where the precursor can be measured can be dependent on local conditions and on the magnitude of the future earthquake.

The local precursors are created mainly by the point-source mechanisms, which are connected directly with the focal area and faults within. The advantage of these local precursors is the fact that they are mapping this focal area, but their disadvantage is the limit of observations and the necessity of the measurement directly in the focal area. They are not detectable outside the focal area with two exceptions – earthquake clouds (Uda & Maeda 2006) and thermal anomalies (Wei et al. 2009), which are detectable from space by spacecraft. Using these local precursors, it is possible to estimate the diameter of the future focus of the earthquake and its magnitude as well.

The short-range precursors are connected, first of all, with the changes of various fields (electromagnetic, gravity, stress, deformation), which have smaller attenuation of measured parameters with the distance than local precursors and, therefore, are detectable on the wider area by a less dense network of observation sites. Many such observation methods are used for a long time (water level measurement, VAN method, measurement of tilt or deformation of massif) Many of them are quite new (measurement of EM anomalies by spacecrafts (Němec et al. 2005), measurement of ionosphere anomalies (Liu et al. 2004) and some of them are more traditional but work empirically (animal behaviour – Li et al. 2003). The short-range precursors can detect the anomalous period and localise the focal area, but they are covered many times by the noise from other sources e.i. local seismicity, human activity or distant large (significant) earthquakes.

The worldwide precursors are based mostly on the changes of the stress field and the deformation of the whole Earth. Therefore, these precursors are able to detect the anomalies preceding the largest earthquakes in the world. The measurement should be executed in the quietest areas to decrease the noise and the consequences of local seismic activity and the whole globe so as to correlate the anomalies in time.

It is possible to correctly estimate the focal area, magnitude and time of future big earthquakes by measurement of all of kinds of precursors and by

merging the information from different sources (areas and measurement devices).

The above described **preliminary earthquakes preparing and triggering model** has the following **properties**:

1) The model is global – this means that all of the lithosphere plates are continuously in mutual contact and the stress redistribution concerns the whole Earth. The model supposes very close stress bounds inside one lithosphere plate and the coincident action of all forces on the whole Earth. As all of the lithosphere plates are in mutual contact (even when sometimes very weakened, e.g. in the mid-ocean rift zones), the movement of one plate causes redistribution of stresses both on margins and inside lithosphere plates. This redistribution of stresses (and deformations) results in the status quo among plates being disturbed, and afterwards they will look for the next optimal position relative to the plates around them.
   This is the difference from all of the previous models, which supposes that the energy accumulation proceeds by a slow tectonic process until the time when the rock stress approaches its limit of strength (Mjachkin et al. 1974, Rikitake 1976, Bolt 1988, Sobolev 2003). According to them, during great earthquakes, the most of accumulated energy is released and the process starts again.
2) The main mechanism of energy accumulation is tied with exogenous forces (tides, thermoelastic waves, Earth's rotation velocity change, atmospherics, dynamic of gravitation and others). The most important source of energy is solar irradiance.
3) The exogenous forces together with ratcheting mechanism and the Earth's rotation results in the preference of unidirectional movement of lithosphere (to the west). Endogenous forces (radionuclide heat, Earth's accretion, gravitational separation of minerals according their density, etc) play only a negligible role in the stress accumulation process.
4) The model enables us to explain the western drift of lithosphere against the mantle (Doglioni 1993, Ostřihanský 1997, 2004, Doglioni et al. 2003, 2005, Scoppola et al. 2006, Crespi et al. 2007) and

therefore the western drift of deformation of lithosphere and/or the stress waves.

5) The effect of exogenous forces is not permanent and uniform as previous models of earthquake preparation presumed (Mjachkin et al. 1974, Rikitake 1976, Bolt 1988, Sobolev 2003). Instead, most of the effects are dynamic because most of these exogenous forces have a cyclic character. The non-linear effects around the strength limit and the ratcheting mechanism make the seismic response to the exogenous forces chaotic.

6) The viscosity of asthenosphere, friction between lithosphere and mantle, and geographic distribution of continents on the Earth decides the velocities of plate movement (Doglioni 1993).

7) Any of the movement mechanisms can be an earthquake trigger. However, each of them has a different importance. As the environmental parameters are not the same (e.g. fault orientation), quite different consequences can be observed in one region at different times. Each earthquake is triggered by a combination of trigger mechanisms. It is extremely complex to determine in advance, which effects will prevail at a given site at any given moment.

8) Observable consequences of exogenous effects are dependent on local conditions at different measurement sites. So, it is necessary to interpret globally the measured data taking into consideration the local conditions at sites of measurement. From this point of view it is possible to compare the Earth's crust to the pile of stones, which has a unified sense of deformation during its displacement by bulldozer, but each stone has its own velocity, sense of rotation and reaction time to external stimulus.

9) The model takes into consideration that the earthquakes are connected with mutual movements of lithospheric plates and with stress redistribution in the crust and upper mantle. So, the lithological content and geometrical displacement of plates, blocks and layers, deals with the stress field and its changes.

10. EARTHQUAKE PREDICTION

We consider the earthquake prediction one of the main but, as it has proved, realistic targets of present-day seismology. The term prediction, however, does not mean so-called 'long-term' or 'medium-term prediction', i.e. statistic prognosis (Keilis-Borok & Kossobokov 1990) but rather, immediate determination of time, place and magnitude of a future earthquake. Let the statistic prognosis continue to serve the purpose of identifying the potentially dangerous areas on which it is necessary to focus the prediction, and especially when applying the anti-seismic construction standards.

The predicted time window for an expected earthquake should be comparable with the nucleation stage immediately preceding the main breakage of rock (see Chapter 2.2), i.e. in the order of several days to one month for major earthquakes with M>7.5 (see Fig. 2.2). On the other hand, the term prediction does not mean the ex-post warning issued after the earthquake occurrence and preceding, in a given area, the seismic waves due to a higher velocity of propagation of electro-magnetic signals than seismic waves (for instance tsunami).

10.1. Prediction Methods

How can we, by means of vertical static pendulums, predict an earthquake, i.e. specify the time window during which we can expect the earthquake to occur, the area in which the accumulated energy is going to be released, and the earthquake's expected magnitude? From our point of view, the easiest one is specifying the time window for the earthquake. Why? This is because (as we have shown in Chapter 7) both the massif deformation and noise of rock mass depend on the amount of stress in the rock layers. More specifically, the pendulum deviations are proportional to the time derivation of relevant components of stress tensor in the rocks surrounding the pendulum. And the noise is proportional to strain. Thus, it is easy to identify the time period during which stress is increasing, and to

estimate its relative value when compared to the strength limit of the rocks surrounding the pendulum.

Hence, **the time window for an expected earthquake** may be estimated based on the development of **the anomalous tilts** of the pendulum and the increase in **noise** detected by the pendulum. As an example, let's take the development of both parameters prior to the Sumatra earthquake that occurred on September 12, 2007 (Ms=8.5) when, approx. two weeks before the earthquake, the largest anomalous tilt in the year 2007 was observed on the P7 pendulum (see Fig.7.4). At the same time, the anomalous noise increase was observed on all pendulums (P1 and P7) (see Fig. 8.8) as well as on the strainmeter (see Fig. 8.3). On the absolute gravimeter at Pecný a higher gravity than average was also observed in the residues (see Fig. 8.7).

Analogically, the earthquakes in Indonesia on January 03, 2009 (M=7.6) and Sumatra on September 30, 2009 (M=7.5) (see Fig.8.2) could be predicted. They were the most powerful earthquakes on our plate during 2009. They followed a pronounced tilt of the pendulums towards south and west and an increase in noise. Additionally, on the relative gravimeter a gravity increase was observed prior to both earthquakes. That gravity increase is, through the rock density, directly proportional to stress.

The second method of establishing the time period of anomalous stress is based on the recognition of so-called **'stress waves'** or **'tectonic waves'**. If the strength limit around the future focal point of a major earthquake is exceeded then the creep, tremors or micro-earthquakes are caused in the surrounding areas. Stress waves originating this way don't need to be of a seismic nature (although they could be) and their repetition period depends on the triggering mechanism of the triggered earthquake. Where the waves are induced by solar irradiance, they show similar behaviour as seen in figures 6.6a, 6.6b, 10.6 and 10.9. Where the stress waves are induced by tidal strain their behaviour looks like Fig. 6.5. The stress waves may also be induced by different triggering mechanisms with longer than semidiurnal or diurnal periods (LOD, Chandler wobble) or even with yearly periods, where we observe something similar to Fig. 7.5 on the NS component. The advantage of detecting stress waves is that they appear in the time period

closely preceding the main rupture only when the stress in a large area is nearing the strength limit of rocks in the focal point area, and the asperity preventing the plate from moving starts to break.

The 'stress waves' are different from seismic waves in that they have super-long periods (semidiurnal and longer) and super-long wavelengths. From this point of view all deformations associated with 'stress waves' occur in the near field of the focus area. This is different from the seismic waves, which are observed mostly in the far-field area and is the reason why the attenuation of these 'stress waves' is very low. We could also observe the 'stress waves' coming from opposite hemisphere, more than 10000 km away.

For the 'stress waves' the relationship

$$\log(r) = 0.5\,M - 1.96 \qquad (10.1)$$

found by Takemoto (1991) based on the stress-tilt measurement in Japan, and the relationship

$$\log(r) = 0.43\,M \qquad (10.2)$$

proposed by Zadro & Breitenberg (1999) are not valid.

Through recognition of a stress wave with a diurnal period, the earthquake that occurred in the Kuril Islands on Novemebr 24, 2008 (M=7.3) was predicted. The stress wave related to the earthquake in Sichuan on May 12, 2008 (M=8.1) (see the following Chapter 10.2) was detected in advance, and the area in a critical state of stress was recognised in Afghanistan on February 27, 2010 (M=5.9) (see Chapter 10.3).

Forecasting an earthquake's expected location is more difficult than determining when it will occur. Since we will probably never be able to measure the complete stress tensor and its changes in an intact environment not affected by the underground working itself or the cave where the pendulums are placed, we will always have to consider the interaction of the stress field and the measured part of the massif. Therefore, we will always have to interpret the results of the massif deformation with regard to the measurement geometry, the geometry of the measured space, the tectonic situation of the space, and other factors. This way, for example, the P7

pendulum in Příbram, 96 m deep under the surface, situated in the northern corner of the chamber, measures almost proportionally the deformations induced by the forces from the northern or eastern directions (see Fig. 6.12). However, this does not apply to the forces from the south or southwest. On the other hand, the P6 pendulum, situated at the southern wall of the road with the EW direction, does a good job of measuring the deformations induced by the forces from E and W. However, it is almost insensitive to the principal component of stress tensor, which is in the NS direction. Even more complicated is the situation when measuring in the field close to large tectonic faults. This way, the pendulum in the 13C cave that is situated directly at the active fault with the NS direction is extremely sensitive to the stress changes in this direction. In contrast, the pendulum in the Ida gallery that is situated near the active Hronov-Poříčí fault with the NW-SE direction is highly sensitive to the stress changes in that direction.

Hence, the basis for the focal point localisation may be the direction in which the relevant component of stress increases, or the direction in which the rock is deformed most. Once again, the earthquake in Sumatra on September 12, 2007 can serve as an example. The anomalous direction of deformation was almost perpendicular to the general trend of the long-term tilt of the massif (see Fig. 7.4). The second possibility is to monitor in which direction sudden tilts of the pendulum occur, when the stress exceeds the strength limit of the rock near the pendulum (see e.g. Fig. 7.7). The third possibility is to compare the behaviour of the pendulums situated near the faults with various orientations. The largest anomalous deviations have been observed with pendulums located near active faults that have the same or similar directions as the applied force.

If we detect the 'stress waves', we have yet another method of forecasting an expected earthquake's location. If we determine which triggering mechanism induces the particular 'stress wave' we are able, in some cases, to localise the asperity on which the waves are induced. In this respect, the easiest case seems to be the detection of a diurnal wave such as the earthquake in the Kurils on November 24, 2008, or the earthquake in Sichuan on May 12, 2008. In both cases, the stress wave was generated by the sunlight irradiation, which, as we already know, generates the thermo-elastic wave with maximum stress in the afternoon hours between 12:00 and

14:00 (local time). Therefore, we are able to assign a relevant longitude to the time of the 'stress wave' arrival. In the case of Sichuan, the maximums of noise on pendulums were observed around 6:00-8:00 UTC, i.e. around 13:00-14:00 LT (see Fig. 10.5 and 10.6). The main event was triggered at 13:28 LT (6:28 UTC), analogically to the largest aftershock on May 25, 2008 8:21 (UTC) 15:21 (LT) (M=6.1 NEIC). In the case of the earthquake in the Kurils, the 'stress waves' arrived at around midnight. So it was obvious that the asperity must lie on the opposite side of the Earth to the Greenwich meridian where the Kurils and Kamchatka are situated. Therefore, the future focal point of the main event was located there (see Fig. 10.9).

Since there are several fault zones in a critical state and near to breaking point on the Earth's surface at any given time, several 'stress waves' are always moving around the Earth. When we evaluate the statistics of the times of their arrivals and we assume that most of them were induced by solar irradiation and generation thermo-elastic waves, and then we may evaluate the longitudes where the breaking asperities are. For example, we analysed the time period of January 17, 2010 to February 17, 2010. We evaluated the anomalous stresses and deformations, which were detected and we discovered that the asperities were likely to be situated in three areas (see Fig. 10.1). Most stress peaks arrived from Afghanistan where immediately after the earthquake in Chile an earthquake was triggered, on February 28, 2010 (M=5.9). It confirmed the accuracy of the asperity localisation. The second maximum of peaks pointed to the New Guinea area and the third one pointed to Haiti - Costa Rica. Unfortunately, on February 27, 2010, the third asperity was situated on the same meridian, but not in Haiti or Costa Rica, but in Chile where at 6:34 UTC a catastrophic earthquake occurred with M=8.8 on the 72W=288E meridian. That, however, could not be predicted from the Central Europe. This shows the need for a cooperative effort involving as many forecasting methods as possible on both global and local scales, not only just deformometric methods.

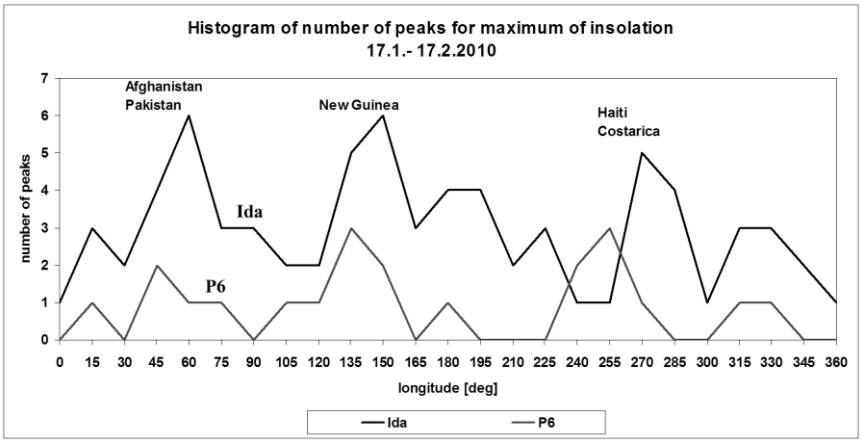

Fig. 10.1: Histogram of the number of 'stress waves' peaks at noon on local meridian.

Through cooperation involving local methods, it was possible to determine the focal point of the earthquake on February 27, 2010 east of Taiwan. Based on the measurement of the massif tilt in the Ida gallery from January 27, 2010 to February 1, 2010 (see Fig. 7.7) it was discovered that the anomalous force acted from ESE and the noise peaks were most frequent around 6:00 – 8:00 UTC corresponding to the asperity longitude of approx. 120E. As the inaccuracy of the stimulation of acting force direction from Central Europe did not allow us to differentiate between many possible focal areas from Japan to Indonesia, the e-mails were sent to Japan and Indonesia on February 2, 2010 with the request for a possible specification of the focal area. The reply from Indonesia was that they had registered the stress anomaly, but the focal point was not on their territory (Wahyudi, personal info). The prediction of a possible earthquake arrived from Tokyo on February 4, 2010. It pointed to the Taiwan area for around February 6, 2010 with a magnitude of M=6.2. The prediction had been made based on the detection of so-called 'earthquake clouds' on the Meteosat Satellite photographs (Shinichi Uda, personal info). The reality outdid the expectations as the earthquake occurred on February 7, 2010 at 06:10 east of Tai-wan. Its magnitude was 6.3 (NEIC). The probability of an accidental occurrence of such Event with M≥6.2 in a 7-day window within a zone of 1000 km from Tai-wan was 3.5%!!!

From our point of view, the most difficult part of forecasting an earthquake has to do with determining its likely magnitude. It is necessary to make use of other forecasting procedures here. One of the most basic ones is to establish the deficit in the expenditure of energy or deformation on some section of a fault or subduction zone, the so-called 'seismic gap'. By adding up the magnitudes of the observed seismic events on a given section of a fault and by their comparison with a long-term mean energy expenditure, it is possible to estimate the amount of energy that could escape. As a good example one can use the estimate of the place and magnitude of the Haiti earthquake, which was presented in 2008 at the Caribbean Conference (Mann et al. 2008).

The time period for which the precursors manifest themselves might help with estimating the magnitude of a future earthquake using pendulums or gravimeters. We can then make a conservative estimate of its magnitude based on the relation (2.4) (see Fig. 2.2) or we can monitor how long there has been a unilateral influence of forces on a global scale before the rock ruptures in some areas. For earthquakes, occurring at the interface of an oceanic and continental lithosphere, such a period of anomalous stress will be longer than 1 month in the case of an earthquake with $M>7.5$ (see Fig. 8.2).

10.2. Case study

Between July 1, 2007 and December 31, 2009, 16 earthquakes with $M\geq7.5$ were registered on the whole Earth (see Tab. 6). For each of them, we have tried to determine if the earthquakes could have been predicted using the instrumentation available to us, the static vertical pendulums in particular. For three of the earthquakes, the nucleation stage was detected in advance and their magnitudes were established. However, no we could not predict the location (Sichuan May 12, 2008, Samoa September 29, 2009, and Indonesia September 30, 2009). Today, ex-post, it shows that the earthquake in Sichuan was completely predictable from Central Europe, including its likely location.

Table 6 Parameters of the worldwide earthquakes with M>7.4 since May 1, 2007 (ANSS 2009, EMCS 2009)

	Lat.	Lon.	Depth	Mag.		Predict.	Method
08/08/2007 17:05	-5.86	107.42	280	7.5	**JAVA, INDONESIA**	?	
15/08/2007 23:40	-13.39	-76.6	39	8	**NEAR COAST OF CENTRAL PERU**	no	
12/09/2007 11:10	-4.4	101.36	10	8.5	**KEP. MENTAWAI REGION, INDONESIA**	yes	tilt, noise P7, gravity
28/09/2007 13:38	22.01	142.67	260	7.5	**VOLCANO ISLANDS, JAPAN REGION**	yes	tilt P7, gravity
14/11/2007 15:40	-22.25	-69.89	40	7.7	**ANTOFAGASTA, CHILE**	yes	noise P7
09/12/2007 07:28	-26	-177.51	152	7.8	**SOUTH OF FIJI ISLANDS**	no	
12/05/2008 06:28	31	103.32	19	7.9	**EASTERN SICHUAN, CHINA**	yes	diurnal waves P7
05/07/2008 02:12	53.88	152.89	632	7.7	**SEA OF OKHOTSK**	no	
03/01/2009 19:43	-0.41	132.88	17	7.6	**NEAR N COAST OF PAPUA, INDONESIA**	yes	tilt, noise P7, gravity
19/03/2009 18:17	-23.05	-174.66	34	7.6	**TONGA REGION**	yes	tilt, noise Lubeník, P7
15/07/2009 09:22	-45.76	166.56	12	7.8	**OFF W. COAST OF S. ISLAND, N.Z.**	?no?	only tilt P7
10/08/2009 19:55	14.1	92.89	4	7.5	**ANDAMAN ISLANDS, INDIA REGION**	no	
29/09/2009 17:48	-15.49	-172.1	18	8.1	**SAMOA ISLANDS REGION**	no	
30/09/2009 10:16	-0.72	99.87	81	7.5	**SOUTHERN SUMATRA, INDONESIA**	yes	tilt, diurnal waves, gravity
07/10/2009 22:03	-13.06	166.34	45	7.7	**SANTA CRUZ ISLANDS**	?yes?	waves
07/10/2009 22:18	-12.53	166.37	55	7.8	**SANTA CRUZ ISLANDS**	?yes?	waves

In addition to those 16 major earthquakes, other earthquakes could have been predicted. One of them, the deep earthquake on the Kuril Islands (M=7.3), was easily predicted 26 days prior to the main event. All those earthquakes will be described later and the forecasts for them will be evaluated.

Event August 8, 2007 Java, M=7.5. In respect of the initial stage of the measurements and their shortcomings, that earthquake was not predicted and would not have been predictable even ex-post. Only the diurnal period was observed on both components, which by no means exceeded the standard, and reduced noise on both components (more on the NS component) from July 22, 2007.

Event August 15, 2007 Peru, M=8. Non-predictable event on our lithospheric plate. It occurred in the relaxation stage of our lithospheric plate (see Fig. 7.4) and no unusual tilts or noise were observed before that. The noise continued decreasing since July 22, 2007.

Event September 12, 2007 Mentawai Region, Sumatra, Indonesia, M=7.9. (One of a few seismic events in 2007 where it was possible to identify several precursors that may have led to its prediction.). Since, in 2007, we were only discovering what it was actually possible to identify from the pendulum tilts and what precursors there might be, we didn't try to predict this earthquake. Today, we know that for that event, the beginning of the nucleation stage could have been identified around August 26, 2007 (see Fig. 10.2), which was characterised by a sudden change of a tilt motion. Simultaneously, the noise was decreasing and peaks related to small-scale earthquakes on the eastern edge of the Eurasian plate started to appear within the noise (from September 1, 2007). The main stage of the earthquake started after the earthquake in Tai-wan (M=6.2) on September 6, 2007 when the pendulum noise doubled in both directions. If we plot the anomalous tilts adjusted by a long-term secular trend of the P7 pendulum in Příbram (see Fig 7.4), then we can see that the total massif deformation in Příbram culminated at the time of the earthquake in Sumatra on September 12, 2007. Since, in 2007, we had just one underground pendulum at the depth more than 30 m, it was not possible to identify unambiguously the direction of the anomalous stress component. The magnitude could be estimated based on the length of the nucleation stage of approx. 16 days according to the relation (2.4) as M≈7.4. The increased strain of the nucleation stage induced a series of anomalies on other instruments (see Chapter 8). Horizontal movements were observed on active faults. Increased noise was observed on the strainmeter at Vyhne (Slovakia), anomalous movements of water levels were observed in the VS-3 borehole in the Eastern Bohemia and increased gravity was observed on the absolute gravimeter at Pecný.

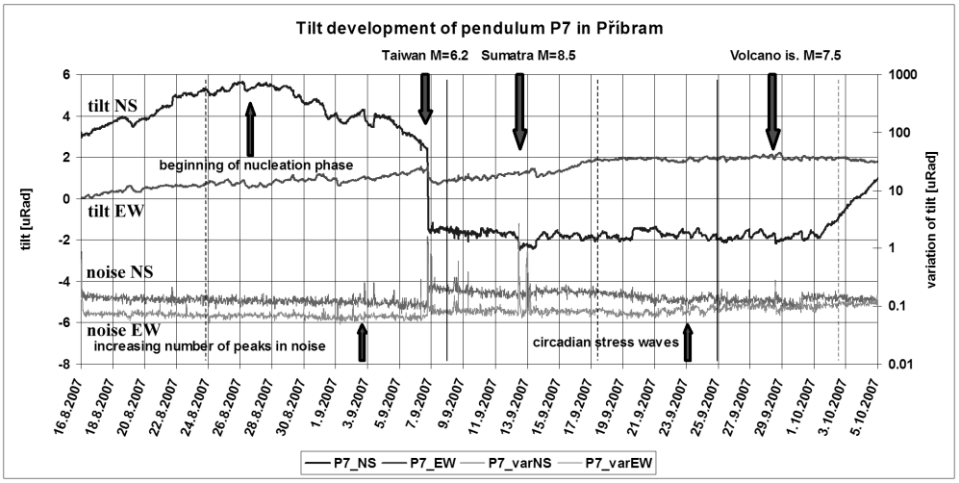

Fig. 10.2: Tilt development on P7 pendulum in Příbram in September 2007.

Event September 28, 2007 Volcano Island, Japan, M=7.5, occurred in the final stage of the same stress wave that triggered the earthquake in Sumatra (see Fig. 10.2). Its only precursor was the fact that after the earthquake in Sumatra, the high noise did not calm down. On the contrary, further increase of noise was apparent on the EW component. Also, the pendulum tilt trend did not get to the original values after the earthquake in Sumatra but only after the earthquake of the Volcano Islands after October 1, 2007.

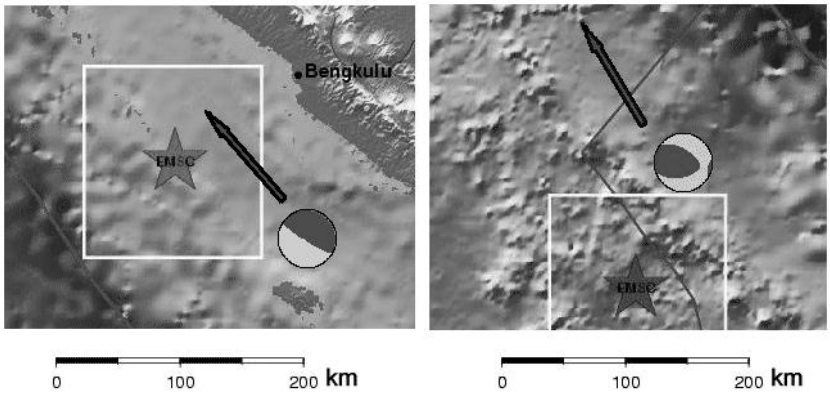

Fig. 10.3a, b: Centroid moment tensor parameters of Sumatra September 12, 2007 and Volcano Islands September 28, 2007 earthquakes (Harvard CMT catalogue (Dziewonski & Woodhouse1983)). Maps by Google maps and tectonic plate boundaries by Bird (2003).

Arrow – direction to Central Europe, star – epicentre by EMSC (2010).

Based on the arrival of the circadian stress wave from September 19, 2007 to September 26, 2007 (see Fig. 10.2), it was possible to expect the increased stress from the E direction. Both the Volcano Islands and Sumatra events point at the 'virtual expansion' of the Philippine plate against the neighbouring plates, especially in the NE-SW direction (see Fig 10.3a, b).

Event November 14, 2007 Antofagasta, Chile, M=7.7, occurred in a relatively 'relaxation' stage of the stress in Central Europe (see Fig. 7.4). In spite of that, it was possible to observe pronounced changes in the tilt motion and the beginning of the nucleation stage on November 03, 2007 accompanied by the arrival of 'stress waves' from November 8, 2007 to November 12, 2007 (see Fig. 10.4). If there had been more pendulums deployed in South America, then this earthquake locality would probably have been predictable. It was impossible to localise the focal point situated on a different plate from Central Europe only. The magnitude estimate according to the relationship (2.4) would have been M≈7.3.

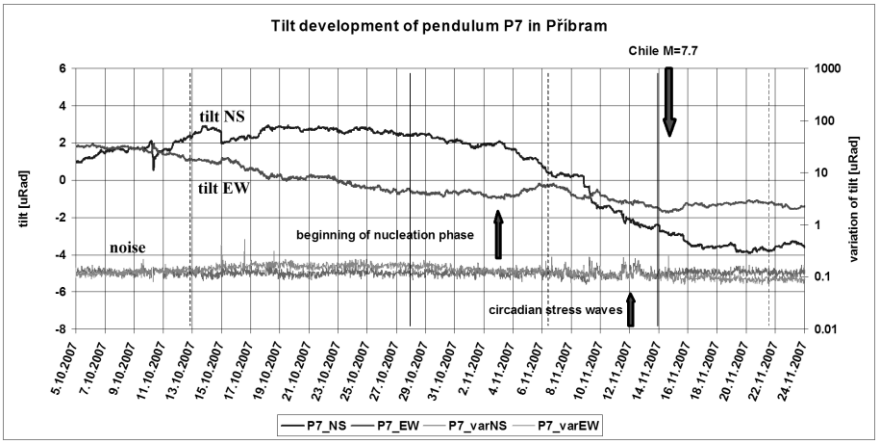

Fig. 10.4: Tilt development on P7 pendulum in Příbram in November 2007.

Event December 9, 2007 Fiji, M=7.8. Except for a reduction of noise on the EW component, no special tilt development was observed on the pendulums (see Fig. 7.4). The earthquake was unpredictable from the Central Europe.

Event May 12, 2008 Sichuan, M=7.9. The first event for which we recognised the 'stress waves' prior to the proper earthquake. We did not identify the epicentre, however, we did estimate the magnitude of approx. 6.9, based on the comparison with creep preceding the earthquake of Loma Prieta 1989. Now we know that it was possible to estimate very precisely the local meridian of the focal area, even when based on the tilt measurement in the Central Europe.

On April 8, 2008 we finished our measurements on the P7 pendulum in Příbram and reconstructed the pendulum. On April 15, 2008, a new measurement commenced with a new rod, which immediately manifested itself in the pendulum noise (variations) reduction from 1/2 to 1/3 of the original values (see Fig. 10.5).

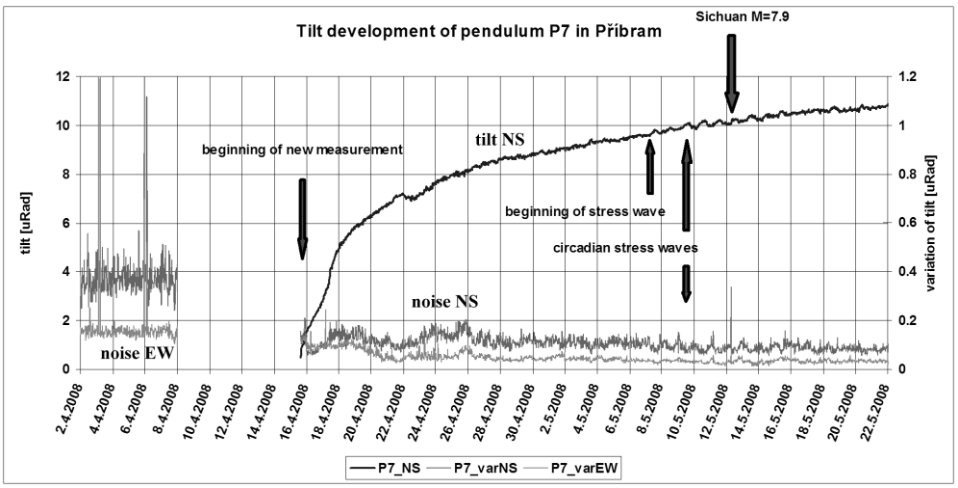

Fig. 10.5: Tilt development on P7 pendulum in Příbram in May 2008.

After the commencement of the measurement, the tilt showed a typical movement given by the relaxation of the new rod on the pendulum. As early as from April 22, 2008, the natural tilts of the pendulum and especially noise were interpretable.

LN wrote on May 11, 2008 at 20:45 UTC: "*I evaluated the data from Příbram and they are interesting. We can see diurnal period, which increases. The noise decreases and noise has diurnal period, too. I wonder where an earthquake will occur*".

PK answered on May 12, 2008 at 4:55 UTC: "*I expected such diurnal thermo-elastic waves before huge earthquakes according to Hvožďara. I had observed them before the Loma Prieta earthquake (1989) on creepmeters in California. The magnitude of a possible earthquake would be greater than 6.9, like in the case of Loma Prieta*".

This partial prediction proved true within two hours when the news brought the information of a large earthquake in Wenchuan (Sichuan). When we look back at the tilt curve on the P7 pendulum in Příbram, we can see that after the pendulum reconstruction we were not able to record the tilt change that could have occurred any time between April 22, 2008 and May 8, 2008. On the other hand, in the low noise, its circadian period was clearly visible starting on May 7, 2008 and ending on May 15, 2008 after the earthquake. Maximum noise was observed exactly at the time when the pendulum displacement reached its maxim towards the south. No significant movement deviations were observed in the EW direction nor did the noise show a pronounced circadian periodicity. From these facts, it was possible to judge that the anomalous additional stress acted from the north.

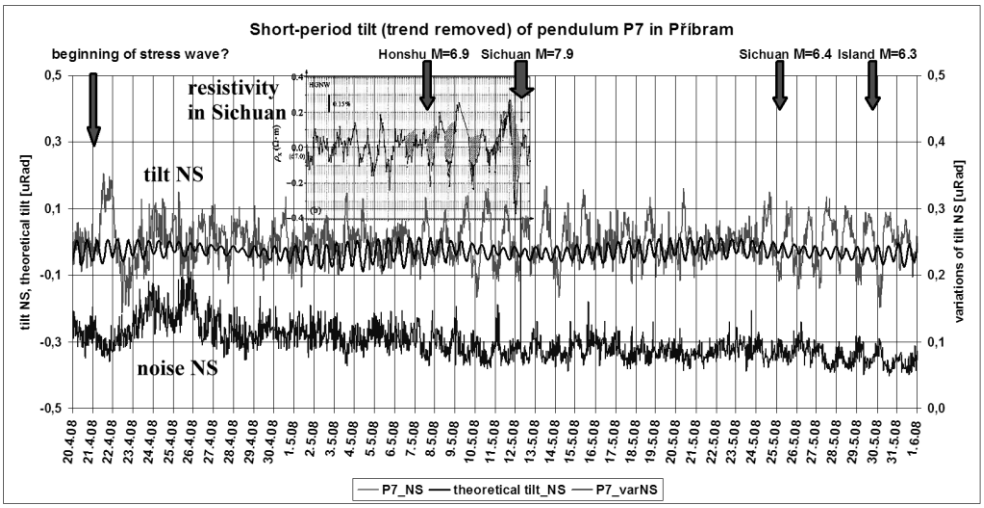

Fig. 10.6: Comparison of tilt development and HRT waves (Qian et al. 2009).

Half a year after the earthquake in Sichuan, after the AGU meeting in San Francisco, we compared our measurement results with those measured right near the focal point in Sichuan. We found that the stress waves we had

measured were identical with those inducing the changes of impedance measured at the Hongge station, approx. 465 km from the epicentre (Qian et al. 2009) (see Fig. 10.6).

Qian et al. (2009) showed that from the fortnightly period point of view, it was possible to establish the beginning of anomalous impedance in the EW direction around April 30, 2008. On the NS component, no anomalous variations of impedance were observed. The beginning of the largest anomalous stage occurred in the seven-day window around May 6, 2008 and five-minute values showed a pronounced circadian variation beginning May 6, 2008 (see Fig. 10.6). The second period of stress increase and reduced impedance was recorded after May 24, 2008. Both periods exactly correspond to the beginning of the 'stress waves' arrival registered in Příbram. Hence, it may be stated that both the observed tilts of the P7 pendulum in Příbram and the impedance changes at Hongge were induced by the same strain changes in the massif.

Which mechanisms are likely to have induced such stress changes? One explanation was offered at the AGU meeting by X. Xiwei et al. (2008). They were of the opinion that the Indian plate pushes towards Asia and the stress is deflected in the EW direction. That, however, does not explain the observed circadian stress periods. Stress maximums in Sichuan and in the Central Europe were observed between 10:00 and 12:00 LT, i.e. 2:00 – 4:00 UT. At that time, a maximal and anomalous exposure of the whole Himalayan area occurred and, as R. Singh et al. (2008) has shown; the relative humidity was anomalously low (20%) in comparison with the average value of 50-60%. So, the thermo-elastic wave, caused by the exposure of the whole of Himalayas, probably acted as a triggering mechanism of that earthquake. This idea is supported by the observed mechanism that manifested itself in Wenchuan as a reverse and oblique-slip, when the Tibetan Plateau in the NW slipped onto the Sichuan Basin (see Fig. 10.7). In Central Europe, we observed the same thermo-elastic wave generated in Central Asia and the Himalayas, only it acted mostly from the northern direction in accordance with the geometric (geographic) position of the source area towards Central Europe.

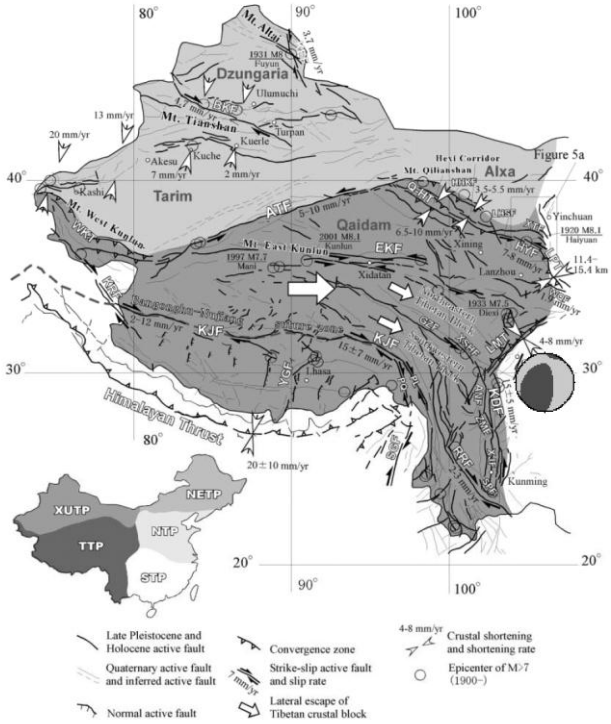

Fig. 10.7: Map of the Western China (according to He & Tsukuda 2003) and earthquake focal mechanism (Harvard CMT catalogue (Dziewonski & Woodhouse 1983)).

As well as the thermo-elastic waves generated by the solar irradiance, other precursors were observed preceding that earthquake. Anomalies were observed on the strainmeter in Shandan on May 11, 2008 (Peng et al. 2009); infra red anomalies in the fifth stage from April 30, 2008 to the earthquake on May 12, 2008 (Wei et al. 2009); noise was heard on the fault near Wenchuan (Smith 2008) and 'earthquake clouds' were observed too (Irrational Geographic 2009). Therefore, we cannot agree with the declaration by G. Purcaru (2008) that Wenchuan earthquake was unpredictable. This earthquake was predictable, but was not predicted by scientists.

Event July 5, 2008 Okhotsk, M=7.7, was preceded by a small drift anomaly only of the pendulum tilt and insignificant stress wave. The event was unpredictable from Central Europe.

Earthquake November 24, 2008 near the Kuril islands, M=7.3, was the first officially predicted earthquake based on the recognition of the circadian 'stress wave'.

The main characteristics of the stress behaviour in Central Europe from April to September 2008 was the 'relaxation' which manifested itself by a general movement of the pendulum P7 tilts towards the north and east (compare to Fig. 10.2 and 10.4). More 'stress waves' (see above) kept arriving on the overall trend. The region of Western Bohemia reacted by a local seismicity to some of them, e.g. on May 24, 2008 after the Sichuan earthquake, or around August 18, 2008 (see Fig. 10.8). At the beginning of the overload stage on April 1, 2008, when the pendulum movement turned to the south and west, the largest seismic swarm during the last 6 years was observed from October 4, 2008 (Horálek et al. 2009). The second sub-swarm was observed from October 27, 2008. In that one, the 'stress waves' with circadian periods were recognised both on the P7 pendulum in Příbram and, in particular, on the pendulum in the 13C cave in Moravian Karst. Since the pendulum is situated in an active fault with the N-S direction it is very sensitive, especially to the stress changes in that direction (see Fig. 10.9).

Pronounced circadian periods of noise were observed on the pendulum in the 13C cave, and the noise itself decreased radically (see Fig. 10.9). Since the noise maximums were observed around midnight UT, we expected that the breaking asperity lay on our lithospheric plate, on the opposite side of the Earth (opposite hemisphere). Since in that area there is a contact between the North American and Eurasian lithospheric plates, we estimated the asperity location to be the region between the Kuril Islands and Kamchatka. Since the peaks on pendulums P7 and 13C coincided with the periods when the diurnal periods prevail in the tides, we estimated that the asperity could have been broken within 28 days from October 31, 2008 when there would be two similar coincidences. We estimated the magnitude of the expected earthquake, based on the nucleation stage length, and also based on the reasoning that we had observed no similar marked peaks prior to other earthquakes in the area of the Sea of Ochotsk and the Kurils.

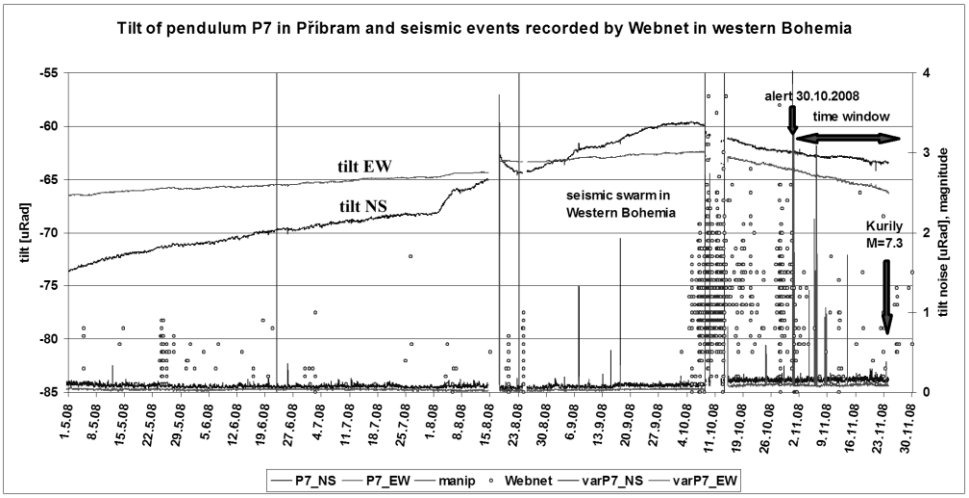

Fig. 10.8: Tilt development on P7 pendulum in Příbram in Autumn 2008 and local seismicity in Western Bohemia, registered by the Webnet network (Horálek & Fischer 2007).

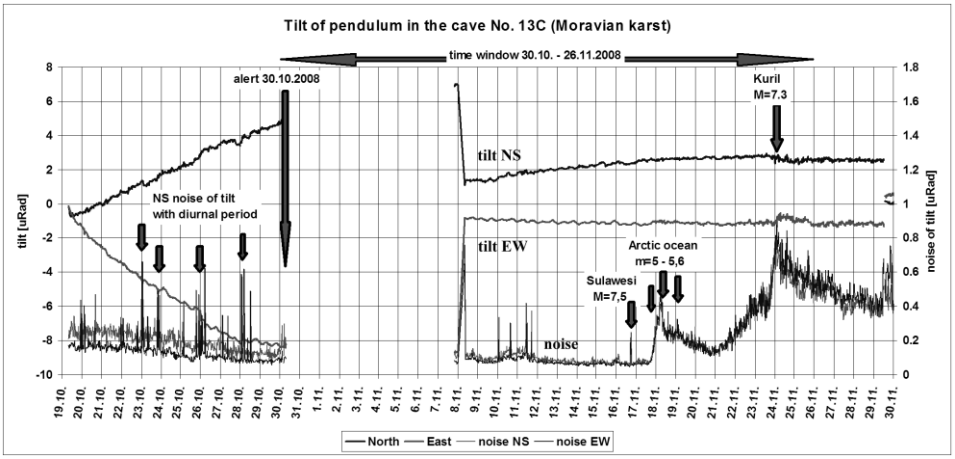

Fig. 10.9: Tilt development on P7 pendulum in Příbram.

The probability, that an earthquake occurring with M≥7 in a given area between the Kurils and Kamchatka in a 28-day window was 6.4%. The probability was calculated, based on the USGS catalogue for the time period from 1973 to 2002, using the program by R. Hunter (2003).

On November 16, 2008, an earthquake was observed near the island of Sulawesi (M=7.5) and exactly one day later a radical increase of noise was observed on the pendulum, which corresponded to an uninterrupted movement of an active fault and occurred simultaneously with a series of medium-size earthquakes in the North Arctic Ocean. The movement on the fault slowly went decreased by November 21, 2008 and then suddenly accelerated and culminated exactly at the time of the main shock on the Kurils on November 24, 2008 (M=7.3). The period from November 21, 2008 to November 24, 2008 may be considered the nucleation stage *sensu stricto*, when the crack development was already unstoppable.

The successful prediction of the Kurils earthquake confirmed the validity of the movement of lithospheric plates (see previous Chapter), correctness of detection and interpretation of the noise peaks that correspond to the maximum of 'stress waves' generated probably in the focal area of the future earthquake on the breaking asperity. We found, surprisingly, the discovery that the 'stress waves' are able to cover the distance of the whole lithospheric plate from one edge to the other, which allows for deformation transfer between the plates in a relatively short time and explains the series of earthquakes on different lithospheric plates.

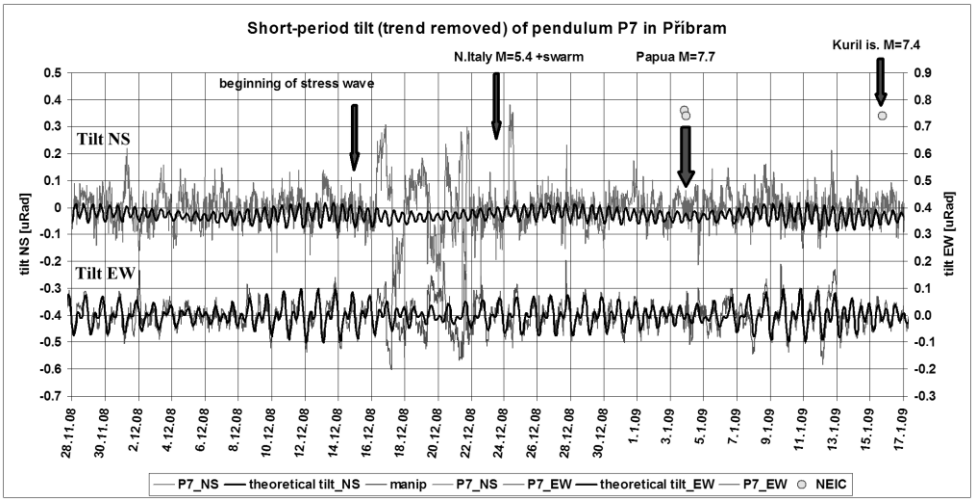

Fig. 10.10: Tilt development on pendulum P7 in Příbram in December 2008.

Event January 3, 2009 Papua, M=7.6, followed 14 days after the arrival of a huge 'stress wave' (see Fig. 10.10). Its direction was from the NE, deduced by the fact that on both components, greater deviations were observed than should have been. On the NS component, one or two-day periods prevailed and on the EW component, the tidal semidiurnal periods were dominant. The direction of the anomalous stress from the NE corresponds to the focal mechanism according to the Harvard CMT (see Fig. 10.11).

It is interesting that the 'stress wave' also triggered a significant seismic swarm in Northern Italy, around the city of Parma in particular. The largest event was observed on December 23, 2008 M=5.4, followed by dozens of smaller aftershocks (EMSC 2008).

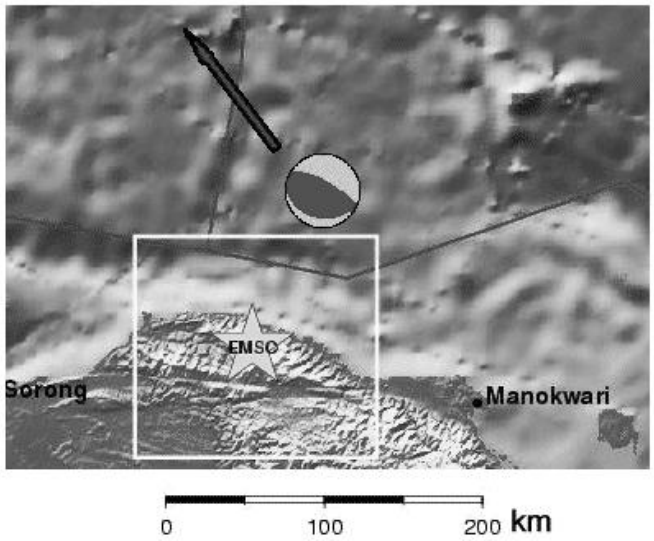

Fig. 10.11: Centroid moment tensor parameters of the Papua earthquake on 5.1.2009. earthquakes (Harvard CMT catalogue (Dziewonski & Woodhouse1983)). Maps by Google maps and tectonic plate boundaries by Bird (2003),
arrow – direction to Central Europe, star – epicentre by EMSC (2010).

After the earthquake near Papua, yet another, less significant, 'stress wave' was observed from the east only. It could have triggered the Kurils earthquake on January 15, 2009 M=7.4. The earthquake near Papua could have been predicted from the time point of view, however, it is not sure whether it could have been localised as it was not clear which triggering mechanism triggered the 'stress wave'.

Event March 19, 2009 at the Tonga Archipelago, M=7.6, was preceded by pronounced anomalies on most pendulums both in Bohemia and in Lubeník, Slovakia (see Figs. 10.12 and 10.13).

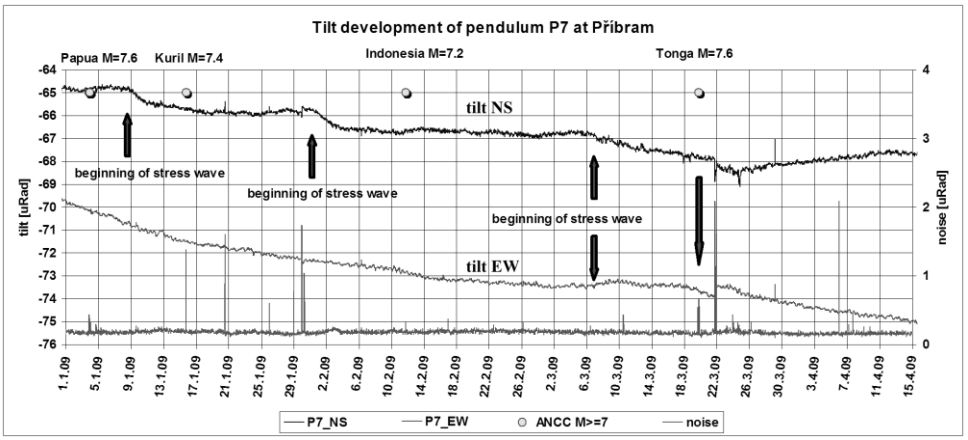

Fig. 10.12: Tilt development on P7 pendulum in Příbram in spring 2009.

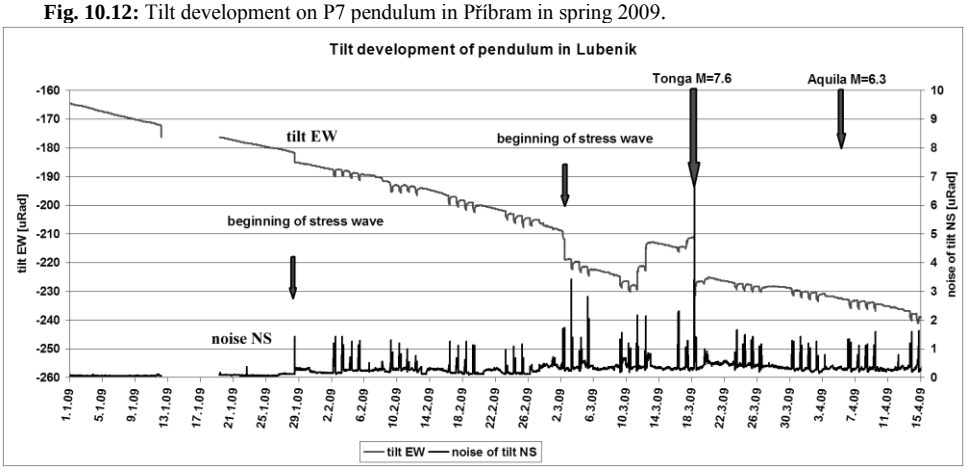

Fig. 10.13: Tilt development of pendulum in Lubeník mine in spring 2009.

Despite the fact that both pendulums are more than 500 km apart, it was possible to observe the arrivals of the 'stress waves' prior to the earthquake in Indonesia (M=7.2) around January 29, 2009 and especially prior to the earthquake in the Tonga Archipelago between June 3, 2009 and June 6, 2009. In the Lubeník mine, even macroscopic deformations of some old roads accompanied by falling top walls were observed at the time of the

'stress wave' and the staple pit where the pendulum is located tilted by several mm per 50m of height.

On April 6, 2009 the earthquake struck in the region of Central Italy near the town of Aquila (M=6.3). As one can see from the tilts of both pendulums, the 'stress wave' from Tonga was fading away at that time and stress redistribution occurred even in Central Europe. According to that scenario, the earthquake of Aquila could have been classified as the aftershock of the Tonga earthquake. Thus, it is similar case to the one after the earthquake in Sichuan after which the earthquake in Iceland (M=6.3) followed on May 29, 2008. The Iceland earthquake was the largest one in the last 18 years (see Fig. 10.6). Nonetheless, those earthquakes differ a lot from other earthquakes, because the earthquake of Aquila was predicted by G. Giuliani based on the radon gas measurement at Aquila and its surroundings (Dorigo 2009). Its anomalies correspond, from the time point of view, with the 'stress waves' that caused the deformations in Bohemia and Slovakia. So, G. Giuliani was performing his measurements, by accident, in the most sensitive area of Italy that was prepared for the earthquake and substantial energy was accumulated there which was released as a result of the earthquake of Tonga and stress change in Europe. Hence, his prediction was successful but a question remains whether or not he would been able to measure such big anomalies comparable with Aquila in other areas of Europe at the same time, since macroscopic deformations and movements on faults were observed even at Lubeník, Slovakia.

Event July 15, 2009 at New Zealand, M=7.8, was preceded by a change of tilt trend on the P7 pendulum in Příbram that occurred after a medium-size event at Baffin Bay on July 7, 2009 (see Fig. 10.14). Other precursors were not observed so that event was unpredictable from Central Europe, as in the case of earthquakes in Honduras (M=7.3) and New Ireland (M=6.8), which were preceded by 'stress waves'.

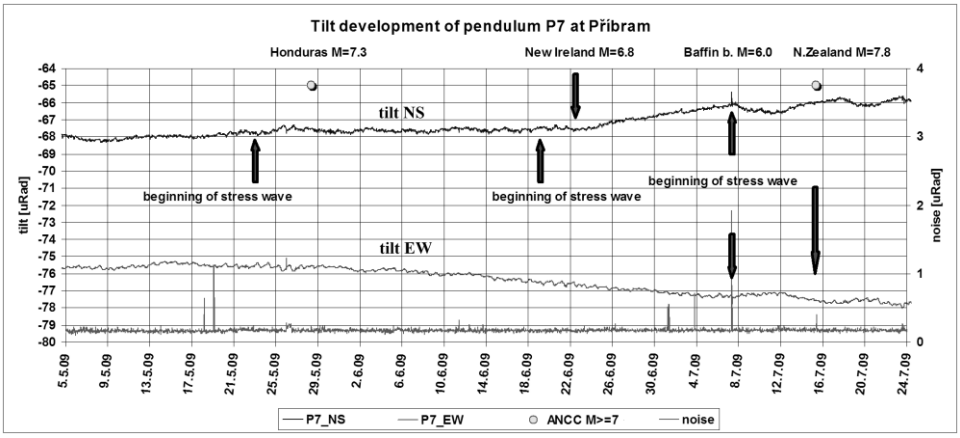

Fig. 10.14: Tilt development on P7 pendulum in Příbram in summer 2009.

By the New Zealand earthquake of July 15, 2009, a period of increased seismic activity began that continued on August 9, 2009 by the earthquake near the Izu Island (Japan) (M=7.1); a day later, on August 10, 2009, at Andaman (India) (M=7.5); on September 2, 2009 at Java (Indonesia) (M=7.0) and ended by a huge earthquake near Samoa on September 29, 2009 (M=8.1), near southern Sumatra on September 30, 2009 (M=7.5) and near Santa Cruz on October 7, 2009 (M=7.8). Except the earthquakes of Samoa and Santa Cruz, which were preceded by clear 'stress waves' (see Fig. 10.15), it was not possible to discover the precursors of the particular earthquakes in a chaotic stress field, as it is obvious already from July 18, 2009 in Fig. 10.14. Neither in the case of the Samoan nor the Santa Cruz earthquake was it possible to localise the relevant asperities. When we analyse the times of stress (noise) maximums then we can see that they fluctuate around 04:00 UT. Therefore, the corresponding local meridian is approx. at 90 to 110E. That meridian corresponds to the Sumatra earthquake. So, the Samoa earthquake could not be predicted as well as the earthquake of Santa Cruz, which was preceded by 'stress waves' with longer periods than one day.

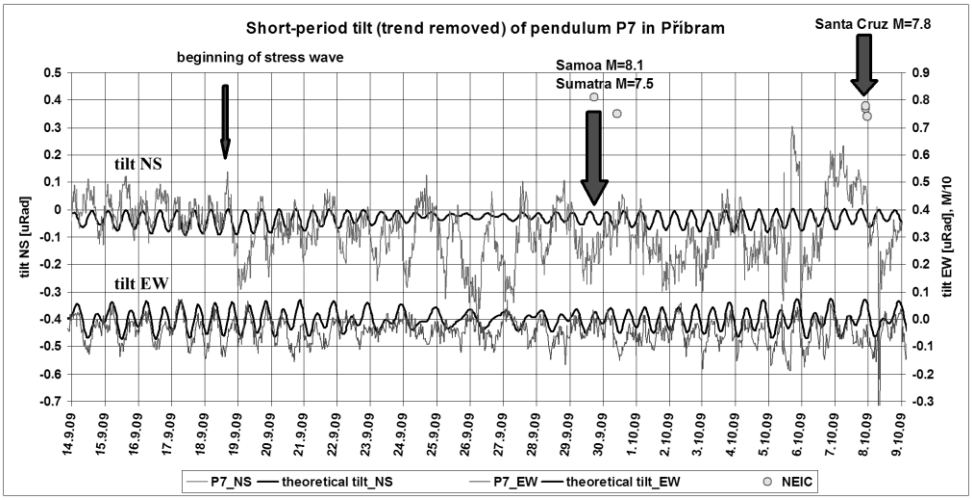

Fig. 10.15: Short-period tilt on P7 pendulum in Příbram in September 2009.

During the earthquake in Sichuan we realised that we were able to recognise the anomalous stress waves induced due, probably, to the asperity breaking in the earthquake focal point. We verified this finding by our first official prediction of the earthquake of the Kuril Islands where we detected the 'stress waves' approx. 26 days prior to the earthquake and we localised its future epicentre. With that event, the nucleation stage *sensu stricto* was observed from the foreshocks in the North Arctic Ocean until the main shock.

We could claim that most predictable earthquakes occurred on our lithosphere plate (see Tab. 6). Only the biggest earthquakes from other lithosphere plates were preceded by precursors. The earthquakes from Southern America or Tonga and Fiji took place mostly in the time of 'relaxation' of the Eurasian plate.

Table 7 Predictions made since 2007

Pre-diction		Beginning of time period	End of time period	Days	Place	Mag. M>=	Prob. %	**Actual**	Place	M	Conf.	Note
Sichuan	unof.	11/05/2008	08/06/2008	28	?	6.9	?	12/05/2008	31N, 103E	7.9	?	
Kuril Is.	off.	30/10/2008	27/11/2008	28	Kuril – Kamchatka	7.0	6.4	24/11/2008	54N, 154E	7.3	Yes	
Euro-Asia	off.	10/03/2009	06/05/2009	57	0-180E, -10 - +90N	No >=7	65.1	07/04/2009	46N, 151E	6.9	Yes	
World-wide	off.	16/12/2009	30/12/2009	14	worldwide	No >=7	42.1	19/12/2009	24N, 122E	6.4	Yes	
East	unof.	04/02/2010	11/02/2010	7	Taiwan area	6.2	3.5	07/02/2010	23N, 124E	6.3	Yes	EQ clouds
East	unof.	19/02/2010	19/03/2010	28	Indon., Philip., Taiwan	7.0	65.1	26/02/2010	26N, 128E	7.2	Yes	
East	unof.	19/02/2010	19/03/2010	28	Tonga, New Guinea	Big	?	27/02/2010	36S, 73W	8.8	**No**	Chile
Pakistan	off.	22/02/2010	22/03/2010	28	25-40N, 60-80E	6.0	17.3	27/02/2010	36N, 70E	5.7-6.0	Yes	
N. Guinea	off.	22/02/2010	22/03/2010	28	15S-5N, 130-155E	6.5	23.2	20/03/201	3S, 152E	6.2-6.5	Yes	
USA	off.	05/03/2010	02/04/2010	28	0-90N, 100-165W	6.5	17	04/04/2010	32N,11W	7.2	**No**	Baja Calif
World-wide	off.	06/03/2010	13/03/2010	7	worldwide	7.0	24.2	11/03/2010	34S, 72W	7.2	Yes	Chile

The most common precursor seems to be ‘stress wave’ or ‘tectonic waves’ (Khalilov 2009). These ‘stress waves’ were probably generated in the focus area of future earthquakes by destruction of asperities, i.e. locked parts of faults or more solid part of rock mass, which are resisted against deformation transfer and which create stress concentrators. The arrival time of such ‘stress waves’ can be recognised by sudden changes of tilt wobble (see Figs. 10.8, 10.12, 10.13 and 10.14) and/or by increasing of noise of pendulums, i.e. variations of movement around average position (see Figs. 10.10, 10.12, 10.13, 10.14 and 10.15). Many of the ‘stress waves’ had circadian periods with the maximum stress in the afternoon of local time in the epicentre area. Such stress waves were probably triggered by solar insolation and thermoelastic wave generation (Hvožďara et al. 1988). This fact could lead to localisation of future mainshock according to local meridian.

We suppose that other external forces can trigger earthquakes and can generate ‘stress waves’ with corresponding periods. The ‘stress waves’ with

semidiurnal period, generated probably by tides, were observed before the Honduras earthquake on May 2009.

All of the recognised 'stress waves' in Central Europe were coming from east or north, even in the case of the catastrophic earthquake in Chile on February 2010 (M=8.8). Such observations confirm the westward drift of lithosphere plates against the mantle (Ostřihanský 1997, 2004, Scoppola et al. 2006) and the westward transfer of deformations.

All earthquakes were connected to each other worldwide by these 'stress waves' and foreshocks and aftershocks could be placed at various lithosphere plates. The preparation area of an earthquake has a global scale from this point of view.

We have also verified the validity of our model idea of mutual movements of lithospheric plates and stress transfer across the whole lithospheric plates on negative predictions when, based on the massif deformation development. We defined the time period when no event with greater than defined magnitude should have occurred on our lithospheric plate or on a global scale. Both predictions proved true despite the fact that one event occurred on the Eurasian plate with M=6.9 prior to which no changes were detected in the pendulum tilt trend or noise or 'stress waves'. In this way we discovered the sensitivity limits of our pendulums in Central Europe since that event came from the Kurils.

Predictions of earthquakes, as we have tried in real time, are possible, but it is necessary to look at the measured data through a prism of a corresponding model on global dimensions. All the lithospheric plates are interconnected into one whole and the movement at one place causes the change in the status and stress in distant places. Therefore it is necessary to perform the measurement of deformation on a global scale and thus analyse the development of deformations and their correlation. In this way it is possible to detect the areas where the deformation will move further and the stress will increase, which may result in a big asperity breaking, thus preventing further movement. This cannot be monitored and measured with one type of equipment only, but it is necessary to build a global network and link up various types of equipment for the measurement, which in co-ordination would show the status and development of stress in a given area, on the whole lithospheric plate and on contacts between the plates.

10.3 Addendum: Case Study – Haiti, Chile and ...

On January12, 2010 Haiti was hit by a catastrophic earthquake the magnitude of which was not high (M=7.1) but it was shallow and close to the capitol Port-au-Prince, so the consequences were extraordinary. Unfortunately, only on a single pendulum (P7 in Příbram) we recorded just the anomalous peaks without any change in the tilt movement (see Fig. 10.16). The earthquake was not predictable from the Eurasian plate but the registered peaks show that if the deformations of other plates had been measured, it would have been predictable. When combined with the knowledge of the accumulated energy and fault position (Mann 2008), the consequences could have been reduced.

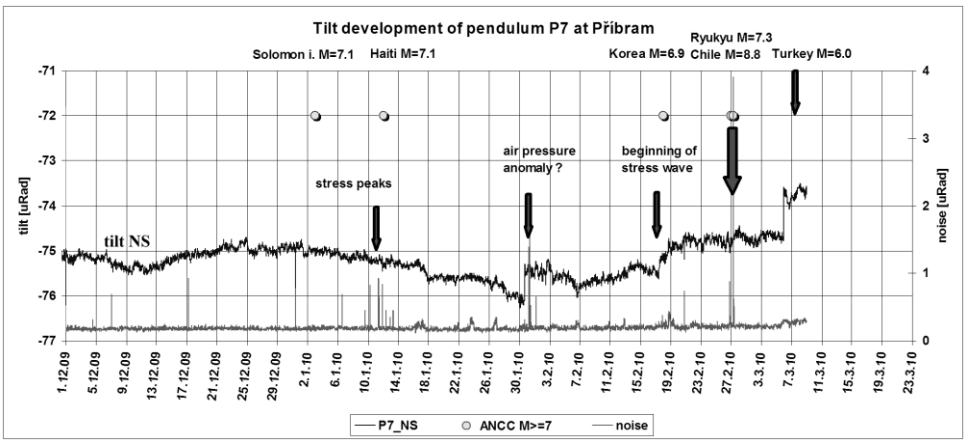

Fig. 10.16: Tilt development on P7 pendulum in Příbram in Winter 2009.

On January 17, 2010, the arrival of an anomalous stress wave was discovered, which continued to January 30, 2010. Since the stress in Central Europe further increased, even after the earthquake in Tai-wan on February 7, 2010 (see Fig. 10.17), and anomalous pressure direction was from the east, enquiries were sent to Japan, Indonesia and Baku whether they could help with localisation. Indonesia, Philippines, Tai-wan, New Guinea and Tonga were identified as probable areas. No official prediction was made and no unambiguous area of the future focal point was identified. On February 27, 2010, an earthquake was observed near the Ryukyu Island (east of Taiwan) with M=7.2 and several hours later a catastrophic earthquake hit Chile with M=8.8. Today, we know that majority of the

observed stress waves anomalies were the precursors of that big earthquake and the preshocks in Tai-wan and near Ryukyu were related to it as well as the subsequent earthquake in Pakistan on February 27, 2010 M=5.9 or in Turkey M=6.0 (see Fig.10.18 and 10.19). The prediction (Table 7) attempts to localise the earthquakes and confirm how marked and unambiguous the registered anomalies were on all the available devices (pendulums, gravimeters, dilatometers (Stemberk, oral communication), differential gravimeters Atropatena (Khalilov, Wahyudi, oral communication)).

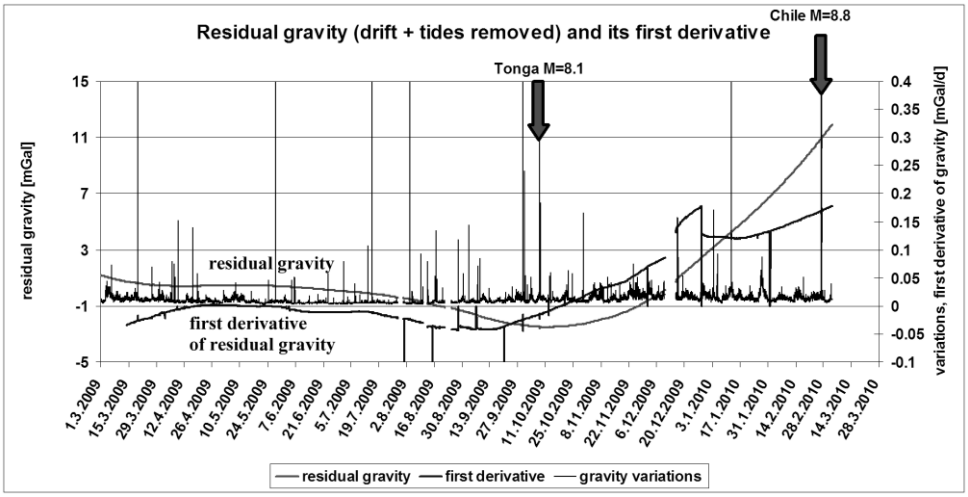

Fig. 10.17: Residual gravity measured in Prague (trend and tides removed).

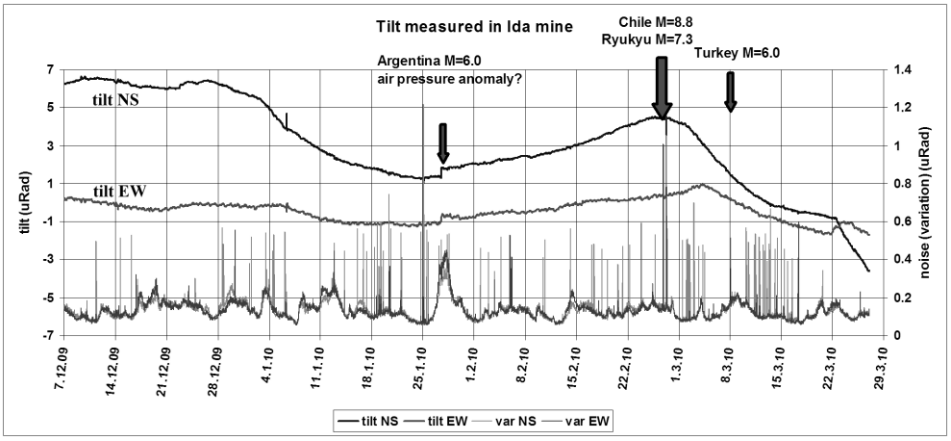

Fig. 10.18: Tilt development of pendulum in Ida mine in Winter 2009.

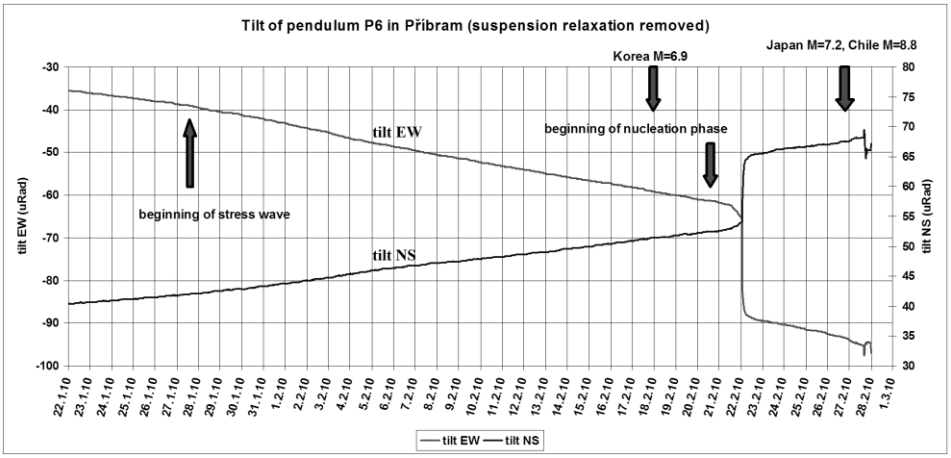

Fig. 10.19: Tilt development on P6 pendulum in Příbram in winter 2009.

The anomalies, we observe today, on all pendulums and gravimeters continues to confirm that the Earth crust blocks have not yet got into a stable position and the accumulated deformation energy may be released in subsequent earthquakes (see Fig. 10.18) and the deformation move further to the west in accordance with the drift of lithospheric plates. That, however, will be a question of further measurements and analyses. The future will show how accurately we have measured our data and, based on our model, interpreted the state of strain. We believe that the model and measurement techniques will be further refined, so in the future we will be able to predict earthquakes more accurately and reliably and thus minimise their consequences.

10.4. CONCLUSIONS

Earthquakes can be predicted!

It is not possible to predict all of them. However, with earthquakes having a magnitude M≥6 it is possible to observe precursors more than 1 day prior to the main shock.

Earthquakes are triggered by a number of possible exogenic factors: solar irradiance, tides, changes of the revolution of the Earth (changes of the length of the day), change of atmospheric pressure, hurricanes, snow cover and precipitation. The main mechanisms are solar irradiation and tides.

The accumulation of energy in rocks is caused by thermo-elastic waves together with the ratcheting mechanism. That leads to the drift of lithospheric plates to the west against the mantle by approx. 0.1 mm/day.

The increased stress in rocks leads to deformation that is measurable through the use of vertical static pendulums in real time. It is also possible to determine the action and consequences of external forces.

Prior to earthquakes, the deformation development is accelerated. Thus, one of the earthquake precursors may be observed.

Prior to the main shock, so-called 'stress waves' have often been observed that are likely to be generated near the breaking asperity. A surprising finding was the fact that the 'stress waves' have been observed to come from places all over the globe. Most frequently, however, 'stress waves' have been observed coming from the edges of the Eurasian lithospheric plate. Those 'stress waves' have periods of triggering mechanisms (most frequently circadian and semidiurnal). Based on the time pattern of the 'stress waves' it is possible to estimate the asperity meridian.

Earthquakes can be studied from a global perspective as all lithospheric plates are in a mutual contact and the deformation or shift of one of them causes the change of stress and movement of the others. Therefore the earthquakes occur in series and the foreshocks and aftershocks can be found not only near the epicentre, but also globally.

By interconnecting the deformometers and other measuring devices globally into one system it should be possible to monitor the mutual interactions of the lithospheric plates and estimate the development of other deformations and stress transfer from one area to the other. In that way, the locations of future major earthquakes can be identified and then predicted.

References

Abbot, C.G. (1911): The solar constant of radiation. *Proceedings of the American Philosophical Society*, Vol. 50, No. 199 (May - Aug., 1911), p.p. 235-245. http://www.jstor.org/stable/984038.

Abidin, H.Z., Andreas, H., Gamal, M., Suganda, O.K., Meilano, I., Hendrasto, M., Kusuma, M.A., Darmawan, D., Purbawinata, M.A., Wirakusumah, A.D. & Kimata, F. (2006): Ground deformation of Papandayan volcano before, during, and after the 2002 eruption as detected by GPS surveys, GPS Solutions, vol. 10, pp. 75-84.

Aki, K. (1965): Maximum likelihood estimate of b in formula logN=a-b.M and its confidence limits, Bull.Earthq.Res. Inst., Tokyo Univ., 43, 237-239.

Allégre C., Manhés G. & Lewin E. (2001): Chemical composition of the Earth and the volatility control on planetary genetics. - Earth. Planet. Sci. Lett. 185, 49-69.

Anderson, Don L., & Dziewonski, A. M., (1984): The Earth's interior: A new frontier and a new challenge for earth scientists: in Global Change, no. 5, eds. T. F. Malone and J. G. Roederer, ICSU Press, p. 345-353..

Anderson, D. L. (1988): Temperature and pressure derivatives of elastic constants with application to the mantle, Jour. Geophys. Res., 93, p. 4688-4700.

Anderson, D. L. (2000): The Thermal State of the Upper Mantle; No Role for Mantle Plumes, Geophy. Res. Lett., v. 27. no. 22, p. 3623-3626, November 2000..

Anderson, D. L. (2001): Enhanced: Top-Down Tectonics? Science 293 2016–18.

ANSS Composite Catalogue (http://quake.geo.berkeley.edu/anss/catalog-search.html).

Aoki,S., Guinot, B., Kaplan, G.H., Kinoshita, H., McCarthy, D.D., Seidelmann, P.K. (1982): The New Definition of Universal Time. Astron. Astrophys. 105, 359-361.

Asada, T. (1982): Earthquake Prediction Techniques: Their Application in Japan (Japan: University of Tokyo Press.

Asteriadis, G. & Livieratos, E. (1989): Pre-Seismic Responses of the Underground Water Level and Temperature concerning a 4.8 Magnitude Earthquake in Greece on 20 October 1988, Tectonophysics, 170, 165–169.

Bachmann , R. (2007): Anatomy of an ancient subduction channel in the depth range of its seismogenic coupling zone - insights from field studies in the Swiss Alps and Southern Chile. PhD thesis. Potsdam. http://www.diss.fu-

berlin.de/diss/servlets/MCRFileNodeServlet/FUDISS_derivate_000000003527/00_start.pdf?hosts=local.

Bak, P. (1996): How nature Works: the Science of Self-Organized Criticality. Copernicus, New York, USA.

Bak, P. & Tang, C. (1989): Earthquakes as an SOC phenomenon, J. Geophys. Res. 94, 15635-15637.

Bak,P, Christensen K., Danon L. & Scanlon T. (2002): Unified scaling law for earthquakes. Phys.Rev.Let. 88, 178501-178504.

Bakun, W.H. & Lindh, A.G. (1985): The Parkfield, California, earthquake prediction experiment. Science, 229, 619-624.

Bakun, W.H., *et al*.(1987): Parkfield earthquake prediction scenarios and response plans, U.S. Geological Survey Open-file Report 87-192, 1987.

Beeler, N. M., & D. A. Lockner (2003), Why earthquakes correlate weakly with the solid Earth tides: Effects of periodic stress on the rate and probability of earthquake occurrence, J. Geophys. Res., 108(B8), 2391, doi:10.1029/2001JB001518.

Ben-Zion, Y. & Leary, P. (1986): Thermoelastic strain in a half-space covered by unconsolidated material, Bulletin of the Seismological Society of America, 76, 1447-1460.

Berger, J. & Wyatt, F. (1973): Some observations on earth strain tides in California, Phil. Trans. Roy. Soc. London, Ser. A, 274, 67-277.

Berger, J. (1975): A Note on Thermoelastic Strains and Tilts, J. Geophys. Res., 80, 274-277.

Berger, W., H. (2008): Solar modulation of the North Atlantic Oscillation : Assisted by the tides? Quaternary international , vol. 188, pp. 24-30 .

Berkland, J. (2009): Earthquake prediction on-line. http://www.syzygyjob.com/.

Berner, R.A. (1991): A model for atmospheric CO2 over Phanerozoic time: American Journal of Science, 291, p. 339–376.

Beroza, G.C. & W. L. Ellsworth (1996): Properties of the seismic nucleation phase, Tectonophysics, 261, 209-227.

Berry, B.L. (1991): Variations and interrelations between helio-geophysical characteristics . Glaciers-Ocean-Atmosphere Interactions (Proceedings of the International Symposium .IAHS Publ. no. 208, 1991.

Biagi, P.F., Caloi, P., Migani, M. & Spadea, M.C. (1976): Tilt variations and seismicity that preceded the strong Friuli earthquake of May 6th, 1976. Ann. Geofis. 29, 137.

Biagi, P.F., et al. (2001): Possible earthquake precursors revealed by LF radio signals. Natural Hazards and Earth System Sciences, 1: 99-104.

Biagi, P.F.,et al. (2004): VLF-LF radio signals collected at Bari (South Italy): a preliminary analysis on signal anomalies associated with earthquakes. Natural Hazards and Earth System Sciences, 4: 685-689.

Bird, P. (2003): An updated digital model of plate boundaries. Geochemistry Geophysics Geosystems, 4(3), 1027.

Bleier, T. & Freund, F. (2005). *"*Earthquake [earthquake warning systems*]".* Spectrum, IEEE *42 (12):22–27.*

Bo, W., Guo, L., Yang, G., & Du, X. (2007): Researches on Application of GPS to Earthquake Monitoring and Prediction. Systemics, Cybernetics and Informatics, Volume 5 - Number 5, 10-15.

Bobova, V.P., Kurbasova, G.S. & Rykhlova, L.V. (1993): Identity of geodynamic, geophysical and heliophysical processes. Astron. Zh., 70, 1281-1288.

Bohannon, R.G. & Geist, E. (1998): Upper crustal structure and Neogene tectonic development of the California continental borderland. *GSA Bulletin*; June 1998; v. 110; no. 6; p. 779-800.

Bolt, B. A. (1988): Earthquakes.(New York: W. H. Freeman and Company.

Boncio, P. & Lavecchia, G., 2000. A structural model for active extension in Central Italy, J. Geodynam., 29, 233-244.

Borghi, A., A. Aoudia, R.E.M. Riva, & R. Barzaghi (2009): GPS monitoring and earthquake prediction: a success story towards a useful integration. Geophysical Research Abstracts, Vol. 11, EGU2009-4091, 2009.

Borisov, N. et al.(2001): A new ionospheric mechanism of electromagnetic ELF precursors to earthquakes. Journal of Atmospheric and Solar-Terrestrial Physics, 63, pp. 3-10.

Bostrom, R.C. (1971): Westward displacement of the lithosphere, Nature, 234, 356–538.

Bowman, D.D., Ouillon, G., Sammis, C.G., Sornette, A. & Sornette, D. (1988): An observational test of the critical earthquake concept. J. Geophys. Res., 103, 24359-24370.

Braitenberg, C. (1999): The Friuli (NE-Italy) tilt/strain gauges and short term observations Annali di Geofísica, 42,. 581. Page 637-664.

Braitenberg, C., Nagy, I., Negusini, M., Romagnoli, C., Zadro, M. & Zerbini, S. (2001): Geodetic measurements at the northern border of the Adria plate. Journal of Geodynamics 32 (2001) 267–286.

Braitenberg, C., Romeo, G., Taccetti, Q. & Nagy, I. (2006): The very-broad-band long-base tiltmeters of Grotta Gigante (Trieste, Italy): Secular term tilting and the great Sumatra-Andaman islands earthquake of December 26, 2004. Journal of Geodynamics 41 (2006) 164–174.

Brázdil, R., et al. (1988): Úvod do studia planety Země. SPN, Praha, 368pp. (in Czech)

Breitkreuz, C. & Kennedy, A. (1999): Magmatic flare-up at the Carboniferous/Permian boundary in the NE German basin revealed by SHRIMP zircon ages. Tectonophysics 302, 307–326.

Brent, D.G., Clague, D. A. & Lanphere, M. A. (1977): Revised age for Midway volcano, Hawaiian volcanic chain. Earth and Planetary Science Letters, Volume 37, Issue 1, p. 107-116.

Briestenský M., Stemberk J. & Petro L. (2007a): Displacements registered around March 13, 2006 Vrbové earthquake M=3.2 (Western Carpathians). Geologica Carpathica, 58,5,487-493, Bratislava.

Briestenský M. & Stemberk J. (2007b): Recent displacements registered in selected caves of Dobrá Voda karst area in Slovakia. - Acta Geodyn. Geomater., 4, 1, 31-38, Praha.

Brimich, L. (2006): Strain measurements at the Vyhne tidal station. Contributions to geophysics and geodesy, Vol. 36/4.

Brudzinski, M.R. & Allen, R.M. (2007): Segmentation in episodic tremor and slip all along Cascadia. Geology, Vol. 35, No. 10, 907-910.

Brune, J.N. (1968): Seismic moment, seismicity, and rate of slip along major fault zones. J. Geophys. Res. 73 (1968), pp. 777–784.

Büllesfeld, F.-J. (1985): Ein Beitrag zur harmonischen Darstellung des gezeitenerzeugenden Potentials. Deutsche Geodätische Kommission, Reihe C (Dissertationen), Heft Nr. 314, München, 1 - 103.

Calais, E. et al. (1995): GPS detection of ionospheric perturbations following the Jan. 17, 1994, Northridge earthquake. Geophysical Research Letters, vol. 22, No. 9, pp. 1045-1048.

Calais, E. et al. (1998): GPS, earthquakes, the ionosphere, and the Space Shuttle. Physics of the Earth and Planetary Interiors, 105, pp. 167-181.

Calais, E. et al. (2003): Detection of ionospheric perturbations using a dense GPS array in Southern California. Geophysical Research Letters, vol. 30, No. 12, 1628, doi:10.1029/2003GL017708.

Caporali, A., Braitenberg, C. & Massironi, M. (2005):Geodetic and hydrological aspects of the Merano earthquake of 17 July 2001. Journal of Geodynamics 39 (2005) 317–336.

Cartwright, D. E. & Tayler, R. J. (1971): New Computations of the Tide-generating Potential. Geoph. Journal Roy. Astr. Soc., 23, 45 - 73.

Cartwright, D. E. & Edden, A. C. (1973): Corrected Tables of Tidal Harmonics. Geoph. Journal Roy. Astr. Soc., 33, 253 - 264.

Cello, G., Mazzoli, S., Tondi, E., & Turco, E. (1997): Active tectonics in the central Apennines and possible implications for seismic hazard analysis in peninsular Italy, Tectonophysics, 272, 43-68.

Charvátová, I. (1988): The solar motion and the variability of solar activity. Advances in Space Res. 8, 7, 147-150.

Charvátová, I. (1997): Solar motion (main article), in Encyklopedia of Planetary Sciences (Eds. J.H.Shirley and R.W.Fairbridge), Chapman & Hall, New York, London, pp.748-751.

Choudhury, S., Dasgupta, S., Saraf, A.K. & Panda, S. (2006): Remote sensing observations of pre-earthquake thermal anomalies in Iran. International Journal of Remote Sensing, 27, pp. 4381–4396.

Chu, J.J., Gui, X., Dai, J., Marone, Ch., Spiegelman, M.W., Seeber, L. & Armbruster, J.G. (1996): Geoelectric signals in China and the earthquake generation process . J. Geophys. Res., Vol. 101, No. B6, Pages 13,869-13,882.

Chyi, L.L., Quick, T.J., Yang, F.T., & Chen, C.H. (2002): Nature of soil gas radon release and earthquake prediction. GSA Abs. with Prog., 34, 262.

Cícha, J. (1991): Kras okolí Ledče, K současnému stavu speleologických lokalit na Ledečsku (Karst in the vicinity of Ledeč. To the present state of speleological localities in Ledeč/Sázava region). - Stalagmite, 1, 20-21, Praha. (In Czech)

Cochran, E. S., J. E. Vidale, & S. Tanaka (2004): Earth tides can trigger shallow thrust fault earthquakes, Science, 306, 1164– 1166.

Cochran, E. S. & J. E. Vidale (2006): Comment on ‘‘Tidal synchronicity of the 26 December 2004 Sumatran earthquake and its aftershocks’’ by R. G. M. Crockett et al. . Geophys. Res. Lett, VOL. 34, L04302, doi:10.1029/2006GL028639, 2007.

Contadakis, M.E. & Asteriadis, G. (2001): Recent results of the research for preseismic phenomena on the underground water and temperature in Pieria, northern Greece. Natural Hazards and Earth System Sciences (2001) 1: 165–170.

Crampin, S. & Gao, Y. (2009): A global earthquake monitoring system that would stress forecast all damaging earthquakes worldwide. Proc. of ISESEP, 8th July, 2009, Beijing. www.geos.ed.ac.uk/homes/scrampin/opinion.

Crespi, M., Cuffaro, M., Doglioni, C., Giannone1, F. & Riguzzi, F. (2007): Space geodesy validation of the global lithospheric flow. Geophys. J. Int., 168, 491–506.

Crockett, R. G. M., G. K. Gillmore, P. S. Phillips, & D. D. Gilbertson (2006): Tidal synchronicity of the 26 December 2004 Sumatran earthquake and its aftershocks, Geophys. Res. Lett., 33, L19302, doi:10.1029/2006GL027074.

Croll, J.G.A. (2005): Thermal buckling of pavement slabs. Jour. of Transportation, Proc ICE., v. 158, p. 115-126.

Croll, J.G.A. (2006): From asphalt to the Arctic: new insights into thermo-mechanical ratcheting processes. III Int. Conf. On Computational Mechanics. Lisbon, Portugal, 5-8 June.

Croll, J.G.A. and Jones, E.W.J. (2006): Thermal ratchetting in periglacial environments. Asian Conf on Permafrost, Lanzhou, China, 7-9 August, 2006.

Croll, J.G.A. (2007a): Mechanics of thermal ratchet uplift buckling in periglacial morphologies. Proceedings of the SEMC Conference, Cape Town, September, 2007.

Croll, J.G.A. (2007b): Thermal ratchet uplift buckling and periglacial morphologies. Presented at Int. Conference Cryogenic Resources of Polar regions, Salekhard City, Russia, 17-22 June, 2007.

Croll, J.G.A. (2007c): A new hypothesis for Earth lithosphere evolution. New Concepts in Global Tectonics Newsletter, no. 45, December, 2007, 34-51.

Croll, J. G. A. (2008): A new hypothesis for the development of blisters in asphalt pavements. Int. Jour. Pavement Engineering, Vol. 9, Issue 1, 59-67.

Dalrymple, G. B.; Clague, D. A.; Lanphere, M. A. (1977): Revised age for Midway volcano, Hawaiian volcanic chain. Earth and Planetary Science Letters, Volume 37, Issue 1, p. 107-116.

Darwin, G. H. (1883): Report of a committee for the harmonic analysis of tidal observations. Brit. Ass. Rep., 48 - 118.

Dehant, V. (1987): Tidal Parameters for an Inelastic Earth. Physics of the Earth and Planetary Interiors, 49, 97 - 116.

DeMets, C., Gordon, R.G., Argus, F. & Stein, S. (1990): Current plate motions. Geophys. J. Int., 101, 425-478.

Denis, C., Schreider, A.A., Varga, P., & Zavoti, J. (2002): Despinning of the Earth rotation in the geological past and geomagnetic and geomagnetic paleointensities. Journal fo Geodynamics, 34, 667-685.

DGFI (2010): Deutsches Geodätisches Forschunginstitut. http://www.dgfi.badw.de/.

Di Giovambattista, R., Tyupkin, Y. (2001): An analysis of the process of acceleration of seismic energy emission in laboratory experiments on destruction of rocks and before strong earthquakes on Kamchatka and in Italy., Tectonophysics, 338, pp. 339-351.

Di Giovambattista, R. & Tyupkin, Y. (2004): Seismicity patterns before the M=5.8 2002, Palermo (Italy) earthquake: seismic quiescence and accelerating seismicity., Tectonophysics, 384, pp. 243-255.

Di Luccio, F., R. Console, M. Imoto, & M. Murru (1997): Analysis of short time-space range seismicity patterns in Italy: further step towards earthquake prediction, Annali di Geofisica, XL, 783-798.

Dieterich, J. (1987): Nucleation and triggering of earthquake slip: effect of periodic stresses, Tectonophys., 144, 127.

Dieterich, J. (1994): A constitutive law for rate of earthquake production and its application to earthquake clustering. J.Geophys. Res.., 99, 2601-2618.

Dobrovlskij, I.P. (1991): Theory of Tectonic Earthquake Preparation. Inst. Fiz. Zemli Akad. Nauk SSSR. (in Russian).

Dodge, D. A. & G. C., Beroza (1995): Foreshock sequence of the 1992 Landers, Calif., earthquake and its implication for earthquake nucleation, J. Geophys., Res. 100, 9865-9880.

Doodson, A. T. (1921): The Harmonic Development of the Tide-generating Potential. Proceedings of the Royal Astronomical Society, 100, London, 305 - 329.

Doglioni, C. (1990): The global tectonic pattern, J. Geodynam., 12, 21-38.

Doglioni, C. (1991): A proposal of linematic modeling for W-dipping subductions – Possible applications to the Tyrrhenian – Apennines system, Terra Nova, 3, 423-434.

Doglioni, C. (1993): Geological evidence for a global tectonic polarity. Journal of the geological society, London, Vol. 150, 991-1002.

Doglioni, C., Carminati, E. & Bonatti, E. (2003): Rift asymmetry and continental uplift. Tectonics, Vol. 22, No. 3, 1024, 8-1 – 8-13. doi:10.1029/2002TC001459.

Doglioni, C., Green, D.H. & Mongelli, F. (2005): On the shallow origin of hotspot and the westward drift of the lithosphere. Geological Society of America Special Paper 388, 735-749.

Douglas, A., Beavan, J., Wallace, L. & Townend, J. (2005): Slow slip on the northern Hikurangi subduction interface, New Zealand. Geophysical Research Letters, Vol. 32, L16305, doi:10.1029/2005GL023607, 2005.

Dorigo (2009): 3 megatons strike in central Italy. A Quantum Diaries Survivor, 6.4.2009. http://dorigo.wordpress.com/2009/04/06/3-megatons-strike-in-central-italy/

Dragert, H., Wang, K. & Rogers, G. (2004): Geodetic and seismic signatures of episodic tremor and slip in the northern Cascadia subduction zone. Earth Planets Space, 56, 1143–1150.

Ducic, V. (2003): Ionospheric remote sensing of the Denali Earthquake Rayleigh surface waves," Geophysical Research Letters, vol. 30, No. 18, 1951, doi: 10.1029/2003GL017812.

Dziewonski, A. M. & Woodhouse, J.H. (1983): An experiment in the systematic study of global seismicity: centroid-moment tensor solutions for 201 moderate and large earthquakes of 1981. J. Geophys. Res., 88: 3247-3271.

Dziewonski, A. M., & Anderson, D. L., (1984): Seismic tomography of the Earth's interior: Am. Scientist, v. 72, no. 5, p. 483-494.

Eftaxias, et al. (2003): Experience of short term earthquake precursors with VLF-VHF electromagnetic emissions. Natural Hazards and Earth System Sciences, 3: 217-228.

Emter, D. (1997): Tidal triggering of earthquakes and volcanic events, in Tidal Phenomena, edited by S. Bhattacharji et al., pp. 293– 309, Springer, New York.

EMSC (2010): Centre Sismologique Euro-Méditerranéen. European-Mediterranean Seismological Centre. http://www.emsc-csem.org/.

Estermann, G., Schuh, H., Crétaux, J.-F. & van Damm, T. (2003): Various models of atmospheric and hyrdological loading investigated by VLBI. Proc. of workshop: „The state of GPS vertical positioning precision: Separation of Earth processes by space geodesy", Luxembourg.

Eötvös, L. (1913): Verhandlugen der 17. Algem. Konferenz d. Internat. Erdmessungen, Part 1, 111.

Farrell, W.E. (1972): Deformation of the Earth by surface loads. Rev. Geophys. Space Phys., No. 10, 761-797.

Favela, J. & Anderson, D.L. (1999): Extensional Tectonics and Global Volcanism. Erice, Italy - Conference Proceedings.

Feigl, K.L., A. Sergent & D. Jacq (1995): Estimation of an earthquake focal mechanism from a satellite radar interferogram: application to the December 4, 1992 Landers aftershock, Geophys. Res. Lett., 22, 1037-1040.

Fischer, T., Kalenda, P. & Skalský, L. (2006): Weak indications of tidal triggering of earthquake swarms in NW-Bohemia/Vogtland, Tectonophysics 424, 259-269.

Foley,S.F., Buhre, S. & Jacob, D.E. (2003): Evolution of the Archaean crust by delamination and shallow subduction. Nature 421, 249-252.

Freund, F. (2002): Charge generation and propagation in igneous rocks., Journal of Geodynamics, 33, pp. 543-570.

Freund, F.T., Takeuchi, A. & Lau, B.W.S. (2006): Electric currents streaming out of stressed igneous rocks –A step towards understanding pre-earthquake low frequency EM emissions. Physics and Chemistry of the Earth 31 (2006) 389–396.

Fujita Research (1997): Earthquake prediction. http://www.fujitaresearch.com/reports/earthquakes.html.

Gadjiyev Y.A., Dadashev R.M. & Sapunov A.G. (1985): Periodicity of mud volcanoes eruptions and solar activity. Transactions of Azerbaijani Academy of Science, v.12, No.11, p.38-42.

Galis M., Moczo P. & Kristek J. (2008): A 3-D hybrid finite-difference—finite-element viscoelastic modelling of seismic wave motion. Geophys. J. Int. 175, 153-184.

Garai, J. (1997): The driving mechanism of plate tectonics, Eos, Transactions, AGU, 78 (46) Fall Meet. Suppl., pp. 712.

Garai, J. & Gasparik, T. (2003): Melting of San Carlos olivine in the presence of carbon at 6-12 Gpa. Physics/0307132.

Garai, J. (2007) Global coupling at 660 km is proposed to explain plate tectonics and the generation of the earth's magnetic field arXiv:0709.1303.

Gasparini, C., Iannaccone, G. & Scarpa, R. (1985): Fault-plane solutions and seismicity of the Italian peinsula, Tectonophysics, 117, 59-78.

Geller, R.J. (1997a): Predictable publicity. SRL 68:4.

Geller, R.J. (1997b): Earthquake prediction: a critical review. Geophys. J. Int. 131, 425-450 (1997).

Geller, R.J., Jackson D.D., Kagan, Y.Y. & Mulargia, F. (1997): Earthquakes cannot be predicted. Science 275, 1616-1618.

Gerstoft, P., Fehler, M. C. & Sabra, K. G. (2006): When Katrina hit California. *Eos Trans. AGU, 87*(52), Fall Meet. Suppl., Abstract S11C-06.

Ghisetti, F. & Vezzani, L. (2002): Normal faulting, transcrustal permeability and seismogenesis in the Apennines (Italy), Tectonophysics, 348, 155-168.

Ghosh, A.; Vidale, J.E.; Peng, Z., Creager, K.C., Houston, H. (2009): Complex nonvolcanic tremor near Parkfield, California, triggered by the great 2004 Sumatra earthquake. J. Geophys., Res., VOL. 114, B00A15, doi:10.1029/2008JB006062.

Gibson, J.M. & Ma, C. (1998): Site displacement due to variation in Earth rotation. J. Geophys. Res., 103, 7337-7350.

Giuliani G. (2004): Apparatus for the detection of radon gas concentration variation in the environment, method for such detection and their use in forecasting of seismic events. European Patent Office, WO2004061448 (A1). http://v3.espacenet.com/publicationDetails/biblio?CC=WO&NR=2004061448A1 .

Glass, E. D. (1996): How Earthquake Sensitives Predict Earthquakes, GeoMonitor: Earthquake Prediction News; April, 1996 – U.S. Copyright TXu000730816, 1996.

Glass, E. D. (1999): Earthquake and tornado precursors, formation, and triggering processes TXu000913900, 1999.

Glass, E. D. (2004): Earthquake and tornado forecasting and research computer program TXu001172397, 2004.

R.G. Gordon, R.G. (1995): Present plate motions and plate boundaries. In: Global Earth Physics, Reference Shelf 1, pp.66-87, ed. T.J. Arhens, Am. Geophys. Un., Washington.

Gorny, V.I., Salman, A.G., Tronin, A.A. & Shilin, B.B. (1988): The Earth outgoing IR radiation as an indicator of seismic activity. Proceedings of the Academy of Sciences of the USSR, 301, pp. 67–69.

Gregory, A. F., Morley, L. W., Bower, Margaret E. & Geological Survey of Canada (1960): Geological interpretation of aeromagnetic profiles from the Canadian arctic archipelago / by A.F. Gregory, Margaret E. Bower and L.W. Morley GSC, Ottawa, Ont.

Gross, R. S. (2000): The excitation of the Chandler wobble. Geophys. Res. Lett., 27(15), 2329–2332.

Grygar, J. (1994): Kosmické katastrofy. Přednáška proslovená v cyklu "Otázky a názory"
dne 6. prosince 1994 na ČVUT v Praze. (in Czech)

Guo, G. & Wang, B. (2008): Cloud anomaly before Iran earthquake . International Journal of Remote Sensing, Volume 29, Issue 7, 1921-1928.

Gutenberg, B. & C. F. Richter (1954): Seismicity of the Earth and Associated Phenomena, Princeton Univ. Press, Princeton, N.J.

Gutenberg, B. & C. F. Richter (1956): Earthquake magnitude, intensity, energy, and acceleration. BSSA, April 1956; v. 46; no. 2; p. 105-145. http://www2.bc.edu/~ebel/GutenberRichterMagnitude.pdf .

Han Y., Guo Z., Wu J. & Ma L. (2004): Possible triggering of solar activity to big earthquakes (Ms ≥ 8) in faults with near west-east strike in China. SCIENCE IN CHINA SERIES G, 2004 47(2).

Harris, R.A. & Arrowsmith, R.J. (2006): Introduction to the Special Issue on the 2004 Parkfield Earthquake and the Parkfield Earthquake Prediction Experiment.

Harrison, J. C. & Herbst, K. (1977): Thermoelastic strains and tilts revisited, Geophys. Res. Lett., 4, 535-537.

Harrison, T.M., Schmitt, A.K., McCulloch, M.T. & Lovera, O.M. (2008): Early (≥4.5 Ga) formation of terrestrial crust: Lu-Hf, δ18O, and Ti thermometry results for Hadean zircons. Earth Planet. Sci. Lett. 268:476–86.

Harward Global Centroid Moment Tensor (CMT) Catalogue (2010): http://www.globalcmt.org/CMTsearch.html.

Havíř, J. & Špaček, P. (2004): Recent tectonic activity and orientations of the principal stresses in the jeseníky region. GeoLines, 17, 38-39.

Hayakawa, M. & Sato, H. (1994): Ionospheric perturbations associated with earthquakes, as detected by subionospheric VLF propagation, in: Electromagnetic Phenomena Related to Earthquake Prediction, edited by: Hayakawa, M. and Fujinawa, Y., Terra Sci. Publ., Tokyo, 391-398.

Hayakawa, M., Y. Sue, & T. Nakamura (2009): The effect of earth tides as observed in seismo-electromagnetic precursory signals. Nat. Hazards Earth Syst. Sci., 9, 1733–1741, 2009. www.nat-hazards-earth-syst-sci.net/9/1733/2009/ .

Hayes, T. J., Tiampo, K.F., Rundle, J.B. & Fernández, J. (2006), Gravity changes from a stress evolution earthquake simulation of California, J. Geophys. Res., 111, B09408, doi:10.1029/2005JB004092.

He, H. & Tsukuda, E. (2003): Recent Progresses of Active Fault Research in China. Journal of Geography, 112, 489-520.

Heaton, T.H. (1982): Tidal triggering of earthquakes. Bull. Seismol. Soc. Am., 72, 6, 2181-2200.

Heezen, B.C. & Tharp, M., (1965): Tectonic fabric of the Atlantic and Indian Oceans and continental drift. Phil. Trans. Roy. .Soc., Ser A, 258, 90-108.

Heki, K. (2004): Ionospheric Perturbation by the Surface Wave of the 2003 Tokachi-Oki Earthquake (MJMA=8.0) Detected Using a Dense GPS Array.

Hervé M. (1999): L'environnement de la Terre primitive : l'Archéen et l'Hadéen. Société Française d'Exobiologie. http://www.exobiologie.fr/index.php/vulgarisation/

Hey, R.N. & Vogt, P.N. (1977): Rise axis jumps and sub-axial flow near the Galapagos hotspot. Tectonophysics, 37, 41-52.

Hill, D.P., et al. (1993): Seismicity in the Western United States remotely triggered by the M 7.4 Landers, California earthquake of June 28, 1992, Science, 1617-1623.¨)

Hiramatsu, Y. & Watanabe, T. (2008): Deep low-frequency tremors as a proxy for slip monitoring at plate interface. Graduate School of Natural Science and Technology, Kanazawa University, Kakuma, Kanazawa, Ishikawa 920-1192, Japan.

Hirose, H. & Obara, K. (2005): Repeating short- and long-term slow slip events with deep tremor activity around the Bungo channel region, southwest Japan. Earth Planets Space, 57, 961–972.

Holmes, A. (1939): Radioaktivity and the Earth movement. Trans. Geol. Soc. Glasg., 28, 559-606.

Holmes, A. (1944): Principles of Physical Geology. (Edinburgh: Thomas Nelson and Sons, 1944 and New York: Ronald Press, 1945).

Holub K., Rušajová J. & Sandev M. (2008): Windstorm of 18-19 January, 2007, an its impact on the features of microseisms. Meteorol. Z., Vol. 17, No. 1, 047-053.

Homola, V. (1952): Krasové zjevy v krystalických vápencích v okolí Ledče nad Sázavou – (Karst phenomena in crystalline limestone near the town of Ledeč nad Sázavou) - Československý kras V, 192-197. (in Czech)

Horálek, J. & Fischer, T. (2007) – Západočeská seismická síť Webnet (West Bohemian seismic network Webnet).- http://www.ig.cas.cz/cz/struktura/observatore/zapadoceska-seismicka-sit-webnet/.

Horálek, J., Fischer, T., Boušková, A., Michálek, J. & Hrubcová, P. (2009): The West Bohemian 2008-earthquake swarm: When, where, what size and data. Studia Geophysica et Geodaetica, vol. 53, No 3, 351-358.

Hough, S. (2009): Predicting the Unpredictable: The Tumultuous Science of Earthquake Prediction. pp 272.

Hunter, R. (2003): Earthquake Probability Estimator. http://www.tarma.com.

Husson, L., Conrad, C.P. & Faccenna, C. (2007): Tethyan Closure, Andean Orogeny, and Westward Drift of the Pacific Basin.

Hvožďara, M., Brimich, L. & Skalský, L. (1988): Thermo-elastic deformations due to annual temperature variation at the tidal station in Vyhne. Studia Geophysica et Geodaetica, Vol. 32, No.2, 129-135.

Ide, S., Shelly, D. R., & Beroza, G. C. (2007): Mechanism of deep low frequency earthquakes: Further evidence that deep non-volcanic tremor is generated by shear slip on the plate interface. Geophysical Research Letters 34 (3), 5.

İnan, S., T. Akgül, C. Seyis, R. Saatçılar, S. Baykut, S. Ergintav & M. Baş (2008): Geochemical Monitoring in the Marmara Region (NW Turkey): A Search for Precursors of Seismic Activity, Journal of Geophysical Research, 113, B03401, doi:10.1029/2007JB005206.

International Earth Rotation Service (1992): IERS Standards (1992), IERS Technical Note 13, edited by D. D. McCarthy (Observatoire de Paris, Paris, France).

IERS (2010): International Earth Rotation And Reference Systems Service. http://www.iers.org/MainDisp.csl?pid=36-9.

Irrational Geographic (2009): Earthquake Fish, Earthquake Weather, Earthquake Clouds, Earthquake Light . http://irrationalgeographic.wordpress.com/category/meteorology/.

ISESEP 09 (2009): 5 – 9 July 2009. Beijing. http://www.cea-igp.ac.cn/English/Symposium/Provisional%20Program.htm .

Ito, K., & Matsuzaki, M. (1990): Earthquakes as self-organized critical phenomena, J. Geophys. Res., 95, 6853-6860.

Ito, Y., Obara, K., Shiomi, K., Sekine, S. & Hirose, H. (2007): Slow Earthquakes Coincident with Episodic Tremors and Slow Slip Events. Science Vol. 315, 26 January 2007., 503-506.

Janssen, V. (2007): Volcano deformation monitoring using GPS. Journal of Spatial Science, 52 (1). pp. 41-54. http://eprints.utas.edu.au/817/1/janssen_JSpSc_2007.pdf .

Jaumé, S.C., & Sykes, L.R. (1999): Evolving towards a critical point: A review of accelerating moment/energy release prior to large and great earthquakes. Pure Appl. Geophys., 155, 279-306.

Jochum, J.P., Hofmann, A.W., Ito, E., Seufert, H.M. & White, W.M. (1983): K, U and Th in mid-ocean ridge basalt. Nature, 306: 431-436.

Johnston, M.J.S., R. D. Borcherdt, A. T. Linde, & M. T. Gladwin (2004): Continuous Borehole Strain and Pore Pressure in the Near Field of the 28 September 2004 M 6.0 Parkfield, California, Earthquake: Implications for Nucleation, Fault Response, Earthquake Prediction, and Tremor. Special Issue on the 2004 Parkfield Earthquake and the Parkfield Earthquake Prediction Experiment.

Jones, L. M., & P. Molnar (1979): Some characteristics of foreshocks and their possible relationship to earthquake prediction and premonitory slip on faults, J. Geophys. Res., 84, 3596-3608.

Jones, L. M., B. Q. Wang, S. X. Xu, & T. J. Fitch (1982): The foreshock sequence of the Feb. 4, 1975, Haicheng earthquake (M=7.3), J. Geophys. Res., 87, 4575-4584.

Jose, P. D. (1965): Sun's motion and sunspots. Astron. J., 70,193-200.

Kachlík V., & Chlupáč I. (1996): Základy geologie. - Skriptum UK, Karolinum. Praha.

Kaczorowski, M. (2007): Preliminary results of investigations of long lasting non-tidal signals observed by means of horizontal pendulums and long water tube tiltmeters in low silesian geodynamic laboratory of Polish Academy of Sciences in Ksiaz. Acta Geodyn. Geomater., Vol. 4, No. 4 (148), 109-119.

Kadlec, J., Hercman, H., Beneš, V., Šroubek, P., Diehl, J.F. & Granger, D. (2001): Cainozoic history of the Moravian Karst (northern segment): cave sediments and karst morphology. - Acta Mus. Moraviae, Sci. geol.: LXXXV (2001), 111-161.

Kagan, Y.Y. (1994): Observational evidence for earthquakes as a non-linear dynamic process, Physica D, 77, 160-192. Kartvělišvili, K.Z. (1988): Issledovanie zemnych prilivov kak spuskovogo mechanizma zemletrjasenij. Prognoz zemletrjasenij, No.8, 112 – 125.

Kalenda,P. & Pompura,I. (1997): Seismic activity development before stress conditioned strong seismic events in Jelšava mine. Acta Montana, Praha, Series A,No.10 (102), 145-153.

Kalenda, P. & Skalský, L. (2002): Verification of the Load-unload response ratio theory in the conditions of induced seismicity in the Ostrava-Karvina Coal Basin. Publ. Inst. Geophys. Pol. Acad. Sci., M-24(340), 35-51.

Kalenda, P., Málek, J. & Skalský, L. (2006): Tidal and non-tidal frequencies found in the seismicity of California. Publs. Inst. Geophys. Pol. Acad. Sci., M-29 (395), 2006.

Kalenda, P., Neumann, L. & Wandrol, I. (2009): Indirect stress measurement by static vertical pendulum. Proceedings of 47th Int. Sci. Conf. Experimentální analýza napětí 2009, 120-128. TU Liberec.

Kanamori, H., Hauksson, E. & Heaton, T. (1997): Real-time seismology and earthquake hazard mitigation. Nature |Vol 390 | 4 December 1997, 461-464.

Kane, R.P., Hari Om Vats & H.S. Sawant (2004): Short-Term Periodicities in the Time Series of Solar Radio Emissions at Different Solar Altitudes . Solar Physics, Volume 201, Number 1 / June, 2001, 181-190.

Kárník,V. & Tobyáš,V. (1961): Underground Measurements of the Seismic Noise Level. Studia Geophys.Geod.; 5 c.3, p.231.

Keilis-Borok, V.I. & Kossobokov, V.G. (1990): Premonitory activation of earthquake flow: algorithm M8. PEPI, Vol. 61, 1-2, 73-83.

Keilis-Borok, V.I & Rotwain, I.M. (1990): Diagnosis of time of increased probability of strong earthquakes in different regions of the world: algorithm CN., Physics of the Earth and Planetary Interiors, 61, pp. 57-72

Keilis-Borok, V.I., Shebalin,P.N. & Zaliapin, I.V. (2002): Premonitory patterns of seismicity months before a large earthquake: Five case histories in Southern California. PNAS December 24, 2002 vol. 99 no. 26, 16562-16567.

Keilis-Borok, V. & Soloviev, A. (2003): Nonlinear Dynamics of the Lithosphere and Earthquake Prediction, Springer Verlag, Berlin, Germany. 344.

Keith, M.L. (1993): Geodynamics and mantle flow: an alternative earth model. Earth-Science Reviews, 33 (1993) 153-337.

Keramova, R.A. (2003): "The Effect of Strong and Catastrophic Earthquakes within the Anatolia–Iran–Caucasus Tectonic Block on the Hydrogeochemical Regime of Fluids in Azerbaijan," in Catalog of Seismic Prognostic Observations in Azerbaijan (1983–2001) (Elm, Baku, 2003) [in Russian].

Keramova, R.A. (2005): Prompt Determination of Seismic Sources of Strong Earthquakes ($M \geq 5.5$) from Geochemical Anomalies of Fluids in Azerbaijan. Izvestiya, Physics of the Solid Earth, Vol. 41, No. 4, April 2005, pp. 279-291.

Kery, P. & Vine, F. (1996): Global Tectonics, Blackwell Science. Surveys in Geophysics, Volume 19, Number 1 / January, 1998.

Khalilov, E. (2009): Global network of forecasting the earthquakes: New technology and new philosophy. SWB, London, pp 65. http://icep-atropatena.com/images/broshura.pdf .

Khain,V.Y. & Khalilov, E.N. (2008): Space-Time regularities of seismic and volcanic activity. Bourgas, 304 p. http://khalilov.biz/pdf/Khain,Khalilov.pdf .

Khain,V.Y. & Khalilov, E.N. (2009): Cycles in geodynamic processes: Their possible nature. Moscow, Scientific World, 520 p.

Kilston, S., &Knopoff, L (1983): Lunar-Solar Periodicities of Large Earthquakes in Southern California. Nature, 1983, vol. 304, pp. 21-25.

King C.-Y., Azuma S., Igarashi G., Ohno M., Saito H. & Wakita, H. (1999): Earthquake-related water-level changes at 16 closely clustered wells in Tono, central Japan. Journal of geophysical research , 1999, vol. 104, noB6, pp. 13073-13082 .

Kinki (2002): Great Hanshin Earthquake Restoration. Kinki Regional Development Bureau. http://www.kkr.mlit.go.jp/en/topics_hanshin.html .

Klein, F. W. (1976), Earthquake swarms and semidiurnal solid earth tide, Geophys. J. R. Astron. Soc., 45, 245– 295.

Knopoff, L. (1964): Earth tides as a triggering mechanism for earthquakes. Bull. Seismol. Soc. Am., 54, 1865-1870.

Knopoff, L. & Leeds, A. (1972): Lithospheric momenta and the deceleration of the Earth, Nature 237, 93-95.

Komitov, B. (2009): An evidence for solar activity influence on the meteorological processes in the south polar region of Mars during the great opposition in AD 1924. "arXiv:0912.2112". http://xxx.lanl.gov/abs/0912.2112.

Kostoglodov, V., Singh, S.K., Santiago, J.A., Franco, S.I., Larson, K.M., Lowry, A.R., & Bilham, R., (2003): A large silent earthquake in the Guerrero seismic gap, Mexico. Geophysical Research Letters, v. 30, doi: 10.1029/2003GLO17219.

Košťák, B. (1991) – patent CZ No. 131631 a 246454, autor Ing. B. Košťák, CSc. – ÚSMH AV ČR.

Landau, L. D & Lifschitz, E. M. (1983): Elastizitätstheorie, (Lehrbuch der Theoretischen Physik, Band VII), Akademie-Verlag, Berlin (5. Auflage 1983, 1.Auflage 1965), translated from L. D. Landau, E. M. Lifšic: Teorija uprugosti, Nauka, Moskva (1965)/(1953).

Levshina, T., & Vorobieva, I. (1992): Application of Algorithm SSE for Prediction of a Strong Repeated Earthquake to the Joshua Tree and Landers., Fall Meeting AGU, 1992, p. 382.

Li, V.,C. (1987): Mechanics of shear rupture applied to earthquake zones. In. Fracture Mechanics of rock (ed. Atkinson, B.K.), Academic Press, London, pp. 351-428.

Liperovsky, V.A., Meister, C.-V., Liperovskaya, E.V., Davidov, V.F. & Bogdanov, V.V., (2005): On the possible influence of radon and aerosol injection on the

atmosphere and ionosphere before earthquakes. Natural Hazards and Earth System Sciences, 5, pp. 783–789.

Li, J.Z., Z. Q. Bai, W. S. Chen, Y. Q. Xia, Y. R. Liu, & Z. Q. Ren (2003): Strong earthquakes can be predicted: a multidisciplinary method for strong earthquake prediction. Natural Hazards and Earth System Sciences (2003) 3: 703–712.

Liu, X. Y. & Z. Y. Shao (1999): Primary analysis of the crustal movement and GPS observation data in Fujian coast. Crust Deformation and Earthquake, 19 (3), 40-47.

Liu, J.Y., et al. (2004): „Pre-earthquake ionospheric anomalies registered by continuous GPS TEC measurements," Annales Geophysicae 22: 1585-1593.

Liu, Ch.-Ch., Linde, A.T. & Sacks, S.I. (2009): Slow earthquakes triggered by typhoons. Nature 459, 833-836.

Lockner, D.A. & Beeler, N.M. (1999): Premonitory slip and tidal triggering of earthquakes. J. Geophys. Res., 104, 20133-20151.

Lomnitz, C. (1994): Fundamentals of earthquake prediction. Wiley, New York, 326 pp.

Lundgren, P. R. (2002): InSAR time series resolution of blind thrust and surface fault creep, 3 pp., Final Report, GESS Requirements. Definition Study.

Ma Zongjin et al. (1990): Nine Major Earthquakes in China. Earthquake Prediction, 178, pp. 105-111.

Main, I. (1995): Earthquakes as critical phenomena: implications for the probabilistic seismic hazard analysis. Bull. Seism. Soc. Am. 85, 1299 -1308.

Main, I. (1996): Statistical physics, seismogenesis and seismic hazard, Rev. Geophys., 34(4), 433-462.

Main, I., et al. (1999): Is the reliable prediction of individual earthquakes a realistic scientific goal? Nature, 25 February, 1999.
http://www.nature.com/nature/debates/earthquake/equake_frameset.html

Mandal, P., Rastogi, B. K., Chadha, R. K., Satyanarayana, H. V. S., Sarma, S. P. C., Kumar, N., Satyamurthy, Ch., Raju, P. I. & Rao, N. A. (2004): Method of short term forecasting of moderate size earthquakes. US Patent No. 6728640.

Mann, P., Calais, E., Demets, Ch., Prentice, C. S. & Wiggins-Grandison, M. (2008): Enriquillo-plantain garden strike-slip fault zone: A major seismic hazard
affecting dominican republic, Haiti and Jamaica. JSG and the 18th Caribbean Geological Conference, Santo Domingo, Dominican Republic.

March, J.G., Lerch, F.J., Putney, B.H. & Cristodoulidis, D.C. (1988): A new gravitational model for the Earth from the satellite tracking data: GEM-T1. J.Geophys. Res., 93, 6169-6215.

Mares, S. (1984): Introduction to Applied Geophysics. Reidel Publishing Company, Dordrecht/Boston/Lancaster.

Marussi, A. (1959): The University of Trieste station for the study of the tides of the vertical in the Grotta Gigante. In: Proceedings of the Third International Symposium on Earth Tides, Trieste, pp. 45–52.

Mason, B. (2010): Chile Earthquake Moved Entire City 10 Feet to the West. http://www.wired.com/wiredscience/2010/03/chile-earthquake-moved-entire-city-10-feet-to-the-west/#ixzz0iHFwr61i.

Matsumoto, N., Takahashi, M. & Koizumi, N. (2007): Groundwater-level Anomalies Associated with a Hypothetical Preslip Prior to the Anticipated Tokai Earthquake: Detectability Using the Groundwater Observation Network of the Geological Survey of Japan, AIST. Pageop, Volume 164, Number 12, 2377-2396.

Masayasu, H. & Yabashi D. (1994): Observation of ELF radiation related to volcanic and earthquake activities. Electromagnetic phenomena related to earthquake prediction, pp. 159-174.

Masood, E. (1995): Greek earthquake stirs controversy over claims for prediction method. Nature 375, 617.

Mauk, F. J., & M. J. Johnston (1973): Triggering of volcanic eruptions by Earth tides, J. Geophys. Res., 78, 3356– 3362.

Meyerhoff A.A., Taner I., Morris A.E.L., Agocs W.B., Kamen-Kaye M., Bhat M.I., Smoot, N.C., & Choi D.R., Meyerhoff Hull D. (editor) (1996): Surge tectonics : a new hypothesis of global geodynamics. Kluwer Academic Publishers, 323 p.

McKinnon, W.B., & Kirk, R.L. (2007). "Triton". in Lucy Ann Adams McFadden, Lucy-Ann Adams, Paul Robert Weissman, Torrence V. Johnson. Encyclopedia of the Solar System (2nd ed.). Amsterdam; Boston: Academic Press. pp. 483–502.

McNutt, S. R., & R. J. Beavan (1981): Volcanic earthquakes at Pavlof Volcano correlated with the solid earth tide, Nature, 294, 615– 618.

Melchior, P.J. (1983): The Tides of the Planet Earth. Pergamon Press, Oxford, 458 pp.

Melchior, P. & Skalský, L. (1969): Station: Příbram/Belg. Mesures faites dans les composantes Nord-Sud et Est-Ouest avec les pendules horizontaux VN No. 76 et No.77 en 1966, 1967 et 1968. Observatorie Royal de Belgique.

The MELT Seismic Team (D.W. Forsyth, D. S. Scheirer, S. C. Webb, L. M. Dorman, J. A. Orcutt, A. J. Harding, D. K. Blackman, J. Phipps Morgan, R. S. Detrick, Y. Shen, C. J. Wolfe, J. P. Canales, D. R. Toomey, A. F. Sheehan, S. C. Solomon, & W. S. D. Wilcock) (1988): Imaging the Deep Seismic Structure beneath a Mid-Ocean Ridge: The MELT Experiment. Science, 280, 1215-1217.

Meschede, M. & Barckhausen, U. (2000): Plate tectonic evolution of the Cocos-Nazca spreading center. Silver, E.A., Kimura, G., and Shipley, T.H. (Eds.) Proceedings of the Ocean Drilling Program, Scientific Results Volume 170. http://www-odp.tamu.edu/publications/170_SR/VOLUME/CHAPTERS/SR170_07.PDF

Milankovich, M. (1930): Mathematische Klimalehre und atsronomische Theorie der Klimaschwankungen. In: Köppen, W., Geiger, R. (Eds.), Handbuch der Klimatologie, vol. 1. Gebrüder Bornträger, Berlin, pp. 1-176.

Mjachkin,V.I., Brace, W.F., Sobolev, G.A. & Dieterich, J.H. (1974): Two models for earthquake forerunners. Pure and Applied Geophysics, Vol. 113, No.1, 169-181.

Moczo, P., Bard, P.-Y. & Pšenčík, I. (1987): Seismic response of two-dimensional absorbing structures by the ray method. J. Geophys., 62, 38-49.

Mogi, K. (1985): Earthquake Prediction (Academic Press, Tokyo).

Molchan, M. & Dmitrieva, E. (1990): Dynamics of the magnitude-frequency relation for foreshocks., Phys. Earth Planet. Inter., 61, pp. 99-112.

Molchanov, O. (2003): „Preseismic ULF electromagnetic effect from observation at Kamchalka," Natural Hazards and Earth System Sciences 3: 203-209.

Molchanov, O. (2004): „Lithosphere-atmosphere-ionosphere coupling as governing mechanism for preseismic short-term events in atmosphere and ionosphere," Natural Hazards and Earth System Sciences 4: 757-767.

Mora, P. & Place, D. (2002): Stress correlation function evolution in lattice solid elasto-dynamic models af shear and fracture zones and earthquake prediction. Pure Appl. Geophys., 159, 2413-2428.

Mukherjee, S. (2006). Earthquake Prediction. Published by Brill Academic Publishers Koninklijke Brill NV, Leiden (The Netherlands) & Boston (USA

Munidasa, K.G.H. (2009): Animals prophesy earthquake. Sunday observer, 3 May, 2009. http://www.sundayobserver.lk/2009/05/03/imp20.asp.

Munk W. H. & MacDonald, G. J. F. (1960): The Rotation of the Earth, Cambridge University Press, London.

Naaman, S.H., et al. (2001): Comparison of simultaneous variations of the ionospheric total electron content and geomagnetic field associated with strong earthquakes. Natural Hazards and Earth System Sciences, 1: 53-59.

NEIC (2004): NEIC Catalogue. http://wwwneic.cr.usgs.gov/neis/epic/epic.html .

Němec, F., Santolík, O., Parrot, M. & Berthelier, J.J. (2005): Statistical study of ELF/VLF emissions observed in the vicinity of earthquakes. AGU meeting 2005, poster T51B – 1347.

Němec, F., Santolík, O. & Parrot, M. (2009): Nízkofrekvenční vlnové emise pozorované družicí DEMETER. Čs. čas. fyz. 59 (2009), č.2, 63-69. (in Czech) http://babeta.ufa.cas.cz/nemec/work/articles/09cesfyz.pdf.

Neumann, L. (2007): Static Pendulum with Contactless 2d Sensor Measurements Open the Question of Gravity Dynamic and Gravity Noise on the Earth Surface. Physics Essays (Vol. 20 No. 4).

O'Nions, R.K. (1987): Relationships between chemical and convective layering in the Earth. J. Geol. Soc. London, 144: 259-274.

Ostřihanský, L. (1997): The causes of lithospheric plates movement. Charles University, Prague, 1-63.

Ostřihanský, L. (2004): Plate movements, earthquakes and variations of the Earth´s rotation. Acta Univ. Carol. Geol., 1-4, pp. 89-98.

Ogata, Y., T. Utsu, & K. Katsura (1995): Statistical features of foreshocks in comparison with other earthquake clusters: Geophys. J. Int., 121, 233-254.

Ohnaka, M. (1992): Earthquake source nucleation: A physical model for short-term precursors, Tectonophysics 211, 249-178.

Ouzounov, D. & Freund, F. (2004): Mid-infrared emission prior to strong earthquakes analyzed by remote sensing data. Advances in Space Research, 33, pp. 268–273.

Owen, H.G. (1983): The Earth is expanding and we don't know why. *New Scientist* 22: 27-29.

Pálinkáš, V. (2006): Precise tidal measurements by spring gravimeters at the station Pecný. Journal of Geodynamics 41 (2006) 14–22.

Pálinkáš, V. & Kostelecký, J. (2008): Superconducting Gravimeter OSG-050 at the Station Pecný, Czech Republic. Poster, ETS, http://www.pecny.cz/cedr/download/Palinkas_ETS_2008_SG.pdf.

Pálinkáš, V.; Šimek, J. & Kostelecký, J. (2008): Státní etalon tíhového zrychlení - absolutní gravimetr FG5 v.č. 215. Metrologie. 2008, roč. 17, č. 2, s.12-18. (in Czech)

Pálinkáš, V. & Kostelecký, J. (2008): Absolute Gravity Measurements and their Applications at the Station Pecný, Czech Republic. EGRSE Journal, Volume XII / 2005, Number 1–2, pp. 2 – 7.

Panza, G., Doglioni, C. & Levshin, A. (2009): Asymmetric ocean basins. XXXX. http://publications.ictp.it

Papazachos, B. (1975): Foreshocks and earthquake prediction: Tectonophysics, 28, 213-226.

Parsons, B. & Richter, F.M. (1981): Mantle convection and the oceanic lithosphere. In: C. Emiliani (Editor), The Sea, Vol. 7: The Oceanic Lithosphere. Wiley, New York, pp. 73-117.

Payero, J.S., Kostoglodov, V., Shapiro, N., Mikumo, T., Iglesias, A., Perez-Campos, X. & Clayton, R.W. (2007): Nonvolcanic tremor observed in the Mexican subduction zone. Geophysical Research Letters, Vol. 35, L07305.

Peng, Z. & Chao, K. (2008): Non-volcanic tremor beneath the Central Range in Taiwan triggered by the 2001 Mw 7.8 Kunlun earthquake. Geophys. Journ. Int., 175, 825–829.

Peng, H., Ma X. & Jiang, J. (2009): Process analysis of in-situ strain during the Ms=8.1 Wengchuan earthquake – data from the stress monitoring station Shandan. Acta Geologica Sinica, vol. 83, No.4, 754-766.

Petrov, L. & Boy, J.-P. (2003): Atmospheric pressure loading for routine data analysis. Proc. of workshop: „The state of GPS vertical positioning precision: Separation of Earth processes by space geodesy“, Luxembourg.

Plotkin, V.V. (2003): GPS detection of ionospheric perturbation before the Feb. 13, 2001, El Salvador earthquake. Natural Hazards and Earth System Sciences, 3: 249-253.

Popov, K.V. (2003): On Precursors of Earthquakes with Scaled of 2-3 Hours in F-Region of Ionosphere,“ Geophysical Research Abstracts, vol. 5, 08416.

Post, G. & Illis, B. (2009): Searching the PaleoClimate Record for Est. Correlations: Temperature, CO2 and Sea Level. Watts up with that?

Pratt, D. (2000): Plate Tectonics: A Paradigm Under Threat. Journal of Scientific Exploration, vol. 14, no. 3, pp. 307-352, 2000).

Prawirodirdjo, L., Ben-Zion, Y. & Bock, Y. (2006): Observation and modeling of thermoelastic strain in Southern California Integrated GPS Network daily position time series, J. Geophys. Res., 111, B02408.

Procházka V. (2008): Monazite in some rocks of Moldanubicum and Central Moldanubian pluton and effects of its radioactivity. - Acta Mus. Meridionale, Nat. Sci. 48, 33-43.

Procházka V. (2009): Phase changes initiated by natural radioactivity in crystalline rocks and their implications. - Geochim. Cosmochim. Acta 73/13 (S1), A 1055 (abstract).

Pulinets, S.A. (1998): „Seismic Activity as a Source of the Ionospheric Variability,“ Adv. Space Res. vol. 22, No. 6, pp. 903-906.

Pulinets, S.A. & Boyarchuk, K. (2004): Ionosferic precursors of earthquakes. Springer. 298pp.

Purcaru, G. (2008): The Great Sichuan Earthquake of May 12, 2008 (Mw7.9) - An Unpredictable Earthquake. American Geophysical Union, Fall Meeting 2008, abstract #S31B-1919.

Qiang Zuji, Xu Xiudeng & Lin Changgong (1990): Thermal anomaly—precursor of impending earthquake. Chinese Science Bulletin, 35, pp. 1324–1327.

Qian, Fuye, Zhao, Biru, Qian, W., Zhao, J., He S.-G., Zhang, H.-K., Li S.-Y., Li, S.-K.,Yan, G.-L., Wang Ch.-M., Sun Z.-K., Zhang, D.-N., Lu J., Zhang, P., Yang, G.-J., Sun J.-L., Guo Ch.-S., Tang Y.-X., Xu J.-M., Xia K.-T., Ju, H., Yin, B.-H., Li M., Yang, D.-S., Qi W.-L., He, T.-M., Guan, H.-P. & Zhao, Y.-L. (2009): Impending HRT wave precursors to the Wenchuan Ms8.0 earthquake and methods of earthquake impending prediction by using HRT wave. Science in China Series D: Earth Sciences. Oct. 2009, vol. 52, no. 10, 1572-1584.

Rasmussen, T.C. & Toll, N.J. (2007): Removal of barometric pressure effects and Earth tides from observed water levels. Ground Water 45 (1), 101 – 105.

Rastogi, B. K. & P. Mandal (1999): Foreshocks and Nucleation of small and moderate size Koyna earthquakes (INDIA), Bull. Seism. Soc. Am. 89(3), 1-8.

Reid, H.F. (1911): The elastic rebound theory of earthquakes. Bull. Dept. Geology. Univ. California, 6, 413.

Ricard, Y., Doglioni, C. & Sabadini, R. (1991): Differential rotation between Lithosphere and Mantle: A consequence of lateral mantle viscosity variations. J. Geophys. Res., 96, 8407-8415.

Richard, Y., Doglioni, C. & Sabedini, R. (1991): Differential rotation between lithosphere and mantle: a consequence of lateral mantle viscosity variations. J. Geophys. Res. 96, 8407-8415.

Richon, P., Sabroux, J.-C., Halbwachs, M., Vandemeulebrouck, J., Poussielgue, N., Tabbagh, J. & Punongbayan, R. (2003): Radon anomaly in the soil of Taal volcano, the Philippines: A likely precursor of the M 7.1 Mindoro earthquake (1994). Geophysical Research Letters, VOL. 30, NO. 9, 1481, doi:10.1029/2003GL016902, 2003.

Riguzzi, F., Panza, G., Varga, P. & Doglioni, C. (2009): Can Earth's rotation and tidal dispinning drive plate tectonics? Tectonophysics. (2009) doi:10.16/j.tecto.2009.06.012.

Rikitake,T. (1976): Earthquake prediction., Elsevier Scientific Pub., Amsterdam, Netherlands.

Rikitake, T. (1982): Earthquake Forecasting and Warning., Kluwer Academic Pub., Amster-dam, Netherlands.

Roeloffs, E. A. (1988): Hydrologic precursors to earthquakes: A review, Pure Appl. Geophys., 126, 177–209, 1988.

Roeloffs, E. & E. Quilty (1997): Water level and strain changes preceding and following the August 4, 1985 Kettleman Hills, California, earthquake, Pure and Applied Geophysics, 149, 21-60.

Rollinson, H. (2008): Secular evolution of the continental crust: Implications for crust evolution models, Geochem. Geophys. Geosyst., 9, Q12010, doi:10.1029/2008GC002262.

Roosbeek, F. (1996): RATGP95: A harmonic development of the tide-generating potential using an analytical method. Geophysical Journal International, vol. 126, 197 - 204.

Rousseau, A. (2005): A New Global Theory of the Earth's Dynamics : a Single Cause Can Explain All the Geophysical and Geological Phenomena. http://hal.archives-ouvertes.fr/docs/00/02/94/00/PDF/global-geodyn.pdf.

Roy, M. & Marone, Ch. (1996): Earthquake nucleation on model faults with rate- and state-dependent friction: Efects of innertia. J. Geophys. Res., 110, B6, 13919– 13932.

Royer, D., L. et al. (2004): CO2 as a primary driver of Phanerozoic climate. GSA Today; v. 14; no. 3, doi: 10.1130/1052-5173(2004)014<4:CAAPDO>2.0.CO;2. http://www.soest.hawaii.edu/GG/FACULTY/POPP/Royer%20et%20al.%202004%20GSA%20Today.pdf.

Royle, G.T. (2006): Comparison of episodic and non-episodic non-volcanic tremors in the Northern Cascadia subduction zone. MSc. degree thesis, Simon Fraser University, Burnaby, Canada.

Rubinstein, J.L., Vidale, J.E., Gomberg, J., Bodin, P., Creager, K.C. & Malone, S.D. (2007): Non-volcanic tremor driven by large transient shear stresses. Nature, Vol 448|2 August 2007| doi:10.1038/nature06017.

Rybach L. (1976): Radioactive heat production: a physical property determined by the chemistry of rocks. In: Physics and Chemistry of minerals and rocks (ed. R.G.J. Strens), 309–318.

Rydelek, P. A., P. M. Davis, & R. Y. Koyanagi (1988), Tidal triggering of earthquake swarms at Kilauea Volcano, Hawaii, J. Geophys. Res., 93, 4401–4411.

Rydelek, P. A., I. S. Sacks, & R. Scarps (1992), On tidal triggering of earthquake at Campi Flegrei, Italy, Geophys. J. Int., 109, 125– 137.

Sammis, C.G., Bowman, D.D. & King, G. (2004): Anomalous seismicity and accelerating moment releas preceding the 2001 and 2002 earthquakes in northern Baja California, Mexico. Pure Appl. Geophys., 161, 2369-2378.

Sandwell, D.T. & Smith, W.H.F. (1997): Marine gravity anomaly from Geosat and ERS1 satellite altimetry. J. Geophys. Res., Vol. 102, B5, 10039-10054.

Saraf, A.K. & Choudhury, S. (2004): Satellite detects surface thermal anomalies associated with the Algerian Earthquakes of May 2003. International Journal of Remote Sensing, 26, pp. 2705–2713.

Saraf, A.K. & Choudhury, S. (2005): NOAA-AVHRR detects thermal anomaly associated with 26 January, 2001 Bhuj earthquake, Gujarat, India. International Journal of Remote Sensing, 26, pp. 1065–1073.

Selvaggi, G. & Chiarabba, C. (1995): Seismicity and P-wave velocity images in the southern Tyrrhenian subduction, Geophys. J. Int., 121, 818-826.

Scholz, C.H. (1988): Mechanisms of seismic quiescence., Pure Appl. Geophys., 126, pp. 701-718.

Scholz, Ch. (1997): What Ever Happened to Earthquake Prediction? Geotimes, *Vol 17, March 1997.*

Schuster, A. (1897), On lunar and solar periodicities of earthquakes, Proc. R. Soc. London, 61, 455–465.

Scoppola, B., Boccaletti, D., Bevis, M., Carminati, E. & Doglioni, C., (2006): The westward drift of the lithosphere: A rotational drag? GSA Bulletin, Vol. 118, No. ½, 199-209.

Scotese, Ch.R. & Golonka, J. (1992): PALEOMAP Paleogeographic Atlas, PALEOMAP Progress Report No. 20, Department of Geology, University of Texas at Arlington, Arlington, Texas, 34 pp.

Scotese, Ch.R. (2003): Paleomap project. http://www.scotese.com/climate.htm.

Shalimov, S.L. (1992): Lithosphere-ionosphere relationship: A new way to predict earthquakes?. pp. 252-254, Dec. 1992.

Shanov S. (1993): Medium-time earthquake prediction based on tectonic fault zone displacement data. Acta Montana 4, 90, 53-62.

Shawe, D.R. (2001): Map of steep structures in part of the southern Toquima Range and adjacent areas, Nye County, Nevada. Miscellaneous Field Studies Map MF–2327–B. U.S. Department of the Interior USGS.

Shi, Y. & Zhang, H., Liu, Ch., Cao, J. & Sun, Y. (2009): How far are we from numerical earthquake prediction? Proceedings of International Symposium on Earthquake Seismology and Earthquake Predictability July 5 to 9, 2009, Beijing, China.

Shirley, J. (1988): Lunar and Solar periodicities of large earthquakes: Southern California and the Alaska Aleutian Islands seismic region., Geophysical Journal, Vol. 92., pp. 403 – 420.

Shlien, S. (1972): Earthquake – tide correlation., Geophys. J. R. Astr. Soc., Vol. 28, pp. 27 – 34.

Shou, Z.H. (2004): Ban earthquake prediction and space technology. Available online at http://www.earthquakecloudpredictions.com/ (accessed 30 December 2009).

Shou, Z.H. (1999): Earthquake Clouds a reliable precursor. Science & Utopia 64, 53~57. (in Turkish).

Sieh, K., Natawidjaja, D.H., Meltzner, A.J., Shen, Ch.-Ch., Cheng, H., Li, K.-S. Suwargadi, B.W., Galetzka, J., Philibosian, B. & Edwards, R.L. (2008): Earthquake Supercycles Inferred from Sea-Level Changes Recorded

in the Corals of West Sumatra. *Science* 12 December 2008: Vol. 322. no. 5908, pp. 1674 – 1678.

Silina, A.S. (2001): Ionospheric phenomena before strong earthquakes. Natural Hazards and Earth System Sciences, 1: 113-118.

Silver, P.G. & H. Wakita (1996): A search for earthquake precursors. Science, 273, 77-78.

Singh, R.P.; Zlotnicki, J.; Prasad, A.K.; Gautam, R.; Hattori, K.; Liu, J.; Parrot, M.; Li, F. & Kafatos, M. (2008): Precursory Signals Using Satellite and Ground data Associated with the Wenchuan Earthquake of May 12, 2008. American Geophysical Union, Fall Meeting 2008, abstract #U22B-06.

Skalský, L. (1963): Tilt Observation Before Rockburst. Studia geoph. et geod., 7, 396 – 403.

Skalský, L. & Pícha, J. (1965): Evaluation of Rockbursts Observed in 1958 - 1961 at Tidal Stations of Březové Hory (Příbram). Travaux Inst. Géophys. Acad. Tchécosl. Sci. No 199, Geofysikální sborník 1964, pp. 97 - 165. NČSAV, Praha.

Skalský, L. (1991): Calculation of theoretical values of the tidal strain components with respect to their practical use. Proceedings from seminary "Advances in gravimetry", December 10 - 14, 1990, Smolenice, pp. 179 - 184. Geophysical institute, Slovak academy of sciences, Bratislava.

Skřivánek, F. (1972): Chráněné podzemí, Jeskyně pod Šeptouchovem (Preserved underground area, Pod Šeptouchovem Cave).- Ochrana přírody, 27/ 10.

Smith, A.D., & Lewis, C. (1999): Differential rotation of lithosphere and mantle and the driving forces of plate tectonics. Geodynamics, 28, 97-116.

Smith, S.W. & Sammis, C.G. (2004): Revisiting the tidal activation of seismicity with a damage mechanics and friction point of view. Pure Appl. Geophys., 161, 2393-2404.

Smith, S. (2008): Rumor and the Sichuan Earthquake.

Sobolev, G.A. & Ponomarev, A.V. (1996): The effect of harmonic oscillations on the deformation and acoustic regime of the fault zone model. ESC XXV General Assembly, Sep. 9-14, 1996, 94-99.

Sobolev, G.A. (2003): Stages of earthquake preparation and mid-term prediction. EGS – AGU - EUG Joint Assembly, Abstracts from the meeting held in Nice, France, 6 – 11 April 2003, abstract #136.

Somoza, R. (2008): Major mid-Cretaceous plate reorganization as the trigger of the Andean orogeny. 7th International Symposium on Andean Geodynamics (ISAG 2008, Nice), Extended Abstracts: 509-512.

Sornette, A. & Sornette, D. (1989): Self-organized criticality and earthquakes, Europhy. Lett. 9, 197.

Staš, L. & Souček, K. (2002): Horizontal Stress field of carboniferous massif in Eastern Czech part of the Upper Silesian Basin. ISRM Regional Symposium - Advancing Rock Mechanics Frontiers to meet the Challenges of 21st Century. Proceedings, 1-10.

Staš, L., Knejzlík, J. & Rambouský, Z. (2005): Conical strain gauge probes for stress measurement. In: P. Konečný (ed.): Eurock 2005. Impact of Human Activity on the Geological Environment. Proceedings. Leiden, A.A.Balkema Publishers, 2005 - pp. 587-592. ISBN 04-1538-042-1.

Stejskal V., Skalský L. & Kašpárek L. (2007): Results of two-years' seismo-hydrological monitoring in the area of the Hronov-Poříčí Fault Zone, Western Sudetes. Acta Geodynamica et Geomaterialia, Vol. 4, No. 4 (148), in 59-76.

Stemberk J., Košťák B. & Vilímek, V. (2003): 3-D monitoring of active tectonic structures. – Journal of Geodynamics, 36, 103-112, Elsevier.

Stemberk, J., Briestenský, M. & Jurková, N. (2008): Posuny registrované ve vybraných jeskyních Českého masivu. - Displacements registered in the selected caves of the Bohemian Massif. Speleofórum 2008, 141 – 144. (in Czech with English abstr.)

Strom, R. G.; et al. (1979). "Volcanic eruption plumes on Io". Nature 280: 733–736.

Stroup, D.F., D. R. Bohnenstiehl, M. Tolstoy, F. Waldhauser, & R. T. Weekly (2007): Pulse of the seafloor: Tidal triggering of microearthquakes at 9°50´N East Pacific Rise. Geophysical Research Letters, VOL. 34, L15301.

Sue, Y. (2009): The effect of earth tides in triggering earthquake as clearly observed in some specific regions of Japan, Journal of Atmospheric Electricity, 29, 53-62.

Sun, W. & S. Okubo (1998): Surface potential and gravity changes due to internal dislocations in a spherical earth - II. Application to a finite fault, Geophys. J. Int., 132, 79-88.

Škrabiš, A. (1977): Předvídání a hodnocení tlakových a deformačních projevů v horizontálních otvírkových a přípravných důlních dílech v podmínkách československé části hornoslezské pánve empiricko-analytickou metodou, doktorská disertační práce, Praha. (in Czech)

Tada, T. (2008): Crustal deformations in the Japanese islands observed. with the nationwide continuous GPS observation system. http://www.slac.stanford.edu/econf/C951114/papers/033.PDF

Takemoto, S. (1991): Some problems on detection of earthquake precursors by means of continuous monitoring of crustal strauns and tilts. J. Geophys. Res., 96, 10377-10390.

Tamura, Y. (1987): A harmonic development of the tide-generating potential., Bulletin d'Informations des Marees Terrestres, 99, pp. 6813-6855.

Tanaka, S., M. Ohtake, & H. Sato (2002a): Evidence for tidal triggering of earthquakes as revealed from statistical analysis of global data, J. Geophys. Res., 107(B10), 2211, doi:10.1029/2001JB001577.

Tanaka, S., Ohtake, M. & Sato, H. (2002b): Spatio-temporal variation of the tidal triggering effect on earthquake occurrence associated with the 1982 South Tonga earthquake of Mw 7,5. Geophys. Res. Let., 29, 16, 3-1-4.

Tanaka, S. (2006a), Tidal triggering of earthquakes in the subducting Phillippine Sea plate beneath the locked zone of the plate interface in the Tokai region, Japan, Tectonophysics, 417, 69– 80.

Tanaka, S. (2006b), Tidal triggering of earthquakes precursory to the 2004 Mw = 9.0 off Sumatra earthquake, paper presented at the 4th International Workshop on Stat. Seismology, Grad. Univ. for Adv. Stud., Kanagawa, Japan, 9– 13 Jan.

Tanaka, S. (2010): Tidal triggering of earthquakes precursory to the recent Sumatra megathrust earthquakes of 26 December 2004 (Mw 9.0), 28 March 2005 (Mw 8.6), and 12 September 2007 (Mw 8.5). Geophysical Research Letters, Vol. 37, L02301.

Tamrazyan, G. (1967): Tide-forming forces and earthquakes., Icarus, 7, pp. 59-65.

Tazief, H. (1975): Niragongo ou le volcan interdit. Flammarion Paris. 194pp.

Thanassoulas, C., (1991): Determination of the epicentral area of three earthquakes (Ms>6) in Greece, based on electrotelluric currents recorded by the VAN network., Acta Geoph. Polonica, Vol. XXXIX, no. 4, pp. 273 – 287.

Thanassoulas, C & Tselentis, G. (1993): Periodic variations in the earth's electric field as earthquake precursors: results from recent experiments in Greece., Tectonophysics, 224, 103-111.

Thanassoulas, C., & Tsatsaragos, J. (2000): The earthquakes of Izmit , Turkey (Ms=7.5R, 17/8/1999) and Athens, Greece (Ms=5.9R, 07/09/1999) as being detected by precursory electrical signals (T=24h period oscillation). Open File report E3906, Inst. Geol. Min. Expl. (IGME), Athens, Greece, pp. 1-18.

Thanassoulas, C., Tsatsaragos, J. & Klentos, V. (2001): Determination of the most probable time of occurrence of a large earthquake., Open File Report A. 4338, IGME, Athens, Greece.

Thomas, A.M., Nadeau, R.M. & Bürgmann, R. (2009): Tremor-tide correlations and near-lithostatic pore pressure on the deep San Andreas fault. Nature, Vol 462| 24/31 December 2009| doi:10.1038/nature08654.

Times of India (2001): A temblor from ancient Indian treasure trove? The Times of India News Service 28 April 2001. http://timesofindia.indiatimes.com/articleshow/39647948.cms

Tolstoy, M., F. L. Vernon, J. A. Orcutt, & F. K. Wyatt (2002), Breathing of the seafloor: Tidal correlations of seismicity at Axial Volcano, Geology, 30, 503–506.

Toomey, D. R., W. S. D. Wilcock, S. C. Solomon, W. C. Hammond, & J. A. Orcutt (1998): Mantle seismic structure beneath the MELT region of the East Pacific Rise from P and S wave tomography, Science, 280, 1224-1227.

Tosi, N. (2007): Numerical modeling of present-day mantle convection. PhD thesis, MFF Charles University, Prague.

Tronin, A.A. (1996): Satellite thermal survey—a new tool for the studies of seismoactive regions. International Journal of Remote Sensing, 17, pp. 1439–1455.

Tronin, A., Hayakawa, M. & Molchanov, O.A. (2002): Thermal IR satellite data application for earthquake research in Japan and China. Journal of Geodynamics, 33, pp. 519–534.

Turcotte D.L. (1992): Fractals, chaos, self-organized criticality and tectonics // Terra Nova. V. 4. № 1. P. 4–12.

Uda, S., Maeda, M. (2006): Characteristic precursors of earthquakes around Metropolitan area in Japan. Poster on the Meeting of JpGU, (E141-P012) (poster session).

Ulomov, V. I. and Mavashev, B. Z. (1971): The Tashkent Earthquake of 26 April, 1966. Acad. Nauk. Uzbek SSR FAN, 188-192.

USGS (1994): Earthquake Research at Parkfield, California, for 1993 and Beyond - National Earthquake Prediction Evaluation Council Working Group, 1994, U.S. Geological Survey Circular 1116, 14 p.

USGS (2009): The Parkfield, California, Earthquake Experiment. http://earthquake.usgs.gov/research/parkfield/index.php .

USGS (2010): http://neic.usgs.gov/neis/epic/epic_rect.html .

Utsu, T. (1965): A method for determining the value of b in a formula log n=a-b.M showing the magnitude-frequency relation for earthquakes, Geophys.Bull. Hokkaido Univ., 13, 99-103.

VAN (1996): Debate on evaluation of the VAN Method (R.Geller, ed.). Geophysical Research Letters, Vol. 23, No.11.

Varga, P., Gambis, D., Bizouard, Ch., Bus1, Z. & Kiszely, M. (2005): Tidal influence through LOD variations on the temporal distribution of earthquake occurrences. Proc. of Conferrence „Earth dynamics and reference systems: five years after the adoption of the IAU 2000 Resolutions“, Warsaw, 19-21 September 2005.

Veizer, J. (2005): Celestial Climate Driver: A Perspective from Four Billion Years of the Carbon Cycle. Geoscience Canada, Vol. 32, No. 1, March 2005, 13-28.

Varotsos, P. et al. (1984a): „Physical Properties of the Variations of the Electric Field of the Earth Preceding Earthquakes, I,“ Tectonophysics, 110 (1984) 73-98.

Varotsos, P. et al. (1984b): „Physical Properties of the Variations of the Electric Field of the Earth Preceding Earthquakes. II. Determination of Epicenter and Magnitude," Tectronophysics, 110 (1984) 99-125.

Varotsos, P. et al. (1987): „Physical properties of the variations in the electric field of the earth preceding earthquakes, III," Tectronophysics, 136 (1987) 335-339.

Veizer, J. (2005): Celestial Climate Driver: A Perspective from Four Billion Years of the Carbon Cycle. Geoscience Canada, Vol. 32, No. 1, March 2005, 13-28.

Venkatanathan, N. (2004): Report of Department of Applied Geology, University of Madras, Guindy Campus, Chennai – 600 025. Email: physics16972@rediffmail.com

Vergnolle, M., Pollitz, F. & Calais, E. (2003): Constraints on the viscosity of the continental crust and mantle from GPS measurements and postseismic deformation models in western Mongolia, J. Geophys. Res., 108(B10), 2502.

Vine, F. J., & Mathews, D.H. (1963): Magnetic anomalies over oceanic ridges. Nature, 199, 947-949.

Vine, F. J. (1966): Sea-floor spreading of the ocean floor: new evidence. Science, 154, 1405-1415.

Special issue "Debate on 'VAN'", GRL, 1996, v. 23, 1,291-1,452.

Verbunt, F. (2002): The Earth and Moon: from Halley to lunar ranging and shells. http://www.astro.utoronto.ca/~mhvk/AST221/verbunt.pdf.

Vidale, J.E., Agnew, D.C., Johnston, M.J.S. & Oppenheimer, D.H. (1998): Absence of earthquake correlation with Earth tides: An indication of high preseismic fault stress rate. J. Geoph. Res., 103 (B10), 24567-24572.

Virk, H. S. & Singh, B. (1994): Radon recording of Uttarkashi earthquake, Geophys. Res. Lett., 21, 737–740.

Voisin, C., J.-R. Grasso, E. Larose, & F. Renard (2008): Evolution of seismic signals and slip patterns along subduction zones: Insights from a friction lab scale experiment, Geophys. Res. Lett., 35, L08302, doi:10.1029/2008GL033356.

Wahr, J.M. (1981): Body tides on an elliptical, rotating, elastic and oceanless earth. Geophysical Journal of the Royal astronomical Society, vol. 64, 677 - 703.

Wahr, J.M. (1985): Deformation induced by polar motion. J.Geophys. Res., 90, 9363-9368.

Wakita, H. (1996): Geochemical challenge to earthquake prediction. Proceedings of the National Academy of Sciences of the United States of America 93, 3781-3786.

Wakita, H. (1975): Water Wells as Possible Indicators of Tectonic Strain. *Science,* Vol. 189. no. 4202, pp. 553 – 555.

Wang, Ch. (1984): Ground-water studies for earthquake prediction in China. Pageoph, Volume 122, Numbers 2-4, 215-217.

Wang, C.M., Wang, Y.L., Zhang, H.P., Li.Y. & Zhao, S. (1984): Characteristics of water level variations in deep wells before and after the Tangshan earthquake 1976. In: EVISON, F.F. (ed), Proceedings of an International Symposium on Earthquake Prediction 1979, Terra Scientific, Tokyo/UNESCO, Paris, 215-232.

Wang, K., Chen, Q. et al. (2006): Predicting the 1975 Haicheng Earthquake. Bulletin of the Seismological Society of America, Vol. 96, No. 3, pp. 757–795.

Wang, Q.-L., Chen, Y.-T., Cui, D.-X., Wang,W.-P. & Liang, W.-F. (2000): Decadal correlation between crustal deformation and variation in length of day of the Earth. Earth Planets Space, 52, 989–992.

Wang, W. X.; Yang, W. Y. & Tian, P. S. (2003): How successful earthquake predictions were achieved by the electromagnetic MDCB method during two earthquake prediction training courses. EGS - AGU - EUG Joint Assembly, Abstracts from the meeting held in Nice, France, 6 - 11 April 2003, abstract #3226. http://adsabs.harvard.edu/abs/2003EAEJA.....3226W

Wang, W. X.; Yang, W. Y. & Tang, F.T. (2002): Studies On Prediction of Damaging Earthquakes By The Mdcb Method (paper Ii) Âthe Relativity Between 12 Types of Graphs and The Location, Time &Magnitude, and Several Earthquake Prediction Cases. EGS XXVII General Assembly, Nice, 21-26 April 2002, abstract #522.

Ward, P.L. (1991): On Plate Tectonics and the Geologic Evolution of southwestern North America. J. Geophys. Res. , Vol. 96, No. B7, Pages 12,479-12,496.

Wegener, A. (1912): *"Die Entstehung der Kontinente"*, Peterm. Mitt.*: 185—195, 253—256, 305—309.*

Wegener, A. (1966): The Origin of Continents and Oceans. *New York: Dover.* - (Translated from the fourth revised German edition by John Biram).

Wei, L., Zhao Y., Guo J., Zeng Z. & Xie H. (2009): Satellite Thermal Infrared Earthquake Precursor to the Wenchuan Ms 8.0 Earthquake in Sichuan, China, and its Analysis on Geo-dynamics. Acta Geologica Sinica, vol. 83, No.4, 767-775.

Wei Sun (2007): Damaging Earthquakes Can be Predicted – The Earthquake Gestation Physical Model and Earthquake Imminent Precursor. Engineering Science, 9 (7): p 7-17 (in Chinese).

Wej Su & Li K., (2007): Of solar activity on the Chinese mid-latitudes 8 earthquake could trigger a Possible Triggering of Solar Activities to Big

Earthquakes (Ms ≥ 8) in the Middle Latitude in China. Astronomy research and technology – National Astronomical Observatory, 2007 Vol. 4, . - Core Journals ISSN: 1672-7673 (2007) 02-0195-04.

Wilcock, W. (2001), Tidal triggering of microearthquakes on the Juan de Fuca Ridge, Geophys. Res. Lett., 28, 3999– 4002.

Williams, G.E. (2000): Geological constraints on the Precambrian history of Earth's rotation and the Moon's orbit. Reviews of Geophysics, Volume 38, Issue 1, p. 37-60.

Willson, R.C. & Hudson, H.S. (1991): The Sun's luminosity over a complete solar cycle. Nature 351: 42–4.

Wright, T.J., B. E. Parsons, J. A. Jackson, M. Haynes, E. J. Fielding, P. C. England, & P. J. Clarke (1999): Source Parameters of the 1 October 1995 Dinar (Turkey) earthquake from SAR interferometry and seismic bodywave modelling, Earth and Planet. Science Lett., 172, 23-37.

Wu S. (2005): S'-čchuan earthquake. Earthquake research in Sichuan.

Wyss, M., Johnston , A.C. & Klein, F.W. (1981): Multiple asperity model for earthquake prediction. Nature 289, 231 - 234 (22 January 1981); doi:10.1038/289231a0.

Wyss, M. & Haberman, E. (1988): Precursory seismic quiescence., Pure Appl. Geophys., 126, pp. 319-332.

Xiwei, X.; Xueze, W.; Guihua, Y.; Guihua, C. & Klinger, Y. (2008): Co-seismic reverse- and oblique-slip surface faulting generated by the 2008 Mw 7.9 Wenchuan earthquake, China. American Geophysical Union, Fall Meeting 2008, abstract #U22B-05.

Xu Xiudeng, Qiang Zuji & Lin Changgong (1991): Thermal anomaly and temperature increase before impending earthquake. Chinese Science Bulletin, 6, pp. 291–294.

Yaltirak, C., Yalcin, T., Yüce, G. & Bozkurtoúlu, E. (2005): Water-Level Changes in Shallow Wells Before and After the 1999 Üzmit and Duzce Earthquakes and Comparison with Long-Term Water-Level Observations (1999-2004), NW Turkey. Turkish Journal of Earth Sciences (Turkish J. Earth Sci.), Vol. 14, 2005, pp. 281-309.

Yamaguchi, R. (1980): Changes in water level at Funabara and Kakigi before the Izu-Hanto-Toho-Oki, Earthquake of 1980, Bull. Earthquake Res. Inst. Univ. Tokyo, 55, 4, 1065.

Yin, X., Xuezhong, C., Ziping, S., & Can, Y., (1995): A new approach to earthquake prediction: the load/unload response ratio (LURR) theory. Pageoph, 145, 701-715.

Yin, X.C., et al. (2000): Development of a new approach to earthquake prediction: Load/unload response ratio (LURR) theory. Pageoph, 157, 2365-2383.

Yin, X., Mora, P., Peng, K., Wang, Y. & Weatherley, D. (2002): Load-Unload response ratio and accelerating moment/energy release critical region scaling and earthquake prediction., Pure appl. Geophys., 159, 2511-2523.

Zachos, J., Pagani, M., Sloan, L., Thomas, E. & Billups, K. (2001): Trends, Rhythms, and Aberrations in Global Climate 65 Ma to Present, *Science* 27, Vol. 292., no. 5517, pp. 686 – 693.

Zadro, M. Braitenberg, C. (1999): Measurements and interpretations of tilt–strain gauges in seismically active areas. Earth-Science Reviews 47_1999.151–187.

Zátopek, A. (1941): O seismickém neklidu. ŘH, 22 (1941), 59, 81. (in Czech).

Zedník, J. (2007): Bulletiny seismických jevů, zaregistrovaných stanicemi České regionální seismické sítě – (Bulletins of seismic events registered in the observatories of Czech regional seismic network).- http://www.ig.cas.cz/cz/seismicka-sluzba/seismicke-bulletiny/

Zhang Guo-min, Fu Zheng-xiang, et al. (2001): EQ Prediction Introduction. Science Publishing House, Beijing, 2001 (in Chinese).

Zhang, T. (2002): Geomagnetic Storm Double Time Method and Prediction of the Three Parameters of Earthquakes, embodied by: Edited by Shuhua Ye and Shupeng Chen, New Approaches and New Methods for Predicting Extremely Strong Natural Hazards, Science Press, Beijing, p104-110

Zhang, Y., Yin, X., Peng, K. (2004): Spatial and temporal verification of LURR and its implication for the tendency of earthquake occurrence in Southern California. Pure Appl. Geophys., 161, 2359-2367.

Zhang S., Cheng Z., Tang L., Zhao X. & Zhang R.. (2008): Study on Relationship Between Precursor Phenomena of Well Water Level and Seismic Source Nucleation. *Earthquake Research In China*, Year 2008, Issue 2, Page 159-171.

Zhang, Ch.-J., Cao, J.-L. & Shi, Y.-L. (2009): Studying the viscosity of lower crust of Qinghai-Tibet Plateau according to post-seismic deformation. Science in China, Ser.D, Vol. 52, No.3, 411-419.

Zschau,J. & Wang, R. (1987): Imperfect elasticity in the Earth's mantle. Implications for Earth tides and long period deformations. Proceedings of the 9th International Symposium on Earth Tides, New York 1987, 605 - 629, editor J.T. Kuo, Schweizerbartsche Verlagsbuchhandlung, Stuttgart.

Acknowledgements

We gratefully acknowledge the research grant from the International Academy of Science H&E-AS, and especially the support from Prof. Elchin Khalilov, Ph.D. from the Azerbaijan section of IAS and Global Network for the Forecasting of Earthquakes (Baku).

We express our gratitude to Dr. Lumír Skalský CSc. and Ing. Václav Polák from the underground research laboratory in Příbram of the Geophysical Institute of Czech Academy of Science, to Ing. Július Kvetko, CSc, from Slovmag Jelšava a.s., to Petr Stolina from Palivový kombinát Ústí s.p., to Ing. Petr Polák, Ing. Tomáš Roth, Franci Musil jun., Ing. Bohuslav Koutecký – speleologists from ZO 6-19 Plánivy – for their help with the instalments and measurements made in underground mines and caves.

We are grateful to Mr. Chen I-wan for the review and translations of many papers from Chinese into English and from English into Chinese.

We would like to thank earthquake researcher E.D. Glass, M.S. Analytical Chemistry for his discussions over the years regarding earthquake triggering processes and for his assistance with proofreading.

We acknowledge help from Dr.Stanka Šebela and David English for their peer reviews and proofreading. We express our sincere thanks to Dr.Petr Rajlich, CSc. for helpful comments and a deep review.

Tomáš Kopf would like to express his thanks to grant MSM4781305904.

Dedication

This book is dedicated to all of the dreamers and visionaries who are able to look at reality from a new perspective, find new connections, sketch new hypotheses, deny generally accepted dogmas, and move our understanding of the universe another step forward.

TILTS, GLOBAL TECTONICS AND EARTHQUAKE PREDICTION

Authors: P. Kalenda, L. Neumann et al.

Reviewer: dr. Stanka Šebela, karst geologist, ZRC SAZU Karst Research Institute, Titov trg 2, 6230 Postojna, Slovenia, sebela@zrc-sazu.si

The manuscript *Tilts, Global Tectonics and Earthquake Prediction* is an interesting work that fits very well in our time period with many strong earthquakes in 2010. I have to stress that I am a karst structural geologist and not a seismologist. In this sense I might not be the right person to give the review remarks.

Most seismologists (or mostly all) that I know are very sceptical in earthquake predictions. They are really not open-minded in this sense. They even don't listen to explanations, because they immediately say: »Earthquakes are not predictable!!!!!«

My personal opinion is that understanding physics of the Earth and causes for an earthquake occurrence still needs some new basic researches and I think that this manuscript (book) can help a lot. Earthquake is not a source but a consequence of different actions that start before earthquake occurrence. L'Aquila (Italy) earthquake on 6th April 2009 (M=6.3) was one of the best examples. We heard from newspapers and TV reports that *Giuliani G.* Called for the attention before this earthquake due to the significant changes in radon concentrations. After the earthquake he was strongly criticiezed by known official Italian seismologists. In 2010 Journal of Zoology published an interesting article about predicting the l'Aquila earthquake regarding the pre-seismic anticipatory behaviour in the common toad (Grant & Halliday, 2010). So not only radon as a precursor signal, but also animal precursors were evident before l'Aquila earthquake as well.

I remember an emotional question of a person from Haiti (12th January 2010, M=7.1) from TV news who was crying and saying: »Why didn't they inform us if they knew this earthquake would strike?« He was addressing the scientists. I read in the newspaper that before the earthquake people noticed that the waters in streams were foaming and some people said:

»Maybe a storm is coming, it is better to sleep out of town.« And in fact some of them survived because they were not in town.

I want to say that it is very important to study and understand precursor impulses to earthquakes and thus also make a step forward in earthquake prediction.
It is important to use more different methods not only one to understand earthquake precursors. And in the manuscript this is well verified. Monitoring of microseismicity is really important. I think that the manuscript gives new approaches that already showed some good results during 2008-2010. The future will evaluate the real weight of the proposed model for earthquake predictions using vertical pendulums. This means still many years of monitoring and interpretations and comparison with other methods.

At the end I have to ask a question. Can the recent increase in strong earthquakes worldwide influence the chaotic stress field and therefore the prediction described in the manuscript can be much more difficult?

Regarding review of the manuscript I suggest that somebody who is more fluent in Physics of the Earth and in Seismology looks over the theoretical part.

I support the publication of manuscript, because it shows an interesting approach in understanding the nucleation stage and stress waves before the earthquakes. I also think that manuscript will be a base for the future research and development giving an important step forward in understanding earthquake precursor.

REFERENCES

Grant, R.A. & T. Halliday, 2010. Predicting the unpredictable; evidence of pre-sesimic anticipatory behaviour in the common toad. Journal of Zoology, doi:10.1111/j.1469-7998.2010.00700.x

Stanka Šebela
Postojna, 19.4.2010

Kalenda, P., Neumann, L., et al. Tilts, Global Tectonics And Earthquake Prediction, SWB 2010, London.

TILTS, GLOBAL TECTONICS AND EARTHQUAKE PREDICTION

Authors: P. Kalenda, L. Neumann et al.

Reviewer: RNDr. Petr Rajlich, CSc.

The book of the authors P. Kalenda, L. Neumann, J. Málek, L. Skalský, L. Ostřihanský, T. Kopf, V. Procházka, I. Wandrol represents alternative and highly innovative contributions/solutions to the utmost difficult issues such as the earthquake prediction. Unlike the latest textbooks and research papers the authors' starting point is not in the current plate tectonic concept. This liberated them from the fairly erroneous concept and allowed them to look for other rather forgotten and unfairly neglected forces such as the Earth rotation, earth tides, solar activity etc. The proposed interpretations are substantiated by the very innovative empirical data sets obtained from several underground pendulum-operating stations in the Czech Republic and the Slovak Republic.

The concept of triggering mechanism dealt with from all possible alternative views is highly desirable because such research has not been carried out for the last 50 years. The present concept of plate tectonics has not allowed the prediction of earthquakes or tremors successfully. But still the great unknown is the nature and functionality of the Earth's core and the extent of its contribution to the mantle and the Earth crust movements.

I recommend this important book to lecturers, students and scientists interested in and dealing with earthquakes and seismic activity prediction.

České Budějovice, November 1, 2010
RNDr. Petr Rajlich, CSc.

TILTS, GLOBAL TECTONICS AND EARTHQUAKE PREDICTION
Authors: P. Kalenda, L. Neumann et al.

Reviewer: Chen I-wan, Advisor, Committee of Natural Hazard Prediction of China Geophysical Society, and Advisor, Committee of Disaster Historical Studies of China Disaster Prevention Association, No.12-6-301, Bai Jia Zhuang Xili, Chaoyang District, Beijing 100020, China, cheniwan@mx.cei.gov.cn

In 1990 I began to investigate and follow the development of earthquake prediction science, which started in China after two devastating earthquakes in Xingtai, North China in 1966. Upon being appointed the advisor of the Committee of Natural Hazard Prediction of China Geophysical Society in 2002, I was able to more closely learn and follow the earthquake prediction work by the most outstanding researchers in China.

Based on what I have learnt during the past 20 years, there is not only no doubt that "earthquakes can be predicted", but furthermore, there is sufficient evidence to demonstrate and prove that "earthquakes can already be rather accurately and reliably predicted" with techniques and instruments already developed and operated today, if necessary support is provided by the government!

I would like to especially recommend three types of techniques/instruments operating with significant success in China:

1) The electromagnetic MDCB[2] network: Each of their MDCB-5 instruments is equipped with 32 sensors in 32 directions, plus one downward sensor, which monitors and records electromagnetic signals from 32 directions. With about 10 such instruments operating in different locations in China, including 3 units on the Taiwan Island, since Sep. 2003 the MDCB network has issued weekly predictions of earthquakes, likely to occur within the coming 7 days, specifying locations (and longitude and latitude) within China and around China, and the likely magnitudes. The MDCB network with only 3 analyst staff they could afford, accomplishes a success rate on average over 65% on earthquakes developing within China. Based on over 350 weekly prediction reports since Sep. 2003, each containing predictions of earthquakes to occur within 5 – 7 specific locations, it should not be difficult to evaluate the overall performance of the MDCB network.

2) The Beijing Liangxiang Dianye Middle School Earthquake Observatory: It is equipped with a series of earthquake precursor monitoring

[2] MDCB stands for Mei (Coal) and Dian Ci Bo (Electro-Magnetic Wave) in Chinese, as Wang Wen-xiang, the chief developer worked at the Xian-Division of the China Coal Science Research Institute.

instruments all developed by Sun Wei, including (1) terrestrial stress, (2) telluric current, (3) pendulum gravimeter, (4) inclinometer, (5) geomagnetic, and (6) earthquake imminent resonance instruments. It is widely known among earthquake prediction researchers that it is impossible to predict the location of earthquakes developing in remote areas with only one observatory, even with multiple types of instruments. Liu Gen-shen, the analyst of the observatory, in June 2007 discovered an interesting phenomenon: The geomagnetic precursors and terrestrial stress precursors before earthquakes developing in the same region but at different times show similar characteristics, even if their magnitudes are quite different and their occurrence times are very much apart. Liu began to use this feature to determine the locations of earthquakes. He normally predicted the occurrence of earthquakes in a 7-day window on the basis of monitoring of precursors with similar characteristics as those of the earthquakes that developed in the same region before. Once the location was determined, the magnitude of the earthquake could be predicted in accordance with the amplitude of the precursors. Based on the above mentioned technique, Liu issued predictions of about 7 – 10 earthquakes worldwide each day, with amazing success. Regarding the results of a very large amount of predictions generated by Liu, it should not be difficult to evaluate the overall performance of Liu's earthquake prediction work.

3) Sun Wei's earthquake imminent resonance instrument: In my opinion, the most difficult issue in earthquake prediction is the following situation: The authorities of a city are presented with a number of dramatically different predictions, i.e. one predicts a strong earthquake might strike within a specific time window, another predicts only a moderate earthquake might strike, and others predict that no earthquake will strike. Therefore, there is a need for a technique/instrument to finally determine whether or not a strong earthquake will occur within the region, or close enough to cause strong effects within the region. Number (6) instrument mentioned above, developed by Sun Wei in 1977, has demonstrated from event to event without failure that it solves this most difficult issue. The principle of the instrument is clear and simple. The resonance frequency of the instrument is finely tuned to exactly match the frequency of the pulse of the earth of the region and thus it is in resonance. Before an earthquake develops within the region, the accumulation of energy and increase of stress within the crust must pass through a phase

during which the pulse of the earth of this region is interrupted. So, the instrument loses resonance and the recording becomes scratchy. If the minimum of two significant pulse spikes appear in the recordings then an earthquake will surely occur. The interval time between the second pulse spike and the occurrence time is shorter for smaller earthquakes, i.e. around 1 – 2 hours, and longer for stronger earthquakes, i.e. 3, 4 or even 12 hours. Furthermore, if the recording becomes scratchy, two spikes appear, but the recording shortly returns to "normal", i.e. resonance, then no earthquake will follow.

Besides investigating and following the development of earthquake prediction techniques and instruments developed in China, I have also established contacts with many researchers in America, Europe and Asia, and among others Pavel Kalenda. I got to know his work in earthquake research "*Influence of tides on global seismicity*" (now one chapter of the book), a very interesting paper by P. Kalenda and L. Skalský in 2003, and helped to translate it into Chinese and presented it at a workshop of our Committee of Natural Hazard Prediction of China Geophysical Society, Nanchang, May, 2004.

In their book "*Tilts, Global Tectonics and Earthquake Prediction*" the authors summarised the results of their work on the earthquake prediction and studies of earthquakes mechanisms accomplished in the past ten years. In my view, the book represents a significant contribution to the development of earthquake prediction worldwide. It looks at the earthquake prediction issues from a new perspective, which could help other researchers around the world. I think it might even raise interest of certain circles of general public.

Therefore I look forward to the publication of this book, and will surely help to introduce this work to researchers in China.

Chen I-wan
Beijing, Oct. 24, 2010

Scientific editor:
Prof. Dr. Elchin Khalilov, IC GEOCHANGE, Germany
Technical editors:
Fuad Damirov; Natalya Ligina

Corrector:
Alena Dukhanina

® Science Without Borders

Secretariat:
19 Kathleen Road, London, SW112JR, United Kingdom of Great Britain and Northern Ireland, Phone: + 44 207 760 633; Fax: + 44 207 691 9560; www.wosco.org; e_mail: publishing_house@wosco.org
Representative office:
Lindenstraße 12 a, 81545 Munich, Germany, GNFE EU, Phone: + 49 157 848-087-65; Germany, GNFE EU e_mail: publishing_house@wosco.org

Date of an order: *02.06.2011*
Order: *103/011*
Size: *60 x 90/16*
Offset printing

ISBN 978-9952-451-18-4